eLoran Service Volume Coverage Prediction

Lebekwe, Caspar

Award date:
2018

Awarding institution:
University of Bath

University of Bath
Department of Electronics and Electrical Engineering

*e*Loran Service Volume Coverage Prediction

Doctoral Thesis

Author:
Caspar K. Lebekwe

Supervisor:
Dr. Ivan Astin

ABSTRACT

This thesis answers the following research questions:

1. Given the current transmitter configuration, what is the accuracy, availability, and continuity performance of the coverage network in the General Lighthouse Authorities of United Kingdom and Ireland's geographical area if differential eLoran is only applicable at harbour and port locations?

2. What is the best method of placing the reference stations in the coverage area given the constraints?

The previous work done by other researchers has been extended to include an improved accuracy model that accounts for the variation of signal delays due to conductivity changes along the path from the transmitter to the user and weather changes experienced at the user's location. Availability and continuity models have been derived using historical transmitter off-air data obtained from Loran control centre located in Brest, France. An analytical model that accounts for additional secondary factor delay over a flat terrain has been modelled and included in the coverage tool. A model which determines the optimization of the separation distance between any two given reference stations has been developed herein. All these techniques have been built into the GLAs coverage software tool thereby extending the software tool's capability to evaluate accuracy, availability and continuity at any location in the GLAs coverage area. Accuracy, availability and continuity are part of the four eLoran system performance parameters. The other performance parameter called integrity is discussed but not modelled in this thesis. The developed coverage software tool enables administrators overseeing the movement of ships into harbours and in coastal waters to ensure that system performance requirements of accuracy, availability and continuity are met within the chosen geographical area. Administrators can select transmitters to be used to predict coverage, identify and plan where new transmitters and reference stations need to be installed to meet international standards for accuracy, availability and continuity, giving a safe and reliable service. The developed coverage tool's outputs serve as a guide to administrators as to whether resources such as reference stations are optimized or not.

ACKNOWLEDGEMENTS

It was in the previous decade that I started this long journey through graduate school. This thesis is a testimony that everything is beautiful at God's time. I would like to thank Jehovah Jireh, Yahweh, God Almighty and His most trusted servants, Major 1, Prophet Shepherd Bushiri Ph.D. and Prophet Isaiah Brian Sovi (The Last Major) for pointing the Way. To God Be the Glory.

I would like to express my sincere gratitude towards my supervisor Dr. Ivan Astin and also to Dr. Nathan Smith. I sincerely thank my sponsors the General Lighthouse Authorities of the United Kingdom and Ireland for giving me the opportunity to study for a postgraduate degree. I would like to thank my colleagues at Botswana International University of Science and Technology (BIUST) for their support.

Finally, I dedicate this thesis to my dearest flower, the rib of my ribs, flesh of my flesh and my wife, Balo Lebekwe, and my two beautiful children Dupri Adriell K. and Raadal for being the reason why I smile everyday.

CONTENTS

ARE	Admiralty Research Establishment
ASF	Additional Secondary Factor
AWGN	Additive White Gaussian Noise
BER	Bit Error Rate
CCIR	International Radio Consultative Committee
CCB	Control Centre Brest
CONUS	Continental United States. All of the US except
CRI	Cross Rate Interference
CWI	Carrier Wave Interference
dB	Decibels
DGPS	Differential Global Positioning System
DHS	Department of Homeland Security
DOT	Department of Transport
DRMS	Distance Root-Mean Square
ECD	Envelope to Cycle Discrepancy
E-FIELD	Electric Field
EMRP	Effective Monopole Radiated Power
eLORAN	enhanced Loran
eDLORAN	enhanced Differential Loran
EUV	Extreme Ultra Voilet
FAA	Federal Aviation Administration
GHz	Gigahertz (Billions of cycles per second)
GLA	General Lighthouse Authorities of UK and Ireland
GNSS	Global Navigation Satellite System
GPS	Global Positioning System
GRF	Group Repetition Frequency
GRI	Group Repetition Interval
HEA	Harbour Entrance and Approach
HDOP	Horizontal Dilution of Precision
H-FIELD	Magnetic Field

HMI	Hazardously Misleading Information
HPL	Horizontal Protection Level
IAT	Independent Assessment Team
IEC	International Electro-Technical Commission
ILA	International Loran Association
ITU	International Telecommunications Union
IMO	International Maritime Organisation
IOC	Initial Operational Capability
kHz	Kilohertz (Kilo Cycles Per Second)
LCAST	Loran Coverage Availability Service Tool
LF	Low Frequency
LOIS	Loran Operational Information System
LOP	Line of Position
LORAN	Long Range Navigation
LORIPP	Loran Integrity Performance Panel
LTE	Long-Term Evolution
MDT	Mean Downtime
MHz	Megahertz (Millions of Cycles Per Second
MTBF	Mean Time Between Failures
MTTR	Mean Time To Repair
NELS	North West European Loran System
NPA	Non-Precision Approaches
PCI	Phase Code Interval
PDF	Probability Density Function
PF	Primary Factor
PNT	Position Navigation And Timing
PRC	Pseudorange Correction
PSD	Power Spectral Density
QoS	Quality of Service
RNP 0.3	Required Navigation Performance of 0.3 Nautical Miles
RTCM	Radio Technical Commission of Maritime Services
SAM	System Area Monitor
SF	Secondary Factor

SGR	Skywave And Ground Wave Ratio
SINR	Signal To Interference Noise Ratio
SNR	Signal To Noise Ratio
SooP	Signals of Opportunity
SSP	Standard Sampling Point
TTF	Time To Failure
RBD	Reliability Block Diagram
RTCM	Radio Technical Commission of Maritime Services
SGR	Skywave And Ground Wave Ratio
TOA	Time of Arrival
TOT	Time of Transmission
TTA	Time to Alert
TPC	Two-Pulse Communication
UK	United Kingdom
US	United States
USCG	United States Coast Guard
UTC	Universal Coordinated Time
UK	United Kingdom
UTC	Universal Coordinated Time
V	Voltage
VLF	Very Low Frequency
WER	Word Error Rate
WGS 84	World Geodetic System 1984
WLS	Weighted Least Squares

LIST OF FIGURES

LIST OF TABLES

Part I

BACKGROUND INFORMATION

1 INTRODUCTION

The World reliance on Global Positioning Systems (GPS) as the primary source of Position Navigation and Timing (PNT) information is well documented in the literature [74, 62]. Though GPS is regarded as superior to other PNT solutions, the risk of relying on a single Global Navigation Satellite System (GNSS) has been assessed in a report [16] popularly known as the 'Volpe report' prepared for the U.S Department of Transportation. The conclusion of the Volpe report pointed that GPS is vulnerable to jamming and signal spoofing, and that critical applications that solely depend on it need to have a redundant system providing backup in the case of GPS outage. The Department of Transport 's (DOT) Undersecretary as the Chair of DOT Positioning and Navigation Committee provided the Federal Administration of Aviation (FAA) evaluation team with a mandate to assess if Loran could meet the current aviation, maritime, timing and frequency requirements [74]. The FAA evaluation team in their findings report recommended a Low Frequency (LF) system known as Loran-C as a viable backup to GPS as long as further enhancements are made to its existing system infrastructure and architecture. According to the FAA report the modernized Loran keeps the Loran-C operating frequency (90 kHz - 110 kHz) and it is synchronized to universal coordinated time (UTC). However, modernized Loran has recapitalized infrastructure and a new communication modulation method to satisfy system performance parameters for both NPA, HEA, timing and frequency applications. The improved Loran-C was termed enhanced Loran *(eLORAN)*, in the FAA evaluation team's report. In 2006, the DOT and Department of Homeland Security (DHS) gave an Independent Assessment Team (IAT) a task to review the need for eLoran [70]. The IAT team unanimously recommended that the eLoran system should be upgraded and made a national backup to GPS for 20 years [4]. The eLoran Definition document published by International Loran Association (ILA) gives a high-level definition of eLoran to policy makers, users and service providers [3]. In that document, eLoran is defined as follows:

- eLoran is a PNT service that is internationally standardized for use by many modes of transport and in other applications. It is the latest in longstanding and proven series of low-frequency, LORAN systems.

- eLoran meets the accuracy, availability, continuity and integrity performance requirements for aviation Non-Precision instrument Approaches (NPA), maritime Harbour Entrance and Approach (HEA) manoeuvres, land-mobile vehicle navigation, and location-based services, and is a precise source of time and frequency for applications such as telecommunications.

- eLoran is a dissimilar and independent complement to GNSS. It allows users to retain the safety, security and economic benefits of GNSS, even when their satellites are disrupted.

eLoran has suffered many setbacks since its inception as a potential backup to GPS, both in U.S and Europe [77]. The U.S Loran-C system was shut down in February 2010 though this did not halt the eLoran research in the

U.S. Several years later, after the termination of operations of Loran Stations in the U.S, organizational bodies were formed to convince the U.S government to rededicate the previous Loran-C infrastructure to eLoran [77]. The General Light House Authorities of United Kingdom and Ireland (GLA) have been at the forefront of eLoran research in Europe since the conception of eLoran. The GLAs provided eLoran radio navigation service to improve the safety of mariners in UK and Irish waters. They have provided Initial Operational Capability (IOC) trial service for eLoran in UK and Ireland. In this service GLAs conducted trials on GPS jamming and proved beyond doubt that a GNSS backup is needed in Europe and that eLoran is a suitable candidate to backup GPS in case of GPS outage [30, 62]. However, in order to keep eLoran running, the GLAs needed to convince the nations hosting eLoran transmitters from shutting them down citing that a backup system for GNSS in Europe is needed. The host nations (France, Norway, Germany, and Denmark) however, disapproved the GLAs' proposal citing cost implications for installing a backup system; besides the conviction that Galileo signal is highly encrypted and robust to any signal manipulations [75]. On the 1^{st} of December 2015, the GLAs issued a public notice that they are discontinuing their IOC prototype/trial service in UK and Ireland, following the Federal governments of France and Norway decisions to switch off the eLoran transmitters in their countries by 31^{st} of December 2015. This marked a sad day for eLoran in Europe. In June 2016, a bill was introduced in the United States House of Representatives that provides the implementation of eLoran systems and assigning the responsibility of the program to the Coast Guard [77]. In Asia, North Korea has made notable advancements in their eLoran research. South Korea has announced plans to implement a nation-wide eLoran system by 2018 due to continued frequent GPS jamming attacks from North Korea [28].

Traditionally, many navigation systems have employed low frequency or very low frequency (VLF) signals. Examples are Datatrak (130 kHz-150 kHz), Decca Navigator (70 kHz-130 kHz) and Omega (10 kHz-14 kHz). These systems provided regional to worldwide coverage for marine and land navigation using terrestrial transmitters [94].

Coverage prediction in Europe started in the early 1990s. A substantial amount of work was done at the University of Bangor (South Wales) under the tutelage of a Loran Expert, Professor Emeritus and Instrument rated pilot, David Last until his retirement in 2004. This thesis describes some of the foundations he has laid on Loran coverage prediction and builds upon it. The next section describes eLoran and its system architecture.

1.1 ELORAN SYSTEM DESCRIPTION

eLoran has many different forms. There is eLoran for maritime harbour entrance and approach (HEA) and eLoran for aviation, each having different system requirements. A good description of eLoran system and the concepts that are used in its operation are described in detail in different research materials [62, 74, 77]. In eLoran, there are four system requirements that need to be assessed in order to satisfy the required navigation performance set out by regulatory bodies.

1.1.1 *System Performance Requirements*

The performance of a position, navigation and timing system is measured using four key performance metrics namely: accuracy, availability, continuity and integrity [61, 74, 62]. These are defined as:

- *Accuracy* is the degree of conformance between the estimated position of a platform and its true position. Rigorous mathematical definitions used for accuracy measures are given in [77]. In that study, accuracy is determined in terms of horizontal position error not exceeded with a probability of 95 %.

- *Availability* is a measure of the availability of the system to provide the required function and performance at the initiation of the required operation. Mathematical rigorous definitions of availability are given in chapter 8.

- *Continuity* is a measure of the capability of the system to perform its function without unforeseen interruptions during the intended operation. It is given by the probability that the system will remain available during the course of the operation, assuming that it was available at the start of the course of operation. Mathematical rigorous definitions of continuity are given in chapter 9.

- *Integrity* is the ability of the system to provide timely warnings to users when the system should not be used for navigation. It is usually specified by the probability of an undetected failure occurring per hour of operation. Integrity is not covered in this thesis.

1.1.2 *eLoran for Harbour Entrance and Approaches*

For maritime HEA, accuracy is of paramount importance. Spatial and temporal variations in the Times Of Arrival (TOA) of signals from the transmitter observed by the receiver have a huge impact on the accuracy of an eLoran system. These variations manifest as errors in the receiver's position solution. Hence, a goal in evaluating eLoran as a backup to GPS is to have a better understanding of the spatial and temporal variations of the TOAs. TOAs are quantified by Additional Secondary Factors (ASFs). Studying the TOA variations due to the conductivity changes along the propagation path made up of the ground is synonymous with studying the effects of the ASFs over the same propagation path. The performance requirements for different sectors of eLoran are set by relevant international bodies such as the International Maritime Organisation (IMO), International Telecommunication Union (ITU) and International Civil Aviation Organisation. The required performance parameters for eLoran for aviation and maritime harbor entrance approaches are different. The required performance parameters for eLoran HEA are summarised in table 1.

1.1.3 *eLoran for Aviation*

eLoran is used for precision approaches in Aviation. Precision approaches include among other things, activities such as aircraft landing in an airport. In aviation, integrity requirement is considered to be more important than other system performance parameters and is assessed by studying the

Table 1: eLoran system requirements for maritime harbour entrance and approaches as documented in [74, 3] .

METRIC	REQUIREMENT
Positioning Accuracy	$(8-20)$ m
Availability	0.999
Continuity	0.999 over 150s
Integrity	$1 \cdot 10^{-7}$ per hour
Frequency Accuracy	$1 \cdot 10^{-11}$
Timing Accuracy	50 ns

sources of phase and cycle errors in the receiver. The error sources are divided into three categories:

- random, uncorrelated and biased errors.
- completely correlated biases
- uncorrelated biases

These errors are denoted by α, β and γ, respectively. The results of the study done by LORIPP [52] suggest that there is a trade off between integrity and availability. Integrity is assessed using the integrity equation.

$$HPL = \kappa \sqrt{\sum_i K_i \alpha_i} + \left| \sum_i K_i \beta_i \right| + \left| \sum_i K_i \gamma_i \right| \tag{1.1}$$

eLoran for aviation is beyond the scope of this work and is described in details in [49, 51]. The required performance standards for eLoran NPA are summarised in table 2.

Table 2: eLoran system requirements for Aviation as documented in [74, 3] .

METRIC	REQUIREMENT
Positioning Accuracy	(307) m
Monitor Limit (target)	556m
Time-to-alert	10s
Availability	99.9
Continuity	0.999 over 150s
Integrity	$1 \cdot 10^{-7}$ per hour

1.1.4 *eLoran System Architecture and Operation*

The principal difference between eLoran and its predecessor Loran-C is the addition of a data channel on the transmitted signal. The data channel transfers application-specific information such as ASF corrections, warnings and signals integrity information to the user's receiver. The data channel enables eLoran to meet very demanding requirements for landing aircraft using non-precision approaches and docking ships in harbour entrance and approaches under low visibility conditions. The modern eLoran system consists of modernized control centres, transmitting stations and monitoring sites. eLoran transmitters are synchronized to UTC by a method independent of GNSS. The eLoran system consists of the transmitters, radio channel and the receivers. The following subsection gives a brief overview of the components of an eLoran system.

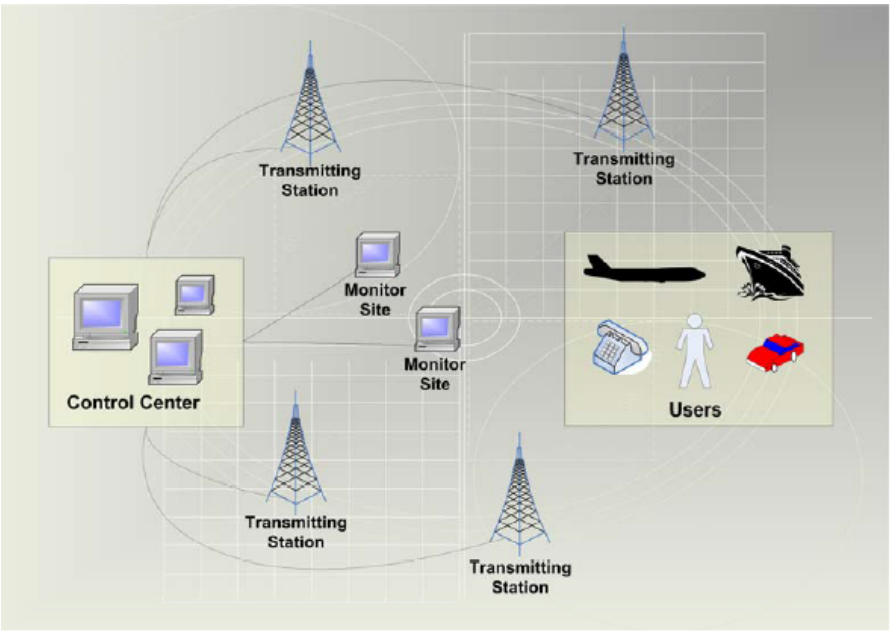

Figure 1: eLoran System Concept (reproduced from [3]) .

Transmitters

eLoran transmitters are arranged in a network and are geographically spaced along the coverage area of interest. They broadcast high powered, accurately timed and phase coherent short group of pulses[1]. The receivers measure their positions by measuring the time of arrival of the signals from at least three transmitters. eLoran transmitter stations are unmanned and use modern solid-state transmitter and control technology. They have an uninterruptible power supply and apply constant phase corrections to their transmitted signals. The transmitter's time reference system uses caesium clocks

1 The master pulse group consists of 8 pulses spaced at 1000 μs, and a 9^{th} pulse 2000 μs after the 8^{th}. All the 8 or 9 pulses are used rather than a single pulse so that more signal energy is available at the receiver, thereby improving SNR without having to increase transmitted power.

to provide a tight synchronization to a timing source. eLoran runs a telemetry system with sufficient personnel at the control centre. Personnel rapidly attend to failures to maintain high levels of system availability and continuity. Scheduled maintenance work is carefully planned to minimize the times the transmitters remain off-air. Poorly scheduled maintenance work degrades the overall system availability and continuity. Care is exercised to ensure that these activities do not disrupt the eLoran service. Transmitters that are out of tolerance are immediately taken off-air to ensure that the receivers do not to use their signals. Blinking is used to show that the transmitter is under test and should not be used (blinking is discussed on page 13). Nautel Inc. and UrsNav have developed the next generation transmitter technology that operates in the Loran band. The next generation transmitter technology provides high performance and is economical to buy, install and operate compared to legacy transmitters [79]. The feasibility of using low powered transmitters and their possible benefits have been investigated in [56].

(a) Low Frequency Transmitter (b) Antenna Tower for LF transmitter

Figure 2: Components of the eLoran transmitter.

eLoran Signal Structure

The basic structure of the eLoran signal is designed to satisfy the requirements given in the specification issued by the United States Coast Guard [32]. Each station transmits pulses with specified standard leading-edge characteristics. The transmitted pulse is defined in terms of current waveform at the base of the transmitting antenna. The standard eLoran pulse is defined as i(t),

$$i(t) = \begin{cases} \mathrm{A}(t-\tau)^2 \exp\left[\dfrac{-2(t-\tau)}{65}\right] \sin(0.2\pi t + PC) & \tau \leq t \leq 65+\tau, \\ 0 & t \leq \tau \end{cases} \tag{1.2}$$

where:

- A is the normalization constant related to the magnitude of the peak antenna current in amperes.
- t is the time measured in microseconds.
- τ is the envelope-to-cycle discrepancy (ECD) measured in seconds.
- PC is the phase code.

The standard eLoran pulse has a tear drop shape and is shown in figure 3. The ECD range is $-5 \leq \tau \leq +5\mu sec$. Various envelopes superimposed on the Loran carrier are depicted in figure 4 The principal transformation of

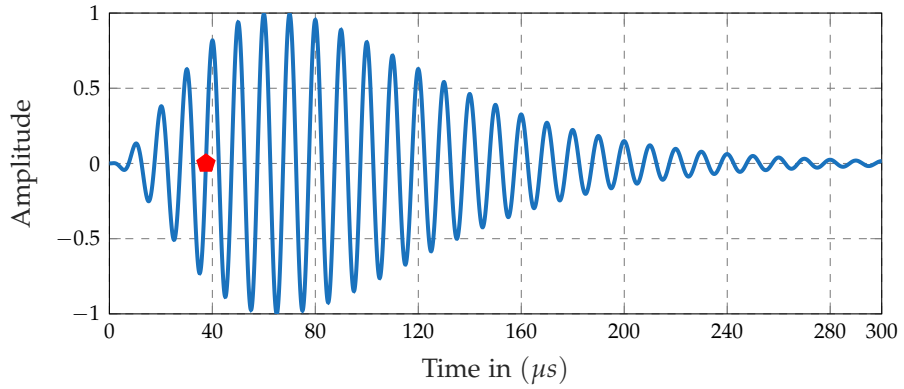

Figure 3: Standard eLoran pulse. The red pentagon denotes the standard zero crossing.

90° carrier phase shift and an ECD change of approximately 2.5μs occurs between the antenna current and E-field in the far field. Figure 5 shows the plot of the antenna current and E-field in the far-field. Loran-C transmitters

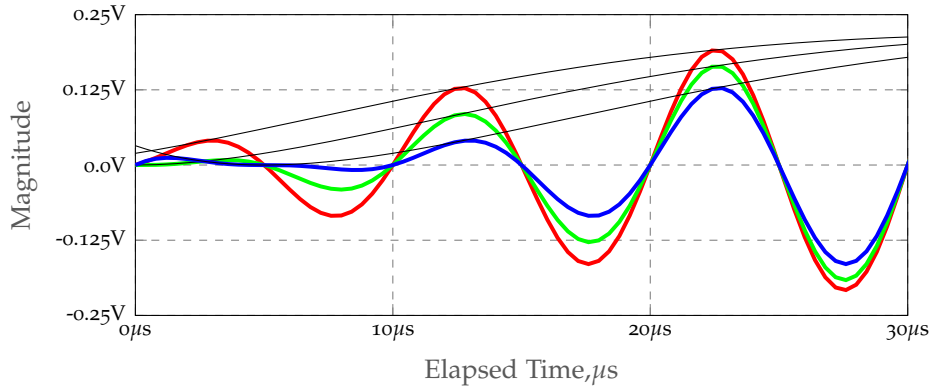

Figure 4: eLoran Signal Pulse with ECD 5,0,-5 μs [3]) .

are arranged in chains, with each chain composed of a master station and two to five secondary stations. Loran uses a time division multiple access scheme in each chain to share the allotted low frequency radio channel. The time of transmissions of stations in each chain is designed such that there is no overlap of pulses from the stations belonging to the same chain anywhere in the coverage area. Each eLoran station operates with a specified Group Repetition Interval (GRI). Permissible GRIs are multiples of 10 μs from

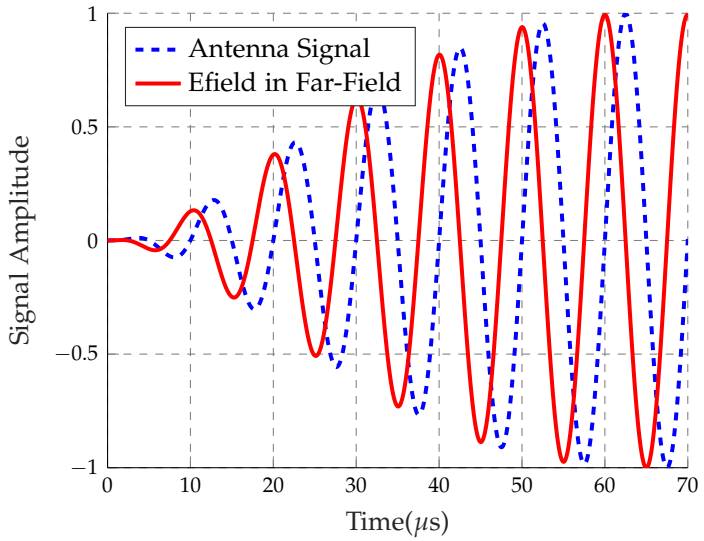

Figure 5: eLoran pulse in the far field.

40000 to 99990 μs. The identifier of each GRI is the GRI code which is the GRI in microseconds divided by 10. For example, the GRI code of Lessay is 7499 which represents the GRI of 74990 μs. Since the GRIs of the chains are different, it is necessary that they are related to a common epoch. This epoch is 0 hrs, 0 minutes and 0 seconds of 1^{st} January 1958. The expected times of coincidence of every master station's transmissions with the UTC second are published by USNO [66]. The secondary station pulse groups are linked in time and are transmitted with the same GRI as the master pulses. The emission delays of the secondary stations with respect to the master station are selected to ensure that the following criteria are met within each chain:

- The minimum time difference between any secondary and master is $10,900$ μs.
- The minimum difference of any two time differences is $9,900$ μs.
- The maximum time difference is the Group Repetition Interval minus $9,900$ μs.
- The minimum spacing between corresponding points of the last pulse of any station's group and the first pulse of the next group in the same chain is 2900 μs, except that the minimum spacing between the master's 9^{th} pulse and the next secondary pulse (of the same chain) may be as little as 1900 μs.

In eLoran, the secondary stations emission delays are synchronised to UTC using Time of Transmission control (TOT) [66]. With this method, the emission delays of the secondary stations are kept constant at all times. The TOT allows the use of *all in view receivers*, which provide improved performance and coverage. The synchronisation of eLoran transmission to UTC is achieved via methods that are independent of GNSS. In Loran-C, a monitor station called System Area Monitor Station (SAM) is set up within a chain's coverage area to adjust the drift in the emission delay times of the

secondary stations. This method is referred to as System Area Monitor control. Emission delays are generally kept as small as possible to allow the use of smaller GRIs. The SAM control is not used in eLoran, however, the old SAM sites are retained to monitor early skywaves [55].

Pulse-Group Phase Coding

eLoran transmitters transmit groups of phase coded pulses in conformance with table 3[2]. For station acquisition and identification, the pulse groups are labelled group A for a duration equivalent to a GRI, group B for next GRI duration. The transmission sequence called phase code interval (PCI) includes both group A and group B; thereafter the sequence repeats. Carefully designed phase codes, which by nature have been designed to be unbalanced, enable the eLoran receiver to have a good rejection capability to *long delay skywaves*.[3]. The downside in the use of unbalanced phase codes is that the eLoran receiver cannot completely eliminate any cross-rating signal by phase coding and comb filtering alone [6]. These codes exhibit a special property where the sum of their autocorrelation is 16 for a given PCI [77]. The autocorrelation properties of the phase codes are shown in figures 6,7 and 8. The phase coding function is conveniently expressed as:

Table 3: eLoran Phase Codes.

Group	Master Station
A	$++--+-+-$
B	$+--+-++$
Group	**Secondary Station**
A	$+++++--+$
B	$+-+-++--$

$$x_k(t) = \sum_{k=0}^{7} C_k \delta(1 - kT_p) + C_{k+8}\delta(t - mT_p + T_{GRI}) \tag{1.3}$$

The amplitude spectrum of the phase code is obtained by taking the Fourier transform of the phase code and is conveniently expressed as:

$$X_k(f) = \mathcal{F}(x_k(t)) = \sum_{k=0}^{7} C_k e^{-j2\pi fkT_p} + C_{k+8}e^{-j2\pi f(kT_p+T_{GRI})} \tag{1.4}$$

where $T_p = 1ms$. T_{GRI} is the GRI in seconds and C_k is the pulse phase code. The plot of the amplitude spectrum of the phase code is shown in figure 9

Blinking

Blinking[4] is the repetitive on-off pattern of the first two pulses of the secondary signal indicating that the baseline is unusable for the following reasons:

2 A similar table for Loran-C provided US Coast Guard includes the codes for 9^{th} pulse of the master station.

3 Sky wave components arriving at the receiver with a differential delay greater than 700μs are referred to as long delay skywaves.

4 A pulse in blinking mode is approximately 0.25s on and 0.375s off.

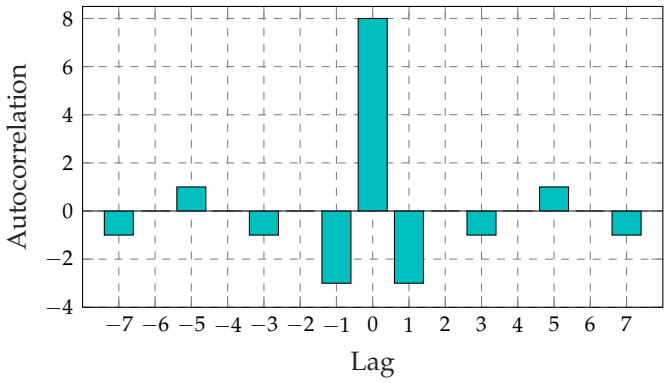

Figure 6: Autocorrelation of GRI,A for Lessay.

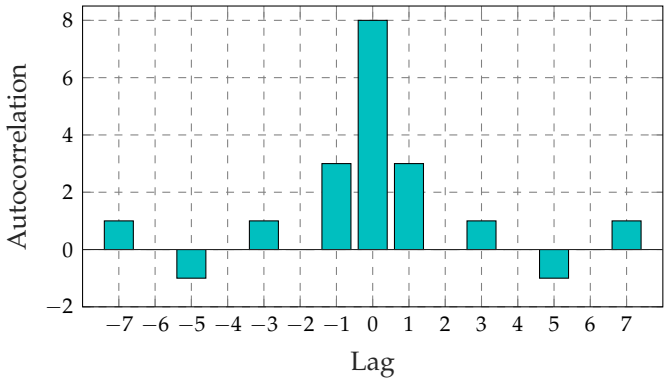

Figure 7: Autocorrelation of GRI,B for Lessay.

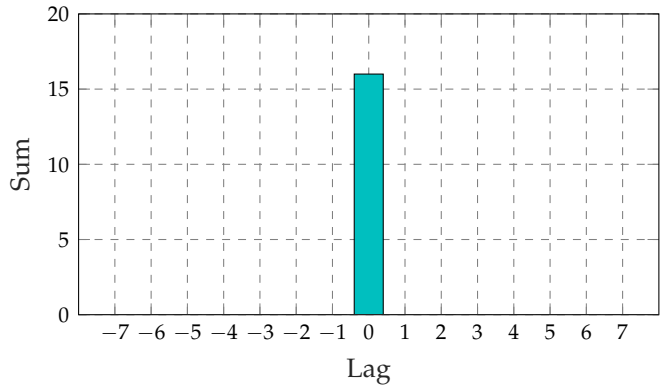

Figure 8: The Autocorrelation sum of GRI,A and GRI,B.

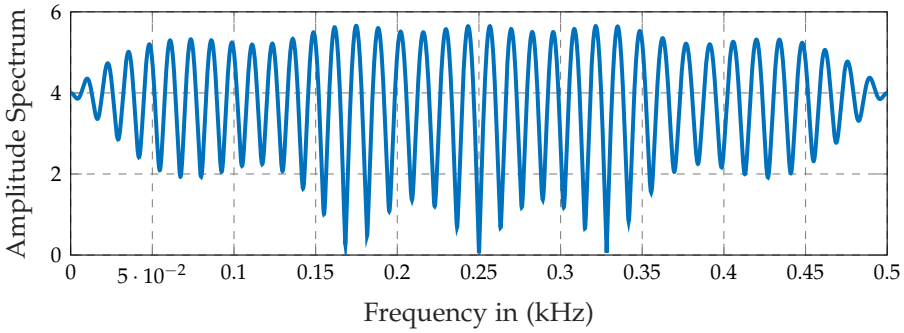

Figure 9: Amplitude Spectrum of a phase code 6731 Master.

- The time difference is out of tolerance
- ECD out of tolerance
- Improper phase code or GRI
- Secondary station operating at an output power of 6 dB lower than the specified output power.

In Loran C, blink is allowed to continue until the out of tolerance condition is eliminated. In eLoran, however, a blinking station is taken off air completely.

Two-Pulse Communication

Two-Pulse communication (TPC) is a synchronous communication which uses two Loran-C pulses to transmit information. Pulse position modulation is used on the 7^{th} and 8^{th} pulses. Each pulse is advanced and delayed once in each Phase Code Interval (PCI) such that the net change of position of each pulse is zero.

Dual-Rate Blanking

To provide full coverage, some stations are operated as members of more than one chain to radiate signals on two GRIs. Such stations are referred to as dual-rated. These stations are periodically faced with the impossible task of having to radiate pulses on both GRIs. In this scenario the pulses radiated on one GRI are blanked in preference to the pulses of the other GRI. Blanking is accomplished by prioritising pulses or alternating the pulse groups of the two GRIs. The longest GRI is often prioritised in this case.

Signal Availability

The performance requirement is to have signals from each transmitting station available in space for 99.9% of the time. A baseline is considered to be unavailable when any of the following conditions exists

- TD out of tolerance
- ECD out of tolerance

- Improper phase code or GRI
- Master or secondary station off-air or operating at less than one half of specified power

Routine equipment change-overs which are accomplished with less than 60 seconds suspension of Loran-C transmissions are considered as continuous transmissions. This standard has been adopted in eLoran.

Spectrum

The $90 - 110$kHz band is a protected Loran band and contains 99% of the total radiated energy. The energy below 90 kHz is not greater than 0.5% and the energy above 110 kHz is also not greater than 0.5% of the total radiated energy. The expression for the power spectral density of the eLoran signal is derived in [77]. The power spectral density of a windowed eLoran signal is shown in figure 10. This plot shows the distribution of signal power across all the frequencies.

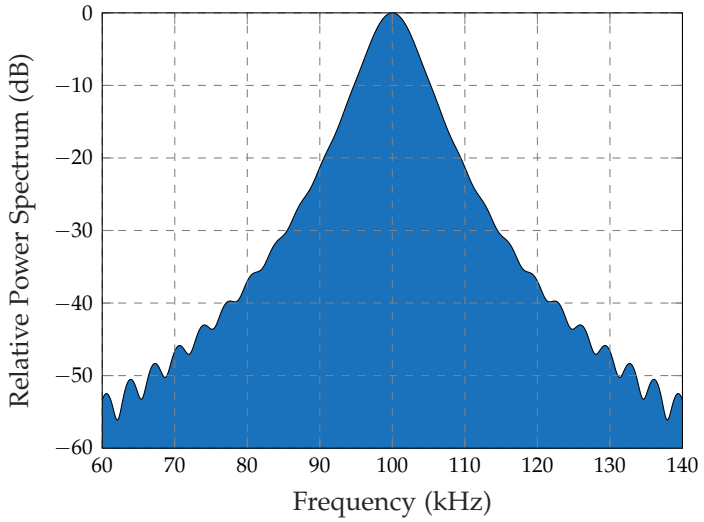

Figure 10: Relative Power Spectrum of the eLoran Signal.

eLoran Radio Channel

Radio energy from an eLoran transmitter emanates omni-directionally. The Loran signals reach the receiver from the transmitter via many paths. For convenience, the propagation paths are grouped into two modes. These modes are: *groundwave* and *skywave* propagation.

Ground Propagation

The groundwave signal propagates in the atmospheric medium below the ionosphere and is assumed to follow the earth surface not the line of sight and is taken to be the most dominant mode for low frequency propagation. The signal reaches the receiver by bending/diffracting around most objects. Propagation due to scattering by rain particles is almost negligible at eLoran wavelength because scattering requires that the scatterer's dimension to

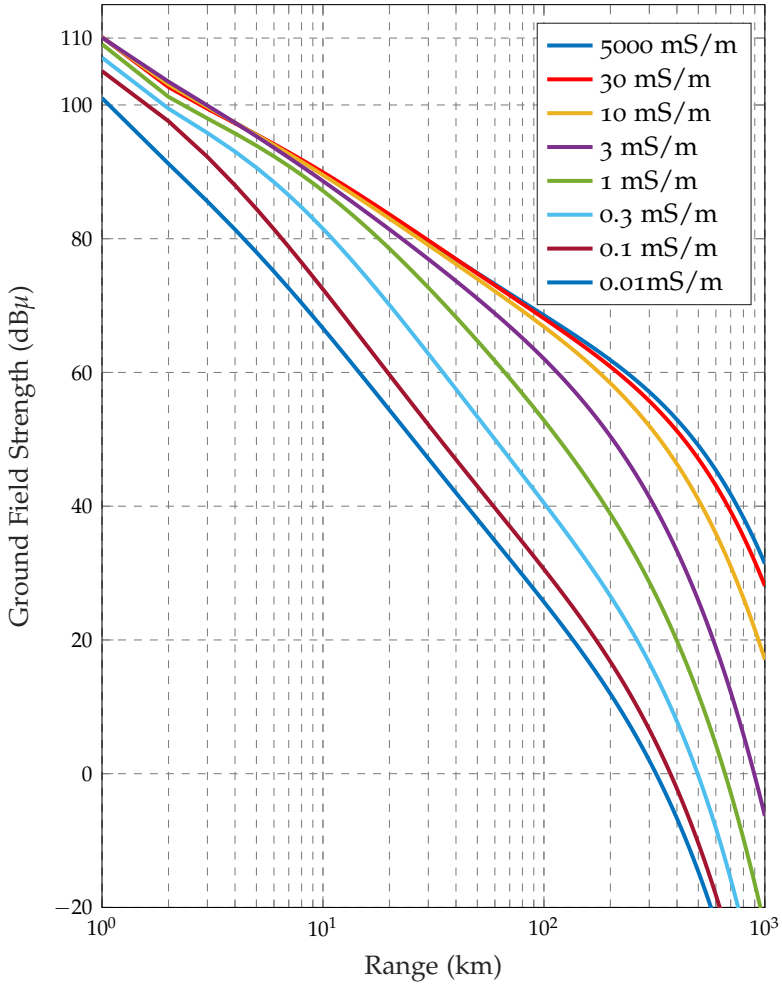

Figure 11: Ground propagation curves for different conductivities.

be greater than the signal wavelength [66]. The groundwave signal is influenced by various physical and electrical factors: ground conductivity, the orientation of the signal path with respect to the earth's magnetic field and physical laws and characteristics of the radio waves. eLoran receivers track the phase of the groundwave because of its stability. However, groundwave signal is attenuated as it travels from the transmitter to the receiver as a result of the conductivity of the terrain[5] over which it propagates. From time to time the conductivity changes due to rain soaking into the earth, freezing and thaw along the propagation path. Signal attenuation is smaller for night paths than for sunlit paths and signals travelling in the east direction experience more attenuation than those propagating in the westerly direction. Based on these factors, the phase of the groundwave signal is not a simple, uniformly increasing function of distance from the transmitters as it would be expected if the signal was traversing through free space. In practice, users must apply propagation corrections to the phase measurements to obtain accurate position fixes [20, 69]. Propagation corrections remove the perturbing influence of the earth on the phase measurements made at the user's location, so that the measured phase is close to what would be observed if the signal traversed through free space. The propagation corrections of course are not perfect and cannot correct all the disturbances of the real world. This is the primary reason why the advertised accuracy of eLoran is $(8 - 20)$ m and not something smaller [64].

Skywave Propagation

Skywave propagation is the 2^{nd} mode of travel for eLoran signals propagating from the transmitter to the receiver via reflections off the layers of the ionosphere. The skywave is reflected at large angles of incidence thereby losing a relatively small fraction of the wave energy to the ionosphere. The existence of the ionosphere allows detection of radio signals at long ranges and indeed, the presence of the ionosphere supported G. Marconi's famous demonstration that radio signals can be transmitted across the Atlantic Ocean. This is true for low frequencies which reflect off the ionosphere at large angles of incidence. The ionosphere is described as the ionised plasma in the atmosphere which is created by photo-ionisation of the neutral atmosphere by extreme ultraviolet (EUV) radiation and high energy solar particles.

The structure and make up of the ionosphere is dependent on the time of the day, season, geomagnetic location, altitude and solar activity. The ionosphere is made up of four layers namely: D region, E-region, F region[6][7] and topside ionosphere. During the day, the D-layer of the ionosphere strongly absorbs the skywaves [55]. At night the D-regions disappears leaving the E region. Part of the skywave is refracted off the E-region of the ionosphere and is received by users at distant locations. Without the ionosphere, most of the radio energy would be radiated into free space with a small fraction being refracted as a surface wave. The propagation of skywaves can be via a single hop or multi-hops depending on the distance of the user from the transmitter. Reception of skywaves at night results in unwanted interference with the desired groundwave at the user's location. Skywaves arriving at the receiver before 37.5 μs pose more problems to the receiver than those

5 Terrain is made up of sea water, land of various conductivities, mountains etc.
6 F region is made up two regions F1 and F2.
7 F1 disappears at night.

that arrive after 60 μs. As stated earlier, the eLoran signal structure is such that this deleterious skywave interference is minimised by the use of carefully designed phase codes. The groundwave signal reception is known to be stable during the day and unstable at night due to contamination by skywaves. The skywave is not tracked because its considered not to be stable and its delay cannot be reliably predicted due to the fact that propagation conditions in the ionosphere change from time to time. The groundwave

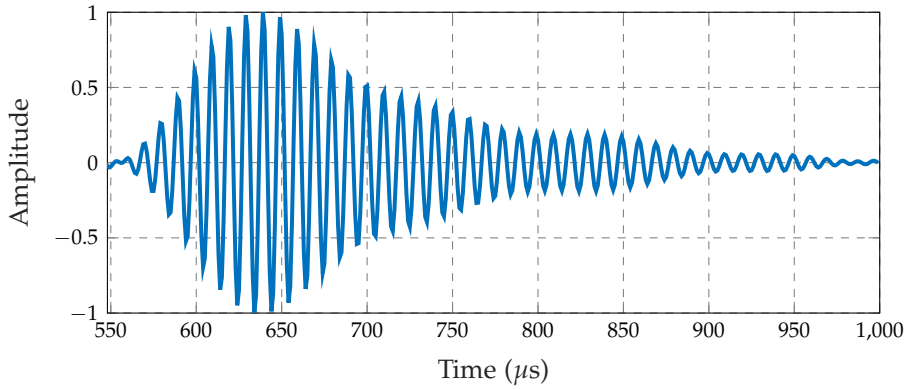

Figure 12: Received Contaminated Loran pulse taken from [2].

and skywave signals are launched at the same time, very often, the skywave part arrives at the receiver later than the groundwave part because the length of the path it takes to the receiver is longer. At large distances, the skywave is higher in amplitude compared to the groundwave because the groundwave is heavily attenuated due to the conductivity of the propagation path. A plot of skywave contaminated signal is shown in figure 12. A closer inspection at the signal in figure 12 reveals some bumps in the received signal which are due to skywave contamination. Skywave delay at any distance from the transmitter can be easily predicted. A plot of relative skywave delay to the groundwave at various distances from the transmitter is shown in figure 13.

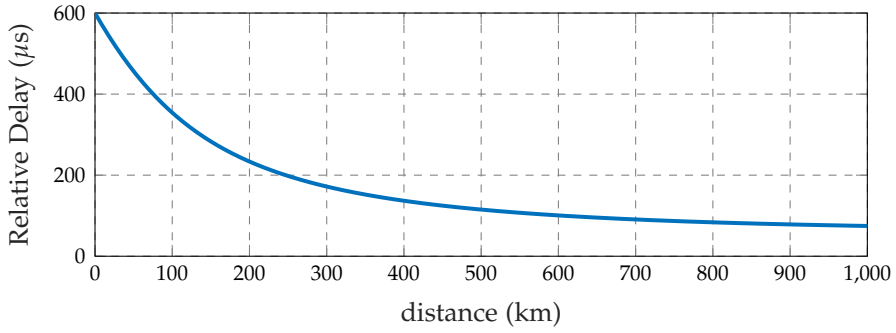

Figure 13: Skywave delay at various distances from the transmitter for a standard ionosphere.

Monitor Sites/Reference Sites

The monitor and reference stations are located in the coverage area to serve two purposes. First, they service the receivers located in their vicinity with real-time differential Loran corrections. The reference stations constantly monitor temporal TOAs caused by changing propagation conditions along the paths from transmitters in real time. The difference between the current TOA and the nominal[8] TOA is called a differential ASF correction and is broadcast via the data channel to one or more transmitters with a Eurofix capability, where it is modulated onto one or more of the transmitted eLoran pulses. Users within a usable range from the reference station receive these differential Loran corrections and use them to compensate for temporal changes in the times of arrival of signals received at their locations. Without differential corrections, it is impossible for the receivers to achieve full eLoran position accuracy. The reference stations are installed in areas where a 10 m accuracy is required. Secondly, reference stations notify the control centres of any anomalies in the signals transmitted by the stations; the control centre thereafter notifies the users not to use the signals infested with such anomalies.

User Equipment

eLoran receivers deploy *all in view* mode rather than the traditional *hyperbolic* mode used in Loran-C receivers. The all in view mode allows for the simultaneous processing of signals from multiple chains resulting in improved coverage performance, integrity and better positioning accuracy. eLoran receivers use carrier phase measurements to determine their position. Knowledge of the signal phase velocity is necessary for the receiver so that the receiver can make a transformation between the measured phase and distance to the transmitter. As it was described earlier, eLoran signals suffer from modal interference at certain ranges from the transmitter. It is generally assumed that modal interference is negligible at distances that are up to 800 km from the transmitters but can be predicted in regions where it is likely to manifest. In such scenario, the receiver is expected to deselect such signals through signal processing techniques. Advanced signal processing techniques deployed in eLoran receivers results in an order of magnitude performance improvement compared to the traditional Loran-C receivers. the eLoran user equipment is required to fulfil the following requirements:

- must be able to coast through 3-second outage.
- must achieve results comparable to at least 12 dB processing gain at the 99^{th} percentile level of atmospheric noise.
- must be able to use government-provided ASF and ECD information.
- Equipment must process cross-rate interference in a way that yields performance comparable to the model proposed by LORRIP.

eLoran receivers generally deploy bandpass filters in their front-end before the signal processing stage. The literature suggests that a Butterworth filter of 8^{th} order with a 28 kHz bandwidth, and passband frequencies, 86 kHz-114 kHz is deployed in the receiver front-end. Generally, the choice of the

8 The TOA measured at the time of reference station installation.

order of the filter is a trade-off between the filter's skywave and CWI rejection capabilities. A good CWI rejection requires filters with steep slopes leading to severe pulse distortions. On the other hand, good skywave rejection requires filters with gentle slopes. Gentle slope filters achieve little pulse distortion but the filtered signals become more prone to CWI contamination. The transfer function of a standard eLoran bandpass filter is given in the *zero-pole gain* form as:

$$H(f) = K\frac{\prod_{i=1}^{N}(j2\pi f - z_i)}{\prod_{i=1}^{M}(j2\pi f - p_i)} \tag{1.5}$$

The phase response of the Butterworth bandpass filter used in the receiver is given by:

$$\angle H(f) = \angle K + \sum_{i=1}^{N}\angle(j2\pi f - z_i) - \sum_{i=1}^{M}\angle(j2\pi f - p_i) \tag{1.6}$$

where f is the operational frequency. In eLoran this is taken as 100kHz. z_i and p_i are zeros and poles respectively. The zeros and poles for a standard eLoran receiver are provided in [77]. The magnitude response of the Butterworth bandpass filter of the eLoran receiver is shown in figure 14; and it

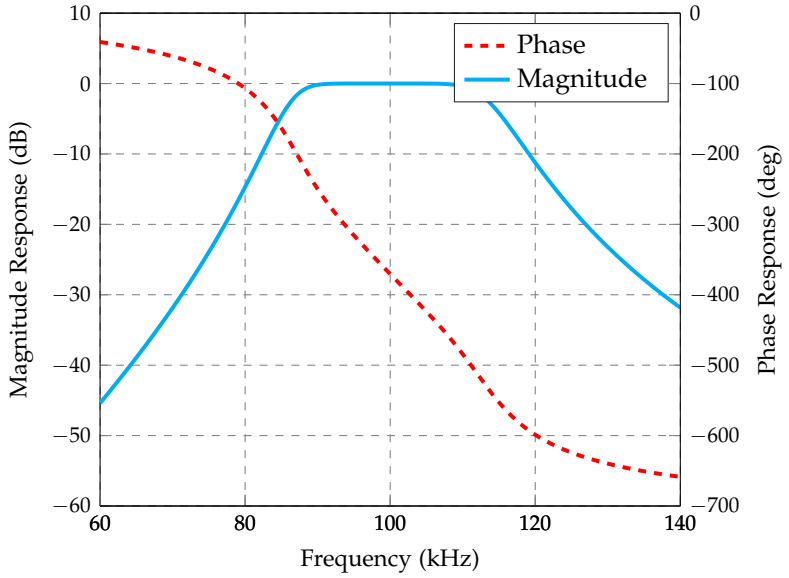

Figure 14: Amplitude and phase response of the front-end filter of the eLoran receiver.

can be seen that the filtering introduces a phase shift of $-10.5°$ at 100 kHz. Safar [77] suggests that this carrier phase shift must be compensated for in all the received signals from various transmitters, to avoid an error in the position measurement. The filtering process also distorts the signal. The envelope of the filtered pulse is a complex function. The group delay and phase delay of the filter is shown in 15. The phase delay is given by:

$$\phi_d(f) = \frac{\angle H(f)}{2\pi f} = -\left[\frac{\angle K + \sum_{i=1}^{N}\angle(j2\pi f - z_i) - \sum_{i=1}^{M}\angle(j2\pi f - p_i)}{2\pi f}\right] \tag{1.7}$$

The group delay is simply the derivative of the phase delay with respect to frequency, f. The phase and group delays are approximately 10μs and 30μs

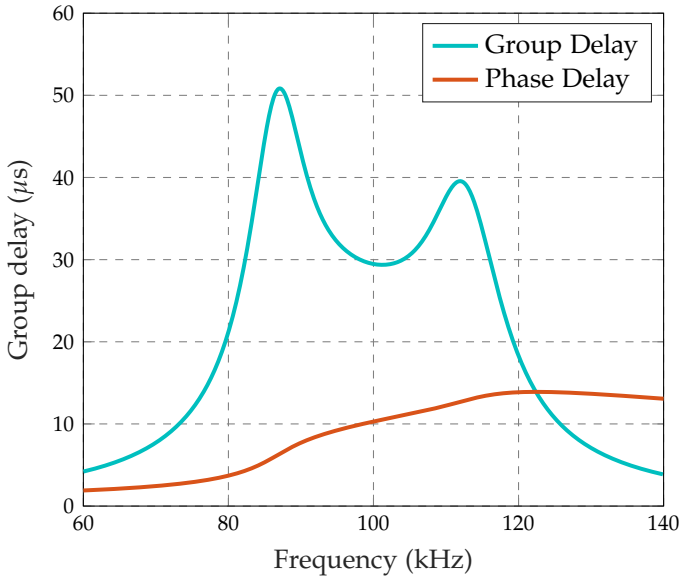

Figure 15: Group delay of the front-end filter of the eLoran receiver.

respectively at the eLoran operation frequency.

The next section describes the project objectives, a summary of the chapters as well as the key contributions made by the candidate.

1.2 PROJECT OBJECTIVES

Aim:

The aim of this thesis is to examine the existing the GLAs accuracy model, identify its shortcomings and develop an improved and realistic accuracy model, particularly for application in Europe; and also to include the availability and continuity capability. The developed coverage prediction techniques are presented in a coverage prediction software that assesses whether the system performance parameters (accuracy, availability, and continuity) at harbour and port locations meet the coverage performance requirements or not.

Objectives:

- To investigate the effects of the changes in conductivity on the accuracy performance of eLoran in the coverage area.
- To investigate the effects of the changes in weather parameters on the accuracy performance of eLoran in the coverage area.
- To develop techniques for predicting the availability for eLoran that is as precise and comprehensive as the state of present understanding allows.
- To develop techniques for predicting the continuity for eLoran that is as precise and comprehensive as the state of present understanding allows.

- To investigate the optimal way of installing reference station in the GLAs coverage area.

1.3 THESIS OUTLINE

This thesis describes the improved coverage prediction techniques developed by the candidate and their implementation in the eLoran coverage prediction tool. Table 4 shows the graphical representation of this thesis. Chapter 1 established the motivation for this research, which stems from the concerns about the increased reliance of society on Global Navigation systems and the need for a backup solution. The basics of the eLoran system as a potential backup to GPS are explained and the aims of this research are defined in this chapter. Chapter 2 reviews the coverage prediction techniques that have been deployed since the 1990s using Loran-C until the times of modernized Loran-C. Chapter 3 describes the various input models of the GLA coverage prediction tool that satisfy various standards set out by international bodies. It also describes the repeatable accuracy model and its assumptions. It also includes some of the author's contributions to the coverage prediction tool such as ECD modelling and an improved skywave field strength model.Chapter 4 describes the author's contributions to the determination of repeatable accuracy. This chapter uses the Land path and weather models to modify the initial assumption that there is differential Loran everywhere in the coverage area. Chapter 5 describes the ASF + SF models necessary to determine the total propagation time taken by the eLoran signals from the transmitter to the receiver. Chapter 6 describes a spatial decorrelation model developed for answering questions like how many reference stations are needed to service a single harbour? The models for interpolating differential corrections are described in detail. Chapter 7 This chapter describes a mathematical model developed using a Taylor Series expansion method to predict the error incurred when applying reference station differential ASF corrections at the user who is within a certain distance from the reference station.Chapter 8 describes an eLoran availability model and produces an availability map for Europe using the transmitter statistics obtained from the Control Centre in Brest (France). Chapter 9 develops a model for continuity using Markov chain analysis and the transmitter availability statistics obtained from the Control Centre in Brest. Chapter 10 describes the results of the case study for finding two suitable places for the Loran transmitters installation with one operating at high power and another operating at low power. Chapter 11 presents the conclusions and the future work needed to improve the coverage tool even further.

1.4 CONTRIBUTION TO KNOWLEDGE

The traditional Loran coverage prediction models are described in chapter 2. In this chapter, it is shown that when applying what was considered as standard practices proposed by the United States Coast Guard, the modelled accuracy figures in Europe were not realistic and were far behind the ones developed in the United States.
Based on these initial results, this thesis is written with the intent to better understand coverage prediction in harbour entrance and approach in Europe and its respective models to estimate accuracy, availability, and continuity at the mariner's location in the coverage area. To this end, this thesis makes contributions in the following areas:

Table 4: Thesis Outline

CHAPTER	AIMS	KEY CONTRIBUTIONS	AUTHOR'S PUBLICATIONS
1 Introduction	Define Research Objectives		
2 Coverage Prediction	Review of the Coverage Prediction techniques used over the years		
3 eLoran	Overview of the status of the GLAs eLoran Coverage Prediction tool	Improved the skywave model Included total field strength due to skywave fading Included ECD modelling	[78, 95]
4 Improved Accuracy Model	To modify the pseudorange error model at regions where differential eLoran is not provided	Proposed the Landpath and Weather models Established that TDOA method is better than TOA method	
5 Spatial ASF Model	To include Spatial ASF and SF models into the Coverage tool	Fitted polynomials to ASF data provided by Johler. Added the model's ability to predict ASF and SF at regions where differential eLoran are not provided. Added the model's ability to predict the total pseudorange from transmitter to receiver.	
6 Reference Station Coverage Prediction Model 4	To develop a Spatial decorrelation method for eLoran differential corrections. To determine the optimal placement of reference stations	Proposed a Spatial decorrelation model. Weighted method for correction of a single reference station. Interpolated method for pseudorange correction from various reference station. Proposed a model for determining the number of reference stations needed to service an area	
7 Spatial Correlation Model	To estimate the error due to applying am ASF correction at the user	Proposed three ASF correction techniques	
8 Availability	To develop an Availability model using Historical transmitter data	Developed and demonstrated the coverage tool's ability to model availability	[95]
9 Continuity Model	To develop a Continuity model for eLoran	Developed and demonstrated the coverage tool's ability to model availability	[95]
10 Irish Case Study	To demonstrate the tools that have been developed in the thesis To study the GRI selection procedure	Found suitable locations for installation of eLoran transmitters in Ireland Completed the tables that were incomplete in Safar's thesis	

- Improved skywave field strength and delay models using the results developed by Alwyin and Poppe in their coverage prediction work using Datatrak and DGPS signals respectively.

- Improved the coverage criteria by merging the work done at the Czech Technical University in Prague on cross rate interference into the existing coverage tools. This work helps in the selection of the transmitters to be used in the position accuracy calculation.

- Established an understanding that most parts of Europe, British Isles, Ireland do not experience a lot of thunderstorms but Spain experiences a lot of thunderstorms. If coverage prediction is to be deployed in Spain, the nature of atmospheric noise experienced there will need to be modelled.

- Improved the repeatable accuracy model, by including the changes in the spatial and temporal ASFs of each transmitter at all points in the coverage area.

- Demonstrated that over a long period of time the temporal ASF changes due to changes in conductivity (Landpath model) contribute more to the eLoran eLoran pseudorange error than the temporal ASF changes due to the weather.

- Included the spatial ASF model in the coverage tool. The coverage tool is capable of predicting ASFs in two ways, analytically (using Monteath's method), and using a set of curves derived from the data provided by other Johler and his colleagues.

- Proposed a weighted ASF correction method from a single reference station using the ratio of BER rather than spatial ASFs as weights.

- Used reference station coverage prediction to assess if the reference stations in the GLA's coverage area are optimally placed or not.

- Proposed a method for calculating the number of reference stations needed to service a harbour.

- Proposed a method for determining an interpolated pseudorange error correction from several reference stations to be applied at the user's receiver.

- Proposed a spatial decorrelation model for eLoran to determine the pseudorange error increase at various distances from the reference station.

- Generated availability and continuity maps in Europe using data from the Control Centre in Brest (France).

- Demonstrated the coverage tool's capability in real-life situations to find suitable locations of two transmitters to be installed in the Republic of Ireland in order to improve the eLoran coverage in the west of the British Isles.

These contributions represent an important part of an overall project by the General Lighthouse Authorities of the United Kingdom and Ireland to demonstrate that eLoran has the potential of being an adequate backup to GPS as well as a backup for position and timing solution to a variety of users and modes of transportation in Europe.

2 COVERAGE PREDICTION

This chapter presents background information on the coverage prediction techniques that have been deployed over the years from the early Loran-C days. This chapter reviews coverage prediction techniques developed by USCG and other researchers in their endeavour to improve upon the USCG coverage prediction techniques. Coverage prediction conveys information about where the system requirements of a radio navigation system (accuracy, availability, continuity, and integrity) are satisfied [76, 95]. The geographical area is divided into equal-sized grid points, and each grid point represents the possible locations of the user's receiver. Various inputs are assessed at each grid point to determine whether the grid point is in coverage or not. Chapter 3 describes the coverage inputs in detail.The next section describes the USCG coverage prediction techniques deployed all over the world.

2.1 UNITED COAST GUARD COVERAGE PREDICTION

The United States Coast Guard (USCG) are by far the most experienced authorities when it comes to Loran-C matters. They operated Loran-C chains around the world and developed coverage prediction tools to address matters pertaining to Loran-C coverage. Their coverage prediction tool assessed the following parameters:

- The level of Signal to Noise Ratio (SNR)

- Skywave to Groundwave Ratio (SGR)

In the USCG model, a location was deemed to be in coverage, if at least three transmitters exceeded an SNR of -10 dB and their SGR exceeded a specified level. SNR values greater than -10 dB were deemed to be sufficient for the Loran-C receiver employing a hyperbolic mode to be able to measure time differences of tracked stations with a standard deviation of less than 0.1 μs [21] . The inputs of the USCG coverage prediction model are shown in figure 16. The following section describes the methods and inputs employed in the USCG coverage prediction tool.

2.2 CALCULATION OF THE COVERAGE PARAMETERS

The USCG coverage prediction tool assessed only four parameters to determine if a grid point is in coverage or not, and these are:

- Groundwave field strength

- Ground conductivity

- Atmospheric noise

- Signal to Noise Ratio

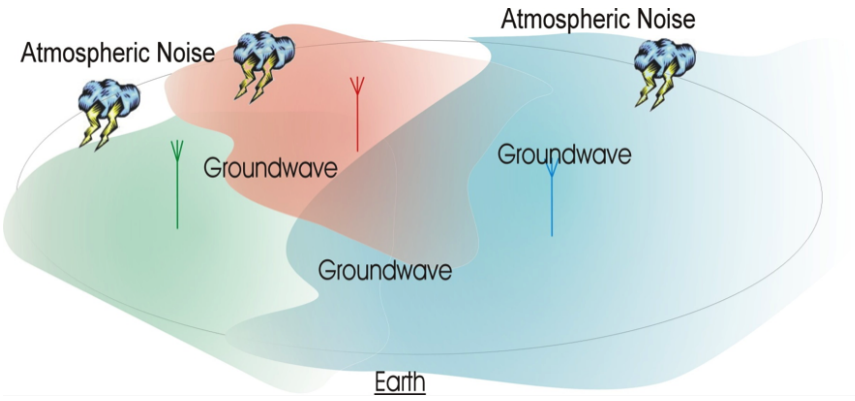

Figure 16: Showing predicted parameters of the USCG coverage model.

Ground Field Strength

Groundwave field strength is the electric field strength of the groundwave signal at any point in the coverage area. Estimation of ground field strengths requires the knowledge of transmitter power, the range of the receiver from the transmitter, signal attenuation curves provided by the International Radio Consultative Committee (CCIR) and the Millington's method [58]. The Millington's method is a quasi-empirical method used for estimating the attenuation of the signals propagating over paths of different conductivities (more description is given in chapter 3). The ground field strength is expressed in dB with respect to $1\mu V$ written as $dB/\mu V$. The USCG employed attenuation curves plotted against distance for a frequency of 100 kHz. These attenuation curves appear to correspond to those that are published in the CCIR report $717-2$ [1] [21] leading to suggestions that they may have been normalised for a transmitter with a radiation peak power of 400 kW. A peak power of 400 kW implies that the signal power at the standard sampling point is 100 kW[2]. Determination of ground field strengths also requires the knowledge of the terrain properties. The ground field strength at a range d from the transmitter is given by:

$$E = \frac{300\sqrt{P}}{d} \tag{2.1}$$

where:
E = the field strength (μV/m),
P = radiated power (kW),
d =range from transmitter (km)

Ground Conductivity

Conductivity affects the rate of attenuation of the signals passing through the terrain [94]. Terrain variants are: fertile ground, mountainous regions, Arctic regions, water lakes, rivers and sea water. Each terrain type has a different conductivity affecting the velocity of the signals differently. For example, propagation velocity is faster over sea water than over land. Apart from terrain type, conductivity also varies with the changes in moisture

1 The CCIR $717-2$ report is superseded by ITU-R P. $372-9$.
2 Standard sampling point is 30 μs from the start of the pulse.

content, temperature, geological structure and the effective depth of penetration of the ground. The ITU publishes attenuation curves for a range of conductivity values. The USCG holds a database of 10000 ground conductivity values covering continental US and Canada [21]. They recommended the CCIR Report $717-2$, for ground conductivity calculations of regions outside USA and Canada. The CCIR Report $717-2$ contains a "World Atlas of Conductivities" and was widely used in Loran-C coverage prediction.

Atmospheric Noise

Atmospheric noise is defined in reference [85] as *a time-varying electromagnetic phenomenon having components in the radio-frequency range, apparently not conveying information and which may be superimposed on, or combined with, a wanted signal*. Atmospheric noise is produced by lightning activity and thunderstorms all over the world [80, 11, 87] and is the dominant form of noise in the Loran band. Since thunderstorms are always present on earth, so is the atmospheric noise. The conductivity nature of the earth surface, allows atmospheric noise produced at distant locations to propagate to the receiver locations. Lightning activity is generally greatest around the equator. The atmospheric noise generated by the lightning activity at the equator propagates as groundwave or skywave signals and is received at medium and higher latitudes. It limits the range of usable signals needed to compute a fix at the receiver's location. Atmospheric conditions affect the operations of Loran receivers resulting in low signal to noise ratios and poor position accuracies. The USCG considered a range at which a transmitter can be used in coverage to be highly limited by atmospheric noise than by other noise sources such as *man-made noise*[3] *and galactic noise*[4]. The atmospheric noise was determined using CCIR Report 322 which has been superseded by ITU-R P. $372-9$ [85]. In this report, the median atmospheric noise at 1 MHz for each of the 24 time blocks is mapped. Each time block represents a period of 4 hours. A complex procedure is used to convert median atmospheric noise at 1 MHz to atmospheric noise not exceeded at various percentiles. This conversion process assumes that the bandwidth of the Loran receiver is 35 kHz [18]. The noise levels are expressed in dB with respect to $1\mu V$ written as $dB\mu V/m$.

Signal to Noise Ratio

SNR is defined as the ratio of the received signal power to the atmospheric noise power experienced at any location in the coverage area. It is measured in decibels (dB). The SNR metric is commonly used in telecommunication systems to assess system performance. The USCG model criterion limited coverage to stations with SNR more than -10 dB at any grid point [21]. If three or more stations met this requirement, then a location was deemed to be in coverage. The USCG method of estimating atmospheric noise in Europe was inconsistent, inadequate and resulted into too much discrepancy between the model and real measurements. In the early 1990s, CWI was prevalent in Europe leading to more interference near the Loran band. The

3 Man-made noise is an aggregated unintended radiation from machinery, electrical and power transmission.

4 Galactic noise is due to radio waves emanating from sources outside the solar system but within the Milky Way. According to NASA, galactic noise can always be heard but not at the same strength.

Loran Working group tried to quantify this interference level by proposing a constant noise level of 61 dB to be used across the coverage area in Europe [21, 94]. This meant that to determine SNR at all grid points; a noise value of 61 dB had to be subtracted from all ground field strengths of all signals received at all those grid points. This suggests that interference and noise were lumped together rather than treating each parameter differently.

Implementation of USCG Coverage Model

Coverage was initially estimated using a pen and paper procedure. Computers were sought after as the model became more complex. The USCG possessed a number of computer programs to aid in the coverage prediction process. Their program called COVERAGE was first written in HP Basic and was later improved upon by a contracted company called Synetics Corporation. The coverage tool developed by Synetics was written in computing language called Pascal and displayed the coverage limit overlaid on a coastline map either on the screen or as a hard copy on a plotter or printer. Its user interface employed menus and a mouse. Ground conductivity data was stored in an array of 5° by 5° [21].

USCG Coverage Model Inadequacies

The USCG model did not include a skywave field strength model in their coverage prediction. Skywaves arriving at the receiver within a specified time difference after the arrival of the groundwave need to be modelled as they result in signal fading, and unusable pulses. The 61 dB proposed by the Loran Working Group was somewhat heuristic and inaccurate because interference is a statistical phenomenon and varies from location to location. Placing an upper bound value on all locations results in pessimistic performance prediction.

2.3 TRINITY HOUSE

As one of the representatives in the Loran working group, the Lighthouse Authority of England and Wales' Engineering department generated coverage diagrams for the proposed new Loran-C system. The model criteria was the same as that of the USCG, except that the SNR criteria of 7 dB was used in the North Sea region because of the cycle selection problems experienced in that area.

2.4 THE COMMISSIONER OF THE IRISH LIGHTS (CIL)

The Commissioner of Irish Lights also adopted the USCG coverage criteria except that an estimated ground conductivity value for Ireland was used. As it was stated earlier, the CCIR $717-2$ did not provide conductivity values for areas outside US and Canada, so a value for Ireland had to be estimated.

2.5 THE ADMIRALTY RESEARCH ESTABLISHMENT

The Admiralty Research Establishment employed coverage prediction techniques that are different to the one used by the USCG. The section describes how the inputs of the ARE model were determined.

Signal Strength

Signal strength was determined using curves developed by Bremmer in favour of those developed by the CCIR. The Millington's method was used to estimate signal attenuation over mixed paths[5]. Farnsworth [21] suggested that the (ARE) model appeared to be flawed in the way ground strength was estimated. He noted that signal power was estimated at the peak of the pulse[6] rather than at the traditional sampling point[7]. The downside of sampling at the peak of the pulse is that the samples are more prone to skywave contamination and skywave fading.

Atmospheric Noise

The ARE atmospheric noise model used atmospheric noise values determined at 90^{th} percentile as opposed to annual average noise as implemented in the USCG model. Atmospheric noise values estimated using this model were found to be 10 dB higher than those obtained using USCG model leading to poor accuracy performance.

SNR Limit

The model used an SNR limit of -10 dB on all the stations. Any station that failed to meet this criteria was not included in the position solution.

Ground Conductivity

Regional geological data was converted to conductivity information. The model uses CCIR conductivity information as well as additional conductivity values of 10 mS/m for urban areas. No justification was given for this extra 10 mS/m. The choice of 10 mS/m could be that perhaps they assumed that the signal delay due to tall buildings is equivalent to delay suffered over a terrain of 10 mS/m. However, such an assumption seems to be pessimistic and should have been validated through analysis of field data.

2.6 MEGAPULSE INC. (USA)

Megapulse Inc. manufactured and sold Loran-C receivers in the 1990s. They developed a prediction model for the North West European Loran-C system. The signal strength, SNR, and noise models appear to be similar to the USCG models. Their ground conductivity model assumes that the world is made up of sea water. The major difference of this model compared to the rest is that the Megapulse model includes the skywave limit.

Skywave Limit

The presence of skywaves limits the range at which the signals from a station can be used in coverage prediction. To avoid contamination of the tracked signals by late skywaves, the model limits the transmitter range to 1800km.

5 Mixed path refers to to an inhomogeneous terrain, i.e path with different conductivities.
6 The peak of the pulse is 65 μs from the start of the pulse.
7 The standard sampling point is 30 μs from the start of the pulse.

Geometrical Fix Accuracy Limit

Geometrical fix accuracy was limited to a distance root mean square error of 463m for 95 % of the time. The next section gives a brief overview of the history Loran in Europe.

2.7 HISTORY AND FORMATION OF THE NELS GROUP

This section summarises the historic report about Loran C in Europe given in reference [1]. The Head of Coordinating Agency office of the Loran-C in the NELS reported that: In the late 50s, the USCG established Loran-C in Europe to provide continuous coverage from north-America across the north Atlantic to continental Europe. In 1976, Norway built two Loran-C stations. In 1981, the nations hosting US military Loran-C stations were notified of the US decision to stop funding the stations in the mid 90s. The Loran-C Working Group with representatives from Germany, Denmark, Iceland, Canada, Norway and USA was set up in 1985 to look into the possibility of setting up an international Loran-C co-operation group in Europe. In 1986, The group recommended an establishment of Northwest European Loran-C chain comprising of existing USCG transmitting stations and that the new stations should also be set up. Following the recommendation from the Loran-C Working Group, in the same year, IALA was invited to an international meeting in London, UK. There was growing interest in Loran-C in Europe, particularly in UK, as DECCA was to be phased out. After the IALA meeting, the Loran-C Policy Group was established. However, there were some challenges afterwards as UK and Canada ceased their interest. In August 1992, the remaining 6 countries met in Norway to sign the NELS International agreement. An interim control centre was set up at Bø to offer NELS control pending finalisation of the NELS control centre at Brest, France (CCB). In mid 1999 when the Brest control centre took over from the control centre located at Keflavik .

In 1997, the committee agreed to upgrade NELS with the Eurofix technology. Eurofix came on-air at the Sylt station in early 1998 as a test setup and, after a long period of cost sharing discussions and Control compliance tests, Bø and Værlandet in Norway and Lessay in France in late 2000 had Eurofix technology installed. The intention was to upgrade all of NELS to include Eurofix as an integral part of the NELS service. NELS started its operation in 1995, but due to delays in the development of the control system/centre in France, it was controlled from an interim control centre co-located with the Bø Loran-C station in Norway until 2000.

Since the agreement was that each country will monitor, control and fund the operation of each transmitter located in their home soil, coverage prediction was therefore needed. This required more rigour in Europe than in the United States. At the University of Wales, Bangor radio navigation group under the stewardship of Professor Emeritus David Last took upon the task of reviewing and improving the coverage techniques developed by the United States Coast Guard. In Europe, the USCG techniques for coverage prediction were considered inadequate [46]. Carrier wave interference was prevalent in Europe due to a lot of Amateur radio station operating near the Loran band. Spectral analysis results of the received Loran signals at the time suggested that there was a lot of interference between 50kHz - 150kHz.

Beckmann studied the effects of carrier-wave interference near Loran band at the University of Delft and the results of his work on interference were included in the Bangor coverage prediction tool. Last and Bian [43] did a statistical evaluation of CWI to Loran C.

2.8 THE BANGOR COVERAGE PREDICTION

The Bangor coverage prediction model kept the same coverage prediction techniques proposed by the USCG and added other parameters such as Envelope Cycle Discrepancy (ECD), Carrier Wave Interference (CWI), and Signal to Noise Ratio (SNR). Coverage criteria was implemented as "modules" in a software suite with each module generating arrays of data. The geographical area over which coverage is to be assessed was divided into equal grid points. The software suite developed, was written in C++, produced repeatable accuracy contours plotted via AutoCAD [46]. Desired coverage parameters were assessed at each grid point to determine whether the transmitter is in coverage or not. The transmitters that were deemed to be in coverage were used to generate accuracy contour plot. Accuracy contour plots were used by authorities as a guidance on where to install new transmitters.

2.8.1 *Bangor Coverage Performance Analysis*

The following sections describe how the coverage parameters are calculated in the Bangor coverage tool called BALOR.

Groundwave field Strength

The calculation of groundwave field strength requires a good conductivity database. Prior to the Bangor coverage prediction tool, conductivity values provided in the world atlas of conductivity maps were found to be limited and inaccurate [29, 21, 94]. Some countries such as France had no assigned conductivity values at all. The Irish conductivity values were found to be 10 times higher than the UK values. The University of Bangor took upon the task of assembling a ground conductivity database for Europe. The UK conductivity values were found to be correct and the Irish conductivities were reduced by a factor of 10 where appropriate. The University of Bangor also employed other alternatives for assembling the conductivity data.

Skywave field Strength and Skywave delay

The skywave field strength is defined as the electric field of the skywave component of the transmitted signal at the receiver whereas the skywave delay denotes time taken for the skywave component to arrive at the receiver after the arrival of the groundwave component of the Loran signal. The skywave field strength and delay of the signals for LF systems is calculated using the models provided by the International Telecommunications Union Recommendation, ITU-R. P 1147 – 2 [84]. At any point in the coverage area, the skywave field strength and delay for each transmitter is calculated and stored in an array, which would be accessed on the fly. This is done so as to save computer-processing power.

Atmospheric Noise

The level of the atmospheric noise at each grid point was determined using the International Telecommunications Union Model Recommendation, ITU-R. P $372-9$ [85]. This resulted in a better coverage approximation than using the 61 dB-μV/m atmospheric noise field strength proposed by the United States Coast Guard [21]. Atmospheric noise at each grid point was calculated and stored in array to save computer-processing power.

Carrier Wave Interference

Loran is prone to two types of interference namely carrier wave interference (CWI) and cross rate interference (CRI). CWI is a form of interference due to spurious signals operating near the Loran band, around (50 kHz-150) kHz. In the early 1990s, CWI was a huge problem in Europe because a lot of amateur radio stations and DECCA were operating near the Loran frequency band [94, 6]. Uncompensated CWI introduces errors in the receiver position solutions. Thus, receivers have to be properly calibrated to solve this problem. CWI affects the receiver's cycle identification process. Cycle identification process determines the proper cycle to be used in extracting phase information from received signals. The extracted phase information is converted into range measurements. Since the cycle identification process is not precise, range errors are introduced. A range error can be determined as:

$$\rho = c \cdot \tau \tag{2.2}$$

where τ is the cycle shift from the tracking point. Loran cycles are integer multiples of 10μs from the tracking point, i.e $\tau = n \cdot 10^{-5}$s, $\forall n \in \mathbb{Z}$. c is the speed of light in vacuum and is equal to $3 \cdot 10^5$ km/s. An improper cycle selection at 100 kHz, leads to a range error of at least 3 km. The resulting position errors can be 1.5 to 4 km depending on geometry. Geometry is defined as the relative position of transmitters with respect to the receiver position. The effect of carrier wave interference on performance of Loran receivers was studied extensively by Beckmann at the University of Delft [6]. In his study, CWI was quantified to be made up of signals of two modulation types:

- Amplitude modulated signals with a modulation frequency less than 1 Hz. These signals include time reference signal which contains a 'marker' for every seconds.
- Data transmission signals employing frequency shift keying modulation. Examples are telex connection and fax pictures.

A common attribute of the modulated CWI signals is that their transmitted spectrum comprises of a set of discrete spectral lines. According to Beckmann [6], these spectral lines can be modelled as a finite set of pure tones with different frequencies and amplitude. To suppress the effects of CWI on the performance of Loran receivers, the interferers are classified into three categories:

- Synchronous: These signals are found on frequencies that are exact multiples of group repetition frequency (GRF), where $GRF = N.\frac{1}{GRI}$.
- Near-Synchronous: These signals fold back to frequencies less than f_b, the tracking bandwidth of the tracking loops. The frequency of the interferer, $f_{CWI} = N.\frac{1}{GRI} + \Delta f$, where $\Delta f < f_b$.

- Asynchronous: These signals fold back to frequencies greater than f_b, the tracking bandwidth of the tracking loops. The frequency of the interferer, $f_{CWI} = N.\frac{1}{GRI} + \Delta f$, where $\Delta f > f_b$.

Synchronous and near-synchronous forms of CWI are considered to be more harmful than asynchronous CWI. Beckmann [6] proposed a CWI elimination method where each synchronous and near-synchronous CWI are multiplied by a weighting function. Synchronous and near-synchronous CWIs are assigned a high weighting factor than asynchronous CWI. Ideally, this weighting function should have a similar amplitude transfer function as that of the tracking loop. However, there is always a risk of having an amplitude transfer function that is different from that of the tracking loop because the amplitude transfer function of the tracking loop is not known exactly. The proper weighting function is therefore used to select and eliminate the most harmful CWI in the receiver using notch filters. Beckmann [6] pointed that not all CWI are eliminated by the use of notch filters and suggested that design goal should be notching out CWI that leads to large position errors. The use of notch filters and the introduction of strict regulations that restrict the amateur radio stations from operating near the Loran band means that CWI is no longer a problem in Europe. Last [19] suggests that amateur radio stations have now come up with techniques of modulating their signals such that the spectral lines of their transmitted signals lie in between the Loran spectral lies. Loran spectral lines are spaced at intervals:

$$\ell_{GRI} = \frac{1}{2 \cdot GRI \cdot 10^{-5}} Hz$$

For a GRI of 7499, the spectral lines are separated by 6.7 Hz. Figure 17

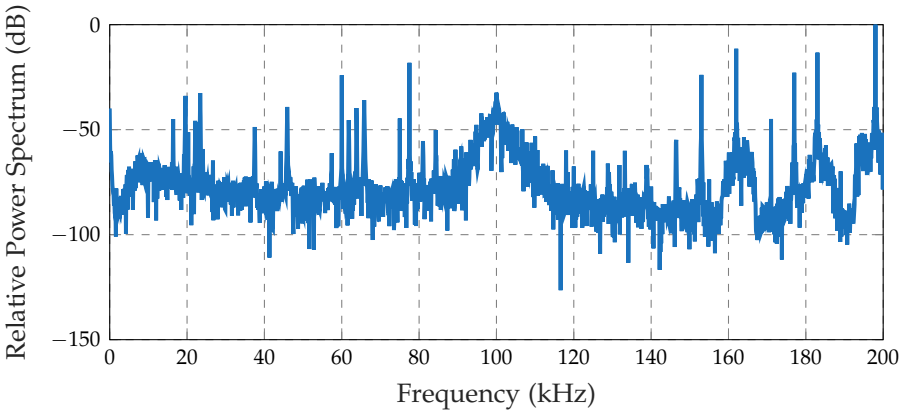

Figure 17: Carrier Wave Interference experienced at Bath using [2].

shows the current levels of CWI in Europe. The data used in producing this plot was recorded at Bath, United Kingdom. The levels of CWI in the frequency range (50 -150) kHz are much lower than it was seen in the illustrations from data measured in the 1990s.

Envelope Cycle Discrepancy

The envelope cycle discrepancy is the measure of signal distortion due to propagation effects [45, 52, 49]. The variation of ECD with distance is a function of conductivity. ECD is used to determine whether there is any

risk of receiver tracking the wrong cycle on the received Loran pulse or not. If the ECD exceeds a certain limit, there is a risk that the receiver, will track a wrong cycle of the Loran signal. A wrong cycle selection poses a threat of getting pseudorange errors that are at least 3 km in error as already explained earlier.

Bangor's Coverage Criteria

Prior to the existence of the Bangor coverage model, the United States Coast Guard proposed that a transmitter is deemed to be in coverage if its skywave to groundwave ratio (SGR) is less than 12 dB when both the skywave and groundwave signal are measured at 37.5 μs from the beginning of the received pulse [21]. The transmitter was also deemed to be in coverage if its SGR is less than 26 dB measured at 60 μs from the beginning of the received pulse. This is depicted by figure 18. A transmitter is said to be in coverage

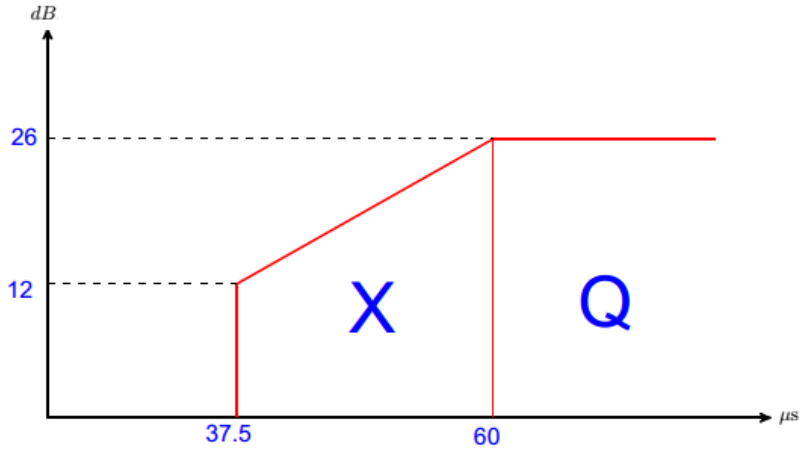

Figure 18: The Skywave Groundwave Ratio (SGR) Criteria.

if its SGR lies in region X. These limits are specified in the Radio Technical Commission for Maritime Services and the International Electro-Technical Commission recommendation [21]. The RTCM and IEC did not specify anything about the usable SGR in region Q [21, 66]. However, it is common practice to use signals with SGR less than $26dB$ measured at times greater than 60 μs from the beginning of the received pulse. Though not specified, it appears that the values specified in the IEC report are for an unfiltered pulse. However, the receiver takes the measurements on the received pulse groups after the bandpass filtering process.[8] This was demonstrated by Safar [77] in his CRI work.

The next section describes the coverage prediction tool developed in Stanford University to estimate eLoran coverage in the US. The Stanford coverage tool was developed at a time when Loran-C was being considered as a possible backup for GPS. This happened at the same time when the Radio navigation group at Bangor was being closed down in early 2005 with retirement of Professor Last. The University of Stanford as part of the Loran

8 A bandpass process results in pulses that are stretched out in time.

Integrity Performance Panel (LORIPP) , took upon a task of reviewing Loran as a potential back up to GPS using coverage prediction software as part of the tasks assigned to LORIPP. The LORIPP team examined the ability of Loran to meet aviation requirements for Required Navigation Performance 0.3 (RNP 0.3) and harbour entrance and Approach.

2.9 THE STANFORD COVERAGE PREDICTION

The coverage prediction techniques developed at Stanford are thorough and focus more on the required navigation performance parameters (RNP) for non-precision approaches (NPA) such as accuracy, availability, continuity and integrity. The techniques used for mitigating these hazards and the methods used for assessing navigation performance parameters were packaged into a coverage software tool called LCAST. The LCAST demonstrated the capability to assess accuracy, availability, continuity and integrity. [52, 49, 51].

The coverage prediction tool developed at Stanford incorporates many features and hazard models to ensure safety by properly analysing the resulting performance against the requirements of the target applications [55]. It is important to realise that integrity is of paramount importance in non-precision approaches while accuracy is an most important coverage parameter in maritime harbour entrance and approach [55, 62]. The various inputs that were used in the LCAST are described in the next section.

2.9.1 *Stanford's Coverage Performance Analysis*

The coverage limiting criteria were kept the same as in the Bangor coverage tool except that they were now more rigorous. The parameters of the coverage limiting criteria deployed in the Stanford Coverage tool are atmospheric noise, skywave, field strength, ground field strength, cycle selection, ECD, cross rate interference and Horizontal Protection limit (HPL) [55, 49]. The following sections briefly describe how each coverage parameter was

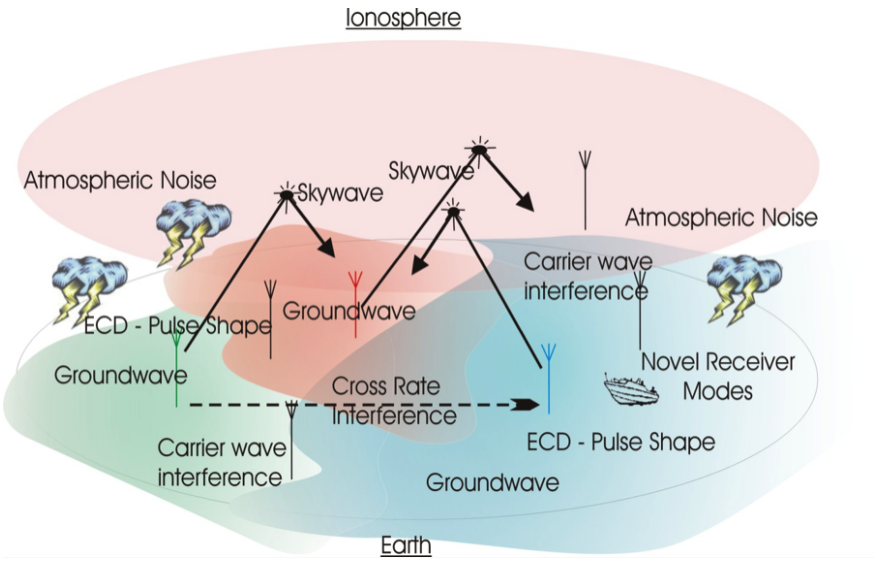

Figure 19: Standford Coverage Prediction Criteria.

determined in the LCAST tool.

Grid Spacing

The nominal user grid for LCAST was 1/4 degree latitude by 1/4 degree longitude. The grid spacing could be set to any value depending on the computing resources available. For example, the grid spacing could be increased to decrease the computation time.

Groundwave field strength

The LCAST included a Loran station database containing station locations, their transmission powers and GRIs. The location and power information were used to calculate ground field strength in conjunction with the Millington's method. The ground field strength was determined using a similar procedure as in the Bangor coverage prediction tool.

Skywave field strength

The skywave field strength was determined using the same models used in the Bangor coverage prediction model. Mitigation of skywave interference was accomplished in two ways:

- Proper phase coding to mitigate the long delay skywave interference
- Shorter skywaves were mitigated by tracking the early portion of the pulse Monitor sites were set up to report to users any skywave anomalies along specific baselines .

Atmospheric Noise

Atmospheric noise was determined using ITU-R P.372 – 9 [85, 66]. Atmospheric noise was studied by Lee Boyce [8, 10, 9] and his results were used to modify the existing noise model used in the LCAST. Atmospheric noise at any grid point was determined at various percentiles and stored. Determination of atmospheric noise requires the antenna noise factor called F_a [9] and the impulsivity of noise, V_d. Boyce [12] improved upon the noise model recommended by ITU and included his improved noise model in the LCAST tool.

Additional Secondary Factors

ASFs are by far the largest source of errors in the determination of Loran positions. A proper understanding of the ASFs and their spatial and temporal variations can substantially reduce their effect on the accuracy of Loran positions. The LORIPP spent a significant effort to model the ASFs. In the LCAST tool, ASFs were treated in three ways:

- The nominal ASF estimate was provided for each station in view at an airport and harbour. Nominal ASF estimates are ASFs measured at the time of reference station installation. These were stored in the receiver's memory and applied only at surveyed airport or harbour.

9 F_a is the power received by the loss free antenna averaged over a 15-minute period.

- A bound was provided on the correlated and uncorrelated temporal variation component of the ASF from the nominal ASF estimate. Johnson et al. studied the effects on ASF on Loran positions obtained at the airports runway [71] and suggested that an ASF bound must be used to account for the yearly ASF temporal variations. However, in HEA performance analysis, the differential Loran corrections account for the temporal ASF variations.

- A bound on the spatial ASF variations from the reference station is provided. Spatial ASF variations are the changes in the ASF as the receiver moves further away from the reference station. These propagation effects are described in more details in chapter 3.

Envelope Cycle Difference

Envelope cycle difference is the discrepancy between the carrier and envelope of the Loran signal as a result of pulse distortion. As it was described earlier, the receiver measures the phase of the carrier of the groundwave signal at the 3^{rd} zero crossing. This is done by sampling the signal at the zero crossing of the carrier cycle that lies underneath the envelope with a slope closest to the predetermined slope of a pure Loran pulse. However, too much pulse distortion can lead to a large ECD difference, and thus, the receiver may end up sampling the received signal at the incorrect zero crossing. ECD bias due to transmitter, receiver, temporal and spatial variations of ASFs is modelled in LCAST. Statistics of all the hazards causing ECD bias are also used in the cycle confidence algorithm. A good model for ECD prediction helps to reduce the probability of getting cycle errors. Since the ECD changes from the time the pulse leaves the transmitter, it is well known that the ECD at the far-field is the time derivative of the ECD in the near-field. Generally, the ECD at the far-field differs with ECD at the near-field by $2.4\mu s$ [65].

Transmitter Range Limit

In LCAST, the range of stations to the user is restricted to 800 km. The reason for this coverage criterion is to mitigate the effects of early skywaves on the desired groundwave signals [47].

Cycle Confidence and Integrity

Cycle selection is a process of choosing the same cycle on the Loran pulse for all signals that are being tracked to ensure consistency between the measurements. Cycle selection algorithm used in LCAST was proposed by LORIPP in order to demonstrate integrity. Cycle selection involves the examination of the envelope of the Loran signal and choosing the desired cycle based on the envelope slope. The determination of the envelope slope is complicated by noise, CRI and CWI. According to the LORRIP team's findings [54], cycle selection is a function of SNR. Having stations with SNR greater than 10 dB guarantees that the correct zero crossings are being tracked all the time. This is stated in terms of the probability of having an incorrect cycle among all the signals tracked by the receiver. This probability is set to be at most 7×10^{-8}.

Cross Rate Interference

Cross Rate Interference (CRI) is a form of interference that occurs due to signals from two chains being received by the receiver antenna at the same time. Alternatively, it can be defined as a form of interference where two groundwave signals from the transmitters operating on different GRIs are being received at the same time. If each chain was operated on a unique frequency, this would not be a problem. Since Loran is time-division multiplexed system, only one chain needs to be on-air at a time. Position errors increase, if no proper attention is paid to the CRI problem. In LCAST, CRI mitigation techniques, though not described in detail, were considered to be relatively effective. CRI mitigation techniques have been extensively described in reference [77]. These mitigation techniques included among others, blanking and cancellation.

Horizontal Protection Level and Time To Alert

Horizontal Protection level (HPL) represents the overall confidence bound on the horizontal position error. The system is said to be available if HPL is less than a set limit. If the system becomes unavailable, the user has to be notified within a specified time called time to alert and the time to alert is usually set to 10 μs. HPL is considered to be valid if the receiver is tracking the correct Loran cycle. In LCAST, the probability of tracking the correct cycles is established first. If this probability is less than a specific bound, then HPL can be determined. Otherwise, HPL cannot be determined.

Other Features of LCAST

The coverage tool displayed plots for accuracy, availability and continuity. The results from various inputs of LCAST demonstrated that accuracy is driven by SNR [55]. Accuracy was determined using a conservative refined noise, weather, basic skywave model and ASF model. The refined noise model was described in detail by Boyce [12] in his work on mitigation of atmospheric noise in the Loran band. The LCAST coverage tool showed output plots of accuracy at a given availability, continuity and integrity .

Table 5: LCAST Models/Algorithms.

Model/Algorithm	Calculation
Signal strength	SNR
Noise Processing	Cycle
ECD	Cycle
Transmitter noise	Cycle, HPL/Accuracy
Spatial ASF	HPL

2.10 SUMMARY AND CONCLUSIONS

Coverage prediction is used to estimate system performance parameters in a geographical coverage area where coverage is desired. It is useful for answering questions on the ability of Loran as a potential back up to GPS. The ability of Loran as a potential back up to GPS is based on the assessment of

potential hazards on the predicted levels of accuracy, availability, continuity and integrity in a chosen geographical area. These hazards manifest at the transmitter, along the radio channel and the receiver resulting in the system not meeting the required performance. The performance of navigation parameters against the set standards can reveal the target areas where error sources can be mitigated. The LCAST tool initially developed for the 2004 FAA Loran technical report provides the best estimate for the coverage parameters for both NPA and HEA in the US.

In Europe, the coverage tool developed at Bangor was far behind compared to the LCAST tool. This thesis presents an improved eLoran coverage prediction tool which has been brought up to date compared to the LCAST tool and have also been developed even further. The coverage tool developed by the author mainly focuses on eLoran for harbour entrance and approaches. The eLoran system proceeding from Loran-C of old is explained in detail in chapter 3.

3 eLORAN SERVICE VOLUME COVERAGE PREDICTION

The previous chapter described the coverage prediction techniques developed by various organisational bodies from Loran-C days to the times of modernised Loran-C. The current chapter gives an overview of the work done by other developers of the GLAs coverage tool since the Loran-C days and also highlights the modifications made by the author. The previous coverage prediction tool was written in C++ language. Fortunately, the Engineer at the General Lighthouse Authorities converted it into MATLAB^{TM} language and handed it to the author at the start of this research. This chapter also describes the various inputs of the coverage tool. The coverage prediction tool described here is most suitable for eLoran harbour entrance and approach and is therefore driven by accuracy. The GLA coverage area lies between 45° to 65° North in latitudes and −15° to 10° East in longitude. The geographical area is divided into grid points of equal size, resulting in 201 by 251 grid points. For simplicity, parameters of interest are assumed to be determined at the centre of each grid point.

3.1 COVERAGE INPUTS

The following inputs are necessary to produce a working coverage prediction tool.

3.1.1 *Shape of the earth*

The properties of the earth surface are adopted from the World Geodetic System 84 (WGS 84) model. WGS 84 is an Earth-centred, Earth-fixed terrestrial reference system and geodetic datum that is based on a set of constants and model parameters describing the Earth's size, shape, gravity and geomagnetic fields. WGS-84 was coined by the U.S. Department of Defence as the standard for a global reference system for geospatial information. The defining parameters of the WGS 84 model are summarised in table 6.

Table 6: Summary of the Defining parameters of the WGS 84 model.

Parameter	Notation	Value
Semi-major Axis	a	6378137.0 m
Flattening Factor of the Earth	$1/f$	298.257223563
Nominal Mean Angular Velocity of the Earth	ω	$7292115x10^{-11}$ rad/s

3.1.2 *Transmitter database*

A database containing the transmitter almanac is needed to determine various coverage parameters. The transmitter almanac contains, among other things, names of the transmitters, coordinates of the transmitters and transmitter operational powers in kilowatts (kW). For each transmitter, various components of its almanac can be used to generate its sky field strength,TOA

variance, SNR, CRI and ground field strength at various grid points representing the possible user locations. These coverage parameters can be stored as files that can be assessed on the fly. The procedure for generating these files is cumbersome and heavy on the computing resources. The ground field and sky field strength files are generated by setting transmitter powers to $1kW$ and stored. Desired transmitter powers can then be factored in on the fly thereby saving computing power. A typical groundwave field strength calculation for the entire GLA coverage area can take about a week to compute on a fast PC.

3.1.3 *Port database*

A port database containing a list of all the ports was sourced from the General Lighthouse Authorities of UK and Ireland. This database is very crucial in determining the position accuracy estimates in and around these ports. In the future, most of these ports will host reference stations and it is expected that the accuracy performance of the system at these ports must be below 10 m (see chapter 4) in order to meet the standards set out by International bodies such as the IMO .

3.1.4 *Conductivity profile*

A conductivity database is useful in determining the signal strength along the propagation path. This database was assembled as a digital conductivity map with a grid resolution of 0.1° by 0.1° in latitude and longitude beforehand at the University of Bangor in the 1990s [21]. Conductivity in the Bangor model was be determined using a world atlas of conductivities [86]. The groundwave field strength at any grid point, can be determined using a two step procedure. First, the conductivity change points along the path between the transmitter and the receiver are determined. These conductivity change points divide the transmitter-receiver path length into segments of different conductivities. Secondly, an appropriate groundwave field strength curve from the ITU-R P. $368-7$ is fitted into each segment to determine the attenuation along that segment. The propagation curves can be used to determine the electric field strength over any particular type of terrain. It is important to emphasize that the ITU-R P. $368-7$ recommendation does not provide the field strength curves for the 100 kHz signals, but provide curves for the 90 kHz and the 120 kHz signals . The 100 kHz curves can be obtained by interpolating the 90 kHz and the 120 kHz curves using curve fitting techniques. The groundwave field strength for various terrain at a distance from the transmitter is illustrated in figure 20. It can be seen that signal attenuation is inversely proportional conductivity. Table 7 shows the possible terrain type, conductivity and relative permittivity of various terrain in the geographical area over which coverage is assessed.

3.1.5 *Groundfield strength model*

The Groundwave propagation is the main mode of propagation of radio waves at frequencies below 2MHz [21, 24, 69]. The Groundwave propagation from the transmitter to the receiver can occur via refraction, reflection, scattering and diffraction depending on the dimensions of the objects in the propagation path. The object's dimensions with respect to the signal wavelength determine whether the signals are affected by scattering and re-

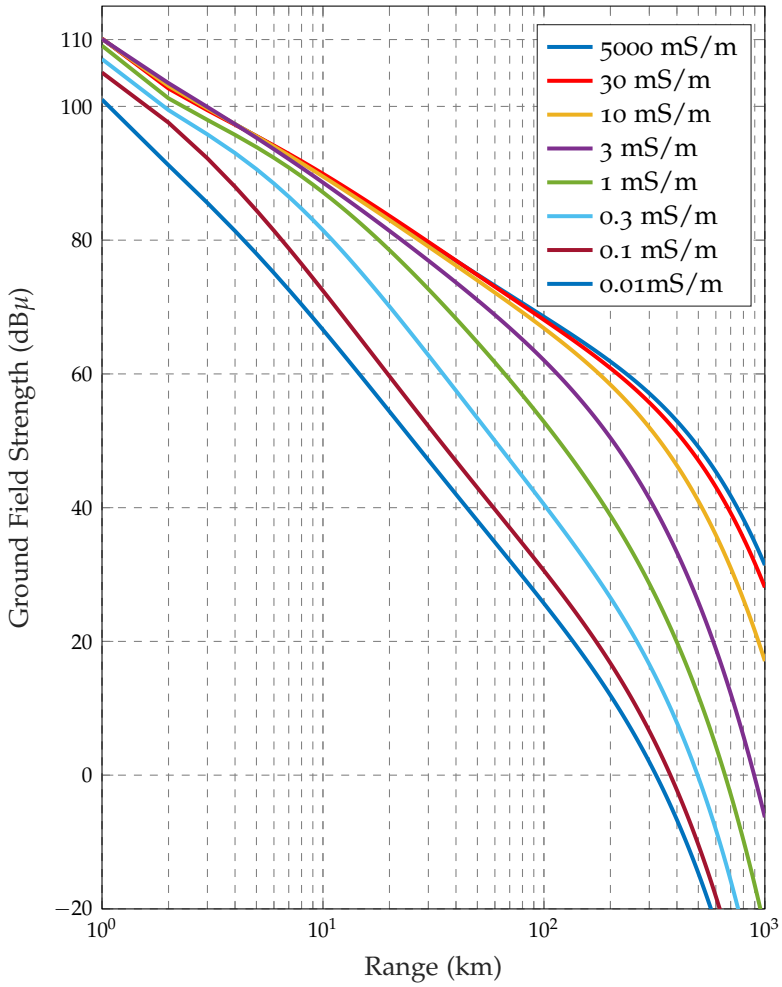

Figure 20: Groundwave propagation curves for different conductivities.

Table 7: Standard ground types as defined by ITU-R.

Ground Type	Conductivity (mS/m)	Relative Permittivity
Sea water	5000	70
Very good ground	30	40
Wet ground; good dry soil	10	30
Fresh water; cultivated ground	3	22
Medium dry, Average ground; Mountainous areas	1	15
Dry ground;permafrost; Snow covered mountains	0.3	7
Extremely Poor, very dry Ground	0.1	3
Glacial Ice	0.01	3

fraction [72]. The propagation velocity of a ground wave is very stable at low frequencies and it is this property that makes ground wave desirable for radio navigation [69]. In addition, ground wave signals are attenuated, delayed and dispersed at a rate that depends on the conductivity of the terrain over which they propagate [44, 46, 78, 95].

Attenuation and Field Strength

The signal modes are attenuated as they propagate from the transmitter to the receiver. Groundwave attenuation is affected by the surface permittivity, temperature, antenna heights above the terrain, frequency and polarisation of the wave [77]. Groundwave field strength at all grid points can be determined using the ITU-R P. 368 − 7 [83]. The ITU-R P. 368 − 7 recommends a quasi-empirical technique called the Millington's method for estimating the groundwave field strength over non-homogeneous paths [58]. The field strength is expressed in decibels with respect to $1\mu V/m$ [66]. The path distance between the transmitter and the receiver is determined using the Vincenty algorithm [78]. Next, the digitized conductivity database based on the world atlas of conductivities [86] is loaded into memory to determine the nature of the propagation path. Each of the segments of the terrain is matched with its corresponding conductivity [78]. Methods of modelling the groundwave field strength are well established in the literature. An exhaustive overview of the existing models was presented by Pelgrum [66].

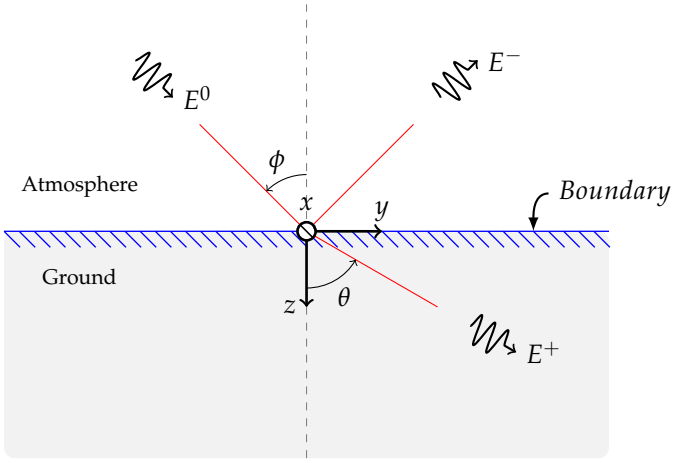

Figure 21: Groundwave Propagation via reflection.

The electric field strength in the forward direction is given by equation 3.1.

$$E_F = E_1(d_1) - E_2(d_2) + E_2(d_1 + d_2) - E_3(d_2 + d_3) + E_3(d_1 + d_2 + d_3) \quad (3.1)$$

The electric field strength along the path can be determined by assuming that the ITU-R curves emanate from the same source. The reverse electric field strength is calculated as follows:

$$E_R = E_3(d_3) - E_2(d_3) + E_2(d_3 + d_2) - E_1(d_1 + d_2) + E_1(d_1 + d_2 + d_3) \quad (3.2)$$

The resultant electric field is determined by averaging equation 3.1 and equation 3.2.

$$E_{field}(1kW) = \frac{E_F + E_R}{2} \quad (3.3)$$

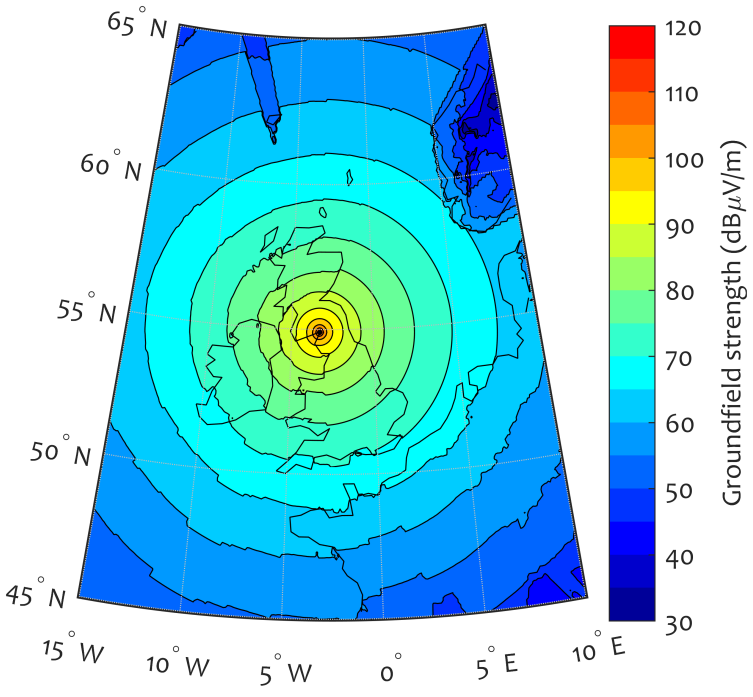

Figure 22: Groundwave field strength for Anthorn.

Equation 3.3 represents the resultant groundwave field strength at the peak of the eLoran pulse assuming a 1 kW of transmission power. However, the eLoran receiver tracks the eLoran pulse by taking measurements at the 3^{rd} zero crossing which is assumed to be 4 dB down from the peak of the pulse. The standard recommendations appear to ignore the effects of receiver front-end filtering on the received pulse. The effects of receiver front-end filtering were investigated in [59, 6, 7]. The groundwave field strength from each transmitter to any grid point in the coverage area is determined by assuming a 1 kW transmission power and is stored in a file which can be accessed on the fly. This approach allows for any transmitter power to be factored in on the fly thereby saving time and computing power. Equation 3.4 can be used to calculate the groundwave field strength at any grid point given the transmitter power.

$$E_{field} = E_{field}(1kW) + 10log_{10}(P_{tx}) - 4\ dB \tag{3.4}$$

where :

- $E_{field}(1kW)$ represents the groundwave field calculated using the Millington's method and,

- P_{tx} is the transmitter power derived from the transmitter database.

Propagation Delay

Position and time can be obtained from eLoran receiver time offset estimates of the groundwave signals that are in view. The time offset of a signal from a particular station at the user's location is modelled as a sum of the station's

emission delay τ_{ED}, the transmitter to receiver propagation delay, τ_{prop}, and the receiver clock bias relative to th system clock, τ_b [77].

$$\tau = \tau_{ED} + \tau_{prop} + \tau_b \tag{3.5}$$

where τ_b is the clock bias relative to the system clock and is determined as part of the receiver position solution. For modelling purposes, τ_b can be assumed to be negligible. The propagation delay, τ_{prop} depends on the properties of the terrain the signal traverses, physical parameters of the atmosphere (see chapter 4) and the distance between the transmitter and the receiver. Phase measurements made by the receiver need to be corrected to compensate for the additional delay accumulated by the signal traversing various media before they are used in computing a position fix. In eLoran, this is done through the use of three correction factors namely, primary factor (τ_{PF}), secondary factor (τ_{SF}) and additional secondary factor (τ_{ASF}). τ_{SF} represents the delay of a signal propagating over sea water with conductivity of 5000 mS/m and is modelled using Brunavs equation [55]. The $\tau_{\Delta PF}$ and τ_{ASF} are modelled in chapter 5. Taking these three correction factors into account, the ground wave propagation delay can be modelled as:

$$\tau_{prop} = \frac{d}{c} + \tau_{\Delta PF} + \tau_{SF} + \tau_{ASF}. \tag{3.6}$$

3.1.6 *The Skywave field Strength Model*

Skywave signals arrive at the receiver via the ionospheric reflection or refraction. Skywave is primarily experienced at night when the D region has faded away and the E-layer of the ionosphere is reflecting the eLoran signal to more distant places. The effective height of the ionosphere varies diurnally and seasonally. The height of the ionosphere is taken to be 73 km during the day and 90 km during the night. The sky field strength also depends on the reflection coefficient of the ionosphere and varies between 0.05 and 0.25 [21, 44]. The skywave field strength criterion limits coverage to only transmitter-receiver paths that are 800 km or less as a mitigation to early skywaves [49, 51, 48] . The ITU-R P. $1147-2$ [84] highlights the slant distance and loss factor due ionospheric absorption as the most important parameters of skywave field strength. Skywave field strength depends on the antenna gain and sea gain. The term antenna gain here, refers to the attenuation of the sky field strength at points close to the antenna rather than the actual gain of the antenna [21]. The antenna gain at the receiver can be determined using Poppe's third order polynomial, developed by fitting a set of curves from the ITU-R P. $1147-2$ [69]. For the purpose of this study, the sea gain term has been assumed to be negligible. Sky field strength assuming a 1kW transmission power, can be determined using equation 3.7 at each grid point. Unlike the groundwave field strength, the skywave field strength is stochastic in nature and is assumed to follow a normal distribution [69]. The ITU-R P. $1147-2$ provides median skywave field strengths as a function of distance for different geomagnetic latitudes. The skywave field strength values are assumed to be for night time. Daily skywave field strength are assumed to be 30 dB lower than the night skywave field strength. Figure 24 shows the night time skywave field strength in the GLA's coverage area. Skywave field strength is modelled as:

$$E_{sky} = G_{ant} + A - 20log10(p) - L_a + season(s) + dbAboveMedian \tag{3.7}$$

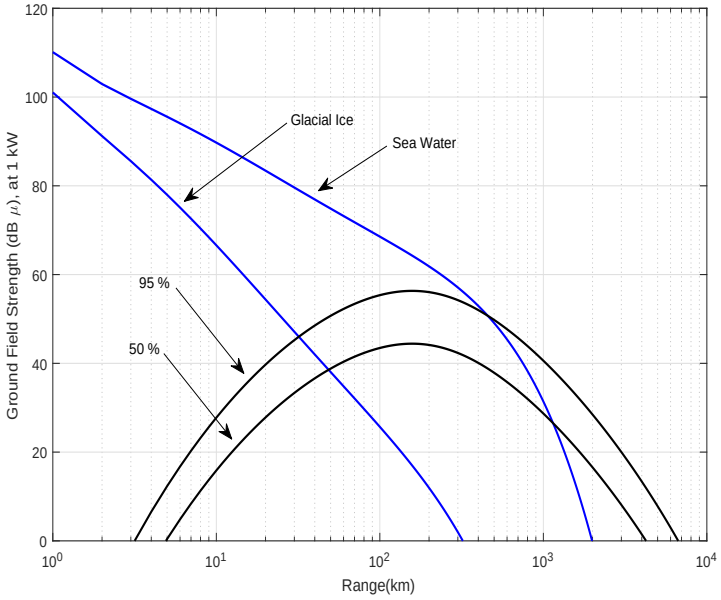

Figure 23: Groundwave field strength and night-time skywave field strength.

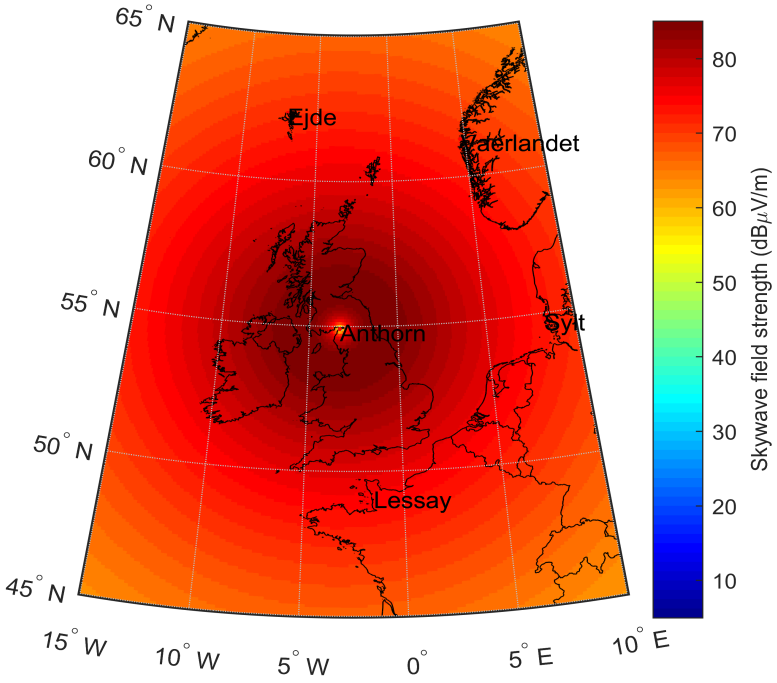

Figure 24: Skywave field strength for Anthorn.

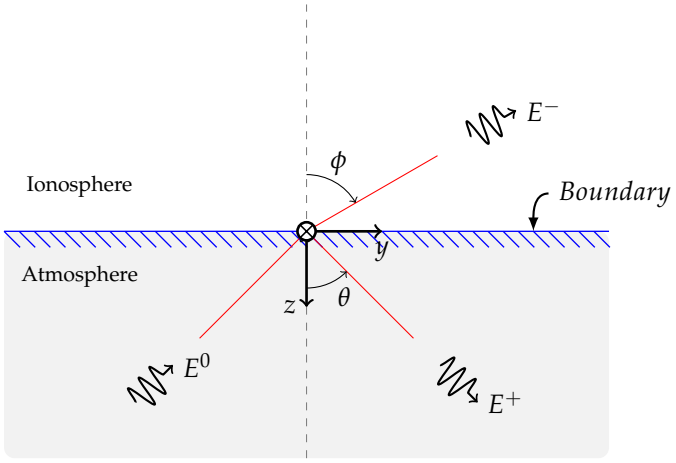

Figure 25: Illustration of skywave Propagation.

where G_{ant} is antenna gain. The antenna gain can be determined using the results of Poppe's work on DGPS. Antenna gain can be calculated as:

$$G_{ant} = -102.4530 + \log_{10} d(91.2214 + \log_{10} d(-26.8642 + 2.6164 \log_{10} d)) \tag{3.8}$$

At 100 kHz, the value of A is assumed to be equal to 110.2. The symbol p in equation 3.10 is referred to as the slant distance and is given by:

$$p = \sqrt{(d^2 + 4h^2)} \tag{3.9}$$

where h is the height of the ionosphere in kilometres. It is assumed that the skywave is perfectly reflected as it strikes the ionosphere on its way down to earth instead of being refracted into the ionosphere. However, there are losses incurred due to signal reflecting off the ionosphere and these losses are incorporated into the model as loss factor l_a. Apart from the effects of ionospheric absorption, the loss factor also includes terminal losses and can be modelled as:

$$l_a = k\sqrt{\frac{p}{100}} \tag{3.10}$$

where k is the basic loss coefficient. The basic loss coefficient can be modelled as:

$$k = (2\pi + 4.95 \tan^2 \Phi) \tag{3.11}$$

where Φ is the dipole geomagnetic latitude of the mid-point of the propagation path between the transmitter and the receiver. The geomagnetic north pole is currently located at the geographic coordinates [78.5° N, 69° W]. From [69], the geomagnetic latitude may be related to geographical latitude by:

$$\Phi = \arcsin(\sin \alpha \sin 78.5^\circ + \cos \alpha \cos 78.5 \cos(-69^\circ + \beta)) \tag{3.12}$$

where:
Φ: geomagnetic latitude,
α: geographic latitude,

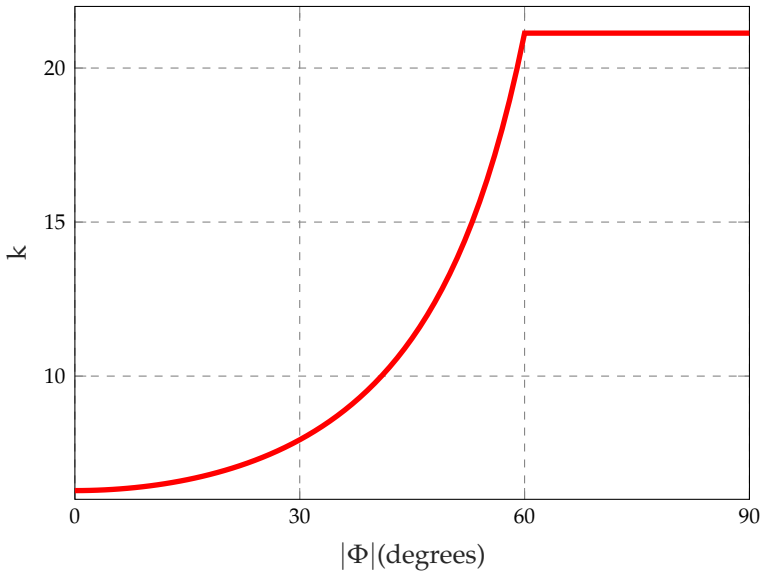

Figure 26: Basic loss factor.

β: geographic longitude.
The geographic latitude of the geomagnetic latitude is given by:

$$\alpha = (\alpha_T + \alpha_R)/2$$

where α_T and α_R are the transmitter and receiver latitudes respectively. The geographic latitude of the geomagnetic latitude is given by:

$$\beta = (\beta_T + \beta_R)/2$$

where β_T and β_R are the transmitter and receiver latitudes respectively. The term d in equation 3.8 is the path distance from the transmitter to the receiver in kilometres. The input parameter called s, in equation 3.7 represents season of the year and is obtained from Farnsworth's work on Loran C coverage prediction [21]. The USCG published curves of rms skywave intensities at distances of 1000 km to 3700 km for night and day. In developing these curves, no distinction was made between summer and winter conditions and ranges that are less than 1000 km were ignored [32]. Decca Navigator Company published tables of experimentally derived values of rms skywave intensities at ranges of 100 km to 500 km [21]. The results from these tables can be broken down into the following categories: full day, dawn/dusk, half-light, winter and summer night. The curves from Decca and USCG were interpolated by Farnsworth to produce a composite curve that includes the ranges from 100 km to 1000 km, which are applicable for Loran-C. Fortunately, these ranges are still applicable for eLoran and are therefore adopted in this work. Table 8 shows the rms skywave field strength of the Decca family of curves. Farnsworth's interpolated the curves (third column) relative to the USCG summer night curve to produce a curve appropriate for Loran-C.

ITU-R P.1147 – 2 [84] gives the annual median field strength values that need to be converted to higher percentiles. The skywave field strength is assumed to follow a normal distribution. The skywave field strength at higher percentile is calculated as shown in table 8. These results are in agreement

to Poppe's work on DGPS.

The term "dbAboveMedian" in equation 3.7, is the increase in the skywave field strength when higher percentiles are used instead of the median values. The values of the "dbAboveMedian" for various percentiles are shown in table 8. This table has been adopted from Poppe's work [69].

Table 8: Skywave field strength for day time and night time.

Time Period	Decca Strength with respect to summer night (dB)	1000 km strength with respect to summer night (dB)	Shape of curve
Winter night	+3	+3	Night
Summer night	0	0	Night
Dawn/Dusk	−6	−6	Day
Half light	−12	−12	Day
Full daylight	−18	−18	Day

$$E_{sky} = E_{sky}(1kW) + 10log_{10}(P_{tx}) - 4dB \tag{3.13}$$

At near-field distances, the groundwave field strength dominates the skywave field strength. However, at greater distances from the transmitter especially at night the skywave interference becomes a problem. This re-

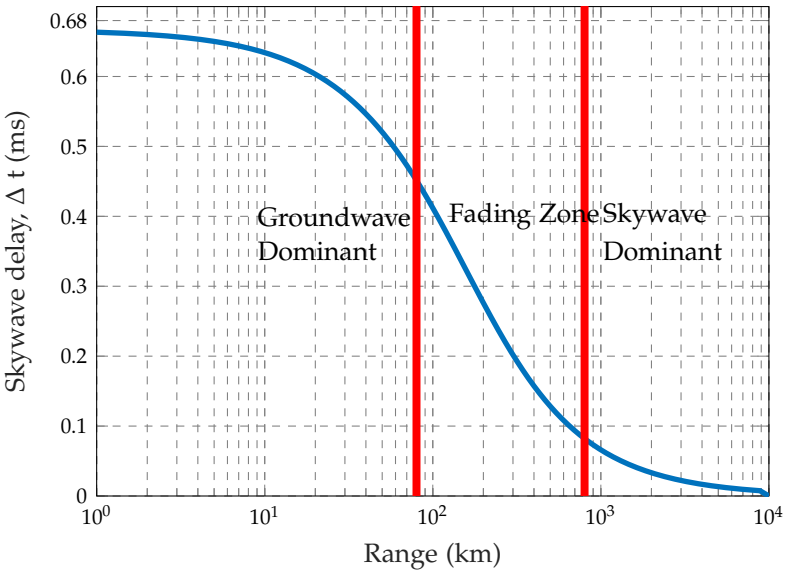

Figure 27: Illustration of skywave delay at various distances from the transmitter.

search, incorporates the IEC and RTCM receiver minimum standards into the skywave propagation model. The RTCM receiver minimum standards document [23] outlines that the receiver should be able to operate with 99 % confidence for skywave ground ratios (SGR) of 12 dB with delays of 37.5μs and 26 dB with delays of 60μs. However, the IEC RTCM minimum performance standard is silent on SGR values for the delays that are beyond 60μs. It is therefore assumed that the receiver can operate with SGR values not greater than 26 dB with the skywave delays that are greater than 60μs . At

each grid point the skywave ground ratio is determined and tested against the RTCM receiver minimum standards.

3.1.7 *The Skywave Delay Model*

The skywave delay always arrives later than the groundwave at the receiver. The differential delay between the skywave and the groundwave is estimated from the effective height of the ionosphere h and the path distance between the receiver and the transmitter r. In this calculation, a spherical earth and single hop skywave is assumed [77].

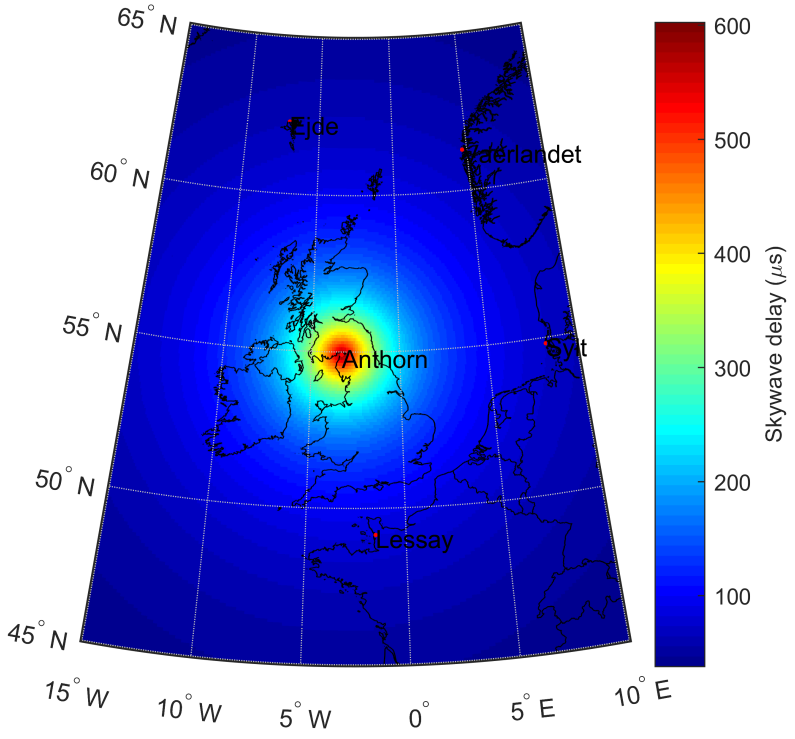

Figure 28: Skywave delay for Anthorn in the coverage area.

$$\tau_{diff} = \frac{2\sqrt{h^2 + 4R_E(R_E + h)\sin^2(\frac{r}{4R_E})}}{c} - \frac{r}{v_{atm}} \tag{3.14}$$

The differential skywave delay τ_{diff} is in μs. In this study the primary velocity is assumed to be equal to 299691162.387 m/s. The propagation velocity of the skywave signal through the ionosphere is assumed to be equal to the velocity of light in vacuum, c and the propagation velocity of the groundwave is set to the velocity of signal in the atmosphere, v_{atm}. The differential delay at any time is dependent on the height of the atmosphere. Figure 29 shows the variation of the differential delay with distance from the transmitter for different ionospheric heights.

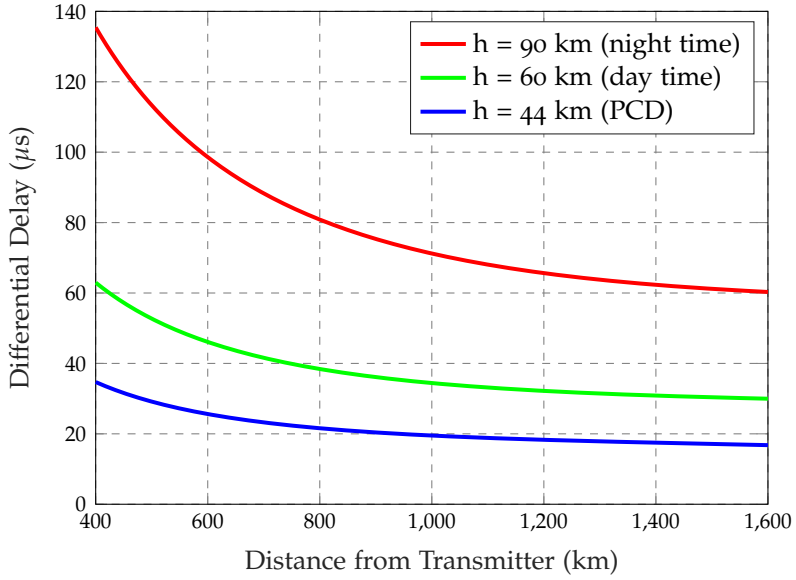

Figure 29: Differential Sky delays at different ionospheric heights, and various distances from the transmitter.

3.1.8 *The Atmospheric Noise Model*

Atmospheric noise is caused by lightning discharges in thunderstorms. There are two forms of lightning discharges; cloud to cloud and cloud to ground discharges [8, 10, 12, 65, 66, 82]. The main form of transference of atmospheric noise is due to the cloud to ground discharges [12]. The conductive nature of the earth allows atmospheric noise to be observed by receivers at distant places as a combination of gaussian noise and impulsive noise. The skywave propagation also allows low frequency energy from these electrical discharges to be detected at thousands of kilometres away from where they have been generated. Pelgrum [65, 66] suggested that a lightning strike on a single received eLoran pulse can render the whole integration of perhaps seconds unusable to the receiver and warned that it is important to detect and drop the distorted pulses before the integration process. In practice, an eLoran receiver averages many pulses before taking a measurement. A more sophisticated eLoran receiver can detect and drop pulses that are severely distorted by the atmospheric noise before averaging. This technique is referred to as hole punching [12, 65, 66, 77].

Atmospheric noise intensity is a stochastic random process and varies with time of the day, season of the year and distances from the thunderstorm centres [29]. Distant sources generate noise that can be considered to be Gaussian distributed in time. Local sources generate additional short-term, high powered spikes thereby making the overall received noise to deviate from its Gaussian nature. Atmospheric noise is greatest in the equatorial regions and the noise generated there can increase the noise levels at mid-latitudes via sky wave propagation [80]. Atmospheric noise has always been an important design and operational parameter since the days of Loran-C. High operational powers radiated by eLoran transmitters are intended to diminish the atmospheric noise to a background phenomenon [65, 66]. In the early 1960s an effort was made to measure the levels of atmospheric noise and its

variation around the globe. The results of this measurement campaign were analysed and published in the CCIR 322 report [18], which has now been superseded by ITU-R P. $372-9$ [85]. The ITU-R P. $372-9$ provides maps showing the statistics of the six, expected median values of the atmospheric noise experienced during the four hour time blocks of the day for all the seasons of the year. At each location, the median noise figure can be determined during the following four hour time blocks: $0000-0400$hrs, $0400-0800$hrs, $0800-1200$hrs, $1200-1600$hrs, $1600-2000$hrs and $2000-2400$hrs [85]. The equations described in this section are used in the coverage software tool at 100 kHz. The most important parameter in determining the atmospheric noise is the external noise factor:

$$f_a = \frac{P_n}{kt_0b} \tag{3.15}$$

where:

p_n is the available noise power from an equivalent lossless antenna,
k: Boltzmann's constant =$1.38 \times 10^{-23} J/K$.
t_0 : reference temperature (K) taken as $290K$
b: noise power bandwidth of the receiving system Hz.
Taking logarithms to base 10 on both sides of equation 3.15 gives:

$$P_n = F_a + B - 204 \tag{3.16}$$

where:

- $P_n = 10\log_{10} p_n$: available power (W) and,
- $B = 10\log_{10} b$, and $-204 = 10log_{10}kt_0$

For a short ($h << \lambda$) vertical monopole above the ground plane, the vertical component of the rms field strength is given by:

$$E_n = F_a - 95.5 + 20\log_{10}(f_{MHz}) + 10\log_{10}(b_{Hz}) \tag{3.17}$$

where: F_a is defined as the power of a loss free antenna for each time block and season. The research scientists at ITU at the time found that the distribution of F_a follows a split log-normal distribution. The term log-normal distribution here means that if the values of F_a are taken in decibels, its distribution will follow approximately a normal distribution centred around the mean noise factor F_{am} [9, 8, 12, 65]. The values of F_a at different locations are determined by interpolating the values of F_a measured at the nearby monitor sites. The ITU-R-P. $372-9$ [85] is used to determine the background atmospheric noise F_{am} and the impulsivity of the noise V_d at every grid point. The value of F_{am} is independent of the bandwidth of the receiver-tracking loop. However, the impulsivity of the noise V_d is dependent on the bandwidth of the receiver-tracking loop. Impulsivity of the noise for a given bandwidth of receiver tracking loop is determined by amplitude probability distribution curves found in ITU-R P. $372-9$.

The atmospheric noise can be determined using the ITU-R curves which have been derived from noise the data measured by a receiver with a front-end filter of 200Hz bandwidth [12, 52]. In the eLoran coverage prediction tool, atmospheric noise at any grid point not exceeded 99.9% to 50% of the time is calculated and stored. The atmospheric noise is a driving input in the accuracy and availability models, which are described in chapter 4

and chapter 9 respectively. Figure 30 shows the atmospheric noise level not exceeded 95 % of the time obtained using the ITU-R P. 372 − 9 recommendation. The impulsivity V_d can be estimated at each grid point. Pelgrum

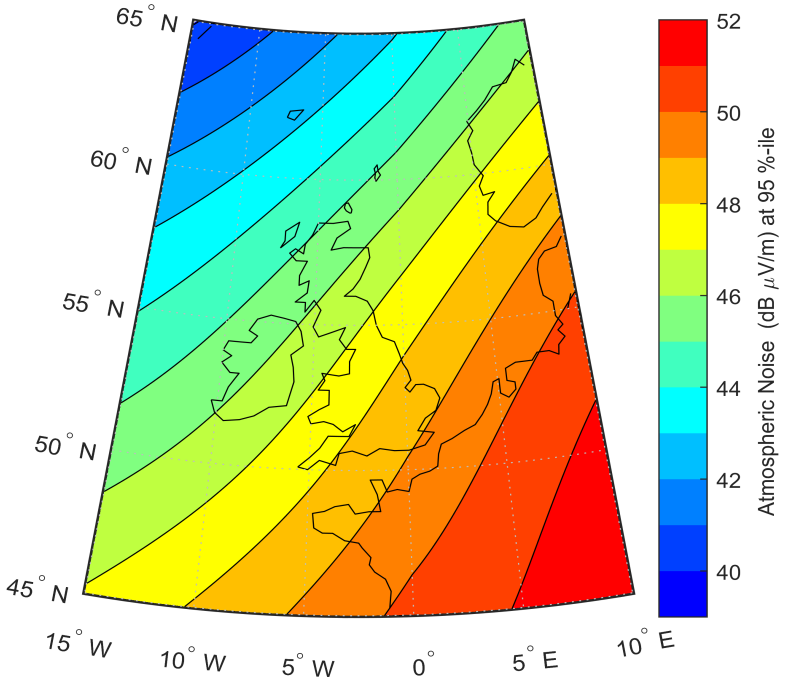

Figure 30: Levels of expected atmospheric noise at 95^{th} percentile.

[65, 66] and Boyce [12] suggested that if the impulsive component of the noise is high, more gain can be achieved through the noise suppressing techniques. In the coverage tool, one option is to assume a constant 12 dB credit everywhere in the coverage area. However, it was found that adding a 12 dB credit in Europe to compensate for the impulsivity of noise is not a reasonable assumption. This is because the number of lightning strikes experienced in Europe are not as prevalent as in the United States. However, if the coverage is to be determined in Italy where thunderstorms occur more frequently, then this may need to be considered [26]. The bandwidth of the receiver used for the purpose of this work is assumed to be 30000 Hz [21]. However, the bandwidth of the receiver used in the ITU-R P. 372 − 9 recommendation was 200 Hz. Generating atmospheric noise for eLoran where receivers of high bandwidth are deployed requires some bandwidth conversion. This conversion factor is a quotient of the bandwidth of the eLoran receiver and the bandwidth of the Loran receiver used for computing the noise statistics in the ITU-R P. 372 − 9. The noise levels experienced in Europe are higher during the summer for all hours of the day compared to other seasons. This is illustrated by figure 31. Atmospheric noise affects the transmitter SNR at the received location. As explained earlier, SNR is used as a coverage limiting criterion. Atmospheric noise generated at 95^{th} percentile is used to determine the SNR. The SNR criterion is such that a transmitter SNR must be greater than −10 dB for a transmitter to be considered to be in coverage. In cases when three or more transmitters have an

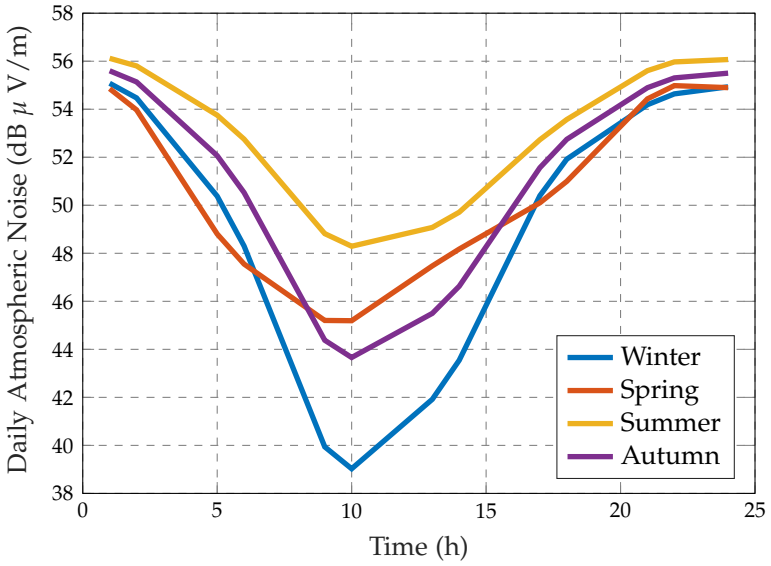

Figure 31: Seasonal 95 %-ile Atmospheric noise experienced at Harwich.

SNR greater than −10 dB, then the grid point is deemed to be in coverage. The SNR across the GLA coverage area is illustrated in figure 32.

3.1.9 *GRI Selection And Cross Rate Interference*

CRI is due to the "collision" of pulses from different transmitters operating on different Group Repetition Intervals (GRI) arriving simultaneously at the receiver. As it was described in chapter 2, this is the worst type of interference in eLoran. However, CRI can be predicted and modern receivers can mitigate the CRI effect to greater or lesser extent. Safar [77] has done some substantial work on CRI and has developed various mitigation algorithms that have been incorporated into the coverage tool. Safar's CRI model determines the number of pulses discarded by the receiver via blanking. These pulses are subtracted from the number of pulses received. The discarded pulses reduce the SNR of the tracked Loran signal, thereby increasing the pseudorange error. Nevertheless, this loss is small when compared to the consequences of not mitigating the CRI contamination at all [77, 78].

CRI Implementation in Modern day Receivers

Safar assessed the effects of CRI on the measurement error in the state-of-the-art eLoran receiver using a series of test bench experiments in which an eLoran signal was contaminated by a band-limited additive white Gaussian noise and interfered with signals of different GRIs. The results of his work suggest that modern day a receiver treats CRIs depending on the following scenarios:

- When SIR > 10 dB, no CRI mitigation algorithm are used. The suppression in this case is done by phase coding and comb filtering operations.

- When SIR < 10 dB, the receiver deploys blanking to mitigate interference

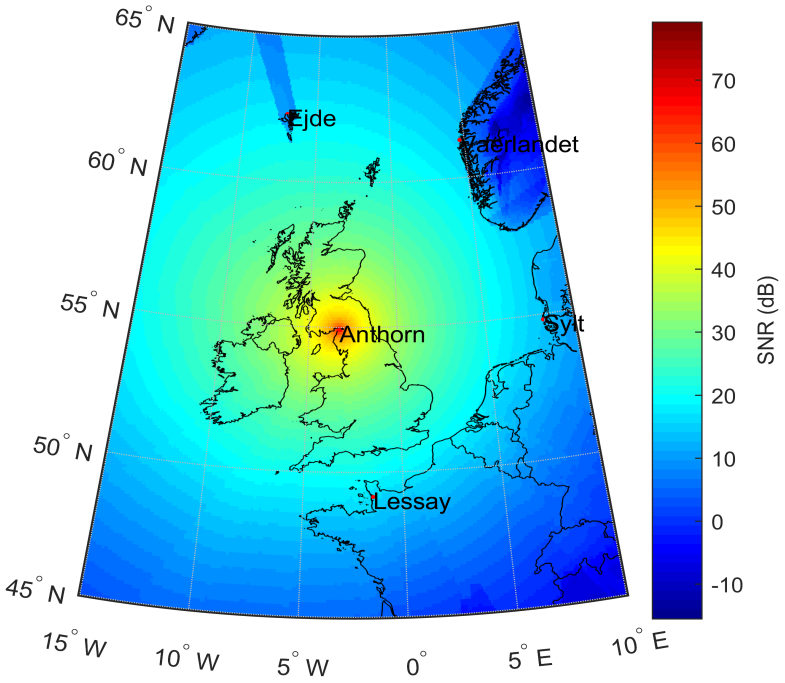

Figure 32: SNR plot for Anthorn.

3.1.10 *Coverage Criteria*

The coverage criteria is based on the skywave limit, SNR limit and the distance limit conditions. The skywave and SNR limits are kept the same as in the Bangor coverage tool. The distance limit is closely linked to the skywave limit condition because at distances greater than 800 km it has been observed that the skywave intensities can become severe and deleterious to the cycle selection process. The criteria adopted thus limits the transmitter range to 800 km. Receiver locations are deemed to be in coverage as long as there are 3 or more received signals whose SNR is more than -10 dB. The SNR limit is influenced by atmospheric noise and CRI. Determination of CRI at each grid point uses the results of Safar's work [77].

3.1.11 *Time of Arrival Variance Model*

The time of arrival variance model was developed by Lo [51] at Stanford University and was analytically derived by Safar [77] using principles of maximum likelihood. The TOA variance is stated as:

$$\sigma^2_{TOA} \approx L_{impl} \frac{337.4^2}{N_p \cdot \gamma} \tag{3.18}$$

where N_p is the number of pulses due to phase averaging and is given by:

$$N_p = (1 - L_p) \frac{8 \times 10^5}{GRI} \tag{3.19}$$

where: L_{impl}, is the implementation loss for the Reelektronika receiver used in Safar's work to ensure that it accurately depicts the performance of the

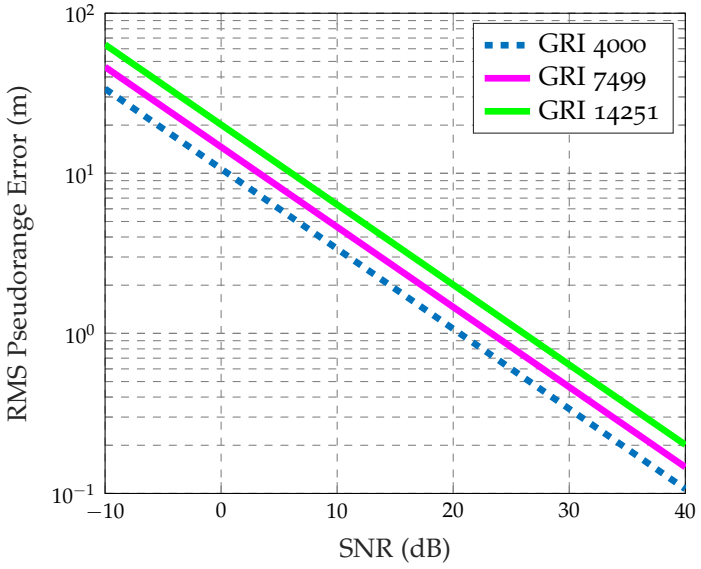

Figure 33: Theoretical lower bound of pseudorange error due Additive White Gaussian Noise vs SNR.

eLoran receiver under test. This value is taken to be approximately equal to 4.8. The term GRI, is the group repetition interval of the chain of the station received while γ is the signal to noise ratio of the transmitter.

The time of arrival variance is used to form the covariance matrix, which is the inverse of the weighting used in the position accuracy solution. The time of arrival variance of a signal from any transmitter is dependent on the SNR, transmitter jitter and the number of pulses averaged [78]. Transmitter jitter is assumed to be Gaussian in nature and thus can be averaged out. The number of pulses averaged is dependent on the group repetition interval (GRI) the station is transmitting on. However, not all pulses are averaged; some are discarded due to CRI contamination. The number of pulses used for averaging affect the time of arrival variance. A small number of pulses results in large TOA variance and vice versa. Stations with large TOA variances are weighted less in the position solution. The next section describes the model for estimating the user's position. The square root of the TOA variance of station is equivalent to the station's pseudorange error. The pseudorange errors of stations operating at different GRI's are illustrated in figure 33. It can be seen that higher SNRs results in lower pseudorange errors and that the pseudorange error is proportional to the GRI, that is the higher the GRI, the greater the pseudorange error.

3.2 POSITION ESTIMATION

The standard eLoran position algorithm used in estimating the user's position is the weighted least squares (WLS) applied to an over-determined set of range measurements. Starting with an initial position estimate, an iterative computation procedure finds a position, which minimises the square of the differences between the measured pseudoranges to the stations and pseudoranges computed from the current estimated position [78]. The cor-

rections in the user's position $\Delta\mathbf{x}$,$\Delta\mathbf{y}$ and $\Delta\mathbf{b}_u$ clock offset are calculated at each iteration point of the algorithm as follows:

$$\Delta u = \left(A^T W A\right)^{-1} \Delta\rho \tag{3.20}$$

$$\Delta u = \begin{pmatrix} \Delta x \\ \Delta y \\ \Delta b_u \end{pmatrix} \tag{3.21}$$

where $\Delta\rho$ is the column vector of the differences between the observed pseudoranges and the pseudoranges computed from the current estimated position using a signal propagation model. W is a weighting matrix. Each station contribution is weighted according to the measure of its signal quality. This allows for the most accurate measurements to have greater influence on the position solution. A is a direction cosine matrix and it describes the geometry of the eLoran stations relative to the user's position. The directional cosine matrix is also referred to as the geometry matrix. It contains the sines and cosines of the bearing β_i of the individual stations from the receiver.

$$A = \begin{pmatrix} \sin\beta_1 & \cos\beta_1 & 1 \\ \vdots & \vdots & \vdots \\ \sin\beta_i & \cos\beta_i & 1 \end{pmatrix} \tag{3.22}$$

There are many different position accuracy measures. The root mean square (RMS) is a convenient choice as it can be easily calculated from the pseudorange error statistics. The RMS error is given by:

$$a_{DRMS} = \sqrt{\lfloor dist^2(\hat{k}, k) \rfloor} \tag{3.23}$$

where $dist^2(\hat{k}, k)$ denotes the distance between the estimated position and the true position of the eLoran receiver. When investigating accuracy, only small position deviations relative to the reference point are of interest. Equation 3.23 can be rewritten as follows:

$$a_{DRMS} = \sqrt{E\lfloor (\underbrace{\hat{\mathbf{x}} - \mathbf{x}}_{\Delta x})^2 + (\underbrace{\hat{\mathbf{y}} - \mathbf{y}}_{\Delta y})^2 \rfloor} \tag{3.24}$$

Using the equality:

$$var(\Delta\mathbf{x}) = E[\Delta\mathbf{x}^2] - E^2[\Delta\mathbf{x}] \tag{3.25}$$

The distance root mean square accuracy can be expressed in terms of the mean and variance of the corrections in the user's position:

$$\delta_{RMS} = \sqrt{\sigma^2_{\Delta x} + E^2[\Delta\mathbf{x}] + \sigma^2_{\Delta y} + E^2[\Delta\mathbf{y}]} \tag{3.26}$$

where $\sigma^2_{\Delta x}$ and $\sigma^2_{\Delta y}$ are the variances of the relative easting and northing respectively. The expected values, $E[\Delta x]$ and $E[\Delta y]$ are assumed to be zero. The terms in equation 3.26 are calculated by examining equation 3.24. It can be shown that the variance $\Delta\mathbf{u}$ is minimized when the weighting matrix is equal to the inverse of the measurement covariance matrix.

$$\mathbf{W} = \mathbf{R}^{-1} \tag{3.27}$$

and,

$$\mathbf{R} = \begin{pmatrix} \sigma_1^2 & 0 & 0 \\ 0 & \vdots & 0 \\ 0 & 0 & \sigma_i^2 \end{pmatrix} \tag{3.28}$$

The mean of the position error can be obtained directly from equation 3.28. The only random variable on the right hand side of the equation is $\Delta\rho$:

$$\begin{aligned} E[\Delta\mathbf{u}] &= E[(\mathbf{A}^T\mathbf{W}\mathbf{A})^{-1}\mathbf{A}^T\mathbf{W}\Delta\rho] \\ &= (\mathbf{A}^T\mathbf{W}\mathbf{A})^{-1}\mathbf{A}^T\mathbf{W}E[\Delta\rho] \end{aligned} \tag{3.29}$$

The variance of the position error is determined using the identity:

$$var(\mathbf{B}\mathbf{x}) = \mathbf{B}var(\mathbf{x})\mathbf{B}^T \tag{3.30}$$

where $\mathbf{x}$ is a vector of size $n \times 1$ and $\mathbf{B}$ is a matrix of size $m \times n$. It is assumed that $\Delta\mathbf{u} = (\mathbf{A}^T\mathbf{W}\mathbf{A})^{-1}\mathbf{A}^T\mathbf{W}\Delta\rho$ and $\mathbf{x} = \Delta\rho$ and by comparing equation 3.29 and equation 3.30, the following equation can be obtained,

$$var(\Delta\mathbf{u}) = (\mathbf{A}^T\mathbf{W}\mathbf{A})^{-1}\mathbf{A}^T\mathbf{W}\underbrace{var(\Delta\rho)}_{\mathbf{R}}\mathbf{W}^T\mathbf{A}(\mathbf{A}^T\mathbf{W}^T\mathbf{A})^{-1} \tag{3.31}$$

The position error variance is minimised when the weight matrix is equal to the inverse of the measurement covariance matrix $\mathbf{W} \equiv \mathbf{R}^{-1}$. Under this assumption, the variance is expressed using the following reduced form:

$$var[\Delta\mathbf{u}] = (\mathbf{A}^T\mathbf{R}^{-1}\mathbf{A})^{-1} \tag{3.32}$$

Equation 3.32 represents the position error variance.

Horizontal Dilution of Precision

Horizontal dilution of precision (HDOP) is defined as the ratio of position error to the range error. The values of the HDOP gives a network designer insight into the areas that are of poor repeatable accuracy based solely on the locations of the transmitter with respect to the receiver [66]. HDOP helps in the optimization of transmitter placement across the coverage area. HDOP is determined using the least squares technique. It is given by the trace of equation 3.32.

Absolute Accuracy

As it has already been discussed, accuracy of the position solution is of paramount importance in HEA. In eLoran, the types of accuracy that are of interest are *absolute* and *repeatable accuracy*. Absolute accuracy depends on the nature of the propagation path between the transmitter and the receiver. The conditions of the propagation path between the receiver and transmitter can also affect the measured pseudoranges and the position solution calculated.

Repeatable Accuracy

Repeatable accuracy is defined as the temporal stability of the position measurement. It determines how well the user gets back to the previously

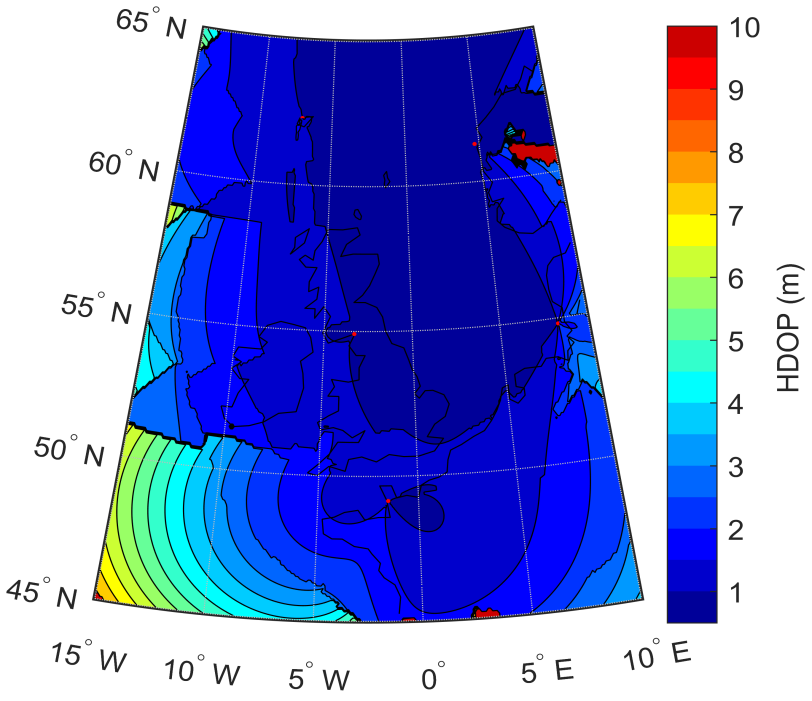

Figure 34: Unweighted HDOP distribution over the British Isles.

measured position at a certain location. In other words it determines the amount of "position scatter" when the user is at the same location. To determine repeatable accuracy, it is assumed that all the phase measurements have the same constant phase uncertainty [94]. This means that the position uncertainty at a location depends on the horizontal dilution of precision there. Various factors may lead to uncertainties in the phase measurements resulting in an increased position fix and poor repeatable accuracy. The main driving factors of the uncertainty in the phase measurements are atmospheric noise, carrier wave interference and cross rate interference [68]. In this study, it is assumed that the effects of carrier wave interference are easily nullified by the receiver signal processing. These are mitigated by using some form of weighting algorithm to ensure that the stations with good SNR contribute more to the position solution than the ones with less SNR. Repeatable accuracy is calculated as:

$$a_{DRMS} = \sigma_\rho \underbrace{\sqrt{(G_{1,1} + G_{2,2})}}_{\text{HDOP}} \tag{3.33}$$

The IMO defines the position error not exceeded 95% of the time. In position based navigation systems,the transmitter placement is practically not optimal with respect to some receiver locations. For this reason, the distribution of the position fixes is elliptical rather than circular. Safar [77] proposed that it is more accurate to use the following expression to calculate position accuracy.

$$a_{R95} \approx (1.960787 + 0.004121 \cdot c + 0.114151 \cdot c^2 + 0.371707 \cdot c^3) \cdot \sigma_{ma} \tag{3.34}$$

where σ_{ma} and c are the semi-major axis and the eccentricity of the error ellipse respectively. The semi-major axis is given by the square root of the

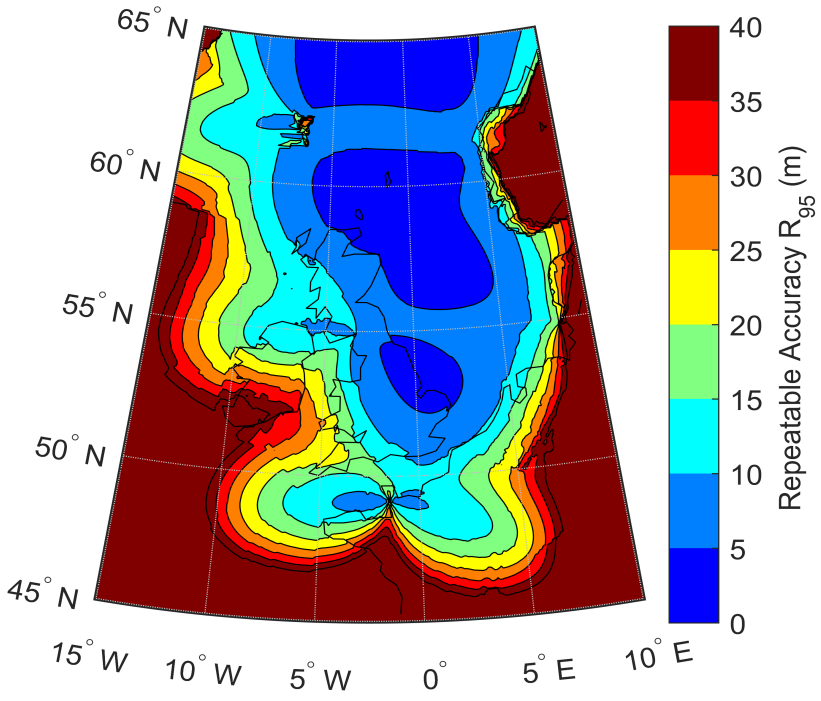

Figure 35: Repeatable Accuracy plot assuming dLoran everywhere .

eigen values of the covariance matrix of the relative northing and the easting coordinates. Equation 3.34 is used to determine the repeatable accuracy throughout this thesis. The repeatable accuracy calculation is summarised by flowchart illustration in figure 36.

3.3 MODEL IMPROVEMENTS

This section describes the improvements made by the author in relation to the models that have already been discussed in this chapter.

3.3.1 *Skywave field Strength*

The skywave field strength model that was handed to the author at the beginning of this study had fundamental errors. In that model, the calculation of the geomagnetic latitude was assumed to be just a single number for all grid points in the coverage area. This has now been modified as explained in section 3.1.6.

Total Field Strength

A method for calculating the effect of own-skywave interference is presented. The implementation of this method into the eLoran model is described . Poppe [69] developed a model using a polynomial curve fit for

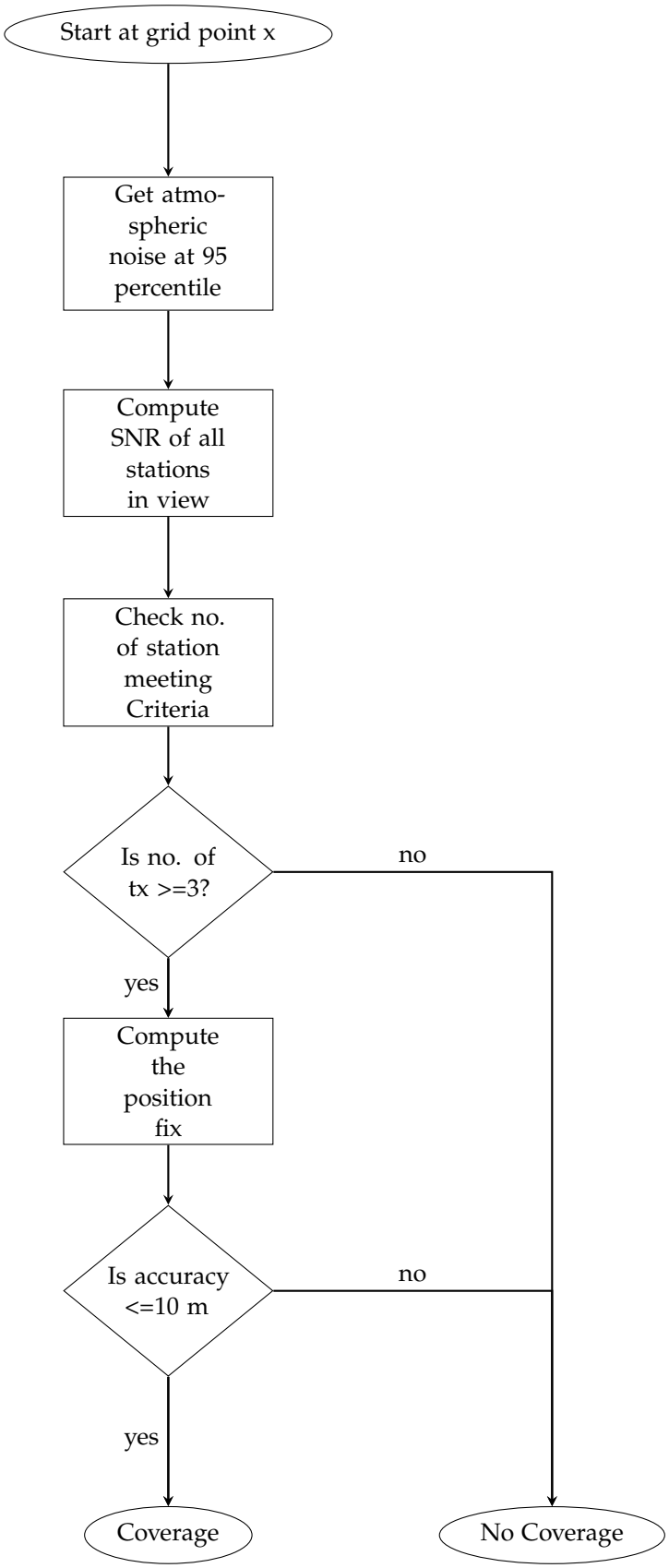

Figure 36: Flow chart depicting the accuracy model.

inclusion in her DGPS model. To keep the complexity of the model low, different curves were applied over various ranges of SGR, as follows:

$$TotalField(dB) = \begin{cases} Field & SGR \leq -30, \\ \\ Field - 11.0087 + \cdots & \\ SGR(-0.8536 + \cdots & \\ SGR(-0.0224 - \cdots & \\ 0.0002SGR)) & -30 < SGR < -5, \\ \\ Field - 8.4614 + \cdots & \\ SGR(0.2005 + \cdots & \\ SGR(0.811 + \cdots & \\ SGR(-0.0014 - \cdots & \\ 3.5e^{-5}SGR))) & -5 < SGR < 15, \\ \\ Field + SGR - 8.45 & SGR \geq 15 \end{cases} \tag{3.35}$$

where Field is the groundwave field strength and SGR is the skywave to groundwave ratio. This model has been adopted by the author to represent the total field strength of the eLoran signal received at user's location. This analysis assumes that fading due to the presence of skywaves. The ITU-R P. $1147-2$ states that fading due to skywave is more prevalent at night than during the day. Figure 37 illustrates the total field strength of an eLoran

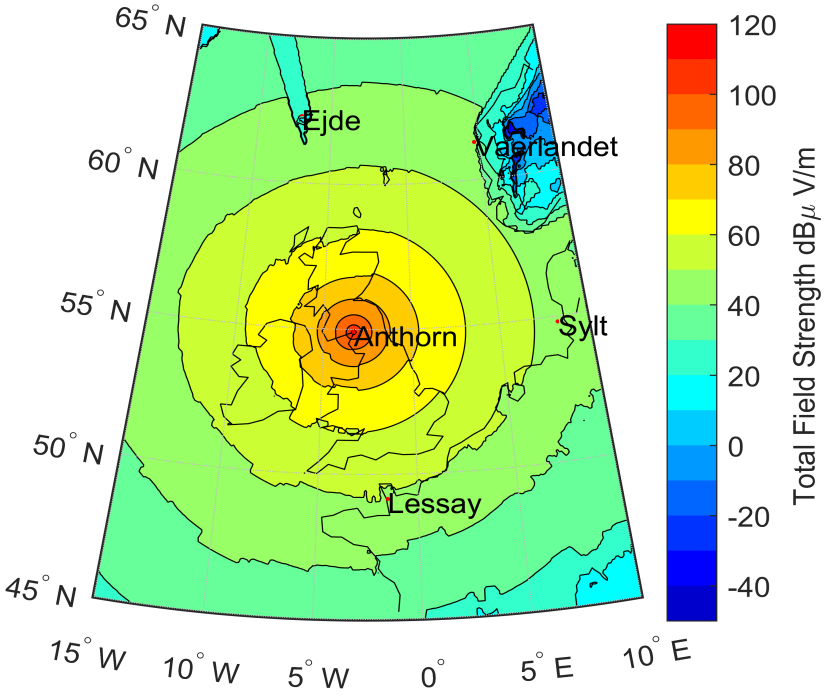

Figure 37: Total field strength due to skywave fading .

signal due to skywave fading. By comparing this figure with figure 22, it

can be seen that the total field strength due to skywave fading is 20 dB worse than the groundwave field strength.

Envelope Cycle Discrepancy

The author has increased the coverage tool's capability to output the ECD plots for all transmitters that are deemed to be in coverage. The modelled ECD plots for Anthorn and Lessay are shown in figures 38 and 39 respectively. It can been seen from these plots that ECD is good in areas near the transmitters and increases with distance from the transmitter.

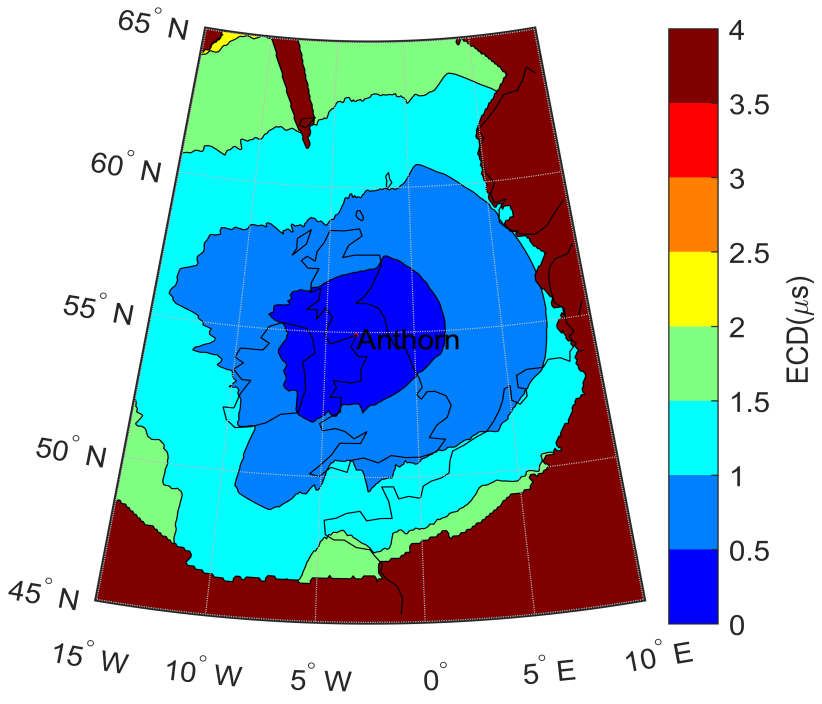

Figure 38: ECD from Anthorn at grid points where Anthorn is deemed to be in coverage .

3.4 SUMMARY AND CONCLUSIONS

This chapter described the various inputs of the coverage tool. Most of the models described in this chapter were developed by other researchers over 26 years. Before the start of this research, the coverage tool displayed predicted repeatable accuracy plots under the following assumptions:

1. Differential ASF corrections are provided everywhere. This assumption is not a realistic but provides a good starting point for a working coverage tool which can then be modified as new data and models become available.
2. ASFs are perfect and receivers are equipped with up to date nominal ASFs.
3. The receiver signal processing is able to mitigate completely the effects of CWI and thus is no longer considered a problem in Europe.

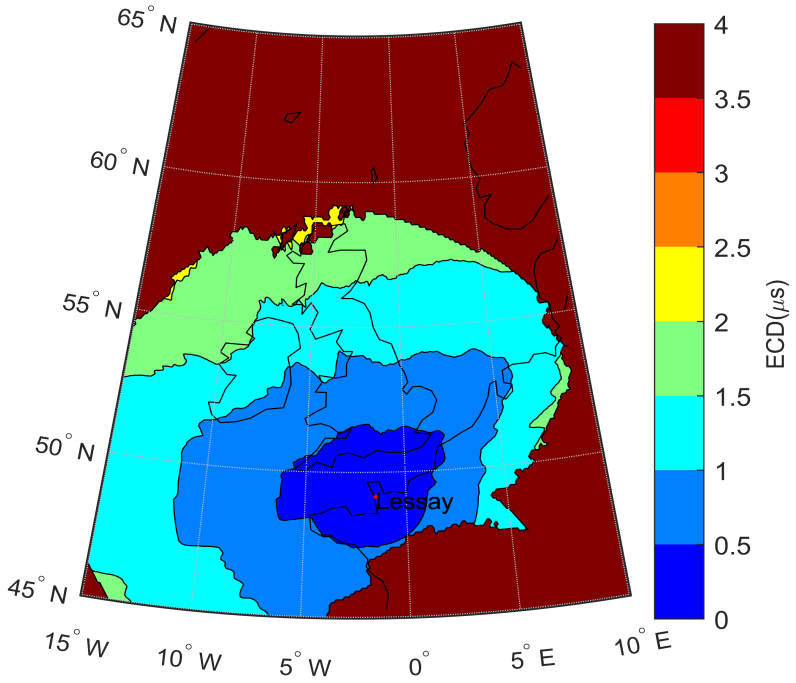

Figure 39: ECD from Lessay at grid points where Anthorn is deemed to be in coverage .

4. The coverage area is entirely made up of a flat terrain. Hence the effects of mountainous terrain on the ASFs are not modelled.
5. The effect of the receiver front-end filtering has no effect on accuracy.
6. Receivers are able to suppress the impulsive noise entering the receiver front-end.
7. Cycle selection is not a problem. Receivers are able to accurately lock onto the correct cycles.

The 1^{st} and 2^{nd} assumption are modified in chapter 7 to make the coverage tool more realistic by diluting the dLoran assumption everywhere in the coverage area except in harbour and port locations. Other model modifications such as ECD, new Field strength and the modified skywave have also been described herein.

Part II

MAIN CONTRIBUTIONS

4

MODIFIED ACCURACY MODEL

The previous chapter described the models used in determining repeatable accuracy by assuming differential Loran everywhere. The assumption of dLoran everywhere is unrealistic although it is helpful in producing a working coverage model. The current chapter describes the framework of the models developed to modify the assumption that dLoran is applicable everywhere in the coverage area. The developed models are conveniently named Landpath and weather models respectively. The Landpath model takes into account the long-term variations of the TOA of transmitted signals received at the user locations due to the changes in the conductivity. On the other hand, the weather model takes into account short term variations of the TOA of the received signals at user locations due to changes in the weather parameters along the propagation paths.

4.1 CRAMER RAO LOWER BOUND FOR PHASE ESTIMATION

The derivation of the TOA variance can be described using the theory of maximum likelihood estimation [25]. The receiver is tasked with the objective of estimating the phase of the sinusoid embedded in additive white Gaussian noise (AWGN) before further processing. The digitised samples in the receiver can be modelled as:

$$x[n] = A\cos(2\pi f_c n + \phi_c) + w[n], n = 0, 1, 2, \ldots, N-1 \tag{4.1}$$

where A is the amplitude and f_c is the frequency of operation. A and f_c are assumed to be known, while w[n] is an Additive Gaussian White Noise with mean $\mu = 0$ and variance σ^2. As described in chapter 1, the eLoran receiver measures the carrier phase of the received samples. The degree of confidence on the efficiency of a measured estimate of the phase of a sinusoid buried in noise is obtained by the Cramer Rao Lower Bound. The probability distribution of the observed sample that is affected by AWGN is given by:

$$p(x;\phi) = \frac{1}{\sqrt{2\pi\sigma^2}} \exp\left[\frac{-(x[n]-\mu)^2}{2\sigma^2}\right] \tag{4.2}$$

The joint probability distribution of the samples is given by:

$$p(x;\phi) = \frac{1}{(2\pi\sigma)^{N/2}} \exp\left[-\frac{1}{2\sigma^2}\sum_{n=0}^{N-1}(x[n]-\mu)^2\right] \tag{4.3}$$

The sample mean is given by:

$$\begin{aligned}\mu =& \frac{1}{N}\sum_{n=0}^{N-1} x[n] \\ =& \frac{1}{N}\sum_{n=0}^{N-1} [A\cos(2\pi f_c n + \phi) + w[n]] \\ =& \frac{1}{N}\sum_{n=0}^{N-1} [A\cos(2\pi f_c n + \phi)] + \frac{1}{N}\sum_{n=0}^{N-1} w[n] \\ =& \frac{1}{N}\sum_{n=0}^{N-1} [A\cos(2\pi f_c n + \phi)] + 0 \\ =& \frac{1}{N}\sum_{n=0}^{N-1} [A\cos(2\pi f_c n + \phi)]\end{aligned}$$

Equation 4.3 can be rewritten as:

$$p(x;\phi) = \frac{1}{(2\pi\sigma)^{N/2}} \exp\left[-\frac{1}{2\sigma^2}\sum_{n=0}^{N-1}(x[n] - A\cos(2\pi f_c n + \phi))^2\right] \quad (4.4)$$

Equation 4.4 can be referred to as the likelihood function and $p(x;\phi)$ can be replaced by $L(x;\phi)$. The log likelihood of function is given by:

$$\ln L(x;\phi) = -\frac{N}{2}\ln(2\pi\sigma^2) - \frac{1}{2\sigma^2}\sum_{n=0}^{N-1}(x[n] - A\cos(2\pi f_c n + \phi))^2 \quad (4.5)$$

The second derivative of equation 4.5 can be explicitly stated as:

$$\frac{\partial^2 L(x;\phi)}{\partial^2\phi} = -\frac{A}{\sigma^2}\sum_{n=0}^{N-1}(x[n]\cos(2\pi f_c n + \phi) - A\cos(4\pi f_c n + 2\phi)) \quad (4.6)$$

Equation 4.6 is still dependent on x[n] and therefore an expected value is taken in order to smooth out the variations. Therefore,

$$\begin{aligned}-E\left[\frac{\partial^2 L(x;\phi)}{\partial^2\phi}\right] =& \frac{A}{\sigma^2}\sum_{n=0}^{N-1}(E(x[n])\cos(2\pi f_c n + \phi) - A\cos(4\pi f_c n + 2\phi)) \\ =& \frac{A}{\sigma^2}\sum_{n=0}^{N-1}\left(A\cos^2(2\pi f_c n + \phi) - A\cos(4\pi f_c n + 2\phi)\right) \\ =& \frac{A^2}{\sigma^2}\sum_{n=0}^{N-1}\left(\frac{1}{2} + \frac{1}{2}\cos(4\pi f_c n + \phi) - A\cos(4\pi f_c n + 2\phi)\right) \\ =& \frac{A^2}{2\sigma^2}\sum_{n=0}^{N-1}(1 - \cos(4\pi f_c n + 2\phi))\end{aligned}$$

The second term is filtered out by the lowpass filter. Thus:

$$-E\left[\frac{\partial^2 L(x;\phi)}{\partial^2\phi}\right] \approx \frac{A^2}{2\sigma^2}(N-0) = \frac{NA^2}{2\sigma^2} \quad (4.7)$$

Equation 4.7 is known as the Fisher Information and is the reciprocal of the CRLB. The variance of any carrier phase estimator is always higher than this CRLB. That is,

$$var(\phi) \geq \frac{2\sigma^2}{NA^2} = \frac{1}{2N\cdot\gamma} \quad (4.8)$$

The phase estimates and the range estimates are related by the following equation:

$$var(\theta_r) = \left(\frac{\lambda}{2\pi}\right)^2 \cdot var(\phi) \tag{4.9}$$

Substituting equation 4.8 into equation 4.9 gives:

$$var(\theta_r) = \left(\frac{\lambda}{2\pi}\right)^2 \cdot \frac{1}{2N \cdot \gamma} = \left(\frac{c}{2\sqrt{2}\pi f}\right)^2 \cdot \frac{1}{N \cdot \gamma} \tag{4.10}$$

The time of arrival variance due to AWGN is expressed as:

$$\sigma^2_{TOA} = \left(\frac{c}{2\sqrt{2}\pi f}\right)^2 \cdot \frac{1}{N \cdot \gamma} = \frac{337.4^2}{N \cdot \gamma} \tag{4.11}$$

where f is the frequency and is equal to 10^5 Hz and c is the speed of light in vacuum taken to be equal to 2.9979245×10^8 m/s. This agrees with the equation proposed by Lo et. al [55]. N is the number of averaged pulses assuming that CRI is negligible. Safar [77] demonstrated that in the presence of CRI contamination, the overall number of averaged pulses is reduced due to blanking and is denoted by N_p.γ is the SNR. The next section adds the contribution of other terms to the TOA variance model using the theory of error propagation laws.

4.2 THE EXTENDED TOA VARIANCE MODEL

The TOA variance model is of the following form:

$$\sigma^2_{TOA} = \sigma^2_{TX} + \sigma^2_{ASF} + \sigma^2_{SF} + \sigma^2_{PF} \tag{4.12}$$

The TOA variance model developed by GLA researchers, was described in chapter 3 as:

$$\sigma^2_{TOA} = \sigma^2_{TX} \approx L_{impl} \frac{337.4^2}{N_p \cdot \gamma} \tag{4.13}$$

By comparing equation 4.12 with equation 4.13, it can be seen that the contributions due to σ^2_{ASF}, σ^2_{SF} and σ^2_{PF} are negligible. Safar's model treated dual-rated and single-rated stations the same way. The averaging process is also assumed to eliminate the transmitter jitter. Safar has also demonstrated that on average 83 % of the samples are discarded due to CRI contamination. The author argues that in some cases N_p may not be sufficiently large enough to diminish the error contribution of the transmitter jitter. Swaszek et al [40] suggested that $\sigma_{jitter} = 60\ ns$ for a single rated station and $\sigma_{jitter} = 90\ ns$ for a dual-rated station. The author has therefore decided to include the contribution of transmitter jitter into the TOA model for completeness. The other terms of the TOA model are derived later in this chapter.

$$\sigma^2_{TOA} = L_{impl} \frac{337.4^2}{N_p \cdot \gamma} + \frac{\sigma^2_{jitter}}{N_p} \tag{4.14}$$

It is common knowledge in the Loran community that the ASFs contribute more to the error budget compared to other propagation factors. The goal of this chapter is to describe a model relating the ASF changes to conductivity

changes. Before proceeding with the development of the TOA variance model, it is important to emphasize that conductivity changes are assumed to be the same throughout the whole coverage area. This assumption leads to two things:

1. The ASF variations can be assumed to be directly proportional to the land path distance traversed by the signal.

2. A model fit can be derived relating the TOA variance to the land path distance from the transmitter to the user's location in the coverage area.

The next section describes the experimental setup used to derive the variance of the ASFs (σ^2_{ASF}) measured over a yearly period, and their contributions in the position error estimation.

4.3 EXPERIMENTAL SET-UP

The TOA from the eLoran stations: Anthorn, Sylt, Lessay, and Soustons was recorded by the Harwich reference station from October 2009 to October 2010 at 5 seconds intervals. The raw TOA data was measured against a local GPS-disciplined Rubidium oscillator while eLoran simulator was used to calibrate out the local channel delays and any receiver processing time. The recorded TOA data had some gaps as the reference station was switched off. However, this data is deemed sufficient for this study. The literature suggests that the thermal and background atmospheric noise sources are the dominant sources of error in eLoran signal tracking and TOA measurements; and that a majority of the $(10-20)$ m position error budget is due to the short measurement noise [49]. It is, therefore, necessary that this short-term measurement noise is smoothed out from the data. The next section describes the process of smoothing out the short-term measurement noise from the TOA data.

Data Preprocessing and Outlier Removal

The TOA data was recorded at 5 seconds intervals, averaged on an hourly basis and smoothed using the Exponential Moving Average (EMA) and the Holt-Winter filters. The comparison in performance of the two filters is shown in figure 40 suggests that the Holt-Winter's filter outperforms the EMA filter on steep upwards trends. On the other hand, the EMA filter performs better when the data has frequent up and down movements. The EMA filter is chosen to remove short-term measurement noise in the data. The short-term measurement noise in the data is assumed to be zero in this experiment.

Exponential Moving Average Parameters

The α parameter of the exponential moving average filter was $1/20$.The filtering algorithm is shown below. Section 4.4 describes the land path model developed using a method of least squares.

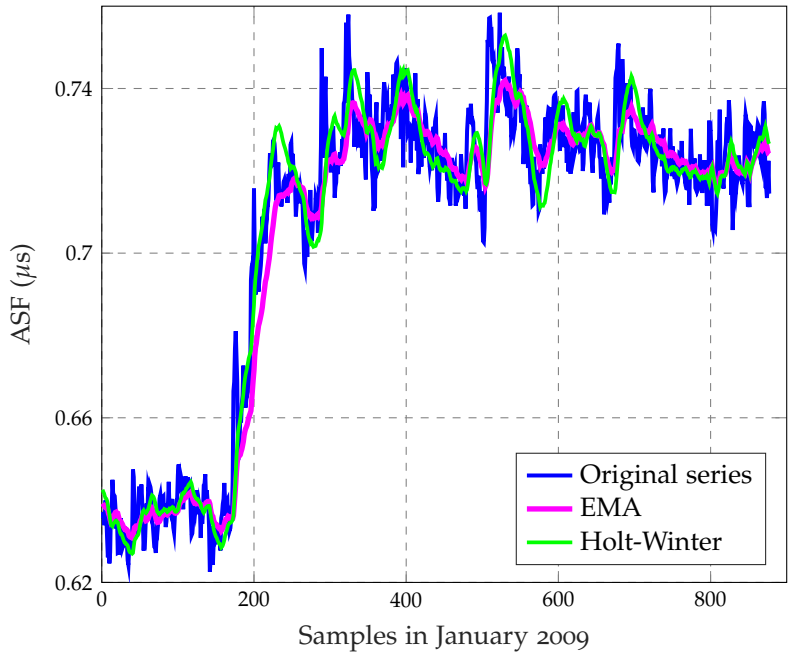

Figure 40: Comparison of the Holt-Winter and Exponential Moving Average filter.

Algorithm 1 Exponential Moving Average Filter.

```
1:  procedure EMA FILTERING
2:      outdata ← zeros(0, length(data))
3:      runningmean ← data(1)
4:      σ² ← 0.0016
5:      α ← 1/20
6:      i ← 2
7:  loop:
8:      if (data(i)-runningmean) < 5σ then
9:          runningmean ← α × data(i) + (1 − α) × runningmean.
10:         residual ← |(data(i) − runningmean)|.
11:         σ² = (1 − α) × σ² + α × residual
12:         outdata(i) ← data(i).
13:     else
14:         outdata(i) ← runningmean.
15:     end
16:     i ← i + 1
17:     goto loop.
18:     close;
```

4.4 DERIVATION OF THE LANDPATH MODEL

This section describes the postulated Landpath model relating the standard deviation of the ASF with the land path distance. The determination of the land distance along the propagation path requires an accurate vector shoreline data[1]. An accurate vector shoreline data can be downloaded from [60]. The land path distance between the transmitter and any grid point in the coverage area was determined and stored in a file. The TOA standard deviations can be normalised by a multiplication factor $(P/P_0)^{1/2}$, where P is the power of the station and P_0 is the highest power transmitted by one of the stations in the mix. The multiplication factor accounts for different power levels transmitted by the Loran stations. The standard deviations of the ASFs plotted against the land path distances were fitted to various models. The exponential model produced a better fit to the data than other models. The proposed exponential model of the normalized standard deviation of the yearly received ASF at the user's location as a function of the land path distance can be expressed as:

$$\sigma = \left[\alpha \left(\frac{P}{P_0} \right)^{1/2} \cdot \exp\left(\beta D\right) \right] \tag{4.15}$$

where D km is the land path distance between the receiver and the eLoran station and σ (m) is the estimated standard deviation. The coefficients α and β of the model can be determined using a method of least squares as: $\alpha = 0.17$m and $\beta = 0.0106 km^{-1}$.

Table 9: ASF measurement statistics from Harwich dLoran reference station.

Station ID	Year's ASF $\sigma(\mu s)$	Land Path Distance (km)	Pseudo range Std Dev. Error (m)
(6731M) Lessay	0.3579	149	4
(6731X) Soustons	1.1631	735	206
(6731Y) Anthorn	0.7829	446	9
(6731Z) Sylt	0.1849	17	2
(7499M) Sylt	0.2219	17	2
(7499X) Lessay	0.3520	149	4

Table 9 shows a summary of the measured ASF data from Anthorn, Lessay, Soustons, and Sylt at the Harwich reference station. The values obtained in this experiment are within the order of magnitude compared to the values

1 A vector shoreline is a digital data file containing the shorelines and international boundaries of the countries. A close inspection of the vector shoreline data suggests that it is made up of splines that join together two neighbouring sample points of a map. The sample points are sparse and may contain some gaps.

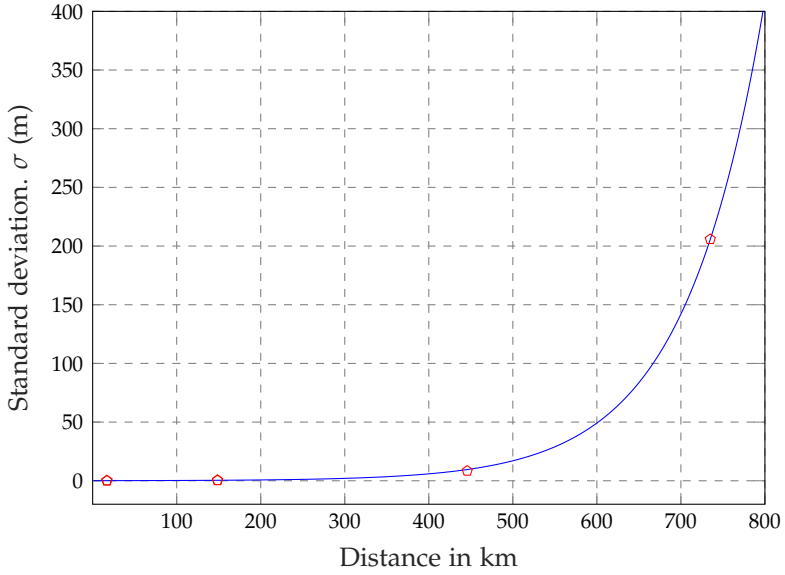

Figure 41: Correlation of σ_{ASF} with distance.

obtained in a similar study that was conducted in the United States [92]. The TOA variance model includes the effect of conductivity changes on the measured ASFs. The procedure described in chapter 3 and proposed TOA variance model is used to model repeatable accuracy throughout the coverage area. Figure 42 shows the repeatable accuracy plot excluding the effects of dLoran. This plot excludes the effects of dLoran. The effects of differential dLoran are included only in harbours and ports. Figure 43 shows the repeatable accuracy plot due to the land path effects. This work assumes that the differential corrections remain valid in a circle of a radius of 50 km centred at the reference station. The system TOA variance is given by:

$$\sigma^2_{TOA} = \begin{cases} L_{impl}\dfrac{337.4^2}{N_p \cdot \gamma} + \frac{\sigma^2_{jitter}}{N_p} & d \leq 50km, \\ L_{impl}\dfrac{337.4^2}{N_p \cdot \gamma} + \frac{\sigma^2_{jitter}}{N_p} + \left[\alpha^2\left(\frac{P}{P_0}\right) \cdot \exp\left(2\beta D\right)\right] & d > 50km \end{cases} \tag{4.16}$$

The figures 42 and 43 show that accuracy is better in the East of the British Isles than in the West. The blue circles in figure 43 represent the coverage due to reference stations. This plot also shows that 19 out of the 21 possible port locations experience repeatable accuracy below 10 m. The assumptions and models used in generating the coverage plots shown in figure 42 and figure 43 are summarised in table 10. The results of the accuracy plot shown in figure 43 suggests that at least two stations are needed in the West of the British Isles, or somewhere in the Republic of Ireland to improve coverage in the sea between Britain and Ireland. Safar [77] developed a CRI compensated pseudorange measurement error model for a transmitter operating under a certain GRI and his model is extended in this work to include the effects of the land path on the on the measured pseudorange errors.

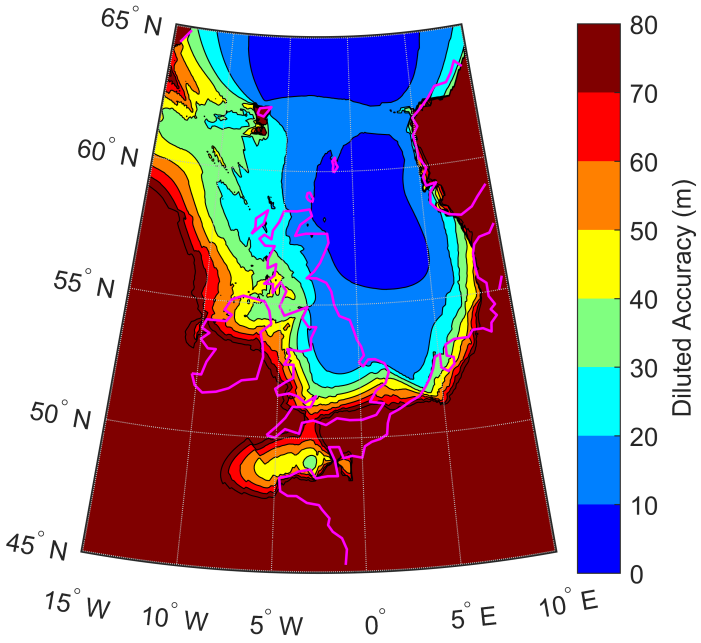

Figure 42: Modified Repeatable Accuracy without the effects of dLoran.

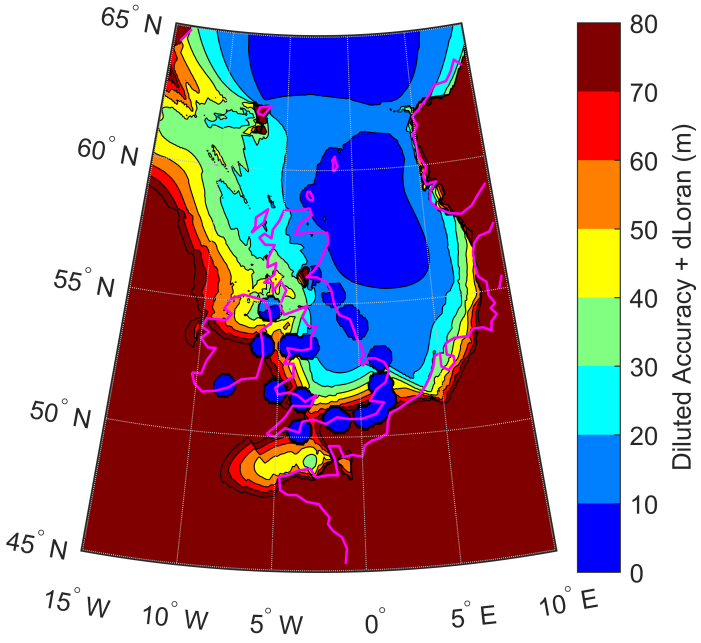

Figure 43: Modified Accuracy including the effects of dLoran.

Pseudorange Error Analysis

A CRI model developed by Safar was summarised in chapter 3. In this study, an extra term showing the effect of conductivity changes on the TOA variance can be added to the TOA variance model as shown in equation 4.17.The pseudorange measurement error is given by:

$$\sigma_p = \sqrt{K_{impl}\frac{GRI}{(1-L_b)\cdot\gamma} + \left[\alpha^2\left(\frac{P}{P_0}\right)\cdot\exp\left(2\beta D\right)\right]} \tag{4.17}$$

where $K_{impl} \approx 0.7$ and L_b represents the blanking loss. The plot of the pseudorange measurement error due to additive white Gaussian noise and changes in conductivity is shown in figure 44. The transmitter jitter is assumed to be negligible.The illustration suggests that the pseudorange error increases with decreasing SNR; and that the pseudorange error increases with increasing land path distance between the transmitters and the user's location

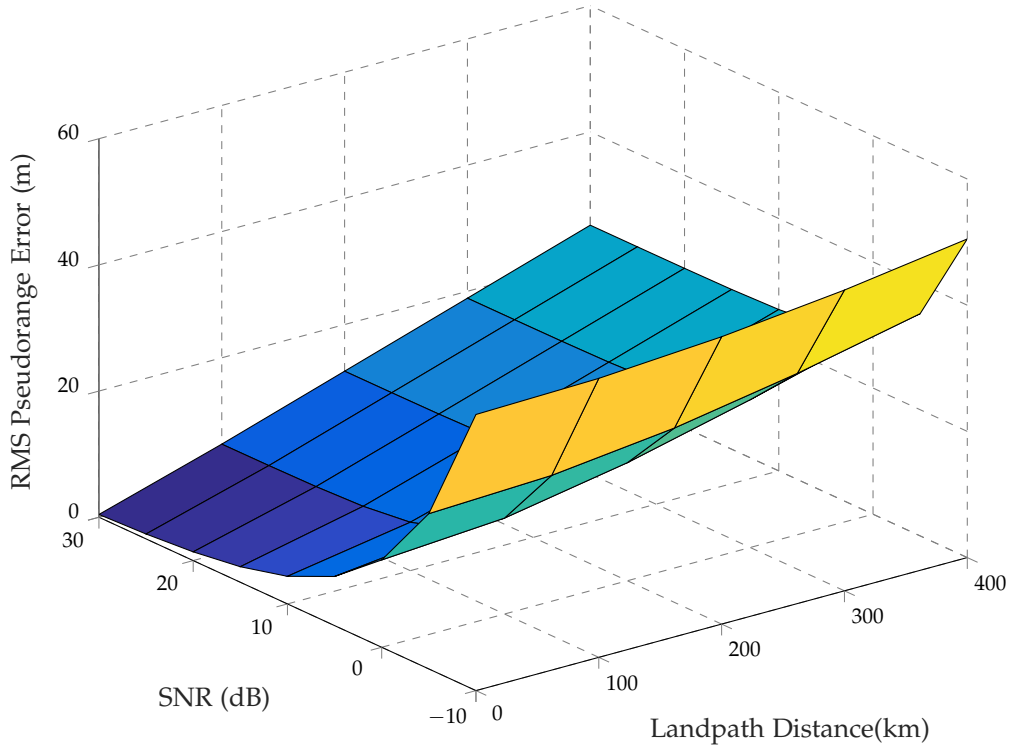

Figure 44: Pseudorange error for GRI 6731 due to additive white Gaussian noise (AWGN) and changes in conductivity. Integration time, $T_i \approx 5$s.

The variance of the primary factor delay is modelled in section 4.5 by studying the effects of the meteorological parameters on the refractive index of the atmosphere along transmitter-receiver paths.

4.5 DERIVATION OF THE WEATHER MODEL

The eLoran signal primary factor delay depends on the following characteristics of the propagation path:

- Transmitter-receiver geodetic range.

Table 10: Summary of assumptions and models used in evaluating coverage performance.

Parameter	Model/Assumptions
Groundwave	
Field Strength	Millington;ITU-R P.368 – 9
Ground Conductivity	ITU-R P.832 – 2
Sky wave	
Field Strength	ITU-R P.1147 – 2
Delay	Morris
Height of Ionosphere	100km
CRI	Safar Thesis [77]
Interfers	All NELS stations
Receiver	

- Atmospheric refractive index at the Earth's surface.
- vertical lapse rate (gradient) of the refractive index.

The Vincenty's algorithm described in chapter 3 can be used to determine the geodetic range from the transmitter to the receiver. Section 4.5.1 describes the model of the refractive index of the atmosphere at the Earth's surface.

4.5.1 *Refractive Index*

Refractive index (η) is related to the meteorological parameters [31] by the following expression:

$$\eta = 1.0 + \left[\underbrace{77.6\frac{P}{T}}_{dry-term} + \underbrace{3730\frac{e_s \cdot RH}{T^2}}_{wet-term} \right] \times 10^{-6} \tag{4.18}$$

Swaszek et. al [93] suggested that the dry term contributes 90 % to the refractive index compared to the wet term.

$$\eta = 1.0 + 77.6\frac{P}{T} \times 10^{-6} \tag{4.19}$$

The temperature and pressure information for a yearly period from October 2009 to October 2010 was extracted from the European Centre for Medium-Range Weather Forecasting (ECMWF) ERA-40 dataset downloaded from the British Atmospheric Data Centre (BADC) [17]. The extracted data were interpolated using a bilinear transformation to fit the grid equivalent to the GLA geographical area. The figure 45 and 46 show temperature and pressure plots.

4.5.2 *Experimental Set-up for Calculation of refractivity*

In practice, the primary delay factor is estimated from the pressure and temperature measured at the reference station since it may not be feasible to monitor the weather parameters at all points in the coverage area. In this case, it is assumed that the measured values at the reference station represent the average values of these parameters along the propagation path.

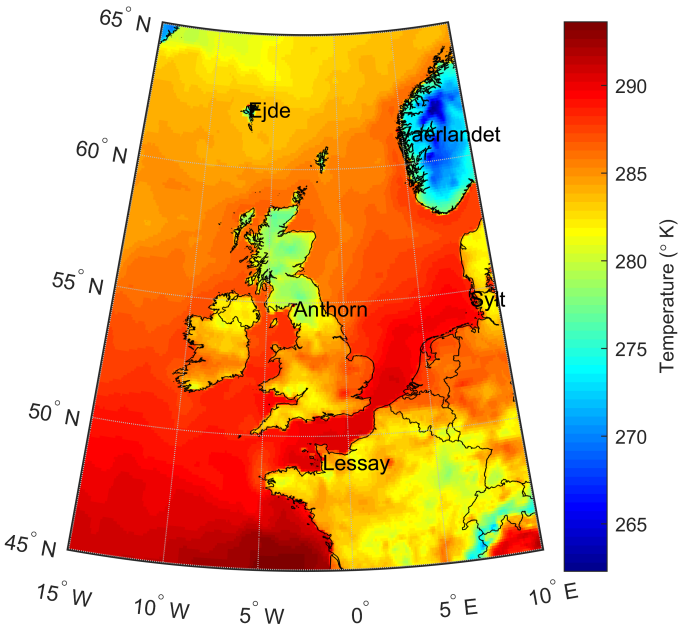

Figure 45: Temperature in the Coverage area. The northern part of the UK is colder than the South. The results suggest that South-East is warmer than anywhere else in the UK and that Norway experiences lowest temperatures in the region.

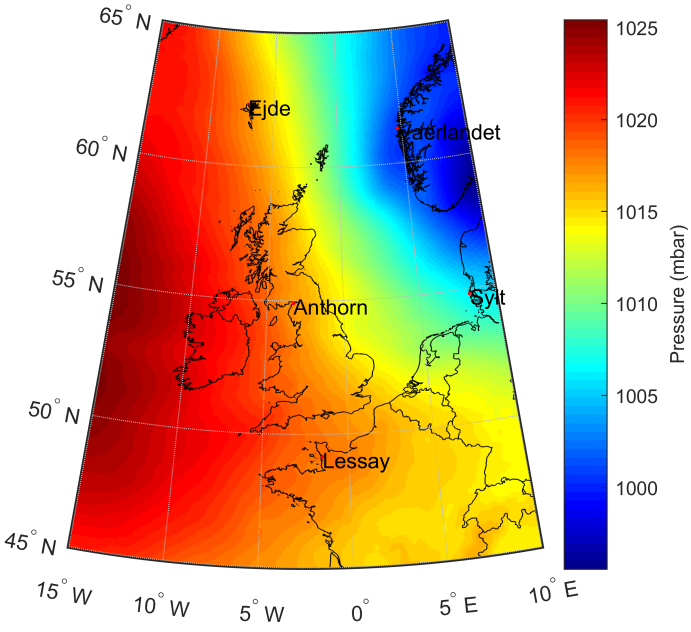

Figure 46: Atmospheric Pressure across the coverage area. The coverage results suggest that high pressure levels are experienced in the Antlantic Ocean.

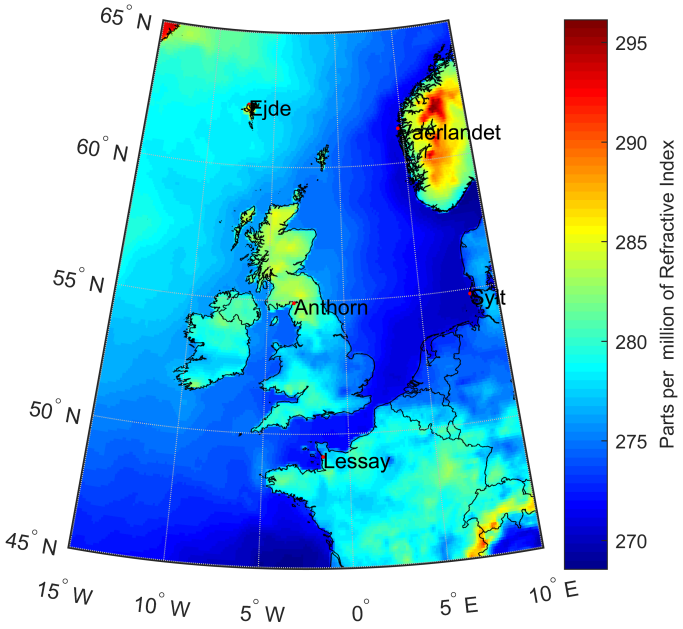

Figure 47: Refractivity across the coverage area.

This assumption is not realistic since the signal delay is not constant and is dependent on the changes in the weather parameters along the propagation path. This procedure provides a good start for a working model. The ECMWF ERA-40 dataset was interpolated to cover the entire coverage area to estimate refractivity at every grid point in the coverage area. Refractivity is determined by the following four-step procedure described below.

1. Divide the path from the transmitter to the receiver into equal segments.

2. Determine refractivity of each path segment.

3. Determine the delay suffered by the signal at each segment.

4. Determine primary factor delay by summing the contributions of all the segments.

The plot of refractivity across the coverage area on a typical day is shown in figure 47. The plot shows that refractivity is higher in Norway and Scotland and lower in the South-West of the British Isles. The primary factor delay is higher in Norway and Scotland, and lower in the South-West of Britain.

The next section discusses the developed framework for approximating the variance of the refractive index of the atmosphere observed at any point in the coverage area. The Harwich location is used here as an example.

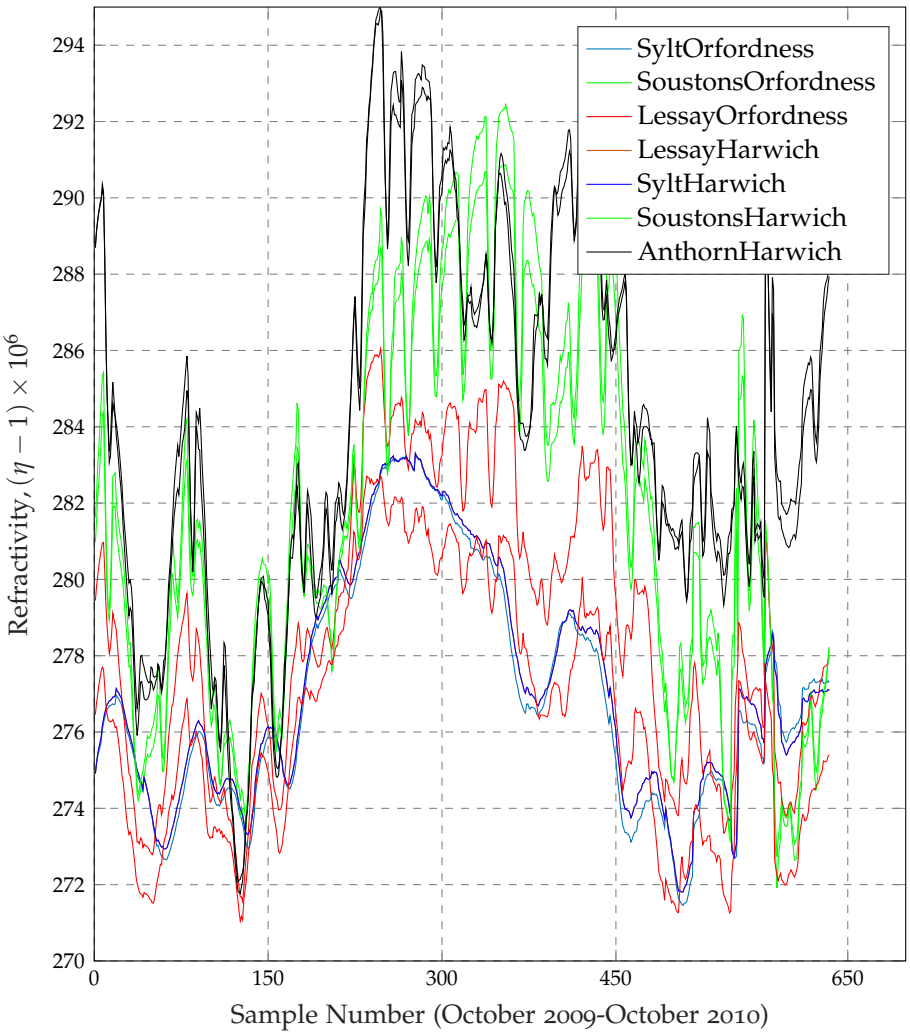

Figure 48: Filtered refractivity of the signals received at Harwich and Orfordness.Harwich and Orfordness are 25.8 km apart. The curves demonstrates that throughout the year, the values of refractivity at the locations are closely correlated.However, there is more decorrelation on the Soustons signal compared to other signals.

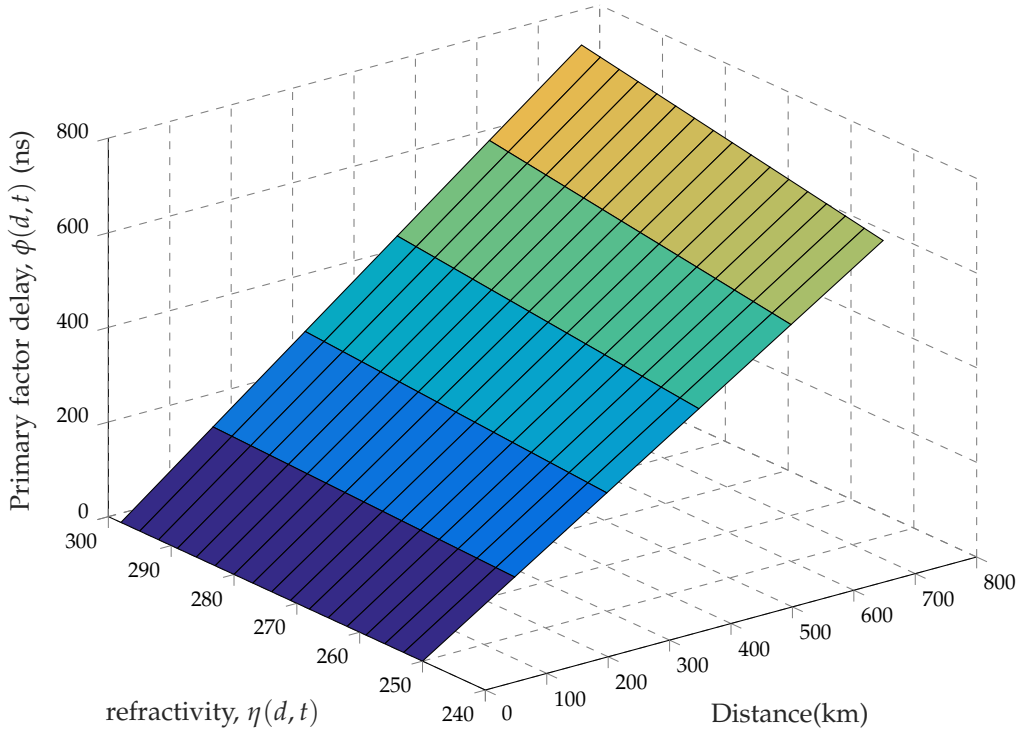

Figure 49: Primary factor delay, $\phi(d,t)$, at distance, d and average refractivity $\eta(d,t)$, from the transmitter.

Determination of the σ^2_{PF} Parameter

The primary factor delay of a signal propagating in the atmosphere is given by:

$$PF = \frac{d}{c}\eta \tag{4.20}$$

The variance of the primary factor delay is derived using equation 4.20 as:

$$\begin{aligned} \sigma^2_{PF} &= (\tfrac{d}{c})^2 \cdot \sigma^2_\eta \\ &= d^2 \cdot \sigma^2_\eta \quad m^2 \end{aligned} \tag{4.21}$$

Taking the variance on both sides of equation 4.18 gives:

$$\sigma^2_\eta = \sigma^2_N \cdot 10^{-12} \tag{4.22}$$

The TOA variance in square meters due to the variations of the refractive index is derived by combining equations 4.21 and 4.22 and is given by:

$$\sigma^2_{PF} = d^2 \cdot (\sigma^2_N \cdot 10^{-12}) m^2 \tag{4.23}$$

where σ_N is the standard deviation of refractivity of the primary factor delay along the propagation path and d is the path distance .

The time series of the hourly refractive index at all the grid points for a yearly period between October 2009-October 2010 was analysed, and their variances used to quantify the contribution of the weather changes in the

primary factor delay of the received signals. The pseudorange error performance of the weather model and the combination of land path and weather models are shown in figure 50 and 51 respectively. The standard deviation of refractivity varies from 9.6 to 17.4 across the whole coverage area. The extended TOA variance model can now be expressed as:

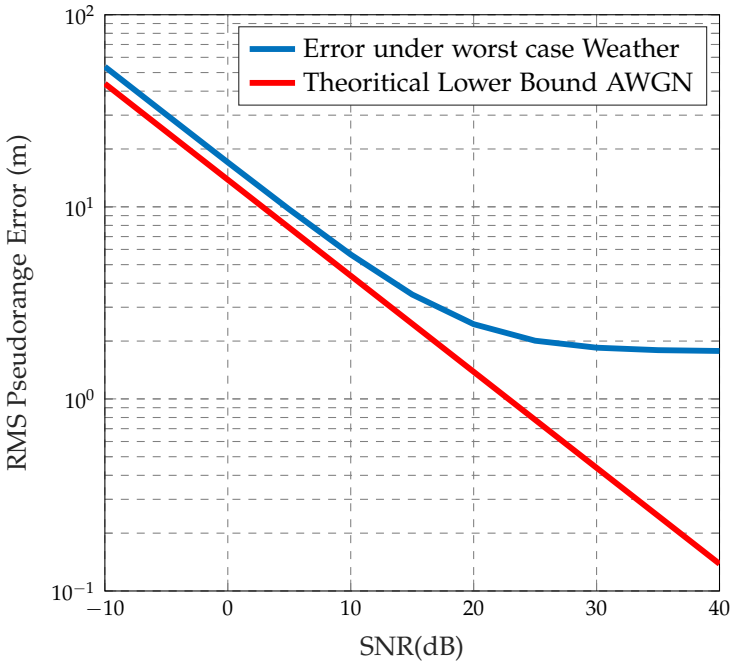

Figure 50: Pseudorange error performance comparison between AWGN and Weather model. It can be seen that as SNR increases the pseudorange error of the weather model asymptotically reaches 1.7 m.

$$\sigma^2_{TOA} = \begin{cases} L_{impl}\dfrac{337.4^2}{N_p \cdot \gamma} & d \leq 50km, \\ L_{impl}\dfrac{337.4^2}{N_p \cdot \gamma} + \left[\alpha^2\left(\frac{P}{P_0}\right) \cdot \exp\left(2\beta D\right)\right] + d^2 \cdot \sigma_N^2 \cdot 10^{-12} & d > 50km \end{cases} \tag{4.24}$$

In the repeatable accuracy coverage plots, σ_N is used to dilute accuracy everywhere except in regions where dLoran is expected.

4.6 MODEL VALIDATION USING REAL DATA

The theoretical results obtained using the Landpath model were tested and validated using measured data recorded at the Blacksod lighthouse, Ireland in 2009. The measurement data used here does not include dLoran. Figure 54 shows the eLoran accuracy performance of 77 m. The Landpath model gives an accuracy of 86.9 m assuming the skywave fading conditions and 69 m without skywave fading. The discrepancy may be due to the inaccuracy of the Landpath model. The accuracy of the model can be enhanced using more data from various monitoring sites. At the time of conducting this

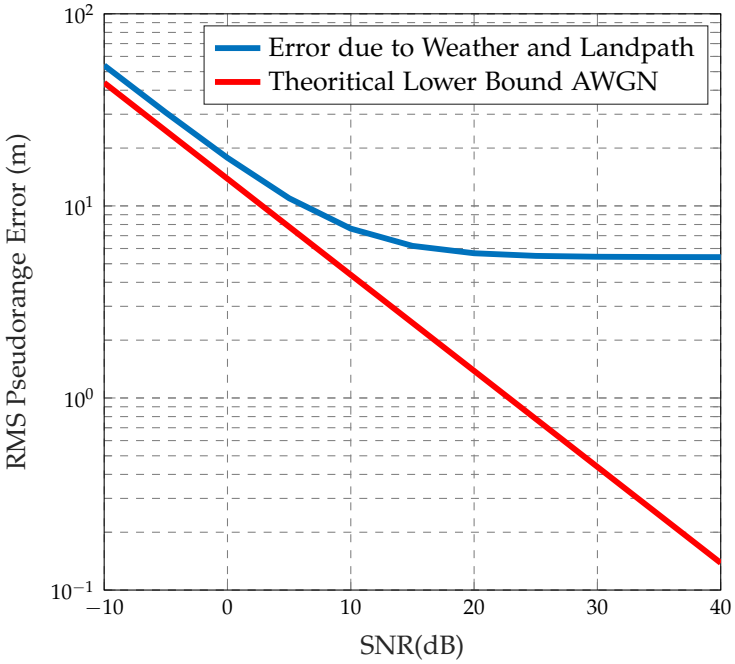

Figure 51: Pseudorange error performance comparison between AWGN and Landpath model. It can be seen that as SNR increases the pseudorange error of the Landpath and the weather models asymptotically reaches 5.5 m.

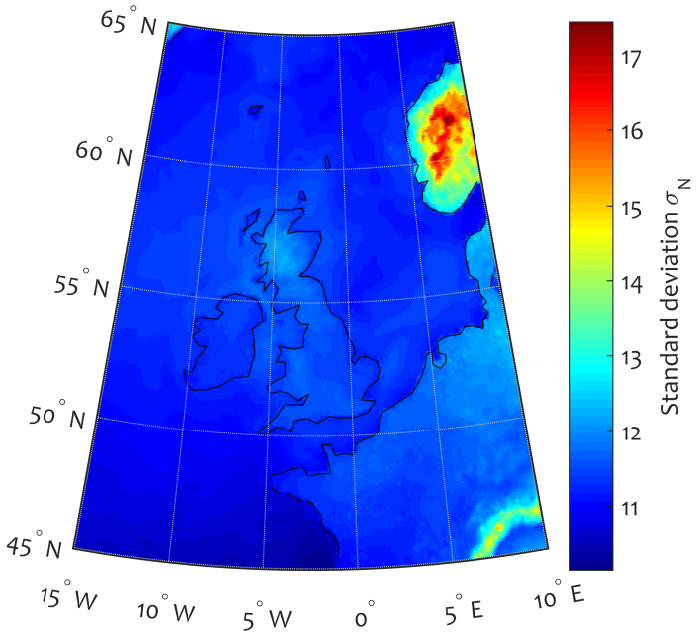

Figure 52: The Standard deviation of Refractivity across the Coverage Area (min =9.6) and (max=17.4) .

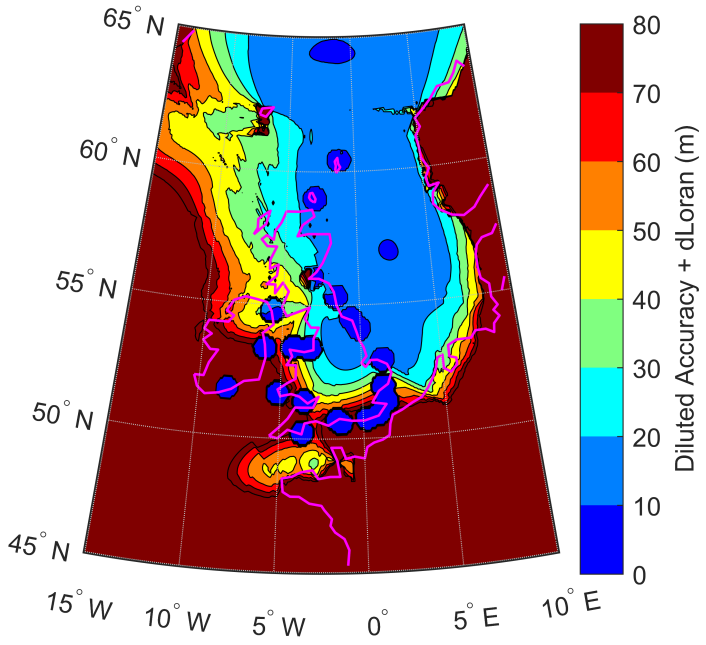

Figure 53: Diluted Accuracy including the effects of dLoran.

experiment, there was only one monitor station across the GLA area. Table 11 compares the measured SNR with the predicted SNRs.

Table 11: Table showing comparison between the measured SNR and Model SNR. The predicted SNR are on average, 6 dB worse than the measured SNRs.

Station	Landpath Distance (km)	Measured SNR (dB)	Predicted SNR (dB)
Anthorn (6731)	234.0	13.1	11.5
Sylt (6731)	299.3	-2.3	-9.0
Lessay (7499)	389.7	5.44	-3
Edje (9007)	31.3	9.8	-3
Vaerlandet (7499)	191.1	-3	-9
Soustons	250.7	-5.4	-11

4.7 POSITIONING ERROR ESTIMATION

This section illustrates the accuracy performance of eLoran in Europe before the eLoran transmissions from France and Norway were switched off. TOA techniques use the information of the signal travel time from transmitters to the receiver. By multiplying the transit time and the speed of light gives the distance between the transmitter and the receiver. Based on the geometrical principle, the receiver lies on a circle centred at the transmitter location. The location of the receiver is determined by the intersection of circles. Three TOA techniques namely; TOA with synchronization, TOA without synchronization and Time of Difference of Arrival (TDOA) are well known in the literature. In the case of TDOA, the transmitters are synchronized, the receivers are not and the knowledge of the time of transmission is not required

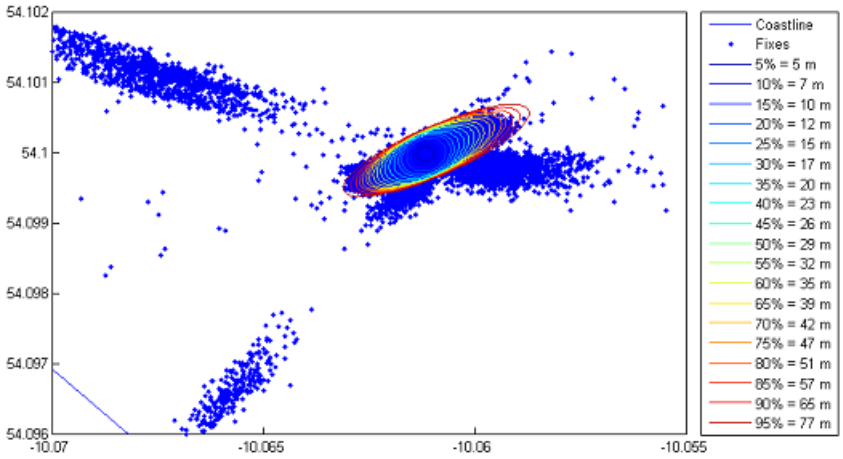

Figure 54: Position accuracy performance at Blacksod, Ireland ,Picture courtesy the GLAs.

either. For any pair of transmitters, TDOA yields a hyperbolic curve with the transmitter at the foci and the position of the user's receiver can be determined as the intersection of the hyperbolic lines of position. The TDOA technique was used in Loran-C.

This section also presents a theoretical analysis of the performance between TOA with and without perfect clock synchronization. The repeatable accuracy plots are also presented using the using the TOA techniques, the developed land path, and weather model. The next section describes the theory of TOA techniques used in positioning estimation.

LOCATION ESTIMATION MODEL

The user's location in a two-dimensional location system can be determined using latitude and longitude of the transmitters using TOA techniques. Let (φ, λ) denote the latitude and longitude of user's receiver. The changes in the latitude and longitude can be conveniently denoted as $(\Delta\varphi, \Delta\omega)$. The location positions (φ, λ) and $(\Delta\varphi, \Delta\omega)$ satisfy the following equations:

$$\tilde{\varphi} = \varphi + \Delta\omega \qquad \tilde{\lambda} = \lambda + \Delta\omega \sec\varphi \tag{4.25}$$

The location equation of the measurement parameter P can be modelled as $P = P(\Delta\varphi, \Delta\omega)$. Since P is non-linear, it can be linearised using first-order Taylor-series expansion as:

$$\bar{P}_i = \hat{P}_i + \frac{\partial \hat{P}}{\partial \varphi} d\varphi + \frac{\partial \hat{P}}{\partial \omega} d\omega \tag{4.26}$$

where $\bar{P}_i$ and $\hat{P}_i$ denote the true measurement and the estimated position of the i^{th} transmitter respectively. Generally, measurements from different

transmitters can be obtained at the same time and conveniently arranged in a matrix form as:

$$\begin{bmatrix} \delta P_1 \\ \delta P_2 \\ \vdots \\ \delta P_n \end{bmatrix} = \begin{bmatrix} \frac{\partial \hat{P}_1}{\partial \varphi} & \frac{\partial \hat{P}_1}{\partial \omega} \\ \frac{\partial \hat{P}_2}{\partial \varphi} & \frac{\partial \hat{P}_2}{\partial \omega} \\ \vdots & \vdots \\ \frac{\partial \hat{P}_n}{\partial \varphi} & \frac{\partial \hat{P}_n}{\partial \omega} \end{bmatrix} \begin{bmatrix} d\varphi \\ d\omega \end{bmatrix} \tag{4.27}$$

where $\delta P_i = \bar{P}_i - \hat{P}_i$. Equation 4.27 can be rewritten as:

$$\mathbf{P} = \mathbf{A}\ \mathbf{d\Psi} \tag{4.28}$$

The least square solution of the estimated position, $(\Delta\varphi, \Delta\omega)$ is now given by:

$$\mathbf{d\Psi} = (\mathbf{A}^T\mathbf{A})^{-1}\mathbf{A}^T\mathbf{P} \tag{4.29}$$

As a result, the latitude and longitude (φ, λ) of the receiver can be obtained using equation 4.29. The effects of the linearisation process can be neglected if the measurement errors are assumed to be small. However, if the measurement errors are significant, then the position matrix can be rewritten as:

$$\mathbf{A}[\mathbf{d\Psi} + \varepsilon_r] = \mathbf{P} + \varepsilon \tag{4.30}$$

where ε_r and ε are the measurement and position error vector respectively. The least solution of the position error vector is given by:

$$\varepsilon_r = (\mathbf{A}^T\mathbf{A})^{-1}\mathbf{A}^T\varepsilon \tag{4.31}$$

Equation 4.31 represents the relationship between the position error and the measurement error. The expectation and the variance of the position error are determined from the measurement error model. In practice, the probability distribution of the measurement error model is not known exactly and thus the following assumptions are often made about the measurement error model:

1. The measurement error, ϵ, follows a normal distribution with mean $E(\varepsilon) = \mathbf{0}$ and variance, $cov(\varepsilon) = \sigma^2\mathbf{I}$. where $\mathbf{I}$ is the identity matrix, and σ is the standard deviation of the measurement error.

2. The measurement errors of signals received from two different transmitters at the receiver are uncorrelated. Thus, the covariance matrix is simply a diagonal matrix:

$$cov(\varepsilon_r) = E(\varepsilon_r\varepsilon_r^T) = (\mathbf{A}^T\mathbf{A})^{-1}\sigma^2$$

The matrix, $(\mathbf{A}^T\mathbf{A})^{-1}$ holds geometric accuracy and correlation information of the position solutions and is used to measure the eLoran accuracy at a location.

From equation 4.27, the following can be obtained:

$$\begin{aligned} \alpha_i &= \frac{\partial \hat{P}_i}{\partial \varphi} = -\cos\kappa_i \\ \beta_i &= \frac{\partial \hat{P}_i}{\partial \omega} = -\sin\kappa_i \\ \delta\hat{P}_i &= \bar{P}_i - \hat{P}_i \end{aligned} \tag{4.32}$$

where κ_i is the estimated azimuth angle seen from estimated position of the receiver to the transmitter i. $\bar{P}_i$ and $\hat{P}_i$ represent the measured and estimated distance between the receiver and the i^{th} transmitter, respectively. The angle κ_i is measured in radians and the distance, P_i can be determined using the following expressions:

$$\begin{aligned} \kappa_i &= \tan^{-1}\left(\frac{\cos(\varphi_2)\sin(\lambda_1-\lambda_2)}{\cos\varphi_1\sin\varphi_2 - \sin\varphi_1\cos\varphi_2\cos(\lambda_1-\lambda_2)}\right) \\ \hat{P} &= \cos^{-1}(\sin\varphi_1\sin\varphi_2 - \cos\varphi_1\cos\varphi_2\cos(\lambda_1-\lambda_2)) \end{aligned} \tag{4.33}$$

If the receiver's clock is perfectly synchronized with the transmitter clock, the time taken from the transmitter to the receiver can be measured precisely and their separation distance is obtained by multiplying the time taken with the signal propagation speed. The coordinates of the receiver can be obtained from at least two transmitters.

$$\mathbf{h} = \mathbf{A} = \begin{bmatrix} -\cos\kappa_i & -\sin\kappa_i \\ \vdots & \vdots \\ -\cos\kappa_n & -\sin\kappa_n \end{bmatrix} \tag{4.34}$$

The position error is given by:

$$\varepsilon_r = (\mathbf{h}^T\mathbf{h})^{-1}\mathbf{h}^T\varepsilon \tag{4.35}$$

The covariance matrix of the position error can be determined from

$$cov(\varepsilon_r) = (\mathbf{h}^T\mathbf{h})^{-1}\sigma^2 \tag{4.36}$$

Time synchronisation is difficult to achieve in reality as it requires expensive clock. Generally, a clock bias is augmented to the two-dimensional position vector to form a three-dimensional vector. In this case, the estimation of the location of the receiver requires three independent TOA measurements. Equation 4.26 can be rewritten as:

$$\bar{P}_i = \hat{P}_i + \frac{\partial\hat{P}}{\partial\varphi}d\varphi + \frac{\partial\hat{P}}{\partial\omega}d\omega + dC \tag{4.37}$$

where $dC = c \cdot dt$. The term dt, denotes the receiver clock bias and c is the signal propagation speed, which is normally taken to be equal to the speed of light in vacuum. The position error at the user's location can be rewritten as:

$$\begin{bmatrix} \delta P_1 \\ \delta P_2 \\ \vdots \\ \delta P_n \end{bmatrix} = \begin{bmatrix} \frac{\partial\hat{P}_1}{\partial\varphi} & \frac{\partial\hat{P}_1}{\partial\omega} & 1 \\ \frac{\partial\hat{P}_2}{\partial\varphi} & \frac{\partial\hat{P}_2}{\partial\omega} & 1 \\ \vdots & \vdots & \vdots \\ \frac{\partial\hat{P}_n}{\partial\varphi} & \frac{\partial\hat{P}_n}{\partial\omega} & 1 \end{bmatrix} \begin{bmatrix} d\varphi \\ d\omega \\ dC \end{bmatrix} \tag{4.38}$$

The least square solution to equation 4.38 is given by:

$$\tilde{\varepsilon_r} = (\mathbf{H}^T\mathbf{H})^{-1}\mathbf{H}^T\varepsilon \tag{4.39}$$

The covariance matrix of the position error is given by:

$$cov(\tilde{\varepsilon_r}) = (\mathbf{H}^T\mathbf{H})^{-1}\sigma^2 \tag{4.40}$$

The above procedure is repeated in the development of the TDOA measurement model.

Measurement Model for TDOA

Unlike the TOA technique that directly estimates the clock bias included in the position state vector, the TDOA eliminates the clock bias from the position state vector. In Loran-C, the master station TOA is selected as the reference and the secondaries' TOA are subtracted from the master station TOA resulting in a TDOA measurement vector. The TDOA can be formulated like in the TOA model as:

$$\begin{aligned} \alpha_i &= \frac{\partial \hat{P}_i}{\partial \varphi} = -\cos\kappa_m + \cos\kappa_i \\ \beta_i &= \frac{\partial \hat{P}_i}{\partial \omega} = -\sin\kappa_m + \sin\kappa_i \\ \delta\hat{P}_i &= (\bar{P}_m - \bar{P}_i) - (\hat{P}_i - \hat{P}_i) \end{aligned} \tag{4.41}$$

The subscript m denotes the master station. For clarity, the master station is assigned, $m = 1$. Then:

$$\mathbf{G} = \mathbf{A} = \begin{bmatrix} -\cos\kappa_1 + \cos\kappa_i & -\sin\kappa_1 + \sin\kappa_i \\ \vdots & \vdots \\ -\cos\kappa_1 + \cos\kappa_n & -\sin\kappa_1 + \sin\kappa_n \end{bmatrix} \tag{4.42}$$

The position error and its covariance matrix are given by:

$$\acute{\varepsilon_r} = (\mathbf{G}^T\mathbf{G})^{-1}\mathbf{G}^T\varepsilon \tag{4.43}$$

$$cov(\acute{\varepsilon_r}) = (\mathbf{G}^T\mathbf{G})^{-1}\sigma^2 \tag{4.44}$$

4.7.1 *Position Error Comparison*

The goal in eLoran coverage prediction is to analyse all the components that contribute to the position error budget and develop techniques that can reduce the contribution of these components so that better position accuracy can be achieved. In this section, the developed position error methods are compared. Comparison of position errors for different techniques is the same as comparing their covariance matrices. In the previous section, the covariance matrices for synchronised TOA, non-synchronised TOA and TDOA were given as:

$$\begin{aligned} cov(\varepsilon_{rTOA}) &= (\mathbf{h}^T\mathbf{h})^{-1}\sigma^2 \\ cov(\tilde{\varepsilon}_{rTOA}) &= (\mathbf{A}^T\mathbf{A})^{-1}\sigma^2 \\ cov(\acute{\varepsilon}_{rTDOA}) &= (\mathbf{G}^T\mathbf{G})^{-1}\sigma^2 \end{aligned} \tag{4.45}$$

If the same measurements are used to compute the TOA and TDOA covariance matrices, then the variances are equal. This reduces the task to a comparison of the weight coefficient matrices of all the given cases.

Comparing TOA with Time Synchronisation with TDOA

From the equations developed above, we can relate the covariance matrices of the position errors derived from the two techniques by a transformation matrix $\mathbf{M}$ given by:

$$\mathbf{M} = [\mathbf{d}_2 \quad -\mathbf{I}_2] \tag{4.46}$$

where $\mathbf{d}_2$ and $\mathbf{I}_2$ are the unit matrix and identity matrix of size 2 respectively. The covariance matrix of the TDOA can be conveniently expressed as:

$$cov(\acute{\varepsilon}_{rTDOA}) = (\mathbf{h}^T\mathbf{M}^T\mathbf{M}\mathbf{h})^{-1}\sigma^2 = (\mathbf{h}^T\mathbf{h} + \mathbf{h}^T\mathbf{N}\mathbf{h})\sigma^2 \tag{4.47}$$

where $\mathbf{N}$ is given by:

$$\mathbf{N} = \begin{bmatrix} 1 & -1 & -1 \\ -1 & 0 & 0 \\ -1 & 0 & 0 \end{bmatrix} \tag{4.48}$$

Using the Sherman-Morrison-Woodbury Lemma for matrix inversions, the following identity holds:

$$(\mathbf{A} - \mathbf{B}\mathbf{D}^{-1}\mathbf{C})^{-1} = \mathbf{A}^{-1} + \mathbf{A}^{-1}\mathbf{B}(\mathbf{D} - \mathbf{C}\mathbf{A}^{-1}\mathbf{B})^{-1}\mathbf{C}\mathbf{A}^{-1} \tag{4.49}$$

By comparing equation 4.47 and 4.49 we get,

$$\mathbf{A} = \mathbf{h}^T\mathbf{h} \qquad \mathbf{B} = \mathbf{h}^T \qquad \mathbf{D}^{-1} = \mathbf{N} \qquad -\mathbf{C} = \mathbf{h} \tag{4.50}$$

Expressing equation 4.47 in the same form as the right hand side of equation 4.49, we get:

$$\begin{aligned} cov(\acute{\varepsilon}_{rTDOA}) &= (\mathbf{h}^T\mathbf{h})^{-1}\sigma^2 - \underbrace{(\mathbf{h}^T\mathbf{h})^{-1}\mathbf{h}^T(\mathbf{N} - \mathbf{h}(\mathbf{h}^T\mathbf{h})^{-1}\mathbf{h}^T)\mathbf{h}(\mathbf{h}^T\mathbf{h})^{-1}}_{\mathbf{F}}\sigma^2 \\ &= (\mathbf{h}^T\mathbf{h})^{-1}\sigma^2 + \underbrace{\left[(\mathbf{h}^T\mathbf{h})^{-1} - (\mathbf{h}^T\mathbf{h})^{-1}\mathbf{h}^T\mathbf{N}(\mathbf{h}^T\mathbf{h})^{-1}\right]}_{\mathbf{F}}\sigma^2 \\ &= 2(\mathbf{h}^T\mathbf{h})^{-1}\sigma^2 - \underbrace{\left[(\mathbf{h}^T\mathbf{h})^{-1}\mathbf{h}^T\mathbf{N}(\mathbf{h}^T\mathbf{h})^{-1}\right]}_{\mathbf{S}}\sigma^2 \end{aligned} \tag{4.51}$$

The matrix $\mathbf{S}$ can either be positive definite[2] or negative definite [3] matrix, and thus it is not easy to determine the performance of TOA with time synchronisation against the TDOA technique. In the next section, the performance of TOA without synchronisation is compared to the TDOA technique.

2 Is a matrix whose symmetric or Hermitian part has all positive eigen values.
3 A negative semi-definite matrix is a Hermitian matrix whose eigen values are non-positive.

Comparing TOA without Synchronisation with TDOA

The covariance of TOA without synchronization can be stated as:

$$cov(\tilde{\varepsilon}_{rTOA}) = (3\mathbf{G}^T\mathbf{R}\mathbf{G})^{-1}\sigma^2 \tag{4.52}$$

where:

$$\mathbf{R} = \begin{bmatrix} 2 & -1 \\ -1 & 2 \end{bmatrix} \tag{4.53}$$

Hence

$$\begin{aligned} & cov(\tilde{\varepsilon}_{rTOA}) \\ &= \left[3(\mathbf{G}^T\mathbf{R}\mathbf{G})^{-1} - (\mathbf{G}^T\mathbf{G})^{-1}\right]\sigma^2 \\ &= \tfrac{1}{|\mathbf{G}^T\mathbf{G}|}\begin{bmatrix} a_{11} & a_{12} \\ a_{21} & a_{22} \end{bmatrix}\sigma^2 \end{aligned} \tag{4.54}$$

where

$$\begin{aligned} a_{11} &= \sin^2\kappa_2 + \sin^2\kappa_3 - 2\sin^2\kappa_2\sin^2\kappa_3 \\ &= (\sin\kappa_2 - \sin\kappa_3)^2 \geq 0, \\ a_{22} &= \cos^2\kappa_2 + \cos^2\kappa_3 - 2\cos^2\kappa_2\cos^2\kappa_3 \\ &= (\cos\kappa_2 - \cos\kappa_3)^2 \geq 0, \end{aligned} \tag{4.55}$$

Equation 4.55 implies that the TOA variance in a receiver without a tight synchronous clock will always be greater than TDOA variance for the same transmitter measurements observed at the receiver. To verify this conclusion, the developed accuracy model for eLoran coverage prediction tool is used, where the receiver is assumed to be located at Harwich and is receiving signals from Anthorn, Sylt and Soustons. Table 12 gives information about the three transmitters. The covariance matrices of the position error

Table 12: ASF measurement statistics from Harwich dLoran reference station.

Location	Latitude	Longitude
Anthorn	54.91120805	−3.2872811
Lessay	49.148673333	−1.5047302778
Soustons	43.73974972	−1.38044000
Receiver location (Harwich)	51.9457	1.2856
Receiver location (Southwold)	52.3227224	1.681382

experienced at Harwich for the proposed positioning techniques using the signals from GRI 7499 are given below:

TOA With Time Synchronization

$$cov(\varepsilon_{rTOA}) = \begin{bmatrix} 0.4591 & -0.0785 \\ -0.0785 & 1.2657 \end{bmatrix}\sigma^2 \tag{4.56}$$

TOA Without Time Synchronization

$$cov(\tilde{\varepsilon}_{rTOA}) = \begin{bmatrix} 1.6668 & 5.0225 \\ 5.0225 & 22.8108 \end{bmatrix} \sigma^2 \tag{4.57}$$

TDOA

$$cov(\varepsilon_{rTDOA}) = \begin{bmatrix} 1.2213 & 4.8487 \\ 4.8487 & 22.7430 \end{bmatrix} \sigma^2 \tag{4.58}$$

Table 13: ASF measurement statistics from Harwich dLoran reference station.

Receiver Location	TOA with time Synchronisation	TOA without the time Synchronisation	TDOA
Harwich	1.313	4.948	4.895
SouthWold	1.263	5.440	5.384

Table 13 shows the traces of the covariance matrices at Harwich using signals from Anthorn, Lessay and Soustons. The results suggest that the performance of the TOA with synchronization is always better than the TDOA performance. However, this is not always true as was demonstrated by Yi Jiang et al in a similar experiment done using AIS signals in China. Nevertheless, the TDOA performance is always better than the performance of the case of TOA without synchronization.

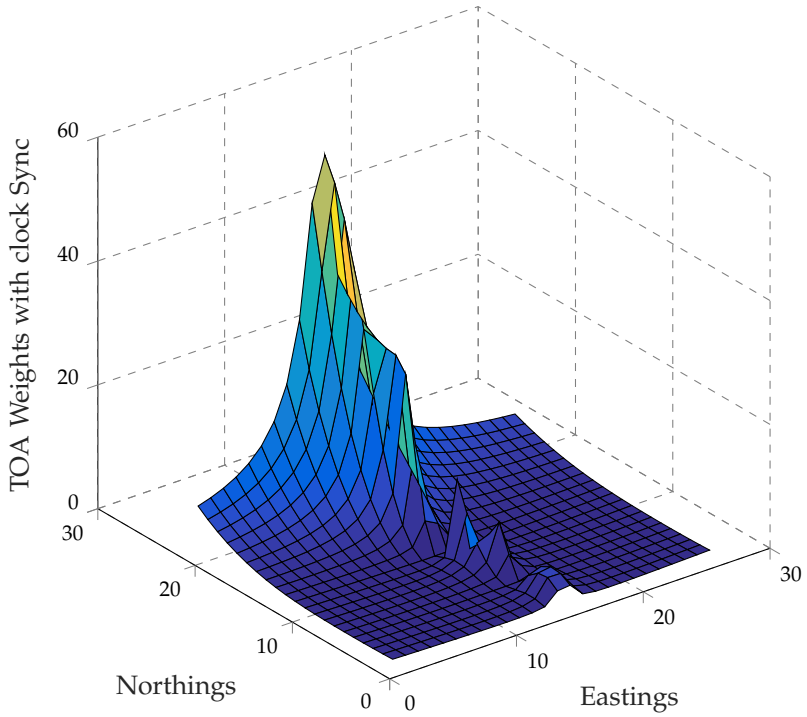

Figure 55: Performance of TOA with Sync. (min=1.16) : max=(57.6), 89.6 %.

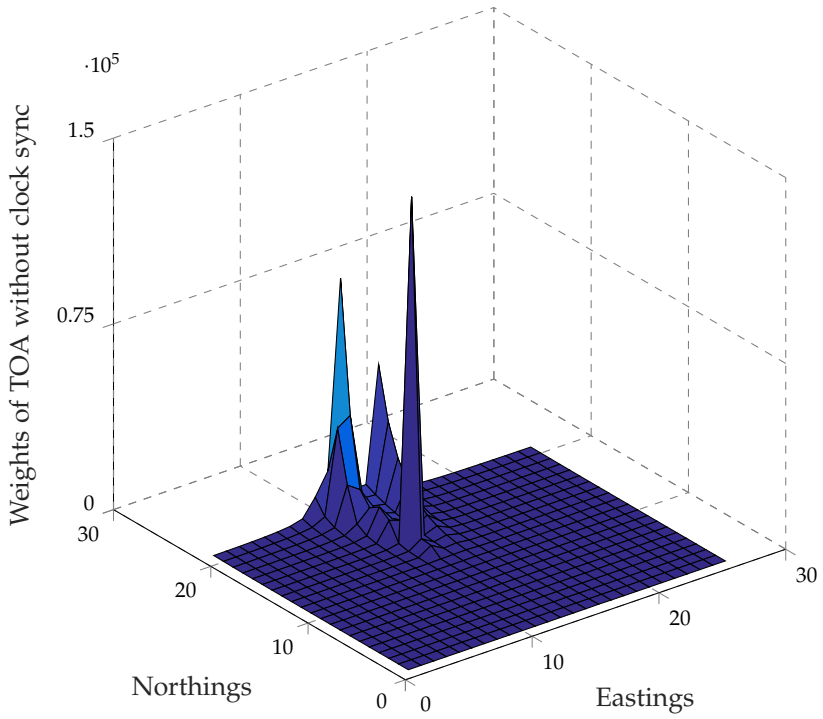

Figure 56: Performance of TOA without Sync.(min=1.45) : max=$(1.40 \cdot 10^5)$, 42.7 %.

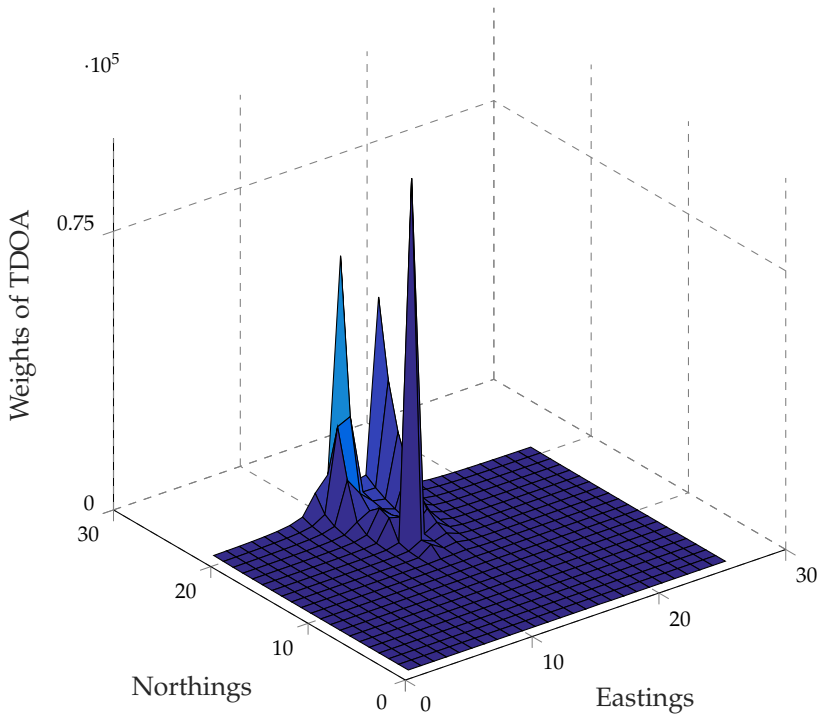

Figure 57: Performance of TDOA.(min=1.19) : max=$(9.81 \cdot 10^4)$, 43.2.

4.8 REPEATABLE ACCURACY WITHOUT NORWEGIAN AND FRENCH STATIONS

It was discussed in chapter 1 that the Federal governments of France and Norway switched off the eLoran transmitters in their countries. Therefore, eLoran cannot meet the accuracy standard required by the governing bodies in most parts of Europe.To demonstrate eLoran capability, the eLoran transmissions from French and Norwegian stations are assumed. Figure 58 illustrates the diluted repeatable accuracy without the effects of dLoran, using a receiver with a tight synchronous clock is used. Without transmissions from Norway and France, a 10 m accuracy is not possible in most parts of Europe. New navigation technologies, called Signals of Opportunity (SooP) brings new possibilities where eLoran can be combined with SooP signals to offer PNT solutions everywhere in the coverage area. Soop navigation is briefly described in section 4.9. Figure 59 illustrates the diluted repeatable

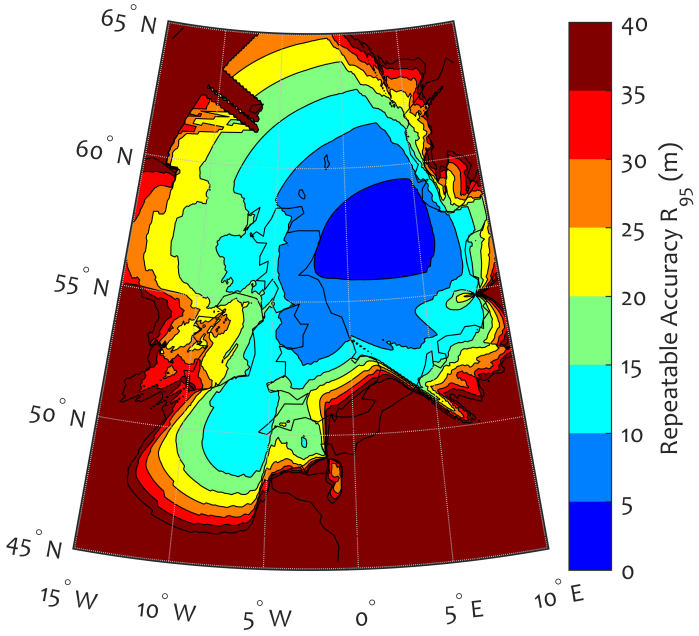

Figure 58: Accuracy for time sync TOA without dLoran.

accuracy due to both land path and weather models but without the effects of dLoran. It is assumed that a receiver with time synchronous clock is used.

4.9 SIGNALS OF OPPORTUNITY NAVIGATION

Signals of Opportunity navigation is a new field in navigation. It requires electronic signals which are not transmitted for navigation purposes [73, 40, 41]. For example, the purpose of these signals may be for communications, wireless networking, radio signals, such as cellular telephone and entertainment. These signals may occur as burst transmission, continuous transmissions, cellular telephone and wireless networking. The main feature for Signals of Opportunity navigation methods is that the time of transmission

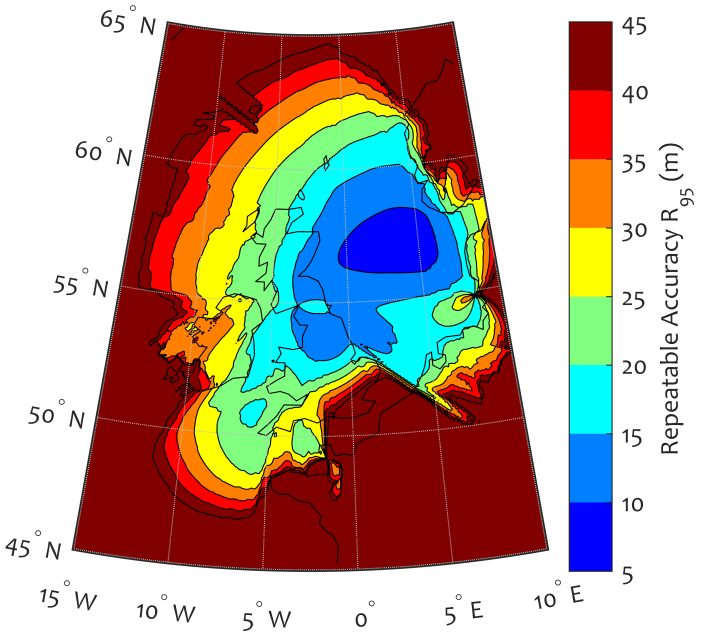

Figure 59: Accuracy for time sync TOA including weather but without dLoran.

is not known. A detailed method for analysing the signals for use with other forms of navigation has been demonstrated by Fisher [22].

4.10 SUMMARY AND CONCLUSIONS

This chapter has presented an improved pseudorange error model that takes into account the effects of the Landpath and weather. These models are useful for modelling repeatable accuracy in areas where dLoran is not required. Repeatable accuracy is the most important system parameter in Harbour Entrance and Approach and remains at the heart of the eLoran Service Volume Coverage Prediction for harbour entrance and approach. The analysis of accuracy maps can help to answer the following questions:

1. How many reference stations are needed to service a harbour?
2. Where to install transmitters among the existing transmitter configuration to improve accuracy at other parts within the coverage area where accuracy does not meet the IMO requirements?

Chapter 7 addresses the first question while the chapter 10 answers the second question. The Accuracy plots generated from the developed coverage tool suggest that there is poor coverage to the west of the British Isles additional transmitters are required somewhere in Ireland. This is further addressed in chapter 10 herein. Accuracy can be used to estimate how far away from a differential-reference station, the ASF corrections remain valid. Chapter 8 discusses spatial decorrelation.

5 SPATIAL ASF MODEL

Chapter 4 described an improved pseudorange error model where the effects of changes in conductivity and weather were modelled to demonstrate an improved repeatable accuracy capability of the coverage tool. The effects of conductivity changes on the eLoran TOAs were modelled by studying the ASF changes measured at Harwich reference station over a yearly period.[1] In that model, it was assumed that the conductivity changes are the same throughout the coverage area. The current chapter describes the analytical propagation delay model derived using the theory and results by Johler [37, 39] and Brunavs [14]. The sum of the propagation delays and the time taken by a wave to propagate the same distance in a vacuum gives the range estimates called pseudoranges needed to showcase the absolute accuracy capability of the coverage tool. Absolute accuracy is the measure of the difference between the computed and true positions. This chapter is divided into two parts the, first part describes the key terms used throughout the rest of this chapter. The second part of this chapter derives the ASF functions by fitting the data provided by Johler into a set of equations for different ground conductivities, σ and relative permeability, ϵ_r. The analytically derived ASF functions are interpolated to estimate the ASF functions for terrain that was not investigated by Johler and his co-workers. Finally, the secondary and primary factor parameters for various terrain are derived from Brunavs work. The work presented here demonstrates the coverage tool's capability to estimate the total propagation time between the user and the transmitter.

5.1 COMPONENTS OF ELORAN PROPAGATION TIME

An eLoran groundwave signal is subjected to delay along the propagation path due to changes in terrain properties. The signal delay is made up of three components, namely:

- primary factor delay (PF)
- secondary factor delay (SF)
- Additional secondary factor delay (ASF)

Additional Secondary Factor (ASF) is the delay of the signal over the ground terrain relative to an all seawater path [38, 21, 66, 44]. ASF variations take up the largest part of the eLoran error budget. Good ASF estimates can significantly increase the accuracy of eLoran. ASFs vary with location as well as time of the day, month, season and year. The variation of ASFs with time, month, season and year is termed temporal ASF variation while the variation of ASFs with location is termed spatial ASFs [15, 71, 36, 62, 35].

5.1.1 *Derivation of the eLoran ASF*

In this section, an ASF model for an eLoran signal propagating over the various ground terrain of different conductivity is derived by fitting analyti-

1 The TOA data used in this study was recorded from October 2009-October 2010.

cally derived data provided in reference [39] into piece-wise functions. The relative permittivity ϵ_r for sea and land used for computing the data were assumed to be 80 and 15 respectively. The following assumptions were used:

- propagation height, h = 0
- Relative permeability of soil, ϵ_r = 15.
- Operational frequency, 100 kHz.
- Plane earth model for distances below 200 miles.
- Spherical earth model for distances above 200 miles.
- The model is applicable to piece-wise homogeneous paths of all ground conductivities.

Table 14 shows the phase lag of the 100 kHz signal for various ground terrain as adopted from [39]. This data was generated by determining the phase of the complex attenuation function of the ground wave at some distance d from the transmitter. Johler and co-workers described the complex groundwave attenuation function as given by:

$$W = \frac{1}{2}\left(\frac{ix}{\pi}\right)^{\frac{1}{2}} \int_{\infty \exp(\frac{i2\pi}{3})}^{\infty} \frac{\exp(-ixt)w_1(t)}{w_1^{'}(t) - qw_1(t)} dt \tag{5.1}$$

where,

$$\begin{aligned} x &= (ka/2)^{1/3}(d/a) \\ k &= 2\pi/\lambda \\ q &= -i(ka/2)^{1/3}\Delta \\ \Delta &= (i\epsilon_0\omega/(\sigma + i\epsilon\omega))^{1/2}(1 - i\epsilon_0\omega/(\sigma + i\epsilon\omega))^{1/2} \end{aligned}$$

a= radius of the earth and is equal to 6368 km. ϵ_0 = dielectric constant of free space and $w_1(t)$ = an Airy function. If the transmitter and receiver are assumed to be on the ground, the attenuation for this case may be specified by the residue series as:

$$W = \exp(-j\pi/4)\sqrt{\pi x} \sum_{s=1}^{\infty} \frac{\exp(-ixt_s)}{t_s - q^2} \tag{5.2}$$

The values of t_s are complex roots to the following differential equation commonly known as Ricatti's equation:

$$w^{'}(t) - qw(t) = 0 \tag{5.3}$$

A number of intricate sub-routines for numerical integration are required to obtain the values of t_s with sufficient accuracy. The mathematically involved procedures for determining the values of t_s have been described in reference [39]. In practice, the summation in equation 5.2 is evaluated until successive results are within a reasonable tolerance. This requires hundreds of iterations before convergence can be achieved. The literature suggests that the series converges rapidly at longer distances and poorly at shorter distances [37]. At ranges that are less than 320 km, the series converges slowly and thus a modified series can be used to approximate the solution.

This modified power series was derived by Bremmer and Wait [91] and is described in [81] as:

$$W = \sum_{m=0}^{10} A_m [\exp(i\pi/4) q x^{1/2}]^m \tag{5.4}$$

where,

$$\begin{aligned}
A_0 &= 1 \\
A_1 &= -i\sqrt{\pi} \\
A_2 &= -2 \\
A_3 &= i\sqrt{\pi}\left(1 + \frac{1}{4q^3}\right) \\
A_4 &= \frac{4}{3}\left(1 + \frac{1}{2q^3}\right) \\
A_5 &= -i\sqrt{\pi}\left(1 + \frac{3}{4q^3}\right) \\
A_6 &= -\frac{8}{15}\left(1 + \frac{1}{q^3} + \frac{7}{32q^6}\right) \\
A_7 &= \frac{i\pi}{6}\left(1 + \frac{5}{4q^3} + \frac{1}{2q^6}\right) \\
A_8 &= \frac{i\sqrt{\pi}}{6}\left(1 + \frac{5}{4q^3} + \frac{1}{2q^6}\right) \\
A_9 &= -\frac{i\sqrt{\pi}}{24}\left(1 + \frac{7}{4q^3} + \frac{5}{4q^6} + \frac{21}{64q^9}\right) \\
A_{10} &= -\left(\frac{32}{945} + \frac{64}{945q^3} + \frac{11}{189q^6} + \frac{7}{270q^9}\right)
\end{aligned}$$

The eLoran phase in microseconds can be determined as:

$$ASF + SF = -\frac{Arg(W)}{2\pi f} \cdot 10^6 \tag{5.5}$$

As mentioned earlier, quality ASF requires the roots of the airy function to highly precise but the available literature does not give a satisfying description of the computation of these roots. Johler et. al [37] provided the time delays for a 100 kHz signal propagating over various ground media using the analytical method described above. This task estimates the ASF by subtracting the sea water propagation delay (SF) from the ground delays (SF + ASF) for the various ground terrain. Figure 61 shows ASFs for terrain of various conductivities. The ASF for the ground terrain that was not part of the data from the U.S Department of Commerce and the National Bureau of Standards was determined using gridded interpolation method. Figure 62 shows the interpolated ASF curves. The coefficients are determined by splitting the ASF curve into two parts. The ASF at distances up to 320 km from the transmitter was estimated using a four parameter logistic regression function. The ASF at distances beyond 320 km, is assumed to follow a linear function. A plane earth model is also assumed for distances that are below 320 km while a spherical earth model is assumed for distances that are beyond 320 km. The ASF data for each ground terrain of different

Table 14: Table showing the ASF+SF values for terrain of various conductivities [39].

Conductivity (S/m)	0.0005 (S/m)	0.001 (S/m)	0.002 (S/m)	0.005 (S/m)	0.05 (S/m)	5 (S/m)
Distance (miles)			SF + ASF (μs)			
0.1	4.4066	4.4108	4.4138	4.4205	4.4196	4.4209
0.2	3.5351	3.5444	3.5537	3.5633	3.5751	3.3802
0.5	1.4287	1.3499	1.2972	1.2522	1.2014	1.1807
1	0.89338	0.77668	0.69438	0.62225	0.53842	0.50384
2	0.78812	0.62924	0.51684	0.41296	0.29406	0.24479
5	0.94579	0.70510	0.52766	0.35307	0.18108	0.10321
10	1.2334	0.90414	0.65748	0.43407	0.16951	0.059424
20	1.7272	1.2250	0.88285	0.56924	0.19652	0.040878
50	2.4964	1.8704	1.3555	0.86959	0.28272	0.036771
100	3.2957	2.5580	1.8814 Plane Earth	1.1919	0.39101	0.043383
100	3.4758	2.6987	2.0331 Spherical Earth	1.3603	0.52711	0.17549
200	4.6994	3.8489	3.0444	2.1180	0.92781	0.42051
500	7.3738	6.5787	5.7176	4.2414	2.2330	1.3579
1000	11.826	10.948	9.9936	7.8031	4.5332	3.0811

conductivity was fitted to a piece-wise function of the form:

$$ASF(d) = \begin{cases} A + \frac{A-D}{\left(1+\left(\frac{d}{C}\right)^B\right)} & d \leq 320km, \\ \\ Ed + F & d \geq 320km \end{cases} \tag{5.6}$$

Table 15 shows the coefficients of the empirically derived ASFs for the various ground terrain. Section 5.1.2 presents the methods for solving the integral equation whose solution is the attenuation factor. It was shown in equation (5.5) that the argument of the attenuation factor is related to the sum of ASF and SF of a wave propagating over a medium of conductivity, σ. The integral equation presented in section 5.1.2 assumes that the receiver's height is zero.

5.1.2 *Integral Equation*

The radiation of a vertical current element on a planar, radially inhomogeneous ground is postulated as a integral equation for the attenuation factor. The study of eLoran radio propagation assumes that the transmitter and receiver are on the ground surface. In this case, the attenuation factor for the inhomogeneous flat earth with respect to the field strength on a perfect conductor is given by the integral equation 5.7.

$$F(d) = F_0(d) - \left[\frac{jd}{\lambda_0}\right]^{1/2} \int_0^d [\Delta(r) - \Delta_0] F(r) \frac{F_0(d-r)}{[r(d-r)]^{1/2}} dr \tag{5.7}$$

In equation 5.7,

$$F_0(r) = 1 - j[\pi p_0(r)]^{1/2} e^{-p_0(r)} \text{erfc}[(jp_0(r))^{1/2}] \tag{5.8}$$

Table 15: Coefficients of 100 kHz ASF propagation curves for soils of different conductivities.

Conductivity (S/m)	Range	Coefficients	95% Confidence bounds	Statistics
0.0005	$d \leq 320$km	A = $1.509 \cdot 10^{-12}$ B = 0.5644 C = 642.6 D = 10.52	(fixed at bound) $(0.4565, 0.6723)$ $(-582.5, 1868)$ $(3.966, 17.08)$	sse: 0.0583 rsquare: 0.9971 dfe: 8 adjrsquare: 0.9964 rmse: 0.0853
	$d \geq 320$km	E = 0.0035 F = 3.1903		
0.001	$d \leq 320$km	A = $1.367 \cdot 10^{-13}$ B = 0.5524 C = 2114 D = 13.07	(fixed at bound) $(0.4533, 0.6515)$ $(-3832, 8060)$ $(-0.4682, 26.61)$	sse: 0.0288 rsquare: 0.9977 dfe: 8 adjrsquare: 0.9972 rmse: 0.0600
	$d \geq 320$km	E = 0.0034 F = 2.3762		
0.002	$d \leq 320$km	A = $3.681 \cdot 10^{-14}$ B = 0.5308 C = $1.832 \cdot 10^{4}$ D = 24.92	(fixed at bound) $(0.431, 0.6306)$ $(-1.128 \cdot 10^{5}, 1.495 \cdot 10^{5})$ $(-51.71, 101.5)$	sse: 0.0162 rsquare: 0.9978 dfe: 8 adjrsquare: 0.9972 rmse: 0.0450
	$d \geq 320$km	E = 0.0033 F = 1.6090		
0.005	$d \leq 320$km	A = $3.144 \cdot 10^{-14}$ B = 0.5241 C = $2.638 \cdot 10^{5}$ D = 58.38	(fixed at bound) $(0.4196, 0.6286)$ $(-6.557 \cdot 10^{6}, 7.085 \cdot 10^{6})$ $(-673, 789.8)$	sse: 0.0072 rsquare: 0.9976 dfe: 8 adjrsquare: 0.9970 rmse: 0.0299
	$d \geq 320$km	E = 0.0023 F = 0.9646		
0.05	$d \leq 320$km	A = $1.14 \cdot 10^{-12}$ B = 0.5437 C = $2.438 \cdot 10^{4}$ D = 5.795	(fixed at bound) $(0.4196, 0.6286)$ $(-6.557 \cdot 10^{6}, 7.085 \cdot 10^{6})$ $(-673, 789.8)$	sse: $5.775 \cdot 10^{-4}$ rsquare: 0.9979 dfe: 8 adjrsquare: 0.9973 rmse: 0.0085
	$d \geq 320$km	E = $7.3228 \cdot 10^{-4}$ F = 0.2772		

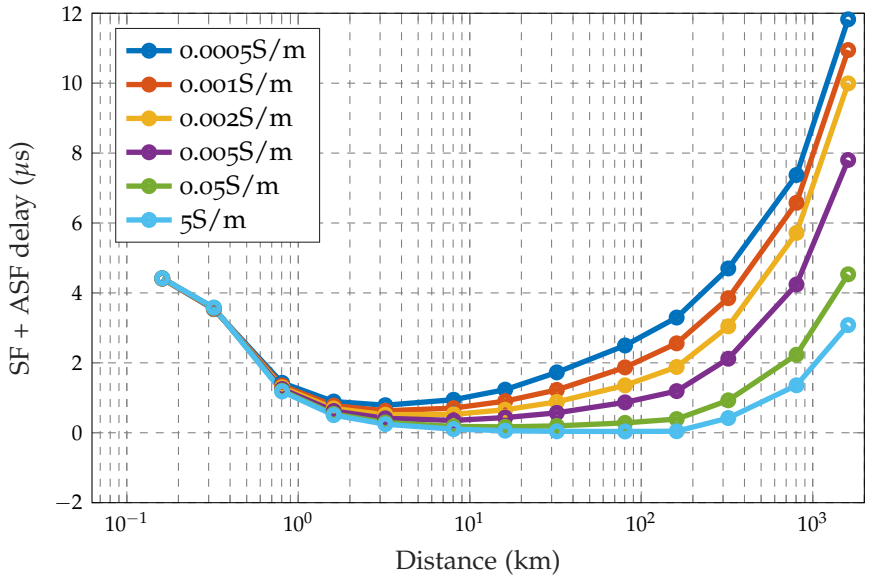

Figure 60: ASF + SF vs. distance for terrain of various conductivities. These graphs are plotted using the data in table 14. The plot of the 5S/m shows zero signal delay over sea water for distances that are 0 to 1800km from the transmitter. For transmitter ranges that are used in eLoran, the SF is always 0μs .

and

$$p_0(r) = -jk_0 r\Delta_0^2/2 \tag{5.9}$$

where Δ_0 is the normalized surface impedance of the ground and $0 \leq \Delta_0 < 1$. $\Delta(r)$ is the impedance of the homogeneous path. It can be seen from equation 5.7, that if $\Delta(r) = \Delta_0$, then $F(d) = F_0(d)$. It can also be seen from equation 5.8 that if $\Delta_0 = 0$, $F_0(r) = 1$. Equation 5.7 can be expressed in the following form:

$$F(d) = F_0(d) - g(d)\int_0^d K(d,r)F(r)dr \tag{5.10}$$

where $g(d) = [jd/\lambda_0]^{1/2}$ and $K(d,r) = (\Delta(r) - \Delta_0)\frac{F_0(d-r)}{[r(d-r)]^{1/2}}$. Wu et. al [96] described and compared four of the available numerical techniques used for solving the integral equations. The following sections detail the methods as described in reference [96]:

1. Linear Approximation
2. Quadratic Polynomial Approximation
3. Simpson's rule
4. Monteath

In the application of the mentioned numerical techniques, the integration length r is divided into N subintervals of length h_n, where $n = 1, 2, \cdots N$, such that

$$\begin{aligned} r_0 &= 0, \\ r_n &= \textstyle\sum_{i=1}^{n} h_i, \\ r_N &= d \end{aligned}$$

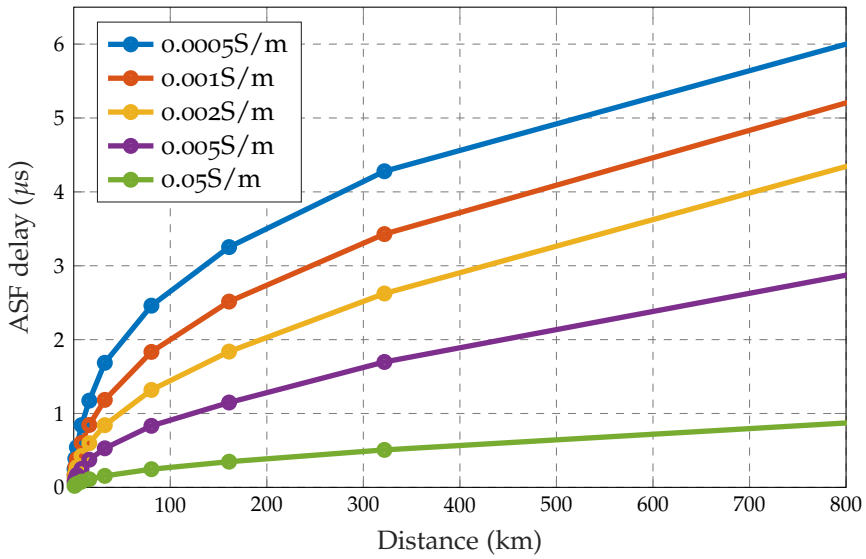

Figure 61: ASF delay for eLoran signals over a terrain of different conductivities,obtained by subtracting the second column (sea water values) from columns (3-7) in table 14.

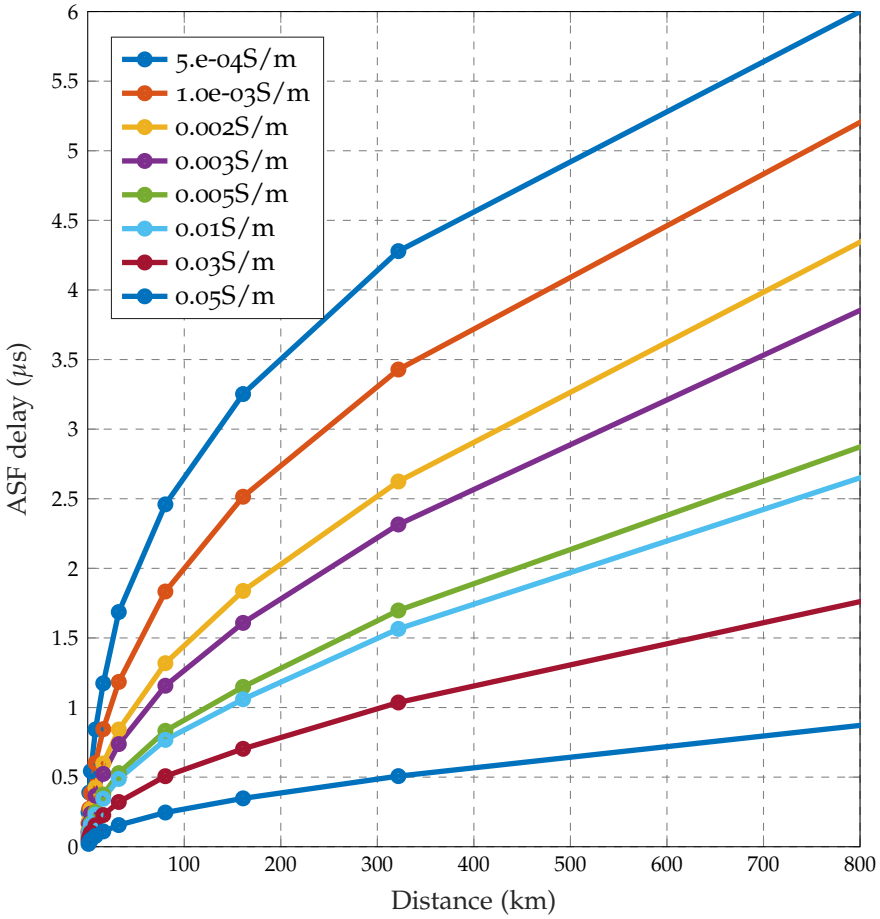

Figure 62: ASF delay for eLoran signals over a terrain of different conductivities including interpolated ASF curves.

The solutions from the four methods as described by Wu et. al are as follows:

5.1.3 *Linear Approximation*

In this method, it is assumed that $F(r)$ and $F_0(d-r)$ vary linearly in the n_{th} interval from r_{n-1} to r_n. In this case, equation 5.10 can be written as:

$$F(d) = \frac{F_0(d)}{1+g(d)R_N} - \frac{g(d)(\sum_{n=1}^{N-1}[Q_nF(r_{n-1}) + R_nF(r_n)] + Q_NF(r_{N-1}))}{1+g(d)R_N} \tag{5.11}$$

where

$$Q_n = -(1/h_n)\Phi(r_n)$$
$$R_n = -(1/h_n)\Phi(r_{n-1})$$

$$\Phi(x) = \int_{r_{n-1}}^{r_n} K_n(d,r)(r-x)dr \tag{5.12}$$

$$\begin{aligned}\Phi(x) = (\Delta_n - \Delta_0)[&-(\alpha_n + \beta_n d)x \arcsin(\frac{2r}{d} - 1)\cdots \\ &+(\alpha_n + \beta_n x)(-[r(d-r)]^{1/2} + \frac{d}{2}\arcsin(\frac{2r}{d} - 1)\cdots \\ &+\beta_n(\frac{1}{4}(2r-d)[r(d-r)]^{1/2}) + \frac{d^2}{8}\arcsin(\frac{2r}{d} - 1)]\end{aligned}$$

5.1.4 *Quadratic Polynomial Approximation*

The terms $F(r)$ and $F(d-r)$ can be approximated by a quadratic polynomial in the n_{th} interval using the following alternative expression:

$$\begin{aligned}F(d) = \frac{F_0(d)}{1+g(d)R_N} - g(d)(&\sum_{n=1}^{N-1}[P_nF(r_{n-2}) + R_nF(r_n)]\cdots \\ &+P_NF(r_{N-2} + Q_NF(r_{N-1}))/(1+g(d)R_N)\end{aligned}$$

where

$$P_n = \frac{1}{h_{n-1}(h_n + h_{n-1})}\Phi(r_{n-1}, r_n)$$
$$Q_n = -\frac{1}{h_{n-1}h_n}\Phi(r_{n-2}, r_n)$$
$$R_n = \frac{1}{h_n(h_n + h_{n-1})}\Phi(r_{n-1}, r_{n-2})$$
$$\phi(y,z) = \int_{r_{n-1}}^{r_n}(r-y)(r-z)K_n(d-r)dr$$

$$\begin{aligned}= (\Delta_n - \Delta_0)(&\frac{F_0(d-r_{n-2})}{h_{n-1}(h_n + h_{n-1})}\Psi(r_{n-1}, r_n, y, z, r_{n-1}, r_n)\cdots \\ &-\frac{F_0(d-r_{n-1})}{h_nh_{n-1}}\Psi(r_{n-1}, r_n, z, r_{n-2}, r_n)\cdots \\ &+\frac{F_0(d-r_n)}{h_n(h_n + h_{n-1})}\Psi(r_{n-1}, r_n, y, z, r_{n-2}, r_{n-1})\end{aligned}$$

where

$$\Psi(a,b,y,z,uq) = yzuqT_1 - [uq(y+z) + yz(u+q)]T_2 \cdots \\ +[uq + (y+z)(u+q) + yz]T_3 - [u+q+y+z]T_4 + T_5$$

and

$$T_1 = [\arcsin(\frac{2r}{d} - 1)]\Big|_a^b$$

$$T_2 = \frac{d}{2}T_1 - [r(d-r)]^{1/2}\Big|_a^b$$

$$T_3 = \frac{3d^2}{8}T_1 - \frac{2r+3d}{4}[r(d-r)]^{1/2}\Big|_a^b$$

$$T_4 = \frac{5d^2}{16}T_1 - [(\frac{r^2}{3} + \frac{5}{12}dr + \frac{5r^2}{8}).\cdot[r(d-r)]^{1/2}]\Big|_a^b$$

$$T_5 = \frac{7d}{8}T_4 - \frac{r^3}{4}[r(d-r)]^{1/2}\Big|_a^b$$

5.1.5 *Simpson's Rule*

To apply the Simpson's rule, the number of terms, N must be tested to check whether it is even or odd. When N is even, the total subintervals, from $r = 0$ to $r = d$ are arranged to form $N/2$ groups. Therefore,

$$F(d) = \frac{F_0(d)}{1 + g(d)R_N} - g(d)\sum_{k=1}^{K}[P_kF(r_{2k-2}) + Q_k(r_{2k-1})\cdots \\ +R_kF(r_{2k})] + P_KF(r_{N-2}) + Q_KF(r_{N-1})/(1 + g(d)R_K)$$

where

$$P_k = \frac{1}{h_{2k-1}(h_2k + h_{2k-1})}\Phi(r_{2k-1}, r_{2k})$$

$$Q_k = -\frac{1}{h_{2k-1}h_2k}\Phi(r_{2k-2}, r_{2k})$$

$$R_k = \frac{1}{h_{2k}(h_2k + h_{2k-1})}\Phi(r_{2k-1}, r_{2k-2})$$

$\Phi(y,z)$ is obtained as described above. However, when N is odd, the Simpson's rule is applied to $(N-1)$ subintervals, while quadratic polynomial approximation is applied on the N-th subinterval. Therefore, for odd N,

$$F(d) = \frac{F_0(d)}{1 + g(d)R_N} - g(d)\sum_{k=1}^{(N-1)/2}[P_kF(r_{2k-2}) + Q_k(r_{2k-1})\cdots \\ +R_kF(r_{2k})] + P_KF(r_{N-2}) + Q_KF(r_{N-1})/(1 + g(d)R_K)$$

P_k, Q_k, R_k, P_N, Q_N and R_N have stated earlier.

5.1.6 *Monteath's Method*

In the Monteath's method, equation 5.11 is arranged in the form:

$$F(d) = F_0(d) - B\int_0^d e(d,r)F(r)[\frac{d}{r(d-r)}]^{1/2}dr \tag{5.13}$$

where $B = [j/\lambda_0]^{1/2}$,

$e(d,r) = (\Delta(r) - \Delta_0)F_0(d-r)$ When all N interval lengths are set to h, $e(d,r)$ can be expressed as:

$$e(d,r) \approx e_n(d,r)$$

$$= [\Delta_n - \Delta_0]F_0(d-r)$$

then,

$$\int_0^d e(d,r)F(r)[\frac{d}{r(d-r)}]^{1/2} \approx h\sum_{n=0}^{N} C(N,n)e_n(d,r_n)F(r_n) \tag{5.14}$$

where

$$C(N,n) = \frac{J(n)J(N-n)}{J(N)}M(N,n) \tag{5.15}$$

with

$$J(m) = \begin{cases} 1 & m = 0 \\ m^{-1/2} & m > 0 \end{cases} \tag{5.16}$$

and $M(N,n)$ are the discrete weighting factors. Equation 5.14 can be approximated as:

$$F(d) = F_0(d) - \frac{BN^{1/2}h^{1/2}\sum_{n=0}^{N-1} J(n)J(N-n)M(N,n)F(r_n)e(d,r_n)}{(1 + Bh^{1/2}M(N,N)e(d,d))} \tag{5.17}$$

Equation 5.17 is the Monteath's iterative equation for F(d).

5.1.7 *Initial Values*

Before all the iterative procedures can start, initial values are required. These are listed in the following section:

Linear Approximation

The initial values of for the Linear Approximation method are given by: $F(0), F(r_1)$

Quadratic Polynomial Approximation

The initial values of for the Quadratic Polynomial Approximation method are given by: $F(0), F(r_1), F(r_2)$

Simpson's Rule

The initial values of for the Simpson's rule are given by: $F(0), F(r_1), F(r_2)$

Monteath's Method

The initial value of for the Monteath's method is given by: $F(0)$ where $F(0) = 1$,

$$F(r_1) = 1 - j[\pi p_1]^{1/2} e^{-p_1} \text{erfc}(jp_1^{1/2})$$
$$p_1 = -jk_0\Delta_1^2 r_1/2$$
$$F(r_2) = 1 - j[\pi p_2]^{1/2} e^{-p_2} \text{erfc}(jp_2^{1/2})$$
$$p_1 = -jk_0\Delta_2^2 r_2/2$$

The intervals for each of the segments can be varied between $(1/2)\lambda_0$ and $5\lambda_0$ depending on the ground properties of the terrain under study.

5.1.8 *Comparison of the four Methods*

Wu et. al [96] compared the performance of the quadratic, Simpson, Linear approximation and Monteath's methods. Their experimental results suggested that Monteath's method performs poorly compared to other methods but is computationally less intensive and is therefore adopted in the Coverage prediction tool.

5.2 COMPARISON BETWEEN ASF OBTAINED BY MONTEATH AND FITTED ASFS

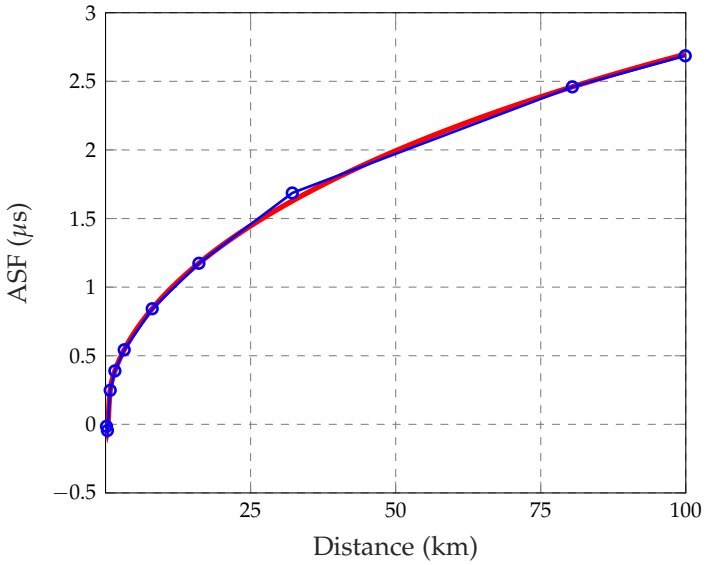

Figure 63: Figure showing the comparison between ASF obtained by Monteath's method (shown in red) and ASF obtained by the author's fitted curve (shown in blue) for ground conductivity of 0.0005 S/m.

This section compares the curve fitted ASFs with the ASFs obtained using Monteath's method. The ASFs curve obtained using Monteath's method (see figure 63) is slightly distorted at $1 - 3$ km compared to the curve fitted ASF. The ASF obtained by Monteath's method and the curve fitted ASFs are 2.6973 μs and 2.728 μs respectively at 100 km from the transmitter giving a 1.1 % error.

5.3 SKIN DEPTH

Sometimes the depth of penetration of a signal into a medium, called the skin depth, may be of interest to the system Engineers. The skin depth can be determined by applying Maxwell's equations in time-varying fields. The existence of radiation in time-varying fields was first predicted by deriving the wave equations from Maxwell's equations. To derive the propagation time for a signal traversing over any terrain with conductivity, σ, consider the following Maxwell's equations, wave equations and the Faraday's Law in the time domain. Applying the curl on both sides gives,

$$\nabla \times \nabla \times \boldsymbol{E} = -\mu \nabla \times \dot{\boldsymbol{H}} \tag{5.18}$$

According to the Ampere's law and that $\boldsymbol{J} = \sigma \boldsymbol{E}$,

$$\nabla \times \boldsymbol{H} = \boldsymbol{J} + \epsilon \dot{\boldsymbol{E}} = \sigma \boldsymbol{E} + \epsilon \dot{\boldsymbol{E}} \tag{5.19}$$

According to Ohm's law,

$$\nabla \times \nabla \times \boldsymbol{E} = -\mu\sigma \dot{\boldsymbol{E}} - \mu\epsilon \ddot{\boldsymbol{E}} \tag{5.20}$$

Expanding the left hand side,

$$\nabla \times \nabla \times \boldsymbol{E} = \nabla\nabla \cdot \boldsymbol{E} - \nabla^2 \boldsymbol{E} \tag{5.21}$$

Comparing equation 5.20 and equation 5.21 gives:

$$\nabla\nabla \cdot \boldsymbol{E} - \nabla^2 \boldsymbol{E} = -\mu\sigma \dot{\boldsymbol{E}} - \mu\epsilon \ddot{\boldsymbol{E}} \tag{5.22}$$

Applying Gauss law:

$$\nabla^2 \boldsymbol{E} = -\mu\sigma \dot{\boldsymbol{E}} - \mu\epsilon \ddot{\boldsymbol{E}}$$

In phasor form, the above equation becomes:

$$\nabla^2 \boldsymbol{E} = j\omega\mu(\sigma + j\omega\epsilon)\boldsymbol{E} = \gamma^2 \boldsymbol{E} \tag{5.23}$$

Propagation Constant γ

The propagation constant γ of the ground terrain can be modelled as complex quantity having both real and imaginary parts. The real part is called the attenuation constant α and the imaginary part is called phase constant β.From equation 5.23, the propagation constant γ is given by:

$$\gamma = \alpha + j\beta = \sqrt{j\omega\mu(\sigma + j\omega\epsilon)} \tag{5.24}$$

Squaring both sides of equation 5.24 gives:

$$\gamma^2 = \alpha^2 - \beta^2 + 2j\alpha\beta = -\omega^2\mu\epsilon + j\omega\mu\sigma \tag{5.25}$$

Comparing the real and imaginary parts of both sides, gives:

$$\alpha^2 - \beta^2 = -\omega^2\mu\epsilon \qquad\qquad 2\alpha\beta = \omega\mu\sigma \tag{5.26}$$

Finding the value of α from the relation in equation 5.26, gives:

$$\alpha = \frac{\omega\mu\sigma}{2\beta}$$

and substituting it into the first relation of equation 5.26, gives:

$$(\frac{\omega\mu\sigma}{2\beta})^2 - \beta^2 = -\omega^2\mu\epsilon \tag{5.27}$$

$$\beta^4 - \beta^2\omega\mu\epsilon - (\frac{\omega\mu\sigma}{2})^2 = 0 \tag{5.28}$$

Solving the quadratic equation 5.28 in β^2, gives:

$$\beta^2 = \frac{1}{2}\left[\omega^2\mu\epsilon \pm \sqrt{1+4\left(\frac{\omega\mu\sigma}{2}\right)^2}\right] \tag{5.29}$$

$$= \frac{\omega^2\mu\epsilon}{2}\left[1 \pm \sqrt{1+\left(\frac{\sigma}{\omega\epsilon}\right)^2}\right] \tag{5.30}$$

Taking the square root both sides, gives the solution to the quadratic equation as:

$$\beta = \sqrt{\frac{\omega^2\mu\epsilon}{2}\left[1 \pm \sqrt{1+\left(\frac{\sigma}{\omega\epsilon}\right)^2}\right]} \tag{5.31}$$

The positive phase shift is usually chosen because the medium is considered to be passive. The simplified expression for the phase constant can also be expressed as:

$$\beta = \omega\sqrt{\frac{\mu\epsilon}{2}\left[\sqrt{1+\left(\frac{\sigma}{\omega\epsilon}\right)^2}+1\right]} \tag{5.32}$$

It is straight forward to show the expression of the attenuation constant, α. This expression for α is:

$$\alpha = \omega\sqrt{\frac{\mu\epsilon}{2}\left[\sqrt{1+\left(\frac{\sigma}{\omega\epsilon}\right)^2}-1\right]} \tag{5.33}$$

The skin depth is also known as the depth of penetration. It gives us an idea of how far the signal can penetrate into the medium. In a conductive medium, the signal gets attenuated as it travels deeper into the medium. The expression for the skin depth is the reciprocal of the attenuation constant, α:

$$\delta = \frac{1}{\omega\sqrt{\frac{\mu\epsilon}{2}\left[\sqrt{1+\left(\frac{\sigma}{\omega\epsilon}\right)^2}-1\right]}} \approx \sqrt{\frac{2}{\omega\mu\sigma}} \tag{5.34}$$

The penetration depth of a signal into a medium is inversely proportional to the square root of the frequency. Lower frequencies penetrate deeper into the medium than high frequencies. Table 16 shows the penetration depth of a 100 kHz frequency signal into various soils. The next section describes the model for determining secondary factor delay (SF) of the eLoran signals over a terrain of different conductivities.

5.3.1 *Brunavs' Model*

Brunavs [14] presented the phase lags (expressed in meters) of a wave front with respect to an imaginary or fictitious wave propagating in vacuum at

Table 16: Table showing the penetration depth of 100 kHz into various soils.

Ground	Conductivity Type (S/m)	Penetration Depth(m)
Sea water	5	0.71
Very good ground	0.03	9.2
Wet ground; good dry soil	0.01	15.9
Fresh water; cultivated ground	0.003	29
Medium dry, Average ground; Mountainous areas	0.001	50
Dry ground;permafrost; Snow covered mountains	0.0003	91
Extremely Poor, very dry Ground	0.0001	159
Glacial Ice	0.00001	503

a speed of 299792.5 km/s. The phase lags were presented using two coefficient formulas named Formula B and Formula C. Formula B produces phase lag values with an accuracy of ± 20 m. Formula C is considered to be more accurate with a precision not exceeding ± 6 m. Based on the reason mention above, Formula C is therefore adopted in this work. Shorter distances less than 2 km were omitted in the development of Formula C coefficients. Formula C can be expressed as:

$$\Delta PF + SF = C_1 + C_2 S + (C_3 S + C_4)\, e^{C_5 S} + \frac{C_6}{(1 + C_7 S + C_8 S^4)} + \frac{2.277}{S} \quad (5.35)$$

where $S = 10^{-5}$, multiplied by the distance in meters. e is the base of natural logarithm and is taken to be equal to 2.71828. The coefficients C_1 up to C_8 are dependent on conductivity. Table 17 shows the coefficients, C_1 up to C_8 adopted from Brunavs' work [14] for various ground conductivities. The relative permittivity for the ground is assumed to $\epsilon_r = 15$. The goal of this

Table 17: Table showing coefficients of Brunavs' Formula C for 100 kHz signal propagating over soils of various conductivities.

Conductivity	C_1	C_2	C_3	C_4	C_5	C_6	C_7	C_8	Conductivity Type (S/m)
Sea water	−111	98.2	−13.51	112.8	−0.254	0	0	0	5
Very good ground	1.9	126.77	43.7	36.9	−0.600	−30.3	13.64	130	0.03
Wet ground; good dry soil	98	148.11	47	−24.0	−0.600	−60.8	14	245	0.01
Fresh water; cultivated ground	297.1	182.95	48.3	−143.1	−0.556	−127.7	10.42	74	0.003
Medium dry, Average ground; Mountainous areas	633.3	207.42	75	−299.4	−0.400	−271.4	6.30	13	0.001
Dry ground;permafrost; Snow covered mountains	855.7	196.04	219.5	−217.3	−0.488	−523.4	5.64	7	0.0003
Extremely Poor, very dry Ground	717.7	183.06	164.2	132.0	−0.510	−690.6	7.25	19	0.0001
Glacial Ice	393.6	173.46	155.7	186.4	−0.522	−402.8	11.29	111	0.00001

chapter is to estimate all the delay components along the propagation path

from the transmitter to the receiver. The pseudorange of the transmitter at the receiver locations is:

$$PR = \frac{d}{c} + ASF + \Delta PF + SF \tag{5.36}$$

5.4 SUMMARY AND CONCLUSIONS

This chapter has described and provided all the necessary methods for estimating the total propagation delay at all the grid points in the coverage area. The equations developed by the author through curve fitting methods have been shown to be accurate, simple and eliminate the need for solving complicated Airy ground attenuation functions. The ASFs for various terrain can be determined from table 15 while the combined primary factor and secondary factor for various terrain can be determined from table 17. The work described in this chapter can be useful for demonstrating the absolute accuracy capability of the coverage tool. However, absolute accuracy could not be modelled due to limitations in the conductivity data supplied by the GLAs to the author.

6 REFERENCE STATION COVERAGE PREDICTION

The various parameters of the signal propagation model of an eLoran signal were described in chapter 5. The current chapter extends the modified accuracy model to include reference station coverage prediction. This chapter is divided into two parts. The first part presents the assumptions and reference coverage prediction models proposed by other researchers. A weighted temporal ASF correction model postulated by the author is also described. The second part of this chapter analyses the estimated coverage of the ports and harbours in the GLA's coverage area to assess whether the proposed reference stations locations are optimized or not. Section 6.1 describes the concept of differential Loran.

6.1 DIFFERENTIAL LORAN (DLORAN)

The role of a reference station is to monitor the temporal TOAs and extract temporal ASF information of the signals measured from the various transmitters that are in view at the reference station and transmit these ASF corrections via a 30 bps data channel to a Eurofix compliant transmitter [15]. The temporal ASFs as part of the DLoran data are sent out as pseudorange corrections per station to mariners doing HEA in the vicinity of the reference station. Traditionally, a single reference station is deployed to service a harbour of an area of up to $2500\pi\ km^2$ if the geometry is good. A set of DLoran correction data takes about 90s to transmit [90]. The UK plan is to send correction data from multiple reference stations via a single Eurofix channel. However, sending correction data from multiple reference stations increases the delay of the data link, which has been stated to be as high as 15 minutes [90]. This large data latency results in position accuracies that are worse than the expected 10 meters in critical areas such as harbours.

6.1.1 *DLoran Shortcomings*

According to Van Willigen et al. [90] the failures of dLoran are as follows:

- The rate at which data can be transmitted through the data link is low thereby introducing significant data latency, which in turn introduces differential Loran errors.

- There is an increased latency experienced by the data channel when a large number of reference stations send a correction data to the user at the same time.

- The system performance is dependent on the accuracy of the atomic clocks at the transmitters.

The designers of dLoran have therefore accepted that their dLoran system does not meet the stringent accuracy requirement in critical areas. They have introduced and tested their new system called enhanced Differential Loran (eDLORAN). The concept of the new DLoran does not mean that Eurofix will be phased out. Van Willigen et al [90] emphasized that Eurofix

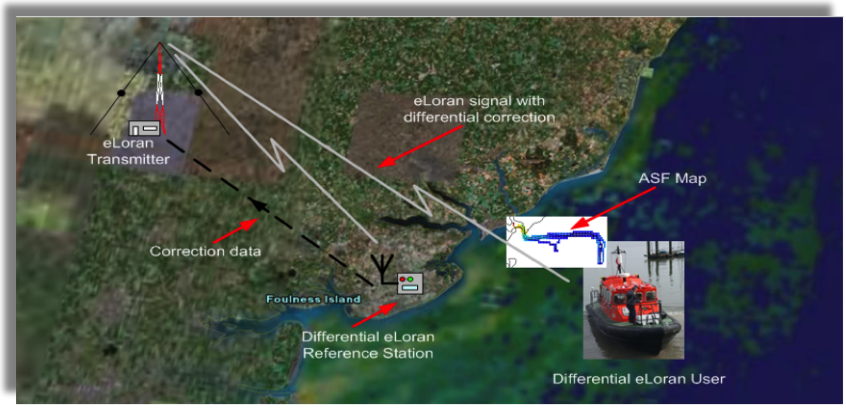

Figure 64: Illustration of the DLoran system [90].

remains the prime GNSS backup candidate for distributing accurate UTC data over large parts of Europe.

6.2 DIFFERENTIAL ELORAN (EDLORAN)

According to its inventors [90], eDLoran uses the public Global System for Mobile (GSM) network to send the differential corrections to the users rather than a Eurofix channel. eDLoran receivers, therefore, have a simple modem for connection to the GSM network and reference stations are also connected to the Internet. This may be implemented using a cabled access or a GSM modem. The user sends the raw position information to the server which determines the optimal correction for that particular information. The inventors of eDLoran stated the following as the advantages of this new system:

- eDLoran offers the best possible eLoran accuracy, as it does not suffer from unstable transmitter antennas, sub-optimal timing control of the transmitter station, and differential data latency. The latency is stated to be just 1 second.

- There is no need to replace the older Loran-C stations to use eDLoran.

- Transmitters can be placed in containers and operated unmanned.

- The installation of eDLoran is fast, simple and cost effective.

- The full data bandwidth that was taken up DLoran can be used for UTC and short-message services over large areas.

- There is no bandwidth limitation and thus multiple reference stations can be installed.

The newly developed eDLoran system is illustrated in figure 65. However, no information has been provided by the receiver manufactures on how the reference station servers process the correction data. The following sections, 6.3 - 6.4.2, describe the methods of applying ASF corrections at the user's locations.

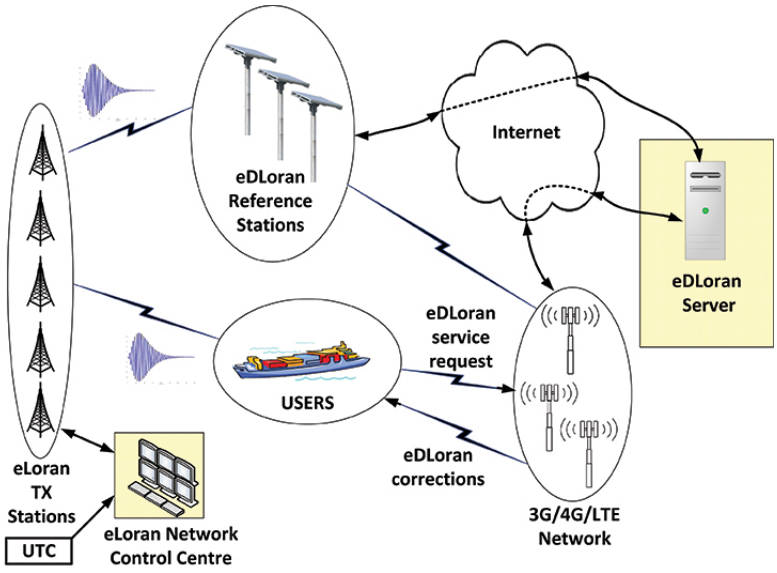

Figure 65: Architecture of the new eDLoran system [90].

6.3 GENERAL ASF CORRECTION TECHNIQUE FOR A SINGLE REFERENCE STATION

It was explained in chapter 5 that the total ASF at the user's location is given by the sum of spatial and temporal variations.

$$ASF = ASF_{spatial} + ASF_{temporal} \tag{6.1}$$

The user's receiver has no knowledge of the temporal ASF variations. Therefore, eLoran reference stations are operated near a harbour to measure these ASF temporal variations which are sent to the mariners near that harbour. The traditional ASF correction technique used in eLoran is illustrated in figure 66. The eLoran reference station measures the TOA of signals from each eLoran transmitter in view and determines the temporal ASF correction. The temporal ASF correction is transmitted to the user who is within the reference station's service area (at a distance of less than 50 km from the reference station) via a transmitter that is Eurofix compliant. The user's receiver adjusts its measured pseudorange by applying the temporal ASF correction. This procedure assumes that the temporal ASF variations at the user and the reference station locations are the same. The ASF at the user's position is given by:

$$ASF_{user} = ASF_{spatial.User} + ASF_{temporal.Ref} \tag{6.2}$$

where, the $ASF_{spatial.User}$ is the spatial ASF at the user's location. This is obtained from the ASF map stored in the receiver's memory[1]. $ASF_{temporal.Ref}$ is the temporal ASF correction at the reference station and is used to adjust the measured pseudoranges at the user's location since the conditions along the transmitter-reference station path are always changing.

1 The harbour is surveyed once and for all to generate an ASF map that is only applicable to that harbour. The generated ASF map is stored in the receiver's memory

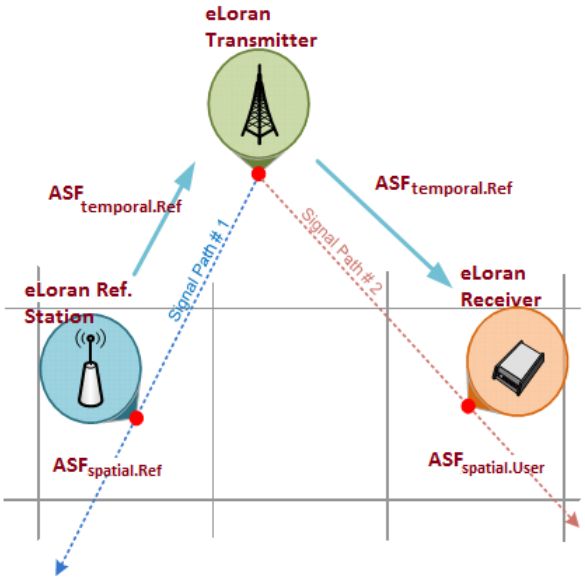

Figure 66: General eLoran ASF Correction Method courtesy [36].

6.4 REVIEW OF EXISTING ASF CORRECTION TECHNIQUES

This section reviews the possible ASF correction techniques that can be used to improve the position accuracy at the user's location. The algorithms described here are basic concepts rather than a description of specific receiver design. Hwang et al. [36] in their work over the Korean peninsula, proposed two ASF correction techniques. They predicted the spatial ASFs using Monteath's algorithm and topography data extracted from NASA Shuttle Radar Topography Mission and evaluated the proposed correction techniques through a simulation study. Their first technique weights the temporal ASF applied at the user's location by the ratio of the user's spatial ASF and the reference station's spatial ASF. The user's ASF can be defined as:

$$ASF_{user} = ASF_{spatial.User} + \left(\frac{ASF_{spatial.User}}{ASF_{spatial.Ref}}\right) \times ASF_{temporal.Ref} \tag{6.3}$$

6.4.1 *Weighted ASF Correction from two Reference Stations*

This technique uses ASF corrections from the reference stations that are in the vicinity of the user. In Hwang et al's experiment, the two reference stations were separated by about 38.7 km. The weighted ASF correction technique is illustrated in figure 67. Their proposed technique is expressed as:

$$ASF_{temporal.User} = s_{3,1} \times ASF_{temporal.Ref1} + s_{3,2} \times ASF_{temporal.Ref2} \tag{6.4}$$

where

$$s_{3,1} = \frac{\left|ASF_{spatial.User} - ASF_{spatial.Ref\#2}\right|}{\left|ASF_{spatial.User} - ASF_{spatial.Ref\#1}\right| + \left|ASF_{spatial.User} - ASF_{spatial.Ref\#2}\right|}$$

and

$$s_{3,2} = \frac{\left| ASF_{spatial.User} - ASF_{spatial.Ref\#1} \right|}{\left| ASF_{spatial.User} - ASF_{spatial.Ref\#1} \right| + \left| ASF_{spatial.User} - ASF_{spatial.Ref\#2} \right|}$$

where the terms, $ASF_{spatial.User}$, $ASF_{spatial.Ref\#1}$ and $ASF_{spatial.Ref\#2}$ are the spatial ASFs at user's receiver, reference station number 1 and reference station 2 respectively. Hwang et. al [36] did not give the reasons for using

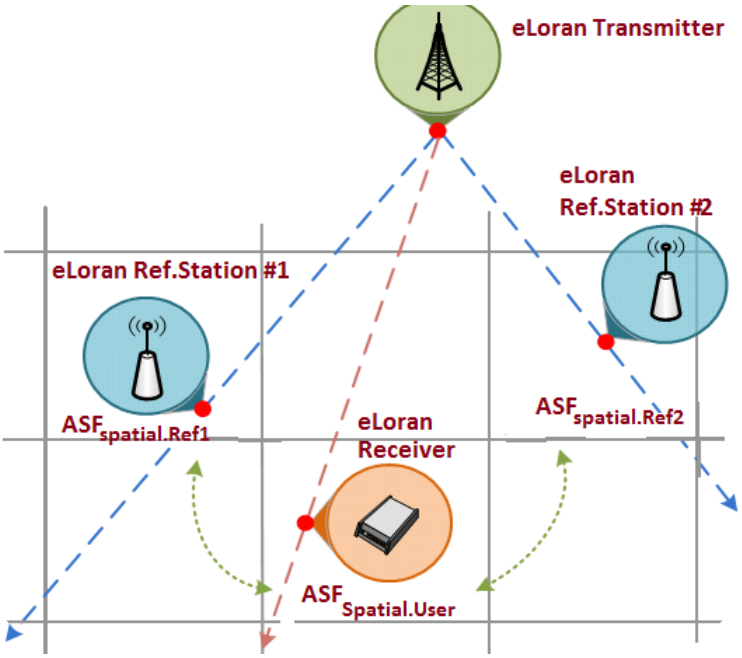

Figure 67: General eLoran ASF Correction Method courtesy [36].

the relative scale factors from the receiver's ASF correction map.

6.4.2 *The Linearly Interpolated Pseudorange Correction Method*

The references [63, 88] presented a linearly interpolated pseudorange correction (PRC) algorithm to improve the DGPS positioning accuracy at the user's position. The regenerated PRC is determined as a linear combination of the PRCs from the multiple reference stations. The criterion is that the same satellites must be in view at the multiple reference stations and the user. Oh et al.'s results showed the positioning accuracy improvement of 40%. Other interpolation techniques are :

1. *Position domain approach*- This algorithm computes a position using each reference station's corrections. The resultant positions are combined by taking a weighted average to produce the final position solution.

2. *Centroid approach*-This procedure combines the pseudorange corrections from all the reference stations to form one correction for each satellite in view. The resulting pseudorange correction should fit the centroid of the area defined by the chosen multiple reference stations. The pseudorange corrections for the centroid can be generated at the user's position or land based hub. The advantage of the latter is that

the user's need only to receive the one set of the pseudorange corrections.

3. *All-in-view approach*- In this procedure, all the pseudorange corrections received from the reference stations are incorporated into one positioning solution without any data preprocessing. For instance, the correction for a specific satellite may be received from 5 different reference stations and used separately to correct the pseudorange observed at the user's receiver from a specified satellite.

The assumptions made in determining the linearly interpolated pseudorange corrections at the user's location are:

- The user only uses the common satellites that are in view at both the user and reference stations to calculate the position.

- Four or more common satellites must exist between the user and reference stations.

- The variation of the correction data of a satellite is small and therefore the characteristic of the PRC variation for each satellite can be assumed to be linear.

6.5 DEVELOPING A LINEARLY INTERPOLATED PSEUDORANGE METHOD FOR ELORAN

The linearly interpolated pseudorange correction method described in this section is being proposed based on the results of the author's own research. This method is similar to existing methods used in other systems such as DGPS [88]. However, important eLoran updates are introduced. Figure 68 shows the statistical distribution of the pseudorange corrections applied at the user's receiver positions that are located at some distances from the reference stations.

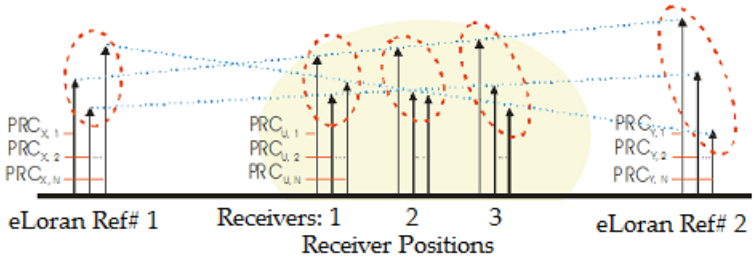

Figure 68: Linearly Interpolated Pseudorange Correction method. It can be seen that the position error ellipse at the user's positions (labelled Receivers 1, 2 and 3) mimics the one seen at the closest reference station [63].

The assumptions made in determining the linearly interpolated pseudorange corrections at the user's location are:

- The user only uses the common transmitters that are in view at both the user and reference stations to calculate the position.

- Three or more common eLoran transmitters must exist between the user and reference stations.

- The variation of the correction data of an eLoran transmitter is small and therefore the characteristic of the PRC variation for each eLoran transmitter came be assumed to be linear.

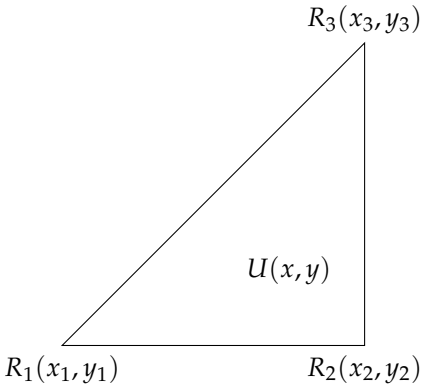

Figure 69: Figure showing the placement of reference stations around the user situated at point U.

The user's unknown position can be derived using the relative geometry information of the transmitters as shown in figure 69. The user's position at $U(x, y)$ can be expressed as:

$$x = \sum_{i=1}^{N} a_i x_i$$
$$y = \sum_{i=1}^{N} a_i y_i$$
$$1 = \sum_{i=1}^{N} a_i$$

The linearly interpolated pseudorange correction at the user's position can be expressed as:

$$\nabla_j^i = \nabla_1^i + a_1^i(x_j - x) + a_2^i(y_j - y) \tag{6.5}$$

The variables x_i and y_i in equation 6.5 represent the latitudes and longitudes in the WGS-84 model. The coefficients a_i and a_j belong to a plane which contains all the reference stations.

$$\begin{bmatrix} a_1 \\ a_2 \end{bmatrix} = (G^T G)^{-1} G^T \begin{bmatrix} \nabla_2^i - \nabla_1^i \\ \nabla_3^i - \nabla_1^i \\ \vdots \\ \nabla_j^i - \nabla_1^i \end{bmatrix} \tag{6.6}$$

The right side of equation 6.6, contains the term $[\nabla_j^i - \nabla_1^i]$ which is determined using the pseudorange corrections from the reference stations. The matrix G contains the location information of the reference stations and the values of a_1 and a_2 are the weights of the linearly interpolated pseudorange correction. This proposed method is suitable for eLoran and can be made robust by a good reference station inclusion criteria.

6.6 PROPOSED DYNAMIC ASF CORRECTION METHOD FROM A SINGLE REFERENCE STATION

This section describes an improved ASF correction method applicable for a single reference station proposed by the candidate. The proposed ASF correction method extends the model proposed by Hwang et. al [36]. Figure 70 and figure 71 show the reference stations situated at points P and Q. In this study, the radius of each circle is assumed to be 50 km and is taken to be the range from a reference at which temporal ASF corrections remain valid. In the scenario depicted by figure 70, the user's receiver can only apply the temporal ASF correction from reference station situated at P if it is within the circle centred at P. The temporal ASF corrections from the reference station situated at Q are considered not applicable to a user's receiver situated within a circle centred at P. The temporal ASF correction method proposed by the author assumes that eDLoran is deployed and the Long-Term Evolution (LTE) communication channel between the reference station and the user's receiver is modelled as an additive white Gaussian noise channel.

$$ASF_{spatial.Ref} : BER_{Ref} = ASF_{Spatial.User} : BER_{User} \tag{6.7}$$

where BER stands for the bit error rate of the channel.In this study, a bit error rate is chosen instead of SNR as the channel may have other impairments.

$$ASF_{user} = ASF_{spatial.User} + \left(\frac{BER_{User}}{BER_{Ref}}\right) \times ASF_{temporal.Ref} \tag{6.8}$$

where BER_{User} and BER_{Ref} are the bit error rates at the user and the reference station. The candidate also argues that since spatial ASF are measured once and for all, using BER ratios is more adaptive to the channel conditions than when the spatial ASFs are used (see section 6.4.1). BER/SNR is related to signal attenuation and it was shown in chapter 5 that the phase lag of the signal can be derived from its attenuation factor.

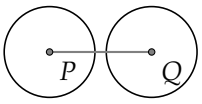

Figure 70: Circle depicting the coverage area of the reference stations located at P and Q.

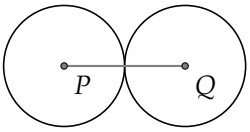

Figure 71: Circle depicting the coverage area of the reference stations located at P and Q.

6.7 TEMPORAL DECORRELATION OF ASF CORRECTIONS

Temporal decorrelation of the pseudorange corrections is due to the time-varying nature of the eLoran error sources. The accuracy of the user's differential position solution becomes worse as the latency between the calculation of a pseudorange correction by the reference station and its application by the user's receiver increases [69]. Most eLoran error types vary relatively slowly, with the pseudorange value only changing significantly over hours. This occurs due to the changes in the ASF and the transmitter clock drift [77, 89].

6.8 SPATIAL DECORRELATION OF ASF CORRECTIONS

The aim of this work is to study and quantify the nature of spatial decorrelation of ASF corrections received at the user's location. The errors associated with differential Loran may occur even though the propagation paths to two receivers are highly correlated. This is mainly attributed to a passing weather front that may be experienced on the transmitter-reference station path but not on the transmitter users receiver path. This work adopts a procedure described in reference [5]. It is assumed that the spatial decorrelation of the eLoran pseudorange error is a stationary process. Let $\Delta\phi_B$ be the measured ASF at the reference station and $\Delta\phi_R$ be the ASF seen by the user's receiver from the transmitter. Let ϕ_B and ϕ_R be the true values of the ASFs for the paths described above. The differential error can be determined as:

$$\varepsilon_D = (\Delta\phi_B - \phi_B) - (\Delta\phi_R - \phi_R) \tag{6.9}$$

The error in equation 6.9 can be attributed to the fact that the transmitter-reference station path does not experience the same ASF changes as the transmitter-user receiver path. This work adopts an autocorrelation technique used by Kasper [42] to describe the pseudorange error due to spatial decorrelation in eLoran. The autocorrelation function can be pragmatically described as:

$$R_{eLoran}(\Delta x) = \sigma^2 e^{-|\Delta x|/50} \tag{6.10}$$

where Δx is receiver-reference station separation distance in kilometres and σ^2 is the variance of the pseudorange error at reference station location. The $R_{eLoran}(\Delta x)$ is an autocorrelation function defined as:

$$R_{eLoran}(\Delta x) = E\{\delta\phi(x)\delta\phi(x + \Delta x)\} \tag{6.11}$$

where $E\{\cdot\}$ is the expected value operator and $\delta(x)$ denotes the uncorrelated pseudorange error at the receiver position x and $\delta\phi(x + \Delta x)$ denotes the uncorrelated pseudorange error at the receiver position $x + \delta x$ where Δx is the separation between the receiver and the reference station. Let us consider a scenario where the differential reference station at position x_0 and the user's receiver is situated at position x. Thus the residual error after correction is:

$$\Delta\phi(x) = \delta\phi(x) - \delta\phi(x_0) \tag{6.12}$$

The RMS error can be determined by squaring equation 6.12. This gives:

$$\Delta\phi^2(x) = \delta\phi^2(x) - 2\delta\phi(x)\delta\phi(x_0) + \delta\phi^2(x_0) \tag{6.13}$$

taking the expected values,

$$\begin{aligned} E\{\Delta\phi^2(x)\} &= E\{\delta\phi^2(x)\} - 2E\{\delta\phi\delta(x)\phi(x_0)\} + E\{\delta\phi^2(x_0)\} \\ &= \sigma^2 - 2\sigma^2 e^{-|\Delta x|/50} + \sigma^2 \\ &= \sigma^2(2 - 2\sigma^2 e^{-|\Delta x|/50}) \end{aligned} \tag{6.14}$$

where Δx and 50 are in kilometres. The value, 50 is in kilometres and is assumed to be the radial distance from the reference station at which the corrections from the reference station become invalid. Taking the square root gives:

$$\begin{aligned} \Delta\phi_{RMS} &= \sigma\left(2 - 2e^{-|\Delta x|/50}\right)^{\frac{1}{2}} \\ &= \left(L_{impl}\frac{337.4^2}{N_p \cdot \gamma}\left(2 - 2e^{-|\Delta x|/50}\right)\right)^{\frac{1}{2}} \end{aligned} \tag{6.15}$$

Equation 6.15 gives the measure of the spatial decorrelation of the PRC error at distances Δx from the reference station. The decorrelation error can be assumed to be a function of the angle between the normal to the reference station's LOP and reference station-receiver baseline(see figure73). In this case, the angular variations are such that the decorrelation error is maximum when the receiver and the reference station are separated along a given line of position and minimum when along the line perpendicular to the line of position (see figures 74 and 75). Assigning a variation of $\sin\alpha$ where α is the azimuth between the normal to the reference station line of position (LOP) and the baseline between the receiver and the reference station. The rms decorrelation error is given by:

$$\begin{aligned} \Delta\phi_{RMS} &= \sigma|\sin\alpha|\left(2 - 2e^{-|\Delta x|/50}\right)^{\frac{1}{2}} \\ &= |\sin\alpha|\left(L_{impl}\frac{337.4^2}{N_p \cdot \gamma}\left(2 - 2e^{-|\Delta x|/50}\right)\right)^{\frac{1}{2}} \end{aligned} \tag{6.16}$$

Discussion of Results

Figure 72 illustrates the growth of the pseudorange error measured on the transmitter in view at the user's location as the user's receiver moves away the reference station. The error is zero, if the user's receiver and the reference station are in the same geographical coordinates. The error grows faster at low SNRs and slower at higher SNRs. Since position error is dependent on the geometry and SNR's of the stations used to determine a position fix, the measured position error due to spatial decorrelation on the measured position grows slowly if there is good transmitter geometry and SNR at the two points.[2]This case represents a low degree of spatial decorrelation. The measured position error grows faster if there is bad transmitter geometry and poor SNR at the two points. This case represents a high degree of spatial decorrelation.

Figure 74 and 75 show that the pseudorange correction (PRC) increases with

2 The term points here refers to receiver and reference station positions.

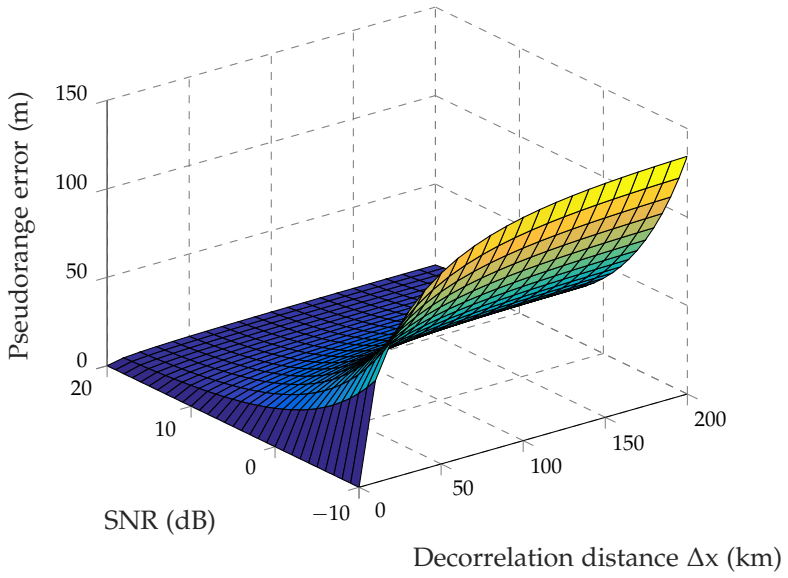

Figure 72: Figure showing an increase in the pseudorange error measured at the reference stations as the user's moves away from the reference station. It can be seen that error increases rapidly if the SNR measured by the reference station is low. At SNR = −10dB, the maximum pseudorange error is: max (σ_r) = 134m.

distance from the reference station. At the same distance from the reference station, the growth of the PRC also depends on the angle between the normal to the reference station LOP and the user's receiver. At 0° and 180°, the growth of the correction depends only on the decorrelation distance. At similar distances, the pseudorange error increase is maximum when the angle between the normal to the reference station LOP and the user's receiver is 90° and 270°.

6.9 OPTIMAL REFERENCE STATIONS PLACEMENT TECHNIQUES

The reference station coverage problem is a measure of quality of service (QoS). The aim of the reference station placement optimization is to have a priori estimate of the number of reference stations to be deployed in an environment to achieve desired coverage. The results of reference station coverage prediction can be used to identify the reference stations that are inefficiently used and perhaps un-install and deploy them elsewhere in the coverage area. It can be seen in figure 76 that some of the reference station resources are not adequately utilized since they are too close to each other.

6.9.1 *Determining the number of Reference station to service an Area*

This section describes the optimal placement method of the reference station resources in a large harbour. Consider a geographical area of the form of a square region with side a. This region can be partitioned into small equilateral triangular subregions with reference stations assumed to be placed at the corners and the centre of the equilateral triangle. The coverage probability, C_p can be estimated as the ratio of the coverage region inside the triangle to the area of the triangle and is represented as:

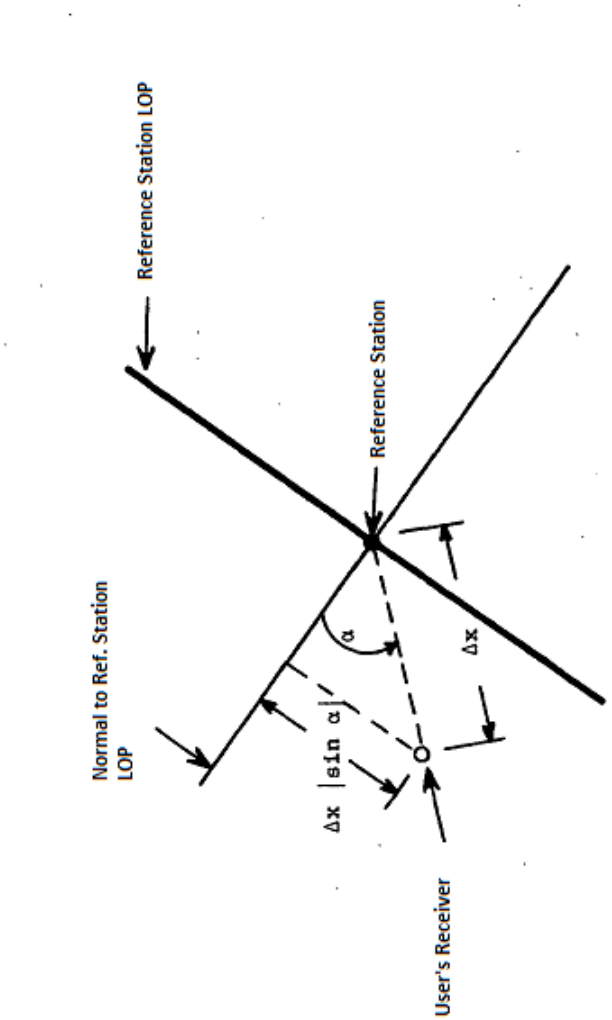

Figure 73: Figure showing the effective decorrelation error when separation distance between the reference station and the user's receiver is Δx.

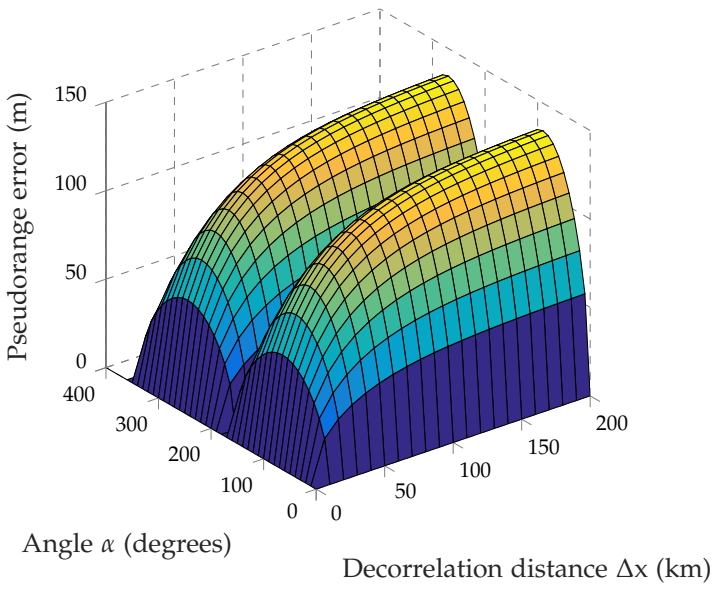

Figure 74: Figure showing an increase in the pseudorange error of the transmitter in view at the user, as the user's receiver moves away from the reference station. The SNR is assumed to be -10 dB. max (σ_r) = 134m.

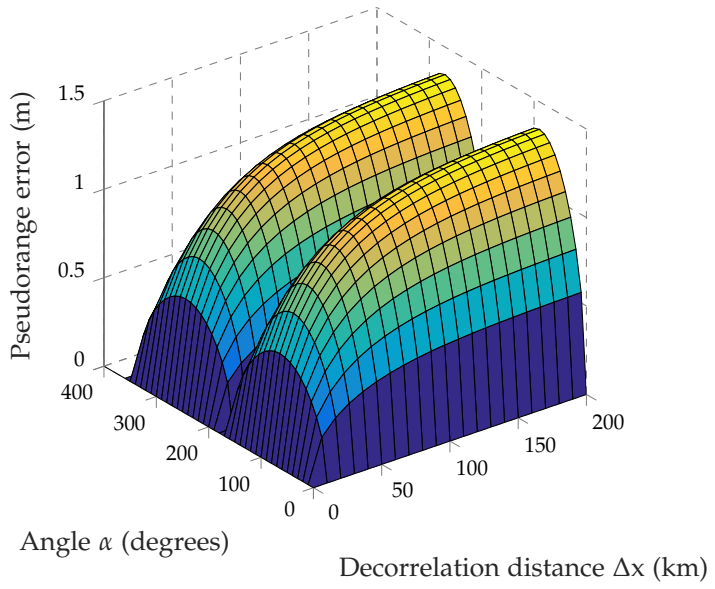

Figure 75: Figure showing an increase in the pseudorange error of the transmitter in view at the user, as the user's receiver moves away from the reference station. The SNR is assumed to be 30 dB. max (σ_r) = 1.3m

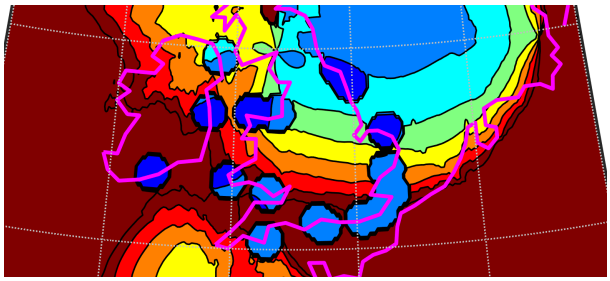

Figure 76: Figure showing possible positions of reference stations in GLA coverage area. The blue circles are show the coverage around the reference station.

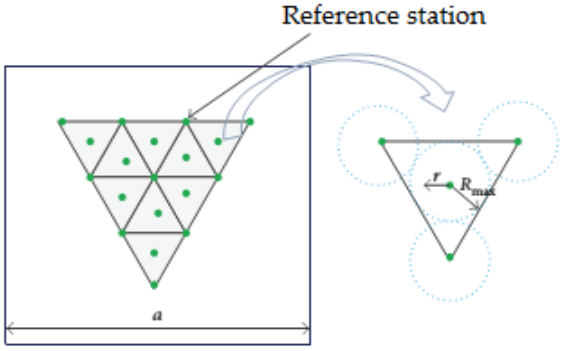

Figure 77: Figure showing optimum placement of reference stations.

$$C_p = \frac{\pi r^2 + \pi r^2/6 + \pi r^2/6 + \pi r^2/6}{3\sqrt{3}R_{max}^2} = \frac{\pi}{2\sqrt{3}}\left[\frac{r}{R_{max}}\right]^2 \tag{6.17}$$

An approximate number of reference stations required to cover a geographical area using triangular reference station deployment can be expressed as:

$$N_{ref} = \frac{1}{2\sqrt{3}}\left[\frac{a}{R_{max}}\right]^2 \tag{6.18}$$

It can be seen in figure 78 that as the range [3]reference station increases, a smaller the of number of reference stations will be needed to cover a specified coverage area. Therefore, the goal is to assess whether the reference stations installed in the GLA's coverage area are optimally positioned or not. It can be seen in figure 76 that the predicted coverage due to the Hurst and St. Catherines reference stations appear as if it is due to a single reference station. The same can be said about the predicted coverage of the reference stations in Whitby and Flamborough. In these scenarios, the reference stations are located close to each other, hence leading to combined coverage.

3 The range of a reference station is the minimum distance from the reference station at which the corrections are not valid

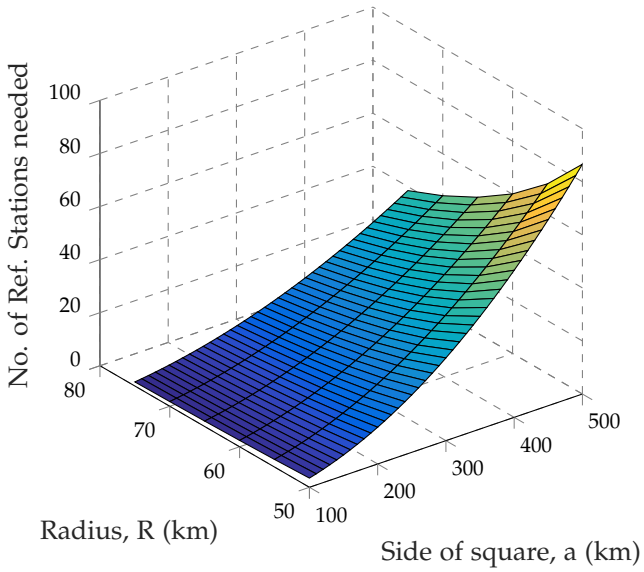

Figure 78: Figure showing the number of reference stations needed, if the reference station radial range is varied from $50 - 75$ km and the square side of the coverage area is varied from $100 - 500$ km. max (N_{max}) = 87.

6.10 SUMMARY AND CONCLUSIONS

This chapter discussed the existing ASF correction methods and presented a method of determining an interpolated ASF correction from multiple reference stations. This interpolated method reduces the pseudorange errors thereby increasing the spatial decorrelation distance. A large spatial decorrelation distance suggests that fewer reference stations will be needed to service the harbour. It is economical the optimize the reference stations' locations. This requires the knowledge of the range of the reference station, therefore, a heuristic method was proposed to determine the spatial decorrelation of the pseudorange errors. An mathematical equation has been derived to work out the number of reference station needed to service a harbour. An ASF correction method using a weighted correction from a single reference has also been presented. These methods can be combined with the ASF correction techniques described in chapter 7 to enhance accuracy performance of the model.

7 SPATIAL DECORRELATION MODEL

This chapter describes the model used to determine the expectation of the error in applying a phase delay correction at the user's receiver. This model is derived using a Taylor series function approximation. The three proposed ASF correction techniques are used to assess the degree of spatial decorrelation of the reference station corrections applied at the user's receiver. The techniques developed in this chapter helps to understand the effects of the long-term and the short-term temporal variations of the ASFs on position accuracies at the receiver locations.

7.1 DERIVATION OF PHASE DELAY

The total phase delay relative to a signal from transmitter to the receiver, travelling at the speed of light in vacuum is given by:

$$\varphi^i(x,t) = \varphi^i_1(x,t) + \varphi^i_2(x,t) + \varphi^i_{2a}(x,t) \tag{7.1}$$

where $\varphi^i_1(x,t)$ is the primary factor delay, $\varphi^i_2(x,t)$ is the secondary factor delay, $\varphi_{2a}(x,t)$ is the additional secondary factor (ASF) delay, x is the location of the user's receiver and t is the time. The expression for the primary factor (PF) delay is related to the parts per million of the refractive index of the atmosphere along the propagation path. The parts per million of the refractive index, $N^i(x,t)$ along the path from transmitter to any given point x at time t is given by:

$$N^i(x,t) = (\eta(x,t) - 1) \times 10^6 \tag{7.2}$$

The primary factor delay is given by:

$$\varphi_1(x,t) = \frac{d^i(x,t)\eta^i(x,t)}{c} - \frac{d^i(x,t)}{c} \tag{7.3}$$

where c is the speed of light in vacuum and $\eta^i(x,t)$ is the refractive index of the atmosphere at time t along the path from transmitter to point x. The $\eta^i(x,t)$ for the primary factor velocity is stated explicitly by the USCG as equal to 1.000338 [32]. The variation of the primary factor is due to the changes in the refractive index. Combining equation 7.2 and equation 7.3 and noting that $d^i(x,t)$ and c are constants, the variation in the primary factor delay can then be expressed as:

$$\varphi(x,t) = \frac{d^i(x,t)}{c} N^i(x,t) \times 10^{-6} \tag{7.4}$$

$N^i(x,t)$ is made up of two components (see chapter 4, section 4.5). The first component is the dry term and the second component is the wet term. The literature suggests that it is sufficient to model just the dry term. Throughout this chapter it is assumed that $N^i(x,t)$ is equivalent to the dry term, N_{dry} [27]. Figure 80 shows the estimate of the variation of $N^i(x,t)$ of the transmitters in view at Harwich. The secondary factor delay can be determined using Brunavs' equations [14] and stored in the receiver memory.

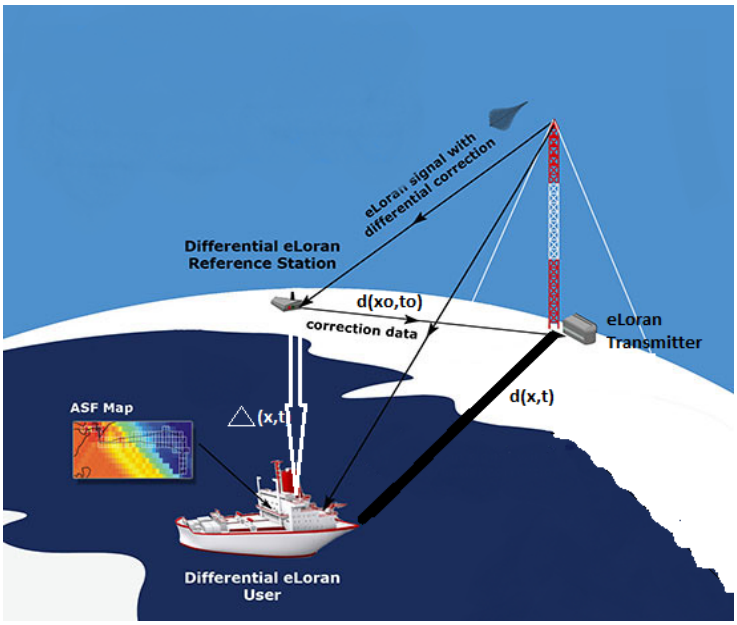

Figure 79: Differential Loran setup.

This work therefore focuses on determining the changes over time of the primary factor and additional secondary factors in the coverage area. Let

$$\vartheta^i(x,t) = \varphi_1^i(x,t) + \varphi_{2a}^i(x,t) \tag{7.5}$$

Equation 7.5 is referred to as the phase delay since in practice the primary factor and the additional secondary factors tend to be lumped together. The Landpath model was discussed in chapter 4. Figure 79 shows the location of a ship doing a harbour entrance and approach. The great circle distance between the transmitter and the ship is given by $d^i(x,t)$. The distance between the reference station and the transmitter is given by $d^i(x_0,t_0)$ and δx is the distance vector between the user's receiver and the reference station. A functional approximation of the phase delay at the locations of the ship and the reference station is postulated as follows: Let the variations of the function at locations x_0 and x at times t_0 and t . The reference station is located at x_0 and the user's receiver is at x . The distance between the reference station and the user's receiver is given by δx while δt is the temporal change of the functional approximation.

The Taylor series expansion can be used to develop the model for the expectation of the ASFs at the user's receiver as well as the error introduced by applying differential ASFs.

7.2 ESTIMATING THE ELORAN PHASE DELAY USING A FIRST-ORDER TAYLOR SERIES EXPANSION

The phase delay of the signal from transmitter i at the user's receiver located at x at time t is given by the sum of $\varphi(x,t) = \frac{d^i(x,t)}{c} N^i(x,t) \times 10^{-6}$ and $\varphi_{2a}^i(x,t) = \beta l^i(x,t)$. where $l^i(x,t)$ is the land path distance between the transmitter and the mariner and β is the long term variation of the ASF with distance. Therefore the phase delay β is given by,

$$\vartheta^i(x,t) = \frac{d^i(x,t)}{c} N^i(x,t) \times 10^{-6} + \beta l^i(x,t) \tag{7.6}$$

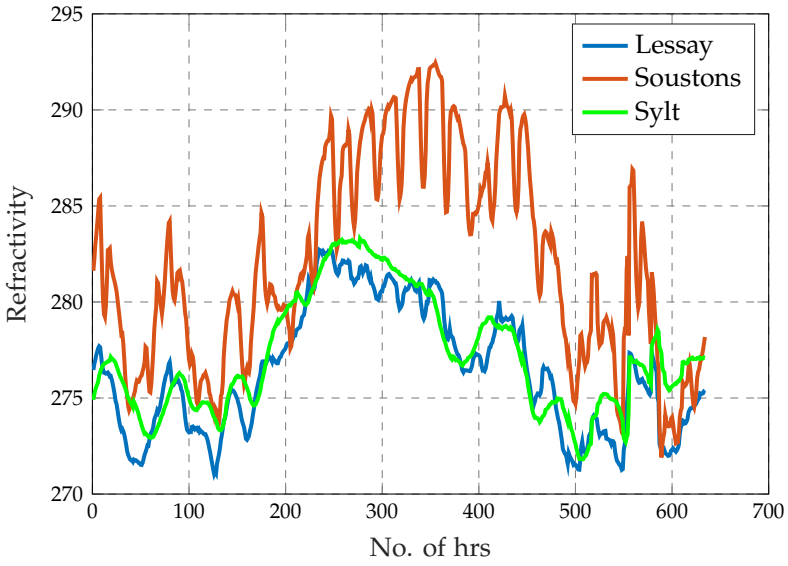

Figure 80: Estimated Refractivity of the signals in view at Harwich.

The first-order Taylor series expansion of the phase delay can be expressed as:

$$\vartheta^i(x,t) \approx \vartheta^i(x_0,t_0) + \frac{\partial \vartheta^i(x_0,t_0)}{\partial x}\delta x + \frac{\partial \vartheta^i(x_0,t_0)}{\partial t}\delta t \tag{7.7}$$

where $\frac{\partial \vartheta^i(x_0,t_0)}{\partial x}$ is the derivative of $\vartheta^i(x,t)$ evaluated at (x_0,t_0). It is assumed that all the derivatives are evaluated at the reference station (x_0,t_0). The estimate of the error in applying the phase delay corrections generated at the reference station located at (x_0,t_0) , at the user's receiver located at (x,t) using first-order Taylor series expansion is given by:

$$\varepsilon^i(x,t) = \vartheta^i(x,t) - \vartheta^i(x_0,t_0) \tag{7.8}$$

so,

$$\begin{aligned}\varepsilon^i(x,t) \approx \frac{\partial \vartheta^i(x_0,t_0)}{\partial x}\delta x \cdots \\ + \frac{\partial \vartheta^i(x_0,t_0)}{\partial t}\delta t\end{aligned} \tag{7.9}$$

where,

$$\begin{aligned}\frac{\partial \vartheta^i(x,t)}{\partial x} = \beta\frac{\partial I^i(x_0,t_0)}{\partial x} \\ +[\frac{\partial d^i(x_0,t_0)}{\partial x}N^i(x_0,t_0) + d^i(x_0,t_0)\frac{\partial N^i(x_0,t_0)}{\partial x}] \times \frac{10^{-6}}{c}\end{aligned} \tag{7.10}$$

since $\beta\frac{\partial I^i(x_0,t_0)}{\partial x} = 0$ and $\frac{\partial d^i(x_0,t_0)}{\partial t} = 0$, therefore

$$\frac{\partial \vartheta(x_0,t_0)}{\partial t} = d^i(x_0,t_0)\frac{\partial N(x_0,t_0)}{\partial t} \times \frac{10^{-6}}{c} \tag{7.11}$$

The expectation of the error in the phase delay correction at location x at time t is given by:

$$E\left\{\varepsilon^i(x,t)\right\} = \beta\frac{\partial l^i(x_0,t_0)}{\partial x}\delta x + \frac{\partial d^i(x_0,t_0)}{\partial x}E\left\{N^i(x_0,t_0)\right\}\frac{10^{-6}}{c}\delta x... \\ +d^i(x_0,t_0)\frac{10^{-6}}{c}\left[E\left\{\frac{\partial N^i(x_0,t_0)}{\partial x}\delta x\right\} + E\left\{\frac{\partial N^i(x_0,t_0)}{\partial t}\delta t\right\}\right] \tag{7.12}$$

The ASFs at the reference station can be assumed to be continuously monitored and over a long period of time. In this case: $E\left\{\frac{\partial N^i(x_0,t_0)}{\partial t}\delta t\right\} = 0$. Therefore,

$$E\left\{\varepsilon^i(x,t)\right\} = \beta\frac{\partial l^i(x_0,t_0)}{\partial x}\delta x + \frac{\partial d^i(x_0,t_0)}{\partial x}E\left\{N^i(x_0,t_0)\right\}\frac{10^{-6}}{c}\delta x... \\ +d^i(x_0,t_0)\frac{10^{-6}}{c}E\left\{\frac{\partial N^i(x_0,t_0)}{\partial x}\delta x\right\} \tag{7.13}$$

where $l^i(x,t)$ and $l^i(x_0,t_0)$ are the land path distances seen by the test site and the reference station respectively; $d^i(x,t)$ and $d^i(x_0,t_0)$ are the actual great circle line distances of the transmitter from the test point and reference station respectively. The actual distance vector of the transmitter from the ship to the reference station is denoted by δx. The distance between transmitter i and the reference station is proposed to be related to the land path distance between the same transmitter and the reference station by some function $\alpha^i(x_0,t_0)$, this can be expressed as:

$$l^i(x_0,t_0) = \alpha^i(x_0,t_0)d^i(x_0,t_0), (0 \leq \alpha^i \leq 1) \tag{7.14}$$

Differentiating 7.14 with respect to x ,

$$\frac{\partial l^i(x_0,t_0)}{\partial x} = \alpha^i(x_0,t_0)\frac{\partial d^i(x_0,t_0)}{\partial x} + d^i(x_0,t_0)\frac{\partial \alpha^i(x_0,t_0)}{\partial x} \tag{7.15}$$

If the coastline is not accurately known, it can be assumed that $\frac{\partial \alpha^i(x_0,t_0)}{\partial x} = 0$,

$$\frac{\partial l^i(x_0,t_0)}{\partial x} = \alpha^i(x_0,t_0)\frac{\partial d^i(x_0,t_0)}{\partial x} \tag{7.16}$$

A plane earth model can be assumed where, $\frac{\partial d^i(x_0,t_0)}{\partial x}$ can be expressed as $-\cos(\theta^i)$. A spherical geometry cosine law can be used to determine the angle θ^i. Points A, B and C in figure 81 represent the locations of the reference station, test point and transmitter respectively and θ^i is the angle subtended by C at A from B. This gives:

$$E\left\{\varepsilon^i(x_0,t_0)\right\} = \beta\alpha^i cos\theta^i \parallel \delta x \parallel \\ +\frac{10^{-6}}{c}\left[-E\left\{N^i(x_0,t_0)\right\}cos\theta^i \parallel \delta x \parallel\right]... \\ +\frac{10^{-6}}{c}d(x,t)E\left\{\frac{\partial N^i(x_0,t_0)}{\partial x}\delta x\right\} \tag{7.17}$$

where $\parallel \delta x \parallel$ is the magnitude of δx and $E\left\{N^i(x_0,t_0)\right\}$ is the average of the refractivity for the i^{th} transmitter path at the reference station. Sections 7.2.1-7.2.2 develops the equations for special cases of equation 7.17.

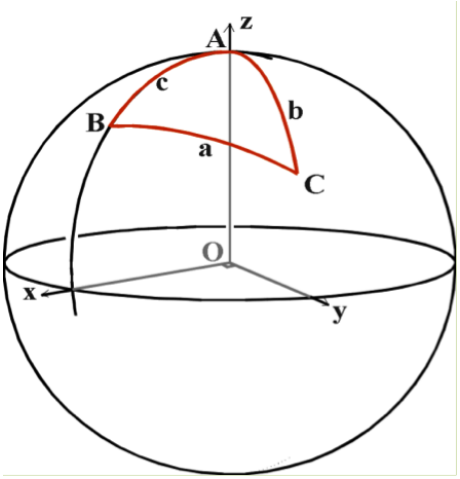

Figure 81: Coordinates of the reference, user and transmitter.

7.2.1 *Similar weather changes at the reference station and user's receiver*

It is reasonable to assume that the weather changes at the reference station, user's receiver and between them are the same. In this case, $\frac{\partial N^i(x_0,t_0)}{\partial x}$ in 7.17 can be set to zero. Thus, the expectation of the error on the phase delay correction for a single transmitter can be expressed as:

$$E\left\{\varepsilon^i(x,t)\right\} \approx -\left[\beta\alpha^i + \frac{10^{-6}}{c} E\left\{N^i(x_0,t_0)\right\}\right] cos\theta^i \parallel \delta x \parallel \tag{7.18}$$

7.2.2 *Passing weather front*

A passing weather front can be simulated by setting $\frac{\partial N^i(x_0,t_0)}{\partial x} = \lambda\ N - units/km$. Under this assumption, the parts per million of the refractive index is assumed to change by λ N-units per kilometre from the reference station. The expectation of the error in the phase delay correction can be expressed as:

$$\begin{aligned} E\left\{\varepsilon^i(x,t)\right\} \approx -\left[\beta\alpha^i + \frac{10^{-6}}{c} E\left\{N^i(x_0,t_0)\right\}\right] cos\theta^i \parallel \delta x \parallel \ldots \\ + d^i(x_0,t_0)\frac{10^{-6}}{c} \times \lambda \parallel \delta x \parallel \end{aligned} \tag{7.19}$$

The next section describes the technique for applying ASFs at the user.

7.3 APPLYING DIFFERENTIAL ASFS FROM THE REFERENCE STATION AT THE USER'S RECEIVER

The differential ASF generated at the reference station is given by:

$$\eta^i(x,t) = \vartheta^i(x,t) - \vartheta^i(x,t_0) \approx \frac{\partial\vartheta^i(x,t_0)}{\partial t}\delta t \tag{7.20}$$

where $\vartheta^i(x,t_0)$ is the nominal ASF and $\vartheta^i(x,t)$ is the ASF measured at time t . By first-order Taylor series approximation:

$$\frac{\partial\vartheta^i(x,t_0)}{\partial t}\delta t \approx \frac{\partial\vartheta^i(x,t)}{\partial t}\delta t + \frac{\partial}{\partial t}\left[\frac{\partial\vartheta^i(x,t)}{\partial x}\delta x\right]\delta t \tag{7.21}$$

The error due to applying the differential ASF from the reference station at the user's receiver is given by the difference in the differential ASFs in 7.20 and 7.21. Hence,

$$\eta^i(x,t) - \eta^i(x,t) \approx \frac{\partial^2 \vartheta^i(x_0,t_0)}{\partial t \partial x} \delta x \delta t \tag{7.22}$$

Taking the variances gives:

$$V\left[\eta^i(x,t) - \eta^i(x,t)\right] = V\left[\frac{\partial^2 \vartheta^i(x_0,t_0)}{\partial t \partial x} \delta x \delta t\right] \tag{7.23}$$

and

$$V\left[\eta^i(x,t)\right] = V\left[\frac{\partial^2 \vartheta^i(x_0,t_0)}{\partial t \partial x} \delta x \delta t + \frac{\partial \vartheta^i(x,t)}{\partial t} \delta t\right] \tag{7.24}$$

Equation 7.23 represents the variance of the error due to applying a dynamic differential ASF correction from the reference station at the user's receiver. Equation 7.24 represents the variance of the error due to applying a static differential ASF correction from the reference station at the user's receiver. Using equation 7.12

$$\frac{\partial \vartheta^i(x_0,t_0)}{\partial t} = d^i(x_0,t_0) \frac{10^{-6}}{c} \frac{\partial N^i(x_0,t_0)}{\partial t} \tag{7.25}$$

and

$$\begin{aligned} \frac{\partial^2 \vartheta^i(x_0,t_0)}{\partial t \partial t} &= d^i(x_0,t_0) \frac{10^{-6}}{c} \frac{\partial^2 N^i(x_0,t_0)}{\partial t \partial x} \cdots \\ &+ \frac{\partial d^i(x_0,t_0)}{\partial x} \frac{10^{-6}}{c} \frac{\partial N^i(x_0,t_0)}{\partial t} \end{aligned} \tag{7.26}$$

The term $\frac{\partial^2 \vartheta^i(x_0,t_0)}{\partial t \partial x}$ is assumed to be zero. Therefore,

$$\frac{\partial^2 \vartheta^i(x_0,t_0)}{\partial t \partial x} = \frac{\partial d^i(x_0,t_0)}{\partial x} \frac{10^{-6}}{c} \frac{\partial N^i(x_0,t_0)}{\partial t} \tag{7.27}$$

The variances of equation 7.26 and equation 7.27 can be determined. So,

$$\begin{aligned} V\left[\eta^i(x,t) - \eta^i(x_0,t)\right] &= V\left[\frac{\partial d^i(x_0,t_0)}{\partial x} \delta x \frac{10^{-6}}{c} \frac{\partial N(x_0,t_0)}{\partial t} \delta t\right] \\ &= \left(\frac{\partial d^i(x_0,t_0)}{\partial x} \delta x\right)^2 \frac{10^{-12}}{c^2} V\left[\frac{\partial N(x_0,t_0)}{\partial t} \delta t\right] \end{aligned} \tag{7.28}$$

And similarly

$$\begin{aligned} V\left[\eta^i(x,t)\right] &= V\left[\left(\frac{\partial d^i(x_0,t_0)}{\partial x} \delta x + d^i(x_0,t_0)\right) \frac{10^{-6}}{c} \frac{\partial N(x_0,t_0)}{\partial t} \delta t\right] \\ &= \left(\frac{\partial d^i(x_0,t_0)}{\partial x} \delta x + d^i(x_0,t_0)\right)^2 \frac{10^{-12}}{c^2} V\left[\frac{\partial N(x_0,t_0)}{\partial t} \delta t\right] \end{aligned} \tag{7.29}$$

The next section describes the accuracy methods to determine position error after applying the phase correction at user's location.

7.4 CALCULATING REPEATABLE ACCURACIES

This section describes the procedure of determining accuracy after applying a correction at the user's position. A vector for the expectation of the errors in the phase delay on all the transmitters in view at the user's receiver is given by:

$$E\left\{\begin{bmatrix} \varepsilon^1(x,t) \\ \varepsilon^2(x,t) \\ \vdots \\ \varepsilon^N(x,t) \end{bmatrix}\right\} = E\left\{\boldsymbol{\Delta\rho}\right\} \tag{7.30}$$

where $\Delta\rho$ is the vector of the pseudorange. The position error can be determined using the weighted least squares.

$$E\left\{\boldsymbol{\Delta u}\right\} = \left(\boldsymbol{A^T W A}\right)^{-1} \boldsymbol{A W} E\left\{\boldsymbol{\Delta\rho}\right\} \tag{7.31}$$

where $E\left\{\boldsymbol{\Delta u}\right\}$ is the position error vector and $\boldsymbol{W}$ is the weighting matrix and $\boldsymbol{A}$ is the geometry matrix of the transmitters in view. Equation 7.31 gives the average repeatable accuracy of the position. The repeatable accuracy is calculated by taking the variance of the position errors. This is given by:

$$V\left[\Delta u\right] = \left(A^T W A\right)^{-1} A^T W V\left[\Delta\rho\right] W A \left(A^T W A\right)^{-1} \tag{7.32}$$

If $\boldsymbol{W} = \boldsymbol{V}\left[\boldsymbol{\Delta\rho}\right]^{-1}$, then repeatable accuracy is just given by:

$$V\left[\boldsymbol{\Delta u}\right] = \left(\boldsymbol{A^T W A}\right)^{-1} \tag{7.33}$$

The distance root mean square of the position error can be expressed as:

$$\boldsymbol{\Delta u_{drms}} = \sqrt{\frac{1}{2}} tr\left(\begin{bmatrix} 1 & 0 & 0 \\ 0 & 1 & 0 \end{bmatrix} \boldsymbol{V}\left[\boldsymbol{\Delta u}\right] \begin{bmatrix} 1 & 0 \\ 0 & 1 \\ 0 & 0 \end{bmatrix}\right) \tag{7.34}$$

7.4.1 *The weighting matrix*

The position algorithm employed in the eLoran receiver weights the received signals in terms of their SNRs. It was stated in chapter 4 that the time of arrival variances of the transmitted signals is used to form a covariance matrix whose inverse is the weighting W for equation 7.31. The time of arrival variance equation for the received signal is given by:

$$V\left[\boldsymbol{TOA^i(x,t)}\right] = L_{impl} \frac{337.5^2}{N_p \cdot \boldsymbol{\gamma^i(x,t)}} \tag{7.35}$$

Equation 7.35 was proposed by Sherman Lo et al [57, 49, 51, 50, 53] and was later modified by Jan Safar et al [77]. In practice, differential ASFs are not provided everywhere in the coverage area. The goal, therefore, is to study the long-term variations of the ASF in the coverage area and dilute the dLoran model in areas where dLoran is not provided. The study of the long-term variations of the ASFs was discussed in chapter 4 to be related to the land path distances under the assumption that conductivity changes are the same throughout the coverage area. It is assumed that the seasonal

variations in the ASFs increase the pseudorange error by the square root of $\left(300\delta\left(l^i(x,t)\right)-l^i(x_0,t_0)\right)^2$where, $\delta = 333ns/Mm$, $l^i(x,t)$ is the land path distance between transmitter i and the user's receiver and $l^i(x_0,t_0)$ is the land path distance between transmitter i and the reference station. According to the propagation error laws, the variances add. Therefore the TOA variance can be expressed as:

$$V^{(1)}\left[\boldsymbol{TOA^i(x,t)}\right] = \left(L_{impl}\frac{337.5^2}{N_p\cdot\boldsymbol{\gamma^i(x,t)}}\right) + \left(300\delta(\boldsymbol{l^i(x,t)}-\boldsymbol{l^i(x_0,t_0)})\right)^2 \tag{7.36}$$

The variance in the time of arrival due to changes in the weather can be added to the existing time of arrival variance equation 7.36:

$$V^{(2)}\left[\boldsymbol{TOA^i(x,t)}\right] = V\left[\boldsymbol{\eta^i(x,t)}\right] + \left(L_{impl}\frac{337.5^2}{N_p\cdot\boldsymbol{\gamma^i(x,t)}}\right) + \left(300\delta(\boldsymbol{l^i(x,t)}-\boldsymbol{l^i(x_0,t_0)})\right)^2 \tag{7.37}$$

and

$$V^{(3)}\left[\boldsymbol{TOA^i(x,t)}\right] = V\left[\boldsymbol{\eta^i(x,t)}-\boldsymbol{\eta^i(x_0,t)}\right]\cdots + \left(L_{impl}\frac{337.5^2}{N_p\cdot\boldsymbol{\gamma^i}(\mathrm{x,t})}\right) + \left(300\delta(\boldsymbol{l^i}(\mathrm{x,t})-\boldsymbol{l^i(x_0,t_0)})\right)^2 \tag{7.38}$$

The TOA variances of the received signals are used to form the covariance matrix.

$$R_{(1)} = \begin{bmatrix} V^{(1)}\left[TOA^1(x,t)\right] & \cdots & 0 \\ 0 & \ddots & 0 \\ 0 & \cdots & V\left[TOA^N(x,t)\right] \end{bmatrix},$$

$$R_{(2)} = \begin{bmatrix} V^{(2)}\left[TOA^2(x,t)\right] & \cdots & 0 \\ 0 & \ddots & 0 \\ 0 & \cdots & V\left[TOA^N(x,t)\right] \end{bmatrix} \tag{7.39}$$

$$and\ R_{(3)} = \begin{bmatrix} V^{(3)}\left[TOA^3(x,t)\right] & \cdots & 0 \\ 0 & \ddots & 0 \\ 0 & \cdots & V\left[TOA^N(x,t)\right] \end{bmatrix}$$

The weighting matrix W is the inverse of the covariance matrix. It can either be $R_{(1)}$ or $R_{(2)}$ or $R_{(3)}$ depending on the test case.

7.4.2 *Repeatable accuracy calculations after applying differential ASFs*

This section describes the methods used to determine the position error after applying differential ASFs at the user's location. Three cases are proposed:

- Apply a differential ASF correction at the user's receiver without the weather effects,

Table 18: Table showing peak-to-peak TOAs recorded in Harwich from various transmitters.

Station	Peak-to-Peak TOA (μs)	Landpath distance from station to Harwich (km)
Anthorn (6731)	0.2828	446.1
Sylt (6731)	0.2616	20.8
Sylt (7499)	0.2765	20.8
Lessay (7499)	0.2186	165.4
Lessay (6731)	0.2204	165.4
Soustons	0.4495	736.6

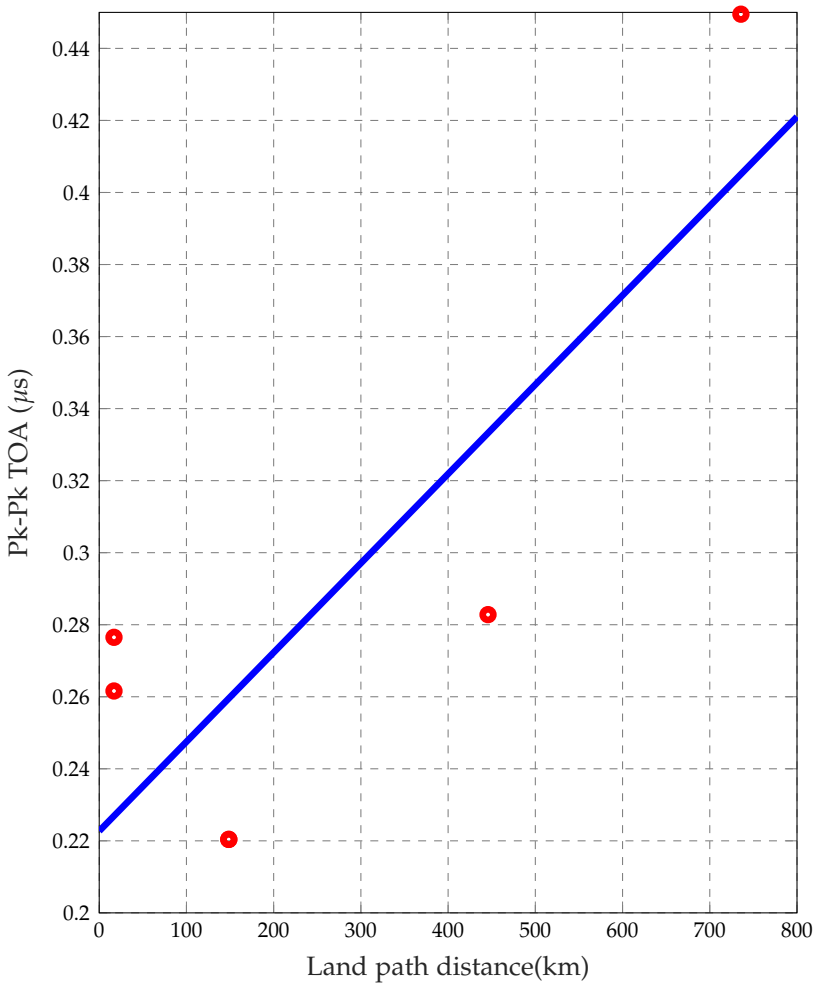

Figure 82: The Linear model for the Landpath vs. TOA peak-to-peak of the stations recorded at Harwich between October 2009 to October 2010. The gradient of the graph is 333 ns/Mm. More points are needed to accurately determine the slope of the graph.

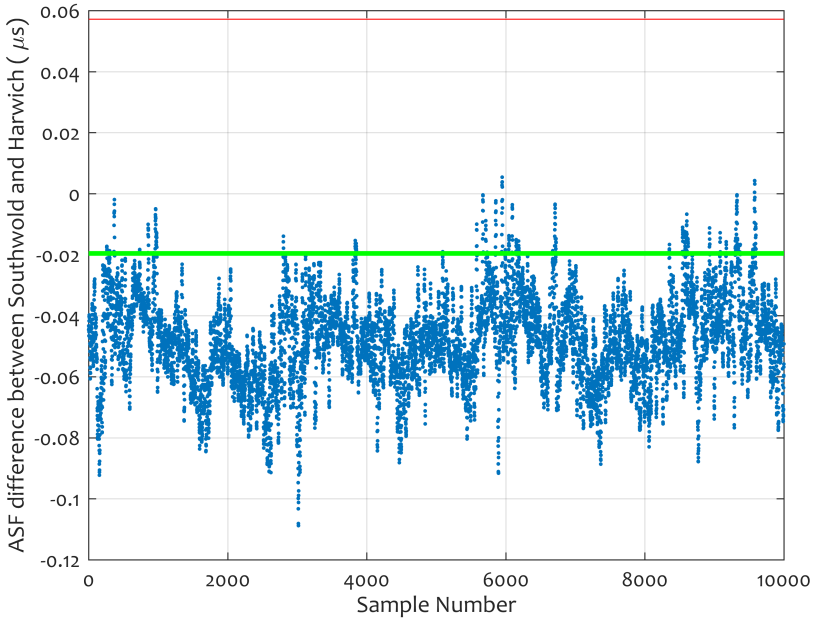

.

Figure 83: The difference between Anthorn ASF corrections from Southwold and Harwich

- Apply a static differential ASF correction at the user's receiver, and
- Apply a dynamic differential ASF correction at the user's receiver

The TOA variance for each case is determined differently. Section 7.4.3-7.4.5 derive the method for determining the position error using the cases mentioned in this section.

7.4.3 *Differential ASF correction applied at the user's receiver without taking the weather effects into account*

The position error for this case is determined using equation 7.36 where $W = R_{(1)}^{-1}$ and $R_{(1)}^{-1}$ is the inverse of $R_{(1)}$. hence,

$$V\left[\triangle u\right] = \left(A^T R_{(1)}^{-1} A\right)^{-1} \tag{7.40}$$

7.4.4 *Applying a static differential ASF correction at user's receiver*

This model assumes that the reference station is sending a static differential ASF to the mariner. A static correction technique is similar to a scenario where a reference station was installed but later transferred elsewhere (that is, the mariners will be using an old correction). This is better than having no differential ASFs at all. The position error for this case can be determined using:

$$s(x,t) = (A^T W A)^{-1} A^T W \eta(x,t) \tag{7.41}$$

where

$$\eta(x,t) = \begin{bmatrix} \eta^i(x,t) \\ \vdots \\ \eta^N(x,t) \end{bmatrix} \tag{7.42}$$

so

$$V[s(x,t)] = (A^T W A)^{-1} A^T W V[\eta(x,t)] W A (A^T W A)^{-1} \tag{7.43}$$

The term $V[\eta(x,t)]$ can be replaced by R_2 to inflate the variance. Therefore

$$V[s(x,t)] = (A^T W A)^{-1} A^T W R_2^{-1} W A (A^T W A)^{-1} \tag{7.44}$$

7.4.5 *Applying a dynamic differential ASF correction at user's receiver*

In reality, the reference station sends dynamic correction information to the users at a specified update rate. It was shown in [95] that a fixed update rate may not be appropriate for the entire year due to poor performance in the winter season. The poor performance can be attributed to broadcast pseudorange corrections lagging the TOA variations. In eDLoran, the users sends their raw position information to the server where dynamic corrections are applied to the raw positions. The position error for this correction technique is given by:

$$s(x,t) - s(x_0,t) = (A^T W A)^{-1} A^T W [\eta(x,t) - \eta(x_0,t)] \tag{7.45}$$

The terms $[\eta^j(x,t) - \eta^j(x_0,t)]$ and $[\eta^i(x,t) - \eta^i(x_0,t)]$ are assumed to be uncorrelated for $j \neq i$. The term $V[\eta(x,t) - \eta(x_0,t)]$ can be replaced by R_3^{-1}. The variance is given by:

$$V[s(x,t) - s(x_0,t)] = (A^T W A)^{-1} A^T W R_3 W A (A^T W A)^{-1} \tag{7.46}$$

let $W = R_2^{-1}$

$$V[s(x,t) - s(x_0,t)] = (A^T R_2^{-1} A)^{-1} A^T R_2^{-1} R_3 R_2^{-1} A (A^T R_2^{-1} A)^{-1} \tag{7.47}$$

The next section uses real data to validate the methods described in this section.

7.5 VALIDATION OF THE NEW PHASE DELAY CORRECTION METHOD AGAINST REAL DATA

This section describes the experiments used to validate the proposed ASF techniques. Four sites (Felixstowe, Orfordness, Aldeburgh and Southwold) were chosen to represent the locations of the receiver. The corrections from the Harwich reference station were applied at the four sites using the proposed techniques. Column 3 of the table 19 shows the position errors at the four sites using equation 7.36. Theere is not much difference in the position between the four sites. This is attributed to the land path distance of the propagation path from the transmitter to Harwich and each site being almost the same. The baseline distance between Felixstowe and Southwold is about 45km, yet the position error difference by 0.3 m. The results suggests that geometry contributes more to the position errors. Column 4 of table 19 shows the position accuracy by applying a static correction to demonstrate the effect of decorrelation due to short-term ASF variations.

Table 19: Table showing the position errors after using the corrections from Harwich.

Test Site	Distance from Harwich (km)	95 % error(m) due to landpath model	95 % error(m) due to Landpath and Weather models
Felixstowe	5.3	8.0	8.4
Orfordness	25.8	8.1	8.4
Aldeburgh	32.1	8.2	8.5
Southwold	51.3	8.3	8.6

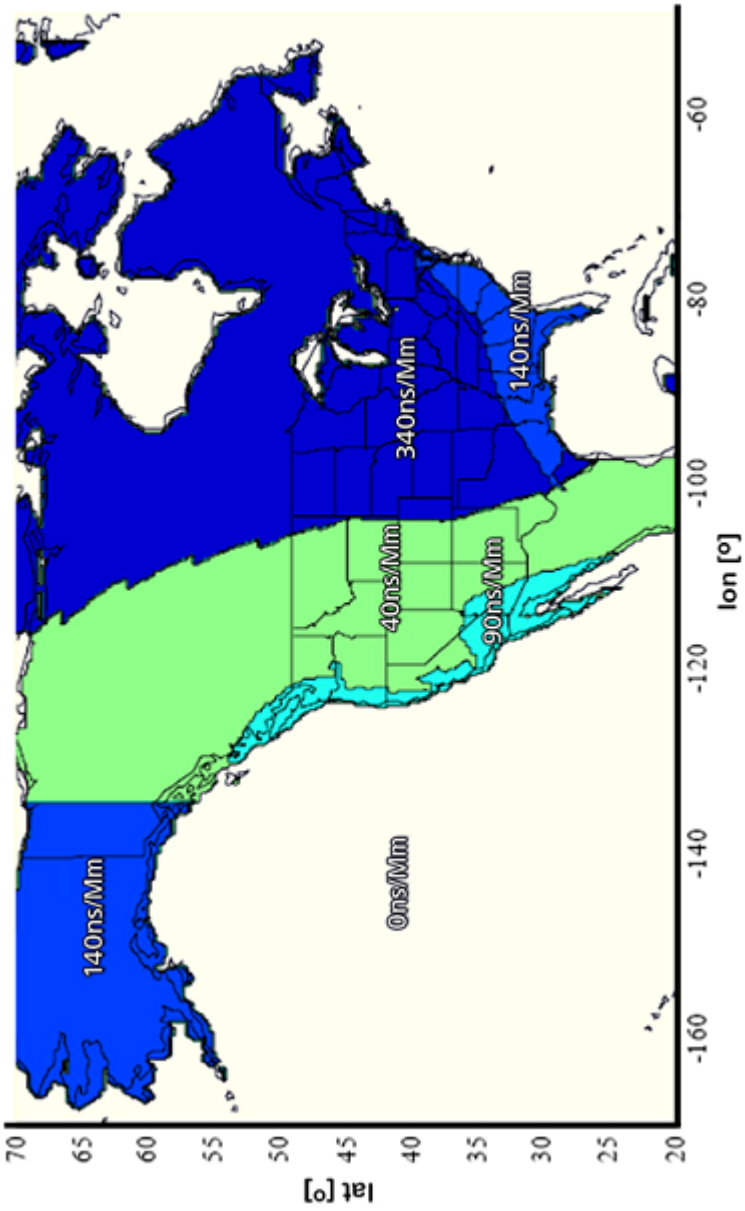

Figure 84: Figure showing the rate of change of TOA with distances over soils of different conductivity [74]. The rate of change of 333ns/Mm closely matches the values in this diagram.

The results suggest that the position error at the test sites increases with distance from the reference station. It can be seen that there is not much difference in position error between the four sites. This is because the pair of sites used in the analysis were within a distance of 50 km from each other. These results agree with the assumption that differential corrections remain valid at 50 km from the reference station. In this experiment, the weather contributes about 4 % to the position errors.

7.5.1 *Applying the ASF correction determined at Harwich Reference Station at the Southwold Reference Station*

The ASF techniques were validated using real data by the applying the Harwich ASF corrections at Southwold. The TOA data was processed to remove outliers. The Harwich and Southwold ASF corrections were time aligned. The error after applying the Harwich pseudorange corrections at Southwold reference station is equal to the difference in their pseudorange corrections. The blue line in figure 83 shows the expected error after applying the Anthorn PRC generated at Harwich on the Anthorn signal received at Southwold. The pseudorange error introduced by this correction technique is about 12m. The effect of these pseudorange errors on accuracy is also dependent on the geometry of the transmitters used to compute the position fix. The green line represents the expectation of the error in approximating the phase delay of the Anthorn transmitter at Southwold using equation 7.18. The red line simulates the expected error due to a passing weather front between the reference station and the test site. The overall position error at Southwold after applying the correction from Harwich is 8.6 m. The position error at Southwold using Southwold corrections is less than 10m.

7.6 SUMMARY AND CONCLUSIONS

The results from the experiments suggest that the model is sensitive to the weather changes. The limitations of the model may be due to ignoring the effects of other short-term ASF variations[1]. The short-term due to rain soaking into the earth will need to be investigated in the future to enhance the model. The model can be enhanced using the second-order Taylor series expansion instead of the first-order. A linear ASF interpolation method was proposed in chapter 6 can be combined with these methods to improve position accuracy at the user's location.

1 The short-term effects investigated here are due to the change in the refractive index. Other short term ASF variations such as rain soaking into the earth, freeze-thaw path are not modelled.

8 AVAILABILITY MODEL

The aim of this chapter is to develop a service availability model for eLoran over the GLA's coverage area. The developed availability model utilises the transmitter availability statistics obtained from the control centre in Brest. This chapter consists of two main parts. The first part introduces the definitions of the key terms and discusses availability models proposed by other researchers while the second part describes the framework of the availability model developed for eLoran over the GLA coverage area.

8.1 AVAILABILITY STANDARDS

Availability is defined by the standards set out by governing bodies. Table 20 summarises the availability requirements set out by international bodies. The Federal Radionavigation Plan (FRP) and the United States Coast Guard (USCG) are examples of the governing bodies that exists and their standards are strictly applicable in the US. For critical areas such as harbours and ports, the availability figure set out by IMO Resolution 860 is adopted. Several definitions of availability have been stipulated in the literature. The following section defines availability as applicable to eLoran.

Table 20: Signal availability specifications.

Document	Availability Requirement
IMO (860)	99.8 % Everywhere
IALA (815)	99.8 % Critical Areas 99.5 % All other Areas
FRP	99.9 % Critical areas 99.7% All other areas
USCG	99.7% Everywhere

8.2 AVAILABILITY DEFINITIONS

Availability is defined as the ability of the system to perform required function at the initiation of the intended operation. Availability provides an indication of the system's ability to provide usable service within the geographical area over which coverage is to be assessed [74, 62].

In Engineering systems, the metric often used in contracts , designs and discussion is availability. A system is said to be available if it is working and unavailable if it has failed. When examined as a statistical quantity, availability can take two different quantitative definitions, namely average availability and instantaneous availability. The average availability of system is defined as the statistical probability that a system is working over a defined period of time. For instance, if a system life cycle is to be considered, then the availability of the system can be expressed as:

$$A = \frac{System\ Uptime}{System\ Operational\ Time} \tag{8.1}$$

The availability equation (8.1) provides no insight with regard to the frequency and durations of outages that are experienced by the system. The technical definition of availability is not limited to its average value. Availability can also be defined in terms of a time independent function $A(t)$ given by:

$$A(t) = Pr(X(t) = 1), \forall t \geq 0 \tag{8.2}$$

where $A(t)$ specifies availability for a moment in time and is thus referred to as the instantaneous availability. Instantaneous availability $A(t)$ is related to the average availability $\tilde{A}(t)$ through the following relationship:

$$\tilde{A}(t) = \frac{1}{t_2 - t_1} \int_{t_1}^{t_2} A\,(t)\,dt \tag{8.3}$$

To visualize the concept of availability, consider two system designs which achieve availability. In this scenario, one system has relatively frequent, short duration outages and is brought back to the operational state quickly. In the second system, the components in use are extremely reliable but due to design constraints repair is difficult and therefore time consuming. This results in infrequent and long outages. Someone who wishes to use the system would need to be advised to understand both the mean time to repair (MTTR) for a system failure as well as its expected failure modes. The most familiar form of availability is in relation to the mean time between failures (MTBF) and the mean time to repair (MTTR). The terms MTBF and MTTR refer to the average time that the system is functioning between failure events and the average time it takes to get the system back into service in the event that it had failed. In telecommunications systems, the achievable availability is often bounded. Developing a clear understanding of system failure modes reduces risk and allows all parties involved to make the best and most informed decisions regarding operations of an eLoran system. Hua [33] in his work for availability assessment for reactor protection systems stated that availability is not only related to safety but is also linked to the economic interests.

Mean Time Between Failures And Mean Time To Repair

The most common metric in radio and telecommunications systems is MTTR. MTTR is the average time that the system is not operational. This restoration period applies to either planned and unplanned outage events. In communication systems two types of downtime are observed. Downtime events can be due to planned system maintenance such as preventative maintenance, system upgrades, system growth and reconfiguration [33]. These types of events are coordinated. The second type of downtime occurs due to a system failure resulting in service outage. This type of downtime is of primary interest to users, designers and operators of system.

In eLoran, the expectation is that the planned maintenance of an eLoran station must be coordinated so that it lasts for shorter durations of time in order to maximise availability [46]. This is because unplanned outages usually require additional time to detect the outage, its location and get to the location of the outage to effect the repair [34]. MTTR is often used interchangeably with mean downtime (MDT). MDT is the sum of MTTR and the time it takes to identify the failure and to start the repair. Failure identification and dispatch can vary from minutes to hours.

Another fundamental metric used in the analysis and design of communication systems is the MTBF. It describes the expected performance to be obtained by a system. MTBF is also stated in hours. Since MTBF is an expected value of the time to failure (TTF). TTF is a statistically distributed random variable. In communication systems it is assumed that TTF follows an exponential distribution. The exponential distribution is used because of its memory-less property and its accurate representation of an electronic component time to failure. The PDF of the exponential function is given by:

$$f(x) = \begin{cases} \lambda e^{-\lambda x}, \forall x \geq 0 \\ 0, \forall x < 0 \end{cases} \tag{8.4}$$

The Control Centre in Brest [13], provides monthly statistical information containing the outages of Loran transmitters providing coverage in Europe. This information is used to calculate the availability of an eLoran transmitter in the GLA's coverage area. With regard to the eLoran system, the GLAs are

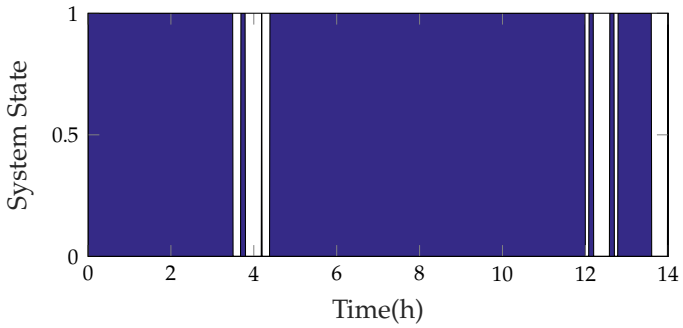

Figure 85: Average availability for a system with frequent short duration outages .

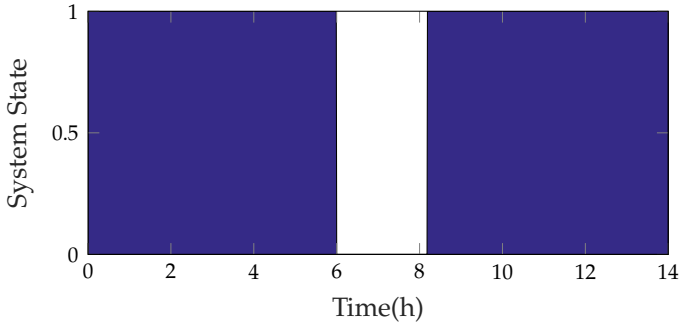

Figure 86: Average availability for system with infrequent long duration outages.

concerned that the number of outages are many and hence affect the levels of system availability experienced in their service area [95]. The GLAs main objective is to ensure that the IMO availability requirements are met at all of their harbours and ports. Ideally, the scheduled maintenance activities should have a predetermined downtime that is carefully controlled. This chapter aims to investigate if the scheduled Loran transmitter maintenance activities comply with the GLAs expectations in their service area.

8.3 REVIEW OF EXISTING AVAILABILITY METHODS

This section reviews the existing availability models used in other systems that are similar in concept to eLoran.

8.3.1 *Grant's Availability Model For Differential Global Positioning System*

Grant [29] reviewed several methods of calculating availability such as the analytical availability method developed by the Polish Naval Academy, Markov Chain Analysis and Fault Tree Analysis [29]. He acknowledged that Markov chain analysis is a powerful tool for modelling complex systems but chose the Fault tree analysis because it is simple and effective. This section therefore briefly describes the model developed by Grant to model availability for Differential Global Positioning system (DGPS) [29]. DGPS uses a network of ground based monitor stations that broadcasts the difference between the measured satellite pseudorange and the actual pseudorange. Grant calculates availability in two parts:

- Transmitter availability plus its signal in space
- Service availability provided by multiple beacons that are on air simultaneously

Grant's availability model is developed in three stages. The first stage deployed the edge-of-coverage method. The edge-of-coverage method is dependent on four factors namely:

1. Beacon/transmitter
2. Own Skywave fading
3. Atmosphere noise
4. Skywave Interference

Each of these four factors were assigned a specific probability. In this model, the transmitter signal was assumed to be deterministic by day. It was also assumed that the signal reaches the receiver by ground field alone. The night time groundwave field strength was assumed to vary in stochastic fashion. In Grant's model, the events [1] are split into two categories: deterministic[2] and stochastic [3]. System availability is determined using the stochastic events described in figure 87 at every location within the coverage area. The availability of a signal in space is expressed as:

$$Q = \prod_{i=1}^{N} (1 - U_i) \tag{8.5}$$

where N is the number of events being processed. U_i is the probability that an event causes the transmitter to be unavailable. Grant proposed that during the day, only the excessive levels of atmospheric noise and transmitter failure cause the transmitter to be unavailable. At night the number of events is increased to four as the skywave propagation becomes a nuisance

1 Events are inputs that determines whether the beacon/transmitter can be used for coverage or not.
2 A deterministic event is a process whose future can be perfectly determined from its past.
3 A stochastic event is random and unpredictable.

while the wanted signal becomes susceptible to excessive self fading. Table 21 shows the individual probabilities of the four events used in calculating the availability of a signal in space. The blank fields indicate that the events are not applicable under that given time of the day. Self fading is

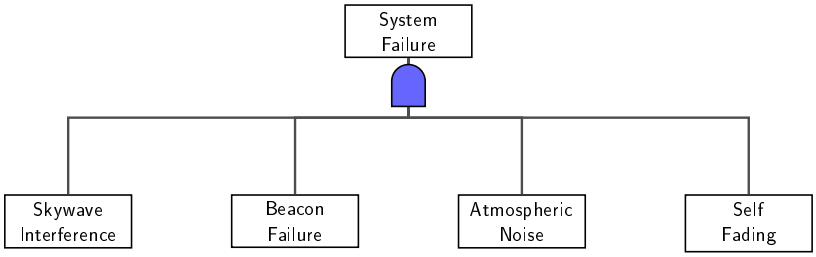

Figure 87: Fault tree diagram from stochastic events alone at night. By day the skywave interference and self fading are considered to be negligible.

determined from the skywave ground ratio (SGR). The availability due to

Table 21: Probability of each event causing unavailability.

	Beacon	Atmospheric Noise	Self fading	Skywave
Probability of Occurence	0.005	0.5	0.5	0.5
Day	0.005	0.5		
Night	0.005	0.5	0.5	0.5

multiple beacons is calculated as follows:

$$Availability = 1 - \prod_{i=1}^{N} (1 - Q_i) \tag{8.6}$$

where N is the number of signals that are received simultaneously and Q_i is the availability of each signal in space. Grant suggested that the equations

Table 22: Availability of Service.

	Grant's Software		Commercial Software	
No of Beacons	Day	Night	Day	Night
1	0.94525	0.85309	0.94525	0.85309
2	0.99700	0.97842	0.99696	0.97618
3	0.99984	0.99683	0.99983	0.99627
4	0.99999	0.99953	0.99999	0.99942

8.5 and 8.6 are only valid if the events that cause non-availability of the service are uncorrelated [29]. Grant validated this by conducting some experiments to investigate if the stochastic events that cause non-availability of service are independent and uncorrelated. His results suggested that there was no correlation between self fading, atmospheric noise and skywave interference. The summary of his results are shown in table 22 are obtained using equations 8.5 and 8.6 as well as information illustrated in table 21. The results suggest that availability is higher during the day than during the night. Grant compared his results with the results obtained from

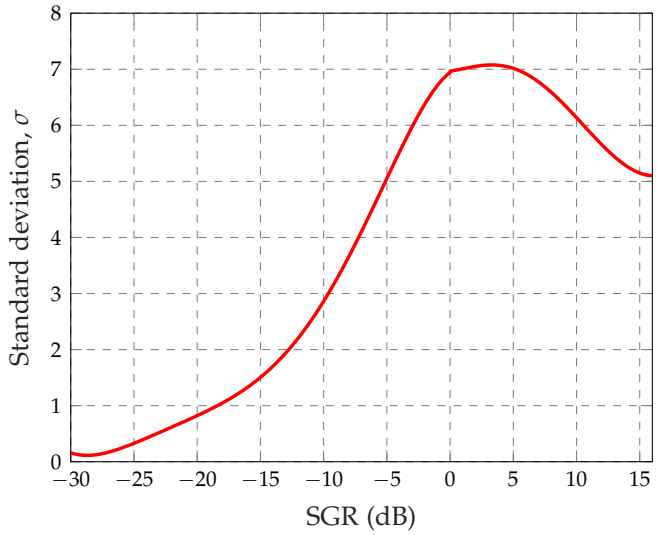

Figure 88: The standard deviation of skywave against SGR.

a borrowed commercial software. It is evident from table 22 that his results closely matched those obtained using a commercial availability software. Grant employed *edge of coverage* technique and fault tree analysis to model availability. He suggested that these methods underestimated availability as they do not take into account the temporal variations of the events. He proposed a statistical availability method to take into account the daily and night variations of the parameters. This approach involves calculating the probabilities of SNR and SIR thresholds being exceeded. Section 8.3.2 gives a description of the events used in Grant's availability model and how each component is determined.

8.3.2 *Factors of Grant's Availability Metric*

This section explains how each of the components of the availability metric is calculated. These components are skywave interference, self fading and atmospheric noise. Skywave interference was described in chapter 3.

Self Fading

Self fading occurs when the tracked groundwave interact destructively with the skywave. This process reduces amplitude of the tracked groundwave significantly. The nature of this fading phenomenon is assumed to be stochastic. Poppe [69] showed that the probability distribution of skywave can be approximated as a Gaussian process. Grant determined the skywave field strengths not exceeded 95% of time at the user's receiver using Poppe's model. The FTA diagram in figure 87, shows that failure to meet any event's probability threshold results in loss of availability. For example, if the field strength is less than the specified minimum field strength, then the availability at that array point is deemed to be zero.

Atmospheric Noise

Atmospheric noise varies stochastically in short term around its mean value and is dependent on the time of the day, location, season and frequency.

ITU provides the median values of atmospheric noise not exceeded 95% of the time per season-time block. Poppe [69] reasoned that using such values places more emphasis on a single season-time block and results into an over-engineering of the problem. She also proposed a method of separating the time-season blocks into day and night. The method of converting the median atmospheric noise values into mean values has also been described by Safar [77]. However, the author has some reservation regarding the atmospheric model proposed by Safar as it outputs the noise levels that are significantly low leading to high SNR values. Safar's method results in position accuracy estimates that does not match the measured position accuracy unless the TOA variance is inflated by a factor of 4.8 and the SNR criterion changed to 0 dB.

8.3.3 *LORIPP's Availability Model*

The LORIPP as part of the team tasked by the FAA to assess Loran as a viable backup option to GPS developed a coverage tool which is capable of producing availability and continuity plots for the eLoran coverage. The factors used by LORIPP to model availability are discussed in section 8.3.4.

8.3.4 *Factors affecting the LORIPP Availability Metric*

According to the LORIPP team, transmitter availability is affected by signal availability[4], physical characteristics of the environment and the technical capabilities of the transmitter system. These are briefly described below:

Signal Availability

Signal availability is defined as the percentage of the time the navigation signals transmitted from the transmitters are available for use within the coverage area [61, 74]. Signal availability is affected mainly by the coverage criteria such as signal to noise ratio, skywave conditions etc.

Physical Characteristics of the Environment

Physical characteristics of the environment include terrain itself, changes in conductivity, passing weather fronts and frozen paths etc. These factors result in large propagation delays (ASFs), large values of an envelope to cycle discrepancies, SNR values less than -10 dB due to lower signal strengths and higher noise values at any given noise percentile.

Technical Capabilities of Transmitter System

In Europe, the Control Centre in Brest (CCB), France monitors the on-air and off-air times of the transmitters in the NELS coverage area. They keep the data loggings of on-air and off-air times and maintenance time information of the European eLoran transmitters. This data is used to determine availability of each transmitter and the overall system availability in the coverage area [51, 61].

4 signal availability here refers to signal in space; this gives us information on whether the transmitter is turned on or not

Inputs of the LORIPP Model

The LORIPP availability model is driven by the following:

1. SNR
2. Availability of the station signal
3. Range of the transmitter to the receiver

The range of the transmitter is limited to 800 km. It is thought the effects of early skywaves are almost negligible under normal conditions at distances that are below this range [55]. The LORIPP model defines availability of the station signal as:

$$\Phi(t) = \frac{MTBF}{MTBF + MTTR} \tag{8.7}$$

where $\Phi(t)$ is the transmitter availability. The MTBF and MTTR are determined using the historical data from Loran Operational Informations System (LOIS). The LORIPP availability model depends on the atmospheric noise because atmospheric noise variations lead to the station availability variations. Atmospheric noise varies significantly over time and location and is an important input to the availability model. Atmospheric noise is generated at various percentiles using ITU-R P. $322-9$ [85], to determine the SNR of the transmitters. The SNR is determined starting at the highest percentile. The transmitter SNR is then tested to checked if it satisfies the SNR criterion or not. If the SNR criterion is not met at 99.9^{th} percentile noise, the model then determines the SNR at the next lower percentile until the SNR criterion is met. The percentile at which the SNR criterion is met is assumed to be the *station's availability due to noise*. The plot in figure 89 suggests that as the percentile increases, the maximum measured noise strength also increases. It can be seen that the level of atmospheric noise not exceeded 50% of the time is approximately 32 dBμV/m. The plot also shows the levels of atmospheric noise at different percentiles. The results suggest that the daytime SNR is lower at higher percentiles than at night since the groundwave field strength is assumed to be deterministic. The overall system availability is equal to the availability of a 10 m accuracy in the coverage area.

8.4 PROPOSED AVAILABILITY MODEL

This research adopts the Fault Tree Analysis method used by Grant for calculating the overall transmitter availability and the noise driven availability proposed by the LORIPP. The components of the fault tree used to work out availability are:

- Signal availability
- SNR criteria
- Range from the transmitter to the receiver criteria
- Skywave to groundwave (SGR) ratio criteria

The SNR criterion stipulates that only transmitters with SNR $\geq$ -10 dB should be used in a navigation solution. The range criterion limits the transmitter range to 800 km. The skywave criterion is described in chapter 3.

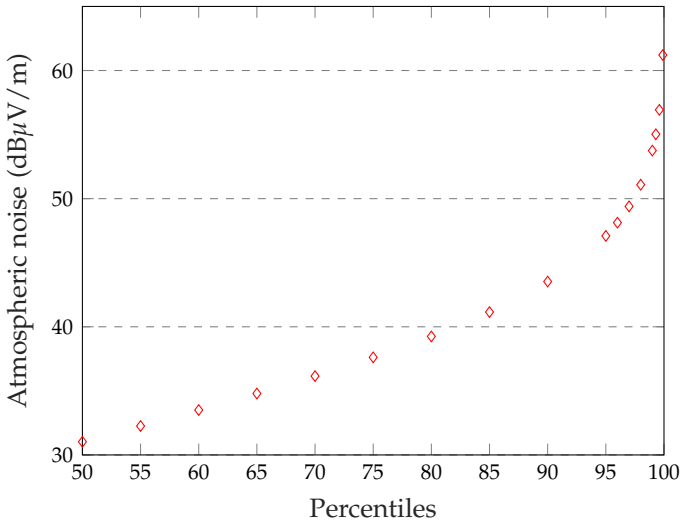

Figure 89: Levels of Atmospheric noise at various percentiles.

The probabilistic model developed herein considers the three aspects of an eLoran system performance criterion which, when appropriately combined, answer the following question:

"What is the probability that an eLoran user can utilize three or more eLoran signals with a properly functioning eLoran receiver system at any location in the coverage area and at any time"

The proposed availability model is described in section 8.5. The components listed in this section are combined to form probability component, P_A.

8.5 PROPOSED AVAILABILITY MODEL

The system availability model is implemented by calculating the system availability index (Ω_{SA}) as:

$$\Omega_{SA} = P_R \cdot P_A \tag{8.8}$$

where P_R is the probability that the eLoran user is available. P_A is the probability that three or more usable eLoran signals are available. The two events are assumed to be independent.

Receiver Availability Component,P_R

The eLoran receiver reliability component, P_R is calculated as:

$$P_R = 1 - \frac{MTTR}{MTBF} \tag{8.9}$$

In general, the MTBF and MTTR depend on the specific eLoran receiver system. These parameters can be taken to be the same for eLoran receivers within the same generic class. The author has struggled to find the MTBF and MTTR information in the receiver specifications. However, it is reasonable to estimate MTBF as equal to 6000 hours and MTTR as equal to 2 hours.

Station Availability Component, P_A

This component is required to calculate the system availability. Station availability is determined by off-air times for each station for each month of the year. Off-air times can be classified as unscheduled and scheduled events. Unscheduled off-air events may occur due to equipment failure. The station availability is derived from the historical off-air data obtained from the Loran control centre in Brest (CCB). Scheduled off-air are planned in terms of occurrence and duration and can be considered random or deterministic. Generally, the scheduled maintenance times are arranged so that each station is maintained in a different month [46]. P_A is calculated from the historic transmitter availability statistics using the following procedure:

1. The MTBF and MTTR are worked out from the unscheduled off-air times for each transmitter

2. An expected value that represents the station availability for a single eLoran transmitter is calculated. From historic data obtained from the control centre in Brest this is set to 99.15%.

8.5.1 *Results And Discussions*

The analysis of the historical data suggests that an eLoran transmitter is on-air for 99.15 % of the time throughout the year. This availability value is assumed to represent any eLoran transmitter. This estimate is reasonable since all the transmitters use the solid-state equipment and caesium clocks. It is also reasonable to assume that their rate of failure is the same. It was shown in chapter 4 that there is good eLoran coverage in the East coast of England than to the West coast due to the current transmitter configuration. If a need to install new transmitters arises, this availability figure will then be assigned to those transmitters. The determination of system availability assumes that three or more transmitters have passed the skywave and SNR criteria. If one of these criterion is not satisfied for any transmitter, then that transmitter cannot be included in the determination of the system availability at that point. The SNR criteria is checked only after the station signal availability has been established. For any given scenario, the coverage tool assesses the noise levels by determining SNR at the highest noise level (99.9^{th} percentile). If the SNR criteria is met at this stage then the system availability is assumed to be 99.9 % availability and no more calculation are done for that location. If the system is not available the coverage software tool will try to calculate system availability at the next lower noise percentiles until it is finally available. The iterative procedure is done steps of 0.01 from 99.9^{th} percentile down to 50^{th} percentile. Determination of System availability requires three or more stations at any given location. This process is complete once availability at all grid points has been determined.

8.5.2 *Determination of Single Station Availability*

The night time single station availability can be determined as follows:

$$Tx_{av} = \prod_{i=1}^{N} (1 - U_i) \tag{8.10}$$

where N is the number of events being processed. U_i is the probability of each event causing the transmitter not to be considered in the determination of the overall system availability. An "event" in this context means excessive noise or excessive skywave interference. The individual probabilities of the three events used in determining the single transmitter availability under night conditions are shown in table 22. The transmitter un-availability figure is 0.0085. This value is determined from the transmitter availability statistics taken from the Control Centre in Brest. The skywave field strength and skywave delay are determined at 99 %-ile using the models described in chapter 3. Therefore the probability of a transmitter being unavailable will be 0.01. At 99 %-ile the probability of transmitter being unavailable due to excessive atmospheric noise is also equal to 0.01.

8.5.3 *Overall Availability Calculations*

The overall system availability at any point in the geographical area can be described as:

$$\begin{aligned} A &= P(all\ tx\ avail) \times P(avail|\ all\ tx\ avail) \\ &+ \sum_{i=1}^{N} P(tx\ m\ unavail\ \&\ other\ tx's\ avail) \times P(avail|tx\ m\ unavail) \end{aligned} \tag{8.11}$$

where A represents the number of ways in which the system can be in an available state. For example, at one instance all the transmitters may be on air while at another instance one of the transmitters could go off air while the remaining $N-1$ transmitters remaining on-air etc. The expression for the overall system availability, A can be re-written as:

$$\begin{aligned} A &= (P_{tx\,avail})^N \times P(avail|\ all\ tx\ avail) \\ &+ \sum_{i=1}^{N} (P_{tx,avail})^{N-1}(1 - P_{tx,avail}) \times P(avail|tx\ m\ unavail) \end{aligned} \tag{8.12}$$

where N is the number of signals received from N different transmitters simultaneously and $P_{tx,avail}$ is the availability of a transmitter being on-air using equation 8.12.Therefore,

$$Normalization\ Factor = (P_{tx,avail})^N + \sum_{i=1}^{N} (P_{tx,avail})^{N-1}(1 - P_{tx,avail}) \tag{8.13}$$

Thus overall system availability is given by:

$$Overall\ System\ Availability \approx \frac{A}{Normalization\ Factor} \tag{8.14}$$

The system availability can be determined by assuming that the probability of two or more transmitters going off the air at the same time is very low. Such cases will not be considered in this study. Only cases with at most two stations going off air will be considered. The overall system availability calculation starts at 99.9 %-ile atmospheric noise and calculates the signal to noise ratio. If the SNR ≥ -10 dB and the skywave limits are satisfied, the transmitter will be included in the calculation of availability. The overall system availability can be determined if three or more transmitters have met the coverage criteria at 99%-ile. However, if there are less than three transmitters satisfying all the necessary criteria for availability then the system is deemed not be available at that percentile. In this case, the SNR criterion is

evaluated at the next highest percentile until the system becomes available. This procedure is done in steps of 0.1 %-iles and stops at 50 %-ile. Using 99.9 %-ile as an example, two transmitters might have an adequate SNR (SNR > -10) at this percentile while some might not be available due to very low SNRs at same percentile. Suppose that the third transmitter meets the SNR criterion using atmospheric noise value not exceeded 70 % of the time. The worked example shows how the overall system availability is determined in this case. At 99.9% -ile, the probability of failure due to excessive noise is equal to 0.001 and the rest of the figures remain the same as in table 22.

$$\begin{aligned} Tx_{av}(99\% - ile) &= (1 - 0.0085)(1 - 0.001)(1 - 0.01) \\ &= 0.9806(98.1\%) \end{aligned}$$

$$\begin{aligned} Tx_{av}(70\% - ile) &= (1 - 0.0085)(1 - 0.3)(1 - 0.01) \\ &= 0.68711(68.7\%). \end{aligned}$$

$$\begin{aligned} Sys_{av} &= 1 - [(1 - 0.9806)(1 - 0.9806)(1 - 0.687)] \\ &= 0.99988(99.98\%) \end{aligned}$$

In determining system availability, it is assumed that the events (atmospheric noise, skywave interference, signal availability) are stochastic and uncorrelated. This assumption was validated by Grant [29] in his work for the availability of radio beacons in a DGPS coverage area. His results suggested that there was negligible correlation between atmospheric noise and skywave interference for any transmitter at any location in the coverage area. Figure 90 shows the availability of a 10 m accuracy of eLoran over the British Isles as it exists today. The plot takes into account the signal availabilities of each transmitter contributing to the position fix at each coverage grid location. This data has been derived from two years worth of transmitter availability statistics. The signal availabilities are then combined into a system availability statistic. It can be seen that availability follows accuracy. The 10 m accuracy was determined using the Land path and the weather models. This plot assumes that the Norwegian and French eLoran stations are on-air.

8.6 SUMMARY AND CONCLUSIONS

This chapter has discussed the availability models employed in various systems. It is assumed that availability is affected by skywave interference, station availability, and atmospheric noise. The availability plot can be used to guide the relevant authorities to minimize the frequency of the maintenance times and the average MDT time. The availability performance figure obtained in this study illustrates the coverage tool's modelling capability and does not represent the true eLoran capability since it was using using the (NELS) standard Loran-C operating procedures. It is expected that availability will improve once all the stations become eLoran compliant.

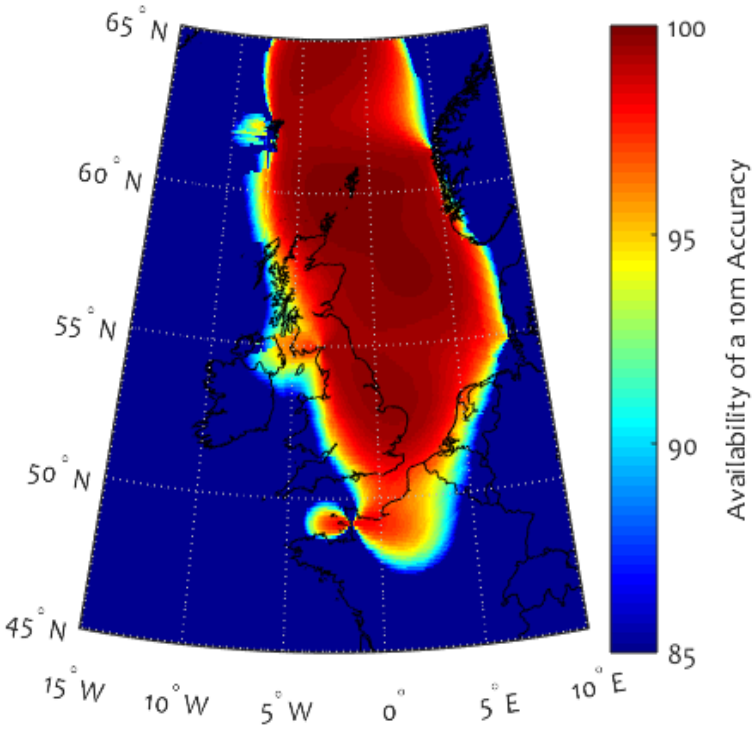

Figure 90: Availability of the 10 m accuracy when the dLoran effects are diluted with Landpath and Weather Models.

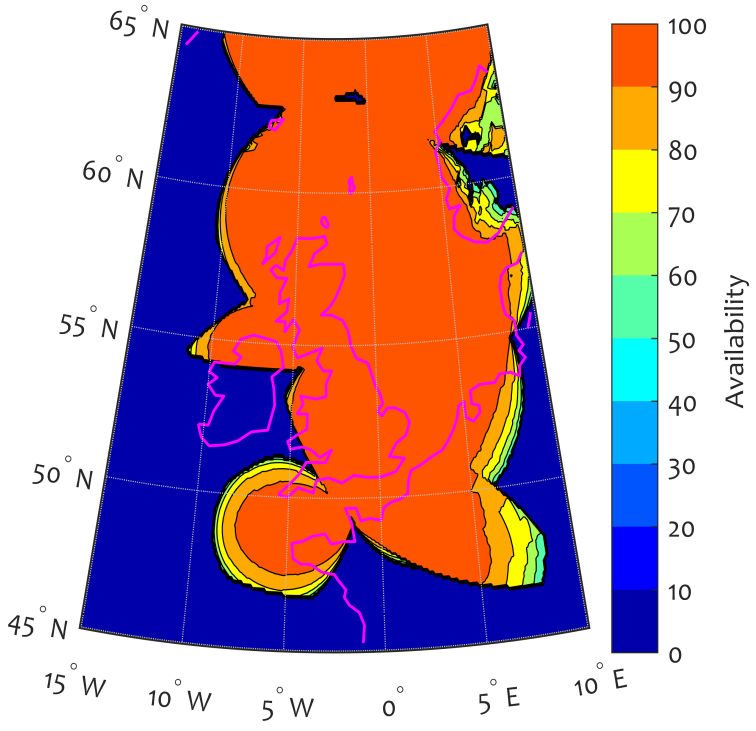

Figure 91: Availability of the 10 m accuracy assuming dLoran everywhere.

9 CONTINUITY MODEL

This chapter describes a continuity model developed for eLoran. In other Engineering disciplines continuity is often referred to as reliability. Continuity is defined as the capability of the system to perform its intended function without unintended interruptions during the intended operation [51, 55]. Continuity is calculated from the conditional probabilities of stations transitioning from one state (off-air) given that they were in another state (on-air) at the start of the intended operation. These conditional probabilities are related to MTBF and MTTR terms which were explained in chapter 8.

9.1 REVIEW OF GRANT'S CONTINUITY MODEL

Grant [29] stated that only the stochastic components of the system contribute to continuity. Stochastic events were examined in chapter 8. Grant also examined each of these factors in detail in respect with their possible effects on continuity. The beacon continuity is determined in accordance with IALA guidelines as

$$continuity = 1 - \frac{CTI}{MTBF} \tag{9.1}$$

where CTI is the duration for which the system is expected to remain in operation. For eLoran harbour entrance and approach, this is expected to be 15 minutes. MTBF is the average time between failures given in hours. Grant's continuity model assumes that there is no scheduled outages between the start of the approach and the time the approach is expected to be completed. This assumption is reasonable since scheduled maintenances are known in advance. Thus, no approach that depends critically on the system can be commenced if the system is forecast to be unavailable for any part of the duration of that approach. Poppe [69] investigated the relationship between SNR and bit error rate (BER). The results of this work were used by Grant in the development of the continuity model. The components, atmospheric noise, self fading and skywave can be classified as stochastic and their probability for affecting system continuity analysed. Grant suggested that continuity increases as one moves towards the beacon/transmitter. This is true since SNR is stronger near the transmitter, and thus the probability of continuity failing due to SNR is significantly reduced. The probability that continuity fails due to self fading is also reduced since near the transmitter the groundwave dominates the skywave. In this scenario, the effect of self fading is generally small. Equation 9.1 shows that continuity depends on $MTBF$ and CTI. However, CTI is set by organisational bodies and cannot be changed. $MTBF$ is the mean between failures due to self fading or atmospheric noise. Section 9.1.1 discusses how each of the components affecting continuity are modelled in Grant's continuity model.

9.1.1 *Components Affecting Continuity*

Grant suggested that skywave though stochastic, does not affect continuity as single entity but affects continuity of a beacon only when it interacts

with the groundwave component of the signal leading to self fading. The probability that continuity fails due to self fading and atmospheric noise are discussed herein.

Atmospheric Noise

The effect of atmospheric noise on continuity was modelled by Grant using indirect evidence from Poppe's investigations on atmospheric noise. Poppe recorded the variation of word error rate (WER) with SNR. The probability of WER can be used to determine the probability of the service becoming unavailable due to noise. This probability is linked with the probability of the correction message being adequately reduced. The probability of the message being received is:

$$P_{success} = [1 - P_{worderror}]^W \tag{9.2}$$

where $P_{success}$ is the probability of receiving the message successfully. $P_{worderror}$ is the probability that the word is received in error. Grant defines failure as the probability of failing to receive four consecutive messages. This probability was determined as a function of SNR. The results from Grant's work suggested that an SNR of 8.5 dB leads to 1 message in 10 being received successfully. The results further suggested that for SNR greater than 9 dB the probability of failure is extremely small.

Self fading

The effect of self fading is taken into account for use in the SNR calculations.

9.2 OTHER CONSIDERATIONS

The author decided not to use Grant's model because it too simple and a lot of model assumptions were made due to lack of appropriate data. The continuity model employed by the author is described in section 9.4.

9.3 CONTINUITY STANDARDS

As with availability, continuity is also defined by the standards set out by governing authorities such as IMO Resolution A.860, IALA, US Federal Radionavigation Plan and United States Coast Guard. The IMO set a single continuity criteria that is applicable everywhere in the coverage area. The European Maritime Radionavigation Forum and IALA set a 99.7 % in harbours and 99.85 % in coastal waters. Table 23 shows the continuity specifications and periods.

9.4 MARKOV CHAIN MODEL FOR CONTINUITY

Many continuity modelling techniques exist. These include reliability block diagrams (RBD), Markov chains and Monte Carlo simulations. RBD give quick and easy results but compromise on the flexibility and accuracy especially when used for a system with a complex topology. Markov Chains provide higher accuracy but can be challenging to apply. Monte Carlo simulations give desirable accuracy at the expense of complexity and can be challenging to apply. They are also computationally intensive even with modern computers. In this work, Markov chains are used in the development of the continuity model.

Table 23: Continuity Specifications and periods.

Document	Continuity Requirement	Calculation Period
IMO (860)	99.97%	1 year
IALA	99.97% 99.85%	3 hours
IALA	99.97% 99.85%	15 minutes
EMRF (815) Revised	99.97% 99.85%	15 minutes

9.4.1 *Assumptions And Notations*

For the purpose of modelling, the following assumptions are made:

- The probability of transition from one state to the other does not depend on the state that was occupied earlier.
- The failure rates and repair rates are constant over time and statistically independent
- There are no more than two simultaneous failures in a time interval
- Repaired transmitters are as good as the new transmitters.

9.4.2 *Transition Diagram*

The transition diagram shown in figure 92 is used to model the Markov chain availability. The diagram shows the states and transitions of the transmitters any time interval. A Markov chain is a stochastic process possessing a Markov Property. A system is said to possess a Markov property if it has no memory about the past processes. This means that the current state is the only state that influences the future events. All historical events are irrelevant in the determination of the future outcomes. The on-air and off-air probabilities are related to the MTTR and MTBF calculated herein. Conditional probability of the station going off-air is calculated from the Markov Chains

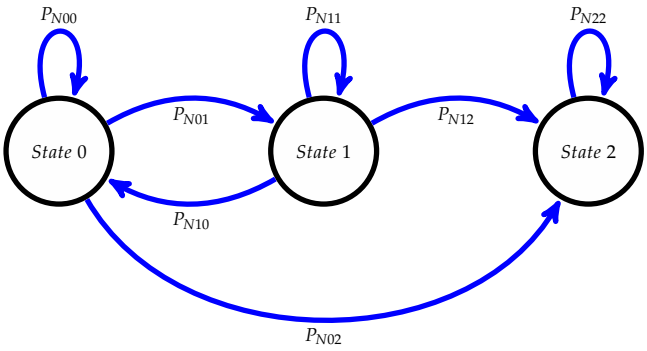

Figure 92: A trapping state Markov Chain.

9.4.3 *Continuity Model Framework*

A transmitter can become unavailable for use due to an increased atmospheric noise leading to SNR falling below -10 dB even though the transmitter is on-air. A transmitter is deemed to be unavailable if it does not meet the skywave to groundwave ratio (SGR) limits set by the IEC/RTCM [21]. The model determines the probability that the transmitter initially available at the start of the operation becomes unavailable during the operation. For harbour entrance and approach, the time needed to complete an approach is assumed to be 15 minutes. A Markov Model simulation traps the stations into a given state. Off-air and on air-times correspond to the states that a transmitter can be in at any given period. In this model, p_{jk} represents the probability that a transmitter can be in state j and going to state k. The transition matrix for these two possible states is given by:

$$C = \begin{bmatrix} p_{00} & p_{10} \\ p_{01} & p_{11} \end{bmatrix} = \begin{bmatrix} p & (1-p_{11}) \\ (1-p_{00}) & p_{11} \end{bmatrix} \tag{9.3}$$

Determination of continuity is related to the probability that the number of off-air transmitters at any time during an approach is less than two since most locations can meet HEA requirements with one station off-air but generally not with two [51]. It is possible that two transmitters go off-air during an approach but not at the same time since the mean time to repair is shorter than the duration of HEA. A Markov model is used to determine the probability that at most two transmitters are off-air at the same time during an approach given that a total of N transmitters are in view at the receiver. At any given period, the system can be in three states:

- All N transmitters in view
- All but one transmitters in view
- All but two transmitters in view

Figure 92 shows a Markov Model for harbour entrance and approach. This model traps instances where two transmitters go off-air at the same time. The transition probabilities of this model are given in terms of, p_{00} and p_{11} . The following are the definition of the probabilities used in the Markov chain: Let p_{00} be the probability that the transmitter is on-air,p_{11} be the probability that the transmitter is off-air, p_{01} is the probability that the transmitter is transitioning from on-air to off-air, and p_{10} be the probability that the transmitter is transitioning from off-air to on-air. If N transmitters are in view at the receiver then the probability that all of them are in view is computed using the Binomial expansion. Let $P_{N,00}$ be the transition probability that all N transmitters are on-air. Using Binomial expansion:

$$P_{N,00} = \begin{pmatrix} N \\ 0 \end{pmatrix} (p_{00})^N (p_{01})^0 = (p_{00})^N \tag{9.4}$$

Let $P_{N,01}$ be the transition probability that all but one transmitter are on-air and one transmitter goes off-air, then,

$$P_{N,01} = \begin{pmatrix} N \\ 1 \end{pmatrix} (p_{00})^{N-1} (p_{01})^1 = N(p_{00})^{N-1} p_{01} \tag{9.5}$$

But $p_{01} = 1 - p_{00}$. Therefore,

$$P_{N,01} = N(p_{00})^{N-1} (p_{01})^1 = N(p_{00})^{N-1} (1 - p_{00}) \tag{9.6}$$

Let $P_{N,02}$ be the transition probability that all but two transmitters are on-air and two transmitters go off-air. Then,

$$P_{N,02} = \left(\begin{array}{c} N \\ 2 \end{array} \right) (p_{00})^{N-2}(p_{01})^2 = \left(\begin{array}{c} N \\ 2 \end{array} \right) (p_{00})^{N-2}(1-p_{00})^2 \tag{9.7}$$

Let $P_{N,10}$ be the transition probability that all but one transmitter are on-air and the transmitter that was off-air initially goes back on-air. This is a conditional probability. Therefore:

$$P_{N,10} = (p_{00})^{N-1}(p_{10}) = (p_{00})^{N-1}(1-p_{11}) \tag{9.8}$$

Let $P_{N,11}$ be the transition probability that one transmitter initially off-air remains off-air or the probability that one transmitter goes off-air and one that was off-air initially goes back on-air again. This is a mutually exclusive event. Therefore,the probabilities for the two mutually exclusive events can be expressed as follows:

$$S = (p_{00})^{N-1}(p_{11}) \tag{9.9}$$

where S is the transition probability that one transmitter initially off-air remains off-air and $N-1$ transmitters remain on-air. This is a conditional probability. Let Q be the probability that one transmitter goes off-air and one that was off-air initially goes back on-air again. There are $N-1$ ways that the $N-2$ transmitters will remain on-air while another one goes off-air.

$$R = \left(\begin{array}{c} N-1 \\ 1 \end{array} \right) (p_{00})^{(N-1)-1}(p_{01}) = \left(\begin{array}{c} N-1 \\ 1 \end{array} \right) (p_{00})^{N-2}(p_{01}) \tag{9.10}$$

Let V be the probability that the transmitter that was off-air initially goes back on-air again. Thus: $V = p_{10}$ hence $Q = R \times V = \left(\begin{array}{c} N-1 \\ 1 \end{array} \right) (p_{00})^{N-2}(p_{01})(p_{10})$
But the probability that is of interest here is:

$$P_{N,11} = S + Q$$

Therefore,

$$\begin{aligned} P_{N,11} &= (p_{00})^{N-1}p_{11} + \left(\begin{array}{c} N-1 \\ 1 \end{array} \right) (p_{00})^{N-2}(p_{01})p_{10} \\ &= (p_{00})^{N-1}(p_{11}) + \left(\begin{array}{c} N-1 \\ 1 \end{array} \right) (p_{00})^{N-2}(1-p_{00})(1-p_{11}) \end{aligned} \tag{9.11}$$

Let $P_{N,12}$ be the probability that one of the $N-1$ transmitters goes off-air and the off-air transmitter remains off-air or the probability that two off-air transmitters remain off-air and the probability that transmitter that was off-air remains off-air. This is a mutually exclusive event.

Let J be the probability that one of the $N-1$ transmitters goes off-air and the off-air transmitter remains off-air. J is then given by:

$$J = \left(\begin{array}{c} N-1 \\ 1 \end{array} \right) (p_{00})^{N-2}(p_{01})(p_{11})$$

Let K be the probability that two of the $N-1$ on-air transmitters goes off-air and the probability that transmitter that was off-air going on-air.

$$K = \left(\begin{array}{c} N-1 \\ 2 \end{array} \right) (p_{00})^{N-3}(p_{01})^2 p_{11}$$

$$= \left(\begin{array}{c} N-1 \\ 2 \end{array} \right) (p_{00})^{N-3}(1-p_{00})^2 p_{10}$$

$$= \left(\begin{array}{c} N-1 \\ 2 \end{array} \right) (p_{00})^{N-3}(1-p_{00})^2(1-p_{11})$$

Therefore,
$P_{N,12} = J + K$
Substituting the expressions for J and K gives:

$$\begin{aligned} P_{N,12} &= \left(\begin{array}{c} N-1 \\ 1 \end{array} \right) (p_{00})^{N-2}(p_{01})(p_{11}) \\ &+ \left(\begin{array}{c} N-1 \\ 2 \end{array} \right) (p_{00})^{N-3}(1-p_{00})^2(1-p_{11}) \end{aligned} \tag{9.12}$$

The probabilities p_{00} and p_{01} are related to the MTBF and MTTR. To derive the terms MTBF and MTTR, a two state Markov Model involving a single transmitter is assumed. It is also assumed that the system starts in state 0 The probability p_{00} is determined by matching the mean time in state 0 to the mean time between failures (MTBF). Assuming the system starts in state 0 with a probability of p_{00}, the only way to leave state 0 is to go to state 1 with a probability p_{01} . The expected time in state 0, $E(time\,in\,state\,0|State\,0)$ is given by:

$$\begin{aligned} E(t_{s0}|s_0) &= 1p_{01} + 2p_{00}p_{01} + 3p_{00}^2 p_{01} + ... \\ &= p_{01}\sum_{t=0}^{\infty}(t+1)p_{00}^t \end{aligned} \tag{9.13}$$

The infinite series $\sum(t+1)p_{00}^t$ can be broken down into the sum of the two series, the Gabriel Staircase and the geometric series. The infinite series on the right side can be expressed as:

$$\sum_{t=0}^{\infty}(t+1)p_{00}^t = \sum_{t=0}^{\infty} t p_{00}^t + \sum_{t=0}^{\infty} p_{00}^t$$

The sum of the geometric series is given by:

$$\sum_{p=0}^{\infty} r^p = \frac{1}{(1-r)}, 0 \leq r < 1$$

and the sum of the Gabriel staircase is given by:

$$\sum_{p=1}^{\infty} p r^p = \sum_{p=1}^{\infty}\sum_{i=p}^{\infty} r^i = \frac{r}{(1-r)^2}, 0 < r < 1$$

Therefore,

$$\begin{aligned}\sum_{t=0}^{\infty}(t+1)p_{00}^{t} &= \frac{p_{00}}{(1-p_{00})^2} + \frac{1}{(1-p_{00})} \\ &= \frac{p_{00}+(1-p_{00})}{(1-p_{00})^2} \\ &= \frac{1}{(1-p_{00})^2}\end{aligned} \tag{9.14}$$

But $p_{01} = 1 - p_{00}$, hence

$$E(t_{s0}|s_0) = p_{01}\sum_{t=0}^{\infty}(t+1)p_{00}^{t}$$

$$= (1-p_{00})\frac{p_{00}}{(1-p_{00})^2}$$

$$= \frac{1}{(1-p_{00})}$$

$$= MTBF$$

Similarly, the relationship between MTTR and can be expressed as:

$$E(t_{s0}|s_0) = p_{10}\sum_{t=0}^{\infty}(t+1)p_{11}^{t}$$

$$= (1-p_{11})\frac{p_{00}}{(1-p_{11})^2}$$

$$= \frac{1}{(1-p_{11})}$$

$$= MTTR$$

The next step is to calculate the probability of the system being in state s_i at time t.
Let S_0 be the chance of being in state 0 when all transmitters are on-air.
Let S_1 be the chance of being in state 1 when one transmitter is off-air.
Let S_2 be the chance of being in state 2 when two transmitters are off-air.
The chances of being in states S_0,S_1 and S_2 at time t = 0 are given by:

$$S_0 = 1$$

$$S_1 = 0$$

$$S_2 = 0$$

Since at time t = 0 (beginning of the harbour entrance and approach given initial availability), it is only after the start of the operation that one or two

transmitters may go off-air at the same time.Hence the probability of having N transmitters in state at time t from the start of the operation is given by:

$$P(S_0(t)) = \sum_{t=1}^{900}((P_{N,00})P(S_0(t-1)) + (P_{N,10})P(S_1(t-1)) \tag{9.15}$$

The probability of having one transmitter in state at time t from the start of the operation is given by:

$$P(S_1(t)) = \sum_{t=1}^{900}((P_{N,01}))P(S_0(t-1)) + (P_{N,11})P(S_1(t-1)) \tag{9.16}$$

The probability of having two transmitters in state S_2 at time t from the start of the operation is given by:

$$\begin{aligned} P(S_2(t)) = \sum_{t=1}^{900}(P_{N,02})P(S_0(t-1))+ \\ (P_{N,12})P(S_1(t-1)) + P_{N,22}P(S_2(t-1)) \end{aligned} \tag{9.17}$$

In eLoran the operation last for 15 minutes which is equivalent to 900 seconds. In the old Loran-C the operation time was 3 hours [51].

9.5 IMPLEMENTATION OF CONTINUITY IN COVERAGE PREDICTION

It is assumed that the system is available at the start of the operation. The system is available when three or more transmitters are in view otherwise continuity of the system is equal to zero. Figure 93 shows the current continuity plot for Europe. It can been seen that continuity is good in the English channel and the North Sea region but poor in the lower part of Ireland. Continuity was determined using the assumption that there is dLoran everywhere.

Table 24: Transition probabilities.

Probability	Description	Value
p_{00}	On-air tx remains on-air	0.999
p_{01}	On-air tx returns off-air	0.001
p_{10}	Off-air tx goes on-air	0.000002
p_{11}	Off-air tx stays off-air	0.999998

9.6 SUMMARY AND CONCLUSIONS

This chapter has presented a continuity model based on the Markov chain analysis.The continuity plot serves as a guide to the administrators about the percentage of the time the system can complete the harbour entrance approach, given that the system was initially available at the start of the operation. The continuity results shows continuity is driven by availability and MTBF. Longer MTBF time has a negative effect on continuity.

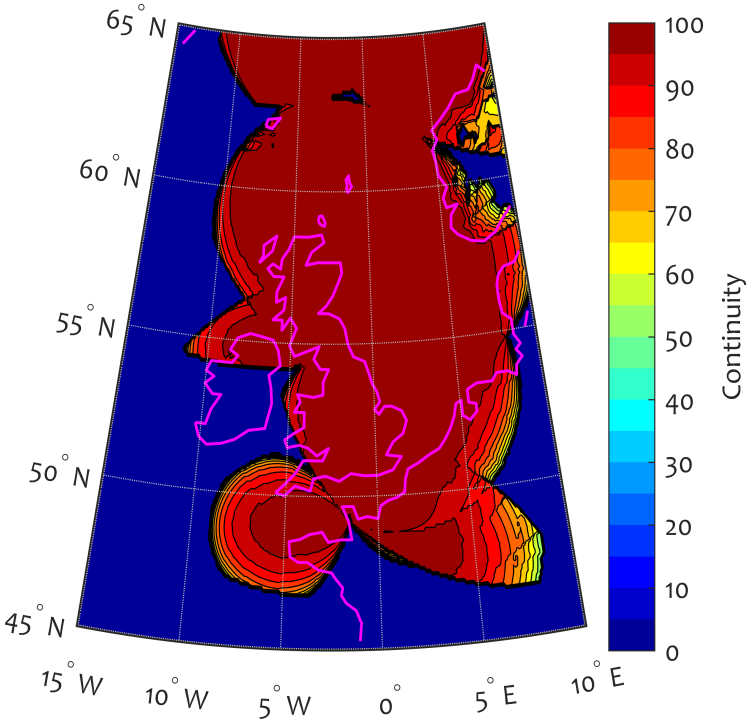

Figure 93: Continuity of eLoran in GLA coverage area assuming dLoran everywhere, min=45.8 % and max=99.9 %.

10 CASE STUDY: NEW TRANSMITTERS IN IRELAND

This chapter presents the analysis and optimization framework on the eLoran coverage performance after placing two eLoran transmitters in Ireland. The intended extension of the transmission network provides an excellent opportunity to demonstrate the models developed in the previous chapters by solving a real-life problem. This chapter adopts the GRI selection procedure proposed by Safar [77] for his work in the same case study. There are two constraints in this optimization problem. These are:

- The levels of the transmitter power suitable for filling the coverage gaps. One transmitter will be high power and the other will be low power.
- The locations of transmitters is limited to specific sites due to political reasons.

In this case study, high power is defined to be the effective radiated power (EMRP) of 250 kW or greater; and "low power" is defined to be the effective radiated power of 50 kW or less. Table 25 shows four candidate locations proposed to host the transmitters . The nature of the site installation is such that only two such locations are suitable for high power transmitters while the other two are suitable for the low power transmitters.

Table 25: Name, location and effective radiated power of candidate transmitters.

Name	Location	Power Type	EMRP(KW)
Tullamore	53.278414°N 7.371781°W	High	250
Bealadangan	53.310893°N 9.608116°W	High	250
Mizen Head	51.450833°N 9.813333°W	Low	50
Ballydavid	52.203770°N 10.337862°W	Low	50

10.1 THE OBJECTIVES OF THE CASE STUDY

The main goal of the case study is to determine the locations of two eLoran transmitters with one high power and the other low power. The choice of the transmitter powers should result in an optimal accuracy performance at a list of ports, harbours and traffic separation schemes in UK and Ireland. The power level can be chosen as long as it is within the constraints depicted by table 25. The results in chapter 4 suggests that the accuracy figures are good in the East of the British Isles but poor in the West of the British Isles. The GLA's plan is to extend coverage to all major ports in the UK and Ireland as well as the English channel. To achieve a full service-wide coverage, the addition of two stations in Ireland is necessary. Table 25 shows the

parameters of the stations operating in the NELS including the Norwegian and French stations that were switched off at end of 2015.

10.2 CHAIN CONFIGURATION

The general procedure in this task is to include the two stations into either an existing chain or a completely new chain or move all the transmitters in NELS into a new chain. These scenarios were also analysed by Safar [77] in his eLoran work. This section reviews and adopts his techniques and completes the columns of the table which were incomplete in Safar's work. The NELS consists of four chains operating on GRIs: 6731, 7001, 7499 and 9007. The inclusion of station into a chain requires the length of its baselines to all the stations to be less than 1200 km. The stations closest to Ireland operate on the following GRIs: 6731, 7499 and 9007. There is a possibility that the new stations can be built into a new chain. Another possibility is to include them in an existing chain. This scenario has the advantage of not having to re-calculate the emission delays of all the stations. Furthermore, the inclusion of new stations into an existing chain results in lower CRI levels than when a new chain is created [77]. The candidate GRIs are assessed to determine if they can accommodate additional stations. The new stations are inserted so that they follow the last secondary in the chain to avoid recalculating the emission delays of the secondary stations of the chain. Once this is done, an accuracy performance is assessed for all the possible scenarios. The configuration that results in the best accuracy performance is chosen. This begs the question, what constitutes the best accuracy performance? Several procedures can be used to answer this question. One may be to assess the overall CRI performance in the coverage area. Another may be to access accuracy improvement at all the grid points while assuming DLoran everywhere. Another possibility is to assess accuracy performance at all the ports and harbour location for each scenario. The author favours the latter because the model that assumes DLoran everywhere does not represent the reality. Assessing the accuracy performance at all ports is in line with the IMO requirements. Section 10.2.1 describes the procedure for determining the minimum GRI of a chain.

10.2.1 *Determination of Minimum GRI*

To determine the minimum GRI for a given chain configuration, the following steps adopted from Safar's work are deployed:

- The minimum time difference between the master and secondary station is assumed to be $\Delta\tau_{n,min} = 10900\mu$s. The time difference between two secondary station is assumed to be $\Delta\tau_{n,min} = 9900\mu$s.

- The smallest time difference between the reception of signals from stations n and $n+1$, denoted $\Delta\tau_n$, can be found at the location of station $n+1$.

$$\Delta\tau_n = \Delta\tau_{ED,n} - \frac{r_n}{v_{prop}} \tag{10.1}$$

  where $\Delta\tau_{ED,n}$ is the difference between the EDs of the stations n and $n+1$, r_n is the distance between the two transmitting stations, and v_{prop} is an estimate of the signal propagation velocity. The signal spec-

ification requires that $\Delta\tau_n$ should be greater or equal to $\Delta\tau_{n,min}$. It follows that:

$$\Delta\tau_{ED,n} \geq \Delta\tau_{n,min} + \frac{r_n}{v_{prop}} \tag{10.2}$$

The minimum GRI can be calculated as:

$$T_{GRI,min} = \sum_{n=1}^{N} \Delta\tau_{n,min} + \frac{r_n}{v_{prop}} \tag{10.3}$$

In our calculations, the ED differences are rounded off to the next highest multiple of $0.1ms$

Table 26: Name, location and effective radiated power of candidate transmitters.

Station	Coordinates	EMRP (KW)	GRI
Lessay	49.14867°N 1.50473°W	250	6731
Soustons	43.73975°N 1.38044°N	250	6731
Anthorn	54.91121°N 3.28728°W	400	6731
Sylt	54.80833°N 8.29357°E	250	6731
Ejde	62.29995°N 7.07391°W	400	9007
Vaerlandet	61.29707°N 4.69628°E	250	9007

Table 27: Showing the name, effective radiated power of candidate transmitters and emission delays.

Station	Status	EMRP (KW)	GRI	Minimum Transmission Delay (ms)
Lessay	M	250		$10.9 + 2.01 = \lceil 12.91 \rceil = 13.0$
Soustons	X	250		$9.9 + 4.2 = \lceil 14.1 \rceil = 14.2$
Anthorn	Y	400		$9.9 + 2.5 = \lceil 12.4 \rceil = 12.5$
Sylt	Z	250		$9.9 + 0.6 = \lceil 10.5 \rceil = 10.6$
Tullamore		250		$9.9 + 0.9 = \lceil 10.8 \rceil = 10.9$
Mizen Head		10		$9.9 + 2.2 = \lceil 12.1 \rceil = 12.2$
Total			Minimum GRI=	73.4

The minimum GRI for the optimum transmission sequence if the emission delays are re-assigned is 7340. This GRI is longer than 6731 and thus the

two stations cannot be configured into 6731 chain. This means that the GRI 6731 has failed the test. However, if only Tullamore is configured into the rest of the 6731 transmitters, the minimum GRI is 6230 and GRI 6731 passes the test.

10.3 INTERFERENCE NATURE OF SUB PERIODIC GRIS

It was explained in chapter 4 that cross rate interference plays a key role in the accuracy performance of the system. The results of cross rate interference analysis and mitigation work as part of this project are presented in reference [77]. The results of that work suggest that cross-rate interference increases the pseudo-range errors leading to poor accuracy. The results of that work also demonstrated that impact of CRI is dependent on the nature of the GRI. The interference from co-prime GRIs with respect to the GRI of the tracked station is deemed to be less harmful than others. It was also demonstrated in that work that the pseudo-range error becomes maximum due to cross rate interference from stations operating on *sub periodic GRIs*[1] and therefore such GRIs should be considered harmful. This leads to the criterion that before GRIs are assigned to new stations, the GRIs of the existing chains that are likely to cause harmful interference must be identified and eliminated. The method of identifying this sub-periodic GRIs uses mathematical procedure called *Farey sequences*[2]. The results from Safar's work suggest that not all sub-periodic GRIs are harmful and that it is only those whose time offset with respect to the tracked GRI falls within a certain threshold, that are considered harmful. The interference due to the sub-periodic GRIs whose time offset falls outside the threshold are assumed to be suppressed by phase coding. This time offset is denoted $\Delta\tau_{sub}$ and is such that $|\Delta\tau_{sub}| < 150\mu$s. The next section summarises the method for identifying the sub periodic GRIs.

10.3.1 *Identification of Sub Periodic GRIs*

The method of identifying the sub-periodic GRIs that are likely to result in harmful interference to the desired GRI is summarised as follows:

- A Farey sequence of order 4 is generated. Although in some scenarios higher order Farey sequences may be required.

- The generated Farey sequence are used to determine the sub-periodic GRIs. These are found by multiplying the desired GRI with the term of the Farey sequence. For example, a modified Farey sequence of order 4 has the following terms $\{\frac{0}{1}, \frac{1}{2}, \frac{2}{3}, \frac{3}{4}, \frac{1}{1}\}$. If the desired GRI is 9007, the sub-periodic GRIs are $\{4504, 6005, 6755\}$.

- Next, $|\Delta\tau_{sub}|$ is determined using the numerator and the denominator of the Farey sequence as: $\Delta\tau_{sub} = a \cdot T_{GRI,1} - b \cdot T_{GRI,2}$ where a and b are the numerator and denominator of the Farey sequence. $T_{GRI,1}$ is the GRI of the desired station while $T_{GRI,2}$ is sub-periodic GRI of the cross rating station. As an example, the $\Delta\tau_{sub,max}$ for the sub-periodic GRIs above are $\{-10, -10, 10\}$.

1 Sub-periodic interference occurs when the ratio of the GRIs of the interfering stations is close to simple fractions such as 1/2, 2/3, 3/4, 4/5 etc.

2 Farey sequence is a sequence of irreducible fractions between 0 and 1 arranged in ascending order. For example, $\{\frac{0}{1}, \frac{1}{2}, \frac{2}{3}, \frac{3}{4}, \frac{4}{5}, \frac{5}{6}, \frac{7}{8}\}$.

The sub-periodic GRIs can be identified from a list of all the Loran chains operating around the world.

10.4 COVERAGE PERFORMANCE OPTIMISATION CRITERIA

The optimisation criterion is to minimise position error within the coverage area while maximising the area covered for a given position accuracy target.

10.5 CHAIN CONFIGURATION

The two probable stations were configured into the three possible chains (6731, 7499 and 9007). The minimum time difference between two consecutive secondary transmissions is $\Delta_{tm,min} = 9900\mu s$. and the minimum separation between the last secondary transmission and master transmission from the next GRI is $\Delta_{Nst,min} = 9900\mu$s.

10.6 GRI SELECTION

Table 28: Cross-over time and sub-periodic CRI for GRI 7499(the cross-over time has to be considered both in terms of the proposed and the existing GRIs, therefore the maximum value of the two,$T_{x,max}$, is shown; a and b are the numerator and denominator, respectively, of the corresponding Farey point.

INTERFERING GRI	$T_{x,max}$	a	b	$\lvert\Delta\tau_{sub}(\mu s)\rvert$
7430	28	323	326	30
7030	5	15	16	50
5543	1	17	23	60

Table 29: Cross-over time and sub-periodic CRI for GRI 9007 (the cross-over time has to be considered both in terms of the proposed and existing GRIs, therefore the maximum value of the two,$T_{x,max}$, is shown; a and b are the numerator and denominator, respectively, of the corresponding Farey point.

INTERFERING GRI	$T_{x,max}$	a	b	$\lvert\Delta\tau_{sub}(\mu s)\rvert$
8970	52	485	487	50
8930	25	116	117	20
8830	11	449	458	30
5543	1	8	13	30

10.7 FACTORS AFFECTING GRI SELECTION

The GRI pre-selection procedures proposed by the USCG, DCN Brest and TU Delft are summarised in reference [77]. In the USCG method, the primary consideration is the estimated groundwave field strength of each station of the interfering chain, not the expected coverage area of each chain. Safar [77] demonstrated that there is a general decreasing trend in the magnitude of the pseudo-range error with increasing GRI of the interfering station. His results suggested that co-prime GRIs results in the errors that are

uniformly distributed while the non-co prime GRIs results in pseudo-range errors that are not uniformly distributed.

10.7.1 *GRI Selection*

The feasibility study of whether an existing chain can accommodate any new stations is first carried out. The procedure for determining if a chain can accommodate any new stations is well understood in the Loran community and has been modified in reference [77] to suit the eLoran specifications. This work adopts the procedure deployed in Safar's work. The incomplete tables in Safar;s thesis are completed here with all the necessary data.

10.7.2 *Cross-Over Time Calculations*

The cross-over time is defined as the number of successive pulse groups affected by the overlaps between two signals transmitted at different GRIs [67] and is determined by:

$$T_x = 1 + \left\lfloor \frac{T_1 + T_2}{T_{GRI,1} - \text{round}\left(\frac{T_{GRI,2}}{T_{GRI,1}}\right) \cdot T_{GRI,1}} \right\rfloor \tag{10.4}$$

where $T_{GRI,2}$ and $T_{GRI,1}$ are the GRIs of the cross rating signal expressed in seconds. T_1 denotes the time taken for each station to transmit a pulse group. Traditionally this was taken to be 11500μs for a master station (since the master was broadcasting 9 pulses) and 9500μs for any other station. In eLoran, all the stations broadcasts 8 pulse groups and T_1 and T_2 are equal to 9500μs. As an example using the transmission of the stations operating on $T_{GRI,1} = 9007$ and $T_{GRI,2} = 8970$, the cross-over time can be calculated as:

$$\begin{aligned} T_x =& 1 + \left\lfloor \frac{(9500 + 9500) \cdot 10^{-6}}{(90070 - \text{round}\left(\frac{89700}{90070} \cdot 90070\right)) \cdot 10^{-6}} \right\rfloor \\ =& 1 + \lfloor 51.35 \rfloor \\ =& 52 \end{aligned}$$

The cross-over times of other interfering chains are shown in tables 28 and 29.

10.7.3 *eLoran Data Channel Considerations*

The newly developed eDLoran is independent of Loran Transmissions and therefore maximum allowable GRI has no influence on the achievable data rates. This offers an opportunity to move all the NELS stations into one GRI chain. The use of longer GRIs results in low data rates in the data link channel used for transmitting correction data to users. The low data rates result in increased latency leading to high temporal decorrelation of the correction data. The use of the new eDLoran improves upon the drawbacks mentioned above.

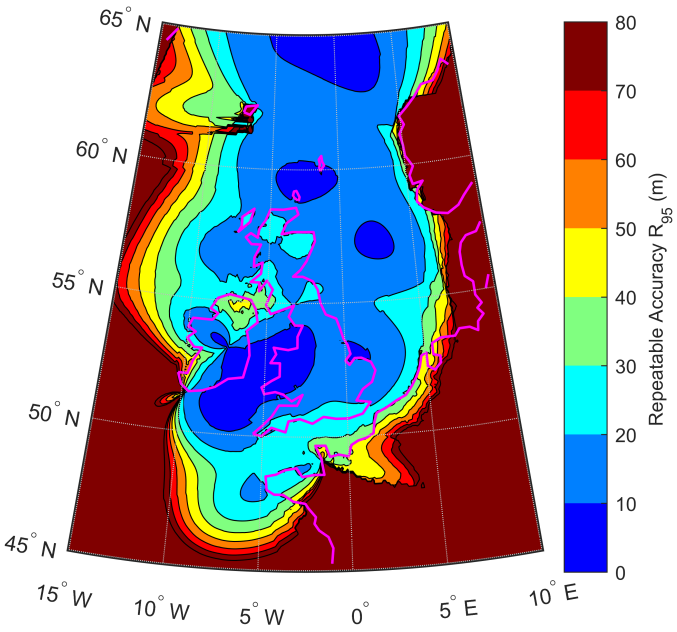

Figure 94: Repeatable Accuracy including the transmitters at Tullamore and Mizen assuming dLoran everywhere.

10.8 REPEATABLE ACCURACY ASSESSMENT

In this section, different transmitter permutations of high and low power are assessed to determine the configuration that produces the best accuracy and an improved coverage at most of the ports around the British Isles.

10.9 RESULTS

The desired output is the one that shows an improved coverage at all the ports in the British Isles as well as improved coverage to the West of the British Isles. Figure 97 shows an accuracy contour plot generated after placing two transmitters at Ballydavid and another one at Tullamore. This accuracy plot is improved compared to the current accuracy plot. There is now a better coverage in the west of the British Isles. There is also a better coverage in the English Channel and the Irish Sea. However, the coverage in the Dovers strip is not so good. Figure 98 shows the repeatable accuracy plot after adding the transmitters at Mizen Head and Tullamore. This transmitter configuration results in a better coverage in Bristol Channel and the entrance of the English Channel but the coverage in the western part of Ireland is poor.

Figure 99 shows the accuracy plot after adding transmitters at Ballydavid and Bealadangan. The accuracy figure is good in the west of Ireland and fairly good in the Irish Sea, Bristol Channel and the English Channel. Figure 100 shows the accuracy plot after adding transmitters at Mizen Head and Bealadangan. There is good coverage in the Bristol Channel and at the entrance of the English Channel but there is poor accuracy in the west of Ireland.

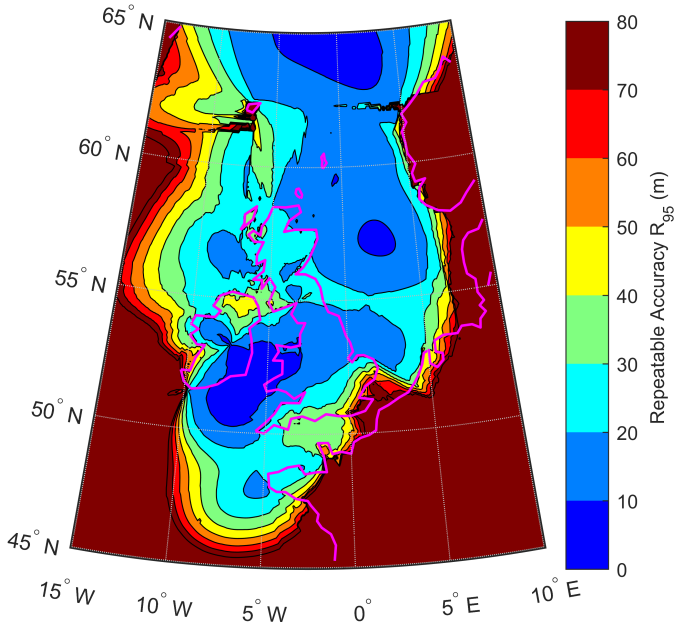

Figure 95: Diluted repeatable accuracy including the transmitters at Tullamore and Mizen.

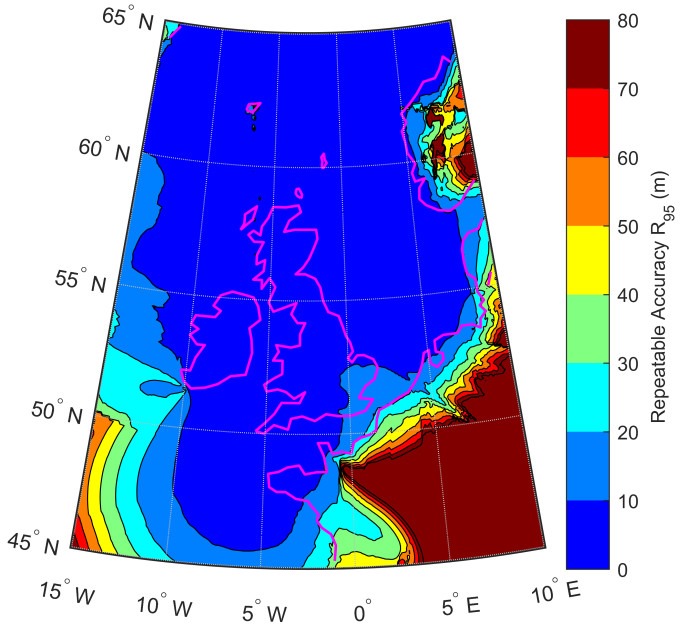

Figure 96: Repeatable accuracy including the transmitters at Tullamore and Mizen. This plot was generated under the assumption that there is no signal fading due to skywave contamination.

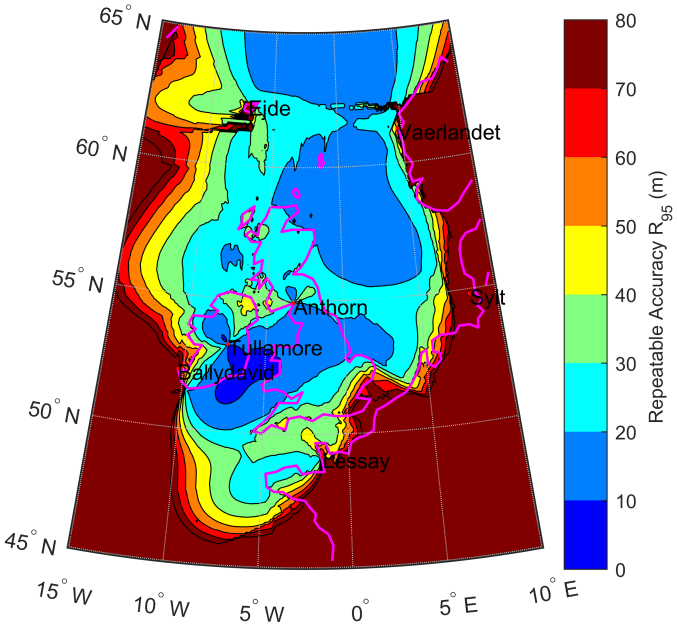

Figure 97: Diluted Repeatable Accuracy including the Tullamore and Ballydavid.

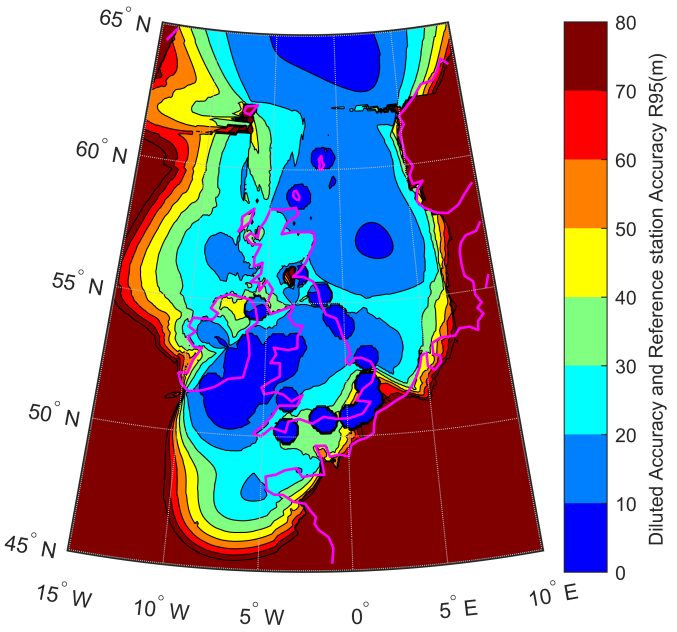

Figure 98: Diluted Repeatable Accuracy including the Tullamore and Mizen.

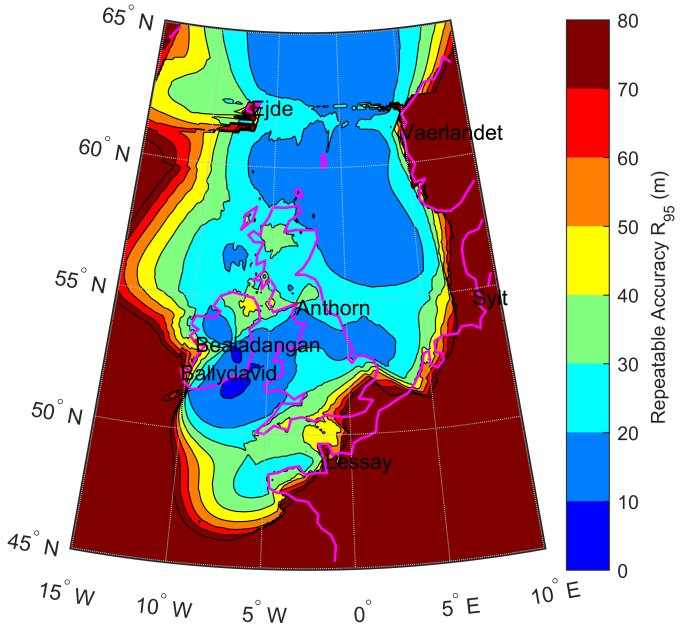

Figure 99: Diluted Repeatable Accuracy after adding transmitters at Ballydavid and Bealadangan.

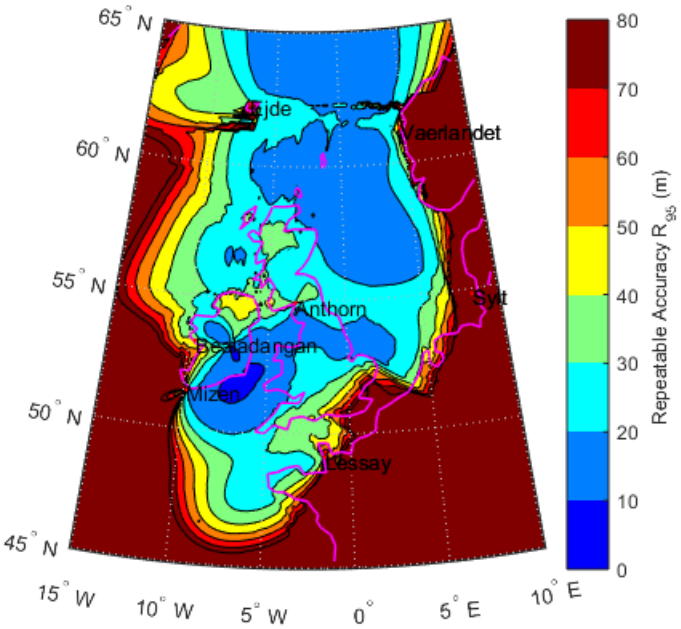

Figure 100: Repeatable accuracy over the GLA coverage area after the inclusion of Mizen and Bealadangan in the republic of Ireland.

10.10 BEST LOCATIONS FOR TRANSMITTERS

The best locations for placing transmitters in Ireland are Bealadangan and Ballydavid. This configuration produces the best accuracy prediction percentage at all of the ports and harbours in the British Isles and Ireland. The coverage produced by this configuration may not be as good as the others in the Bristol and English Channel, but it gives good coverage in Ireland compared to all of them. However, for reasons beyond the GLA's control, it was later decided that the two stations be placed at Mizen and Tullamore [46].

Table 30: Table showing the eLoran accuracy around the ports around UK and Ireland.

Port Name	Latitude	Longitude	Pos error (m)
Belfast	54.668	-5.851	9.6
Bristol Avonmouth	51.506	-2.728	8.3
Brixham	50.401	-3.511	11.4
Clyde	55.942	-4.638	8.2
Cork	51.785	-8.264	15.7
Dover	51.107	1.329	7.9
Dublin	53.346	-6.175	10.4
Fawley	50.829	-1.307	7.7
Felixtowe	51.938	1.307	7.2
Fishguard	52.001	-4.974	10.9
Folkestone	51.069	1.168	7.9
Forth	56.029	-3.072	6.3
Grimsby	53.585	-0.066	6.2
Harwich	51.949	1.272	7.2
Holyhead	53.313	-4.619	9.1
Hull	53.737	-0.334	6.3
Immingham	53.634	-0.184	6.3
Liverpool	53.409	-3.007	7.9
London	51.496	0.743	7.2
Medway	51.399	0.566	7.4

10.11 SUMMARY AND CONCLUSIONS

This chapter has studied and implemented the eLoran GRI selection procedure developed by Safar [77] for the same case study involving the integration of two new transmitter stations at Tullamore and Mizen Head in Ireland into the existing Northwest European network. The objective of this case study was to investigate the options for improving the eLoran coverage on the West Coast of the Britain Isles and over Ireland. The first part of this case study investigated the possibility of including the new stations into an existing eLoran chain in Northwest Europe. It has been determined that there is not enough space for the new stations in the 6731 Lessay GRI. However, it was determined that it is possible to integrate them into either the 7499 or 9007 chain. This analysis has assumed that the Norwegian and French stations are operational. Both GRIs provide a similar level of coverage performance. GRI 9007 seems to achieve better accuracy results in the northern part of the coverage area with 7499 performing better in the south. Safar [77] did a case study where he considered the option of putting the additional stations on a new GRI. He identified a range of candidate GRIs

with the optimum one determined to be GRI 8581. As a consequence of the additional CRI introduced in the system, the coverage performance is slightly worse when the new stations operate on a new GRI than if they were integrated into an existing chain. It is, therefore, preferable to use one of the existing GRIs for the new stations. The possibility of eliminating CRI within the Northwest European system by moving all stations to a single GRI has been investigated. Moving all stations onto a single GRI minimises interference and may also be useful if eLoran is used R mode navigation. Unfortunately, all of the cases studied do not provide full 10m accuracy coverage in Ireland. Further research should, therefore, investigate the possibility of using the transmitter locations that are further west and how eLoran can be combined with other signals of opportunity to back up GPS.

11 CONCLUSIONS

This thesis posed the following questions:

1. Given the current transmitter configuration, what is the accuracy, availability, continuity performance of the coverage network in the General Lighthouse Authorities of United Kingdom and Ireland's geographical area if differential eLoran is only applicable at the harbour and port locations?

2. What is the best method of placing the reference stations in the coverage area given the constraints?

The primary objective of this research was to develop coverage software with its models for predicting accuracy, availability and continuity for maritime harbour entrance and approach in Europe. However, this research has accomplished a good deal more. This research has investigated a number of possible coverage-limiting factors such as changes in conductivity and weather on repeatable accuracy by developing and implementing methods for predicting those effects. Comparisons between predicted and measured data have been used to verify that the methods have been correctly developed and implemented.

Prior to this research, the coverage tool could only model accuracy under the assumption that the ASFs are provided everywhere in the coverage area. However, this assumption is not realistic but served as a starting point for producing a working accuracy model. This assumption was modified by investigating long-term and short-term effects of ASFs changes on accuracy. The long-term effects of ASF changes were investigated by monitoring TOA signals at the reference station in Harwich from October 2009 to October 2010. In this study, a change in conductivity was assumed to be related to the land path distance. This assumption was deemed reasonable and was validated using real data measured in Ireland at a Blacksod lighthouse. The developed model is termed the Landpath model. The Landpath and the weather models were added to the TOA variance model to dilute accuracy in regions where dLoran is not desired. The results of the accuracy plot suggests that one or two stations are needed in the West coast of the British Isles. It is important to emphasize that the initial dLoran assumption is preserved at the locations which are expected to host reference stations.

This thesis has presented the models to determine the degree of spatial decorrelation of the pseudorange corrections from reference station. In order to quantify the number of reference stations needed to service a harbour, the increase of the pseudorange error with distance needs to be determined. This question was addressed in chapter 6. It was shown that the spatial decorrelation depends on the baseline length and the angle between the reference station and the user's receiver. It was postulated that the spatial decorrelation is maximum when the angle between the user and the normal to the reference station's Line of Position is 90° and 270° and minimum when the angles are 0° and 180° (transmitter,reference station and the user in a straight line). This analysis assumed that the receiver is within 50 km

from the reference station. An equation for working out the number of reference stations needed in a harbour of a specified size has also been given in chapter 6.

This research has demonstrated the coverage tool's capability to determine availability and continuity in the GLA coverage area. The determination of availability and continuity uses a similar model developed for eLoran in the US using the transmitter availability statistics obtained from the Control Centre in Brest. The availability results suggest that the scheduled maintenance times need to be minimised in order to meet IMO standards. This is for the first time availability and continuity plot has been produced for eLoran in Europe.

The results of the coverage suggested that eLoran coverage was poor in the West of the British Isles therefore two transmitters were needed in order to improve accuracy in the West of the British Isles. Therefore, a decision had to be made regarding the optimum placement of those transmitters. The development of the coverage tool has deployed several standards for accuracy, availability and continuity and has been used to the find suitable locations of two new transmitters in Republic of Ireland. The coverage software results suggested that the best location would be at Tullamore and Mizen Head. The coverage software is now adequate to help administration to make informed decisions regarding what needs to be accessed in relation to accuracy, availability and continuity.

11.1 REVIEW OF THE THESIS

This thesis described the improved coverage prediction techniques developed by the candidate and their implementation in the eLoran coverage prediction tool. Table 4 shows the graphical representation of this thesis. Chapter 1 established the motivation for this research, which stems from the concerns about the increased reliance of society on Global Navigation systems and the need for a backup solution. The basics of the eLoran system as a potential backup to GPS are explained and the aims of this research are defined in this chapter. Chapter 2 reviews the coverage prediction techniques that have been deployed since the 1990s using Loran-C until the times of modernized Loran-C. Chapter 3 describes the various input models of the GLA coverage prediction tool that satisfy various standards set out by international bodies. It also describes the repeatable accuracy model and its assumptions. It also includes some of the author's contributions to the coverage prediction tool such as ECD modelling and an improved skywave field strength model.Chapter 4 describes the author's contributions to the determination of repeatable accuracy. This chapter uses the Land path and weather models to modify the initial assumption that there is differential Loran everywhere in the coverage area. Chapter 5 describes the ASF + SF models necessary to determine the total propagation time taken by the eLoran signals from the transmitter to the receiver. Chapter 6 describes a spatial decorrelation model developed for answering questions like how many reference stations are needed to service a single harbour? The models for interpolating differential corrections are described in detail. Chapter 7 This chapter describes a mathematical model developed using a Taylor Series expansion method to predict the error incurred when applying reference station differential ASF corrections at the user who is within a certain

distance from the reference station.Chapter 8 describes an eLoran availability model and produces an availability map for Europe using the transmitter statistics obtained from the Control Centre in Brest (France). Chapter 9 develops a model for continuity using Markov chain analysis and the transmitter availability statistics obtained from the Control Centre in Brest. Chapter 10 describes the results of the case study for finding two suitable places for the Loran transmitters installation with one operating at high power and another operating at low power. Chapter 11 presents the conclusions and the future work needed to improve the coverage tool even further.

11.2 CONTRIBUTION TO KNOWLEDGE

This thesis makes contributions in the following areas:

- Improved skywave field strength and delay models using the results developed by Alwyin and Poppe in their coverage prediction work using Datatrak and DGPS signals respectively.

- Improved the coverage criteria by merging the work done at the Czech Technical University in Prague on cross rate interference into the existing coverage tools. This work helps in the selection of the transmitters to be used in the position accuracy calculation.

- Established an understanding that most parts of Europe, British Isles, Ireland do not experience a lot of thunderstorms but Spain experiences a lot of thunderstorms. If coverage prediction is to be deployed in Spain, the nature of atmospheric noise experienced there will need to be modelled.

- Improved the repeatable accuracy model, by including the changes in the spatial and temporal ASFs of each transmitter at all points in the coverage area.

- Demonstrated that over a long period of time the temporal ASF changes due to changes in conductivity (Landpath model) contribute more to the eLoran eLoran pseudorange error than the temporal ASF changes due to the weather.

- Included the spatial ASF model in the coverage tool. The coverage tool is capable of predicting ASFs in two ways, analytically (using Monteath's method), and using a set of curves derived from the data provided by other Johler and his colleagues.

- Proposed a weighted ASF correction method from a single reference station using the ratio of BER rather than spatial ASFs as weights.

- Used reference station coverage prediction to assess if the reference stations in the GLA's coverage area are optimally placed or not.

- Proposed a method for calculating the number of reference stations needed to service a harbour.

- Proposed a method for determining an interpolated pseudorange error correction from several reference stations to be applied at the user's receiver.

- Proposed a spatial decorrelation model for eLoran to determine the pseudorange error increase at various distances from the reference station.

- Generated availability and continuity maps in Europe using data from the Control Centre in Brest (France).

- Demonstrated the coverage tool's capability in real-life situations to find suitable locations of two transmitters to be installed in the Republic of Ireland in order to improve the eLoran coverage in the west of the British Isles.

These contributions represent an important part of an overall project by the General Lighthouse Authorities of the United Kingdom and Ireland to demonstrate that eLoran has the potential of being an adequate backup to GPS as well as a backup for position and timing solution to a variety of users and modes of transportation in Europe.

11.3 CONCLUSIONS

In summary, the following conclusions can be drawn from this research:

- Repeatable accuracy is dependent on the long-term and short-term ASF variations. The long-term ASF variations at the user's locations depend on the land path distance between the transmitter and the user's receiver.

- The pseudorange correction is highly sensitive to passing weather fronts. Dissimilar weather conditions along the paths from transmitter-receiver and transmitter-reference station leads to poor repeatable accuracy at the receiver.

- The number of reference stations needed to service a harbour is dependent on the spatial decorrelation distance.

- The pseudorange correction (PRC) increases with distance from the reference station. At the same distance from the reference station, the growth of the PRC also depends on the angle between the normal to the reference station LOP and the user's receiver. At 0° and 180°, the growth of the correction depends only on the decorrelation distance. At similar distances, the pseudorange increase is maximum when the angle between the normal to the reference station LOP and the receiver-reference baseline is 90° and 270°.

- Availability depends on the level of the atmospheric noise.

- Availability and Continuity depend on the mean time between failure (MTBF). Since the MTBF is affected by scheduled maintenance times, an increase in availability then depends on the shorter scheduled maintenance times.

11.4 SUGGESTIONS FOR FUTURE WORK

In this thesis, it was assumed that the receivers are always tracking correct Loran cycles. Although, this is a good assumption for producing a working coverage model, this is not always the case in practice. Therefore, a cycle

selection method will need to be modelled by calculating the probabilities of getting a cycle error at all the grid points. This is part of integrity requirement, which has not been discussed in this thesis. A cycle selection method can be incorporated into the coverage criteria model to make the coverage prediction model more realistic.

A model for determining Horizontal Protection Limits (HPL) in the coverage area is needed. The improved accuracy model developed using the variances of the measured ASFs over a year at a reference station against the land path distance between the transmitter and the reference station. The relationship between ASF variations of each transmitted signal measured at the reference was postulated to have an exponential relationship with the land path distance between the transmitter and the reference station. However, this model can be improved by including more data from other installed monitor sites around the UK.

In the quest to model how differential ASFs vary as the receiver moves away from the reference station, the ASF was estimated using Taylor series approximation of first-order. This is deemed sufficient for the work developed in this thesis, but for future research that intends to improve these results, a Taylor series approximation of higher order may be used to improve the estimated ASFs everywhere in the coverage area.

This thesis has presented a model for determining the propagation time of the signals from the eLoran transmitters to receivers and as such a finer conductivity grid and topography data needed to determine ASFs with a high degree of confidence.

Part III

APPENDIX

APPENDIX CHAPTER

JAN ŠAFÁR
Czech Technical University in Prague

CASPAR K. LEBEKWE
University of Bath

PAUL WILLIAMS
General Lighthouse Authorities of the United Kingdom and Ireland

ACCURACY PERFORMANCE OF ELORAN FOR MARITIME APPLICATIONS

ABSTRACT

E-Loran, or enhanced Loran, is the latest in the longstanding and proven series of low frequency, LOng-RAnge Navigation systems. eLoran evolved from Loran-C in response to the 2001 Volpe Report on GPS vulnerability. It improves upon previous Loran systems with updated equipment, signals, and operating procedures. The improvements allow eLoran to provide better performance and additional services when compared to Loran-C, and enable eLoran to serve as a backup to satellite navigation in many important applications.

Different applications impose specific requirements on the navigation system's accuracy, availability, integrity and continuity performance. In the maritime sector, accuracy requirements are the most stringent. In order to comply with the requirements of the International Maritime Organisation (IMO) for harbour entrance approach, eLoran has to provide an accuracy of better than 10 m (95%).

Achieving this target is possible if the eLoran navigation receiver is equipped with an up-to-date database of signal propagation corrections and if real-time differential Loran corrections are applied. When these conditions are met, the achievable accuracy is largely determined by the transmitters' geometry, signal strengths and atmospheric noise levels, but also by the mutual interference among eLoran stations. This is also referred to as Cross-Rate Interference (CRI) and is inherent to the way all Loran systems operate.

In this paper we present results of the eLoran research that is being conducted at the Czech Technical University in Prague (CTU) and the University of Bath (UK) in cooperation with the General Lighthouse Authorities of the United Kingdom and Ireland. In our work we have focused on questions that arise when considering introducing new eLoran stations into an existing network. This particular paper investigates the achievable accuracy performance of eLoran for maritime applications. The sources of measurement error in eLoran are reviewed, and an eLoran accuracy performance model is presented. Special attention is paid to the problem of CRI and possible ways of its mitigation.

This paper is an abridged version of a more detailed unpublished paper which can be found at the following address: http://safar.me.uk/pub/js_cl_pw_navsup_2010.pdf.

Keywords:
enhanced Loran, accuracy, maritime applications.

INTRODUCTION

Over the past years, the US Global Positioning System (GPS) has become an integral part of modern society. Be it on land, at sea or in the air, GPS is an important and often the primary means of Positioning, Navigation and Timing (PNT). Although its qualities make it, in many aspects, superior to other PNT solutions, there are also some serious shortcomings and vulnerabilities common to all Global Navigation Satellite Systems (GNSS) — present, as well as future (e.g. Galileo). These are largely a consequence of the extremely low GNSS signal levels at the surface of the Earth[1] and have been documented many times before [2, 4].

The concerns about the vulnerability of GNSS has sparked a renewed interest in the Loran PNT system, or rather in its upgraded version now widely called *enhanced Loran* or simply *eLoran*. The nature of the eLoran system makes its potential failure modes highly independent of GPS. eLoran is a terrestrial system, which operates in the low-frequency band, uses high-power transmitters and completely different navigation signals. Its signals are also data modulated, which enables eLoran to deliver differential corrections, integrity messages and other data to users. Despite the fundamental dissimilarities, both eLoran and GPS are ranging systems and the observables from these systems can naturally be combined into an integrated position solution. In recent years, considerable effort has thus been put into investigating whether eLoran can provide a viable backup to GPS as well as other GNSS.

In Europe, the General Lighthouse Authorities of the United Kingdom and Ireland (GLAs) lead the way in eLoran research. The work presented in this paper is part of the GLAs' effort to develop a comprehensive eLoran coverage and performance model. Coverage prediction in general tells us over what geographical region the eLoran service can be used and to what level of quality. There are four system requirements that need to be assessed in order to satisfy the required navigation performance. These are accuracy, availability, continuity and integrity. This paper concentrates only on the accuracy performance of eLoran.

[1] The received minimum RF signal level for block IIR-M/IIF GPS satellites, for example, is –158.5 dBW [17].

ACHIEVABLE POSITIONING ACCURACY OF ELORAN

When referring to accuracy of a positioning system, we need to distinguish between its absolute accuracy and repeatable accuracy. In [12], the *absolute accuracy* is defined as the accuracy of a position with respect to the geographic or geodetic coordinates of the Earth. The *repeatable accuracy*, then, is the accuracy with which a user can return to a position whose coordinates have been measured at a previous time with the same navigational system. Due to the nature of low-frequency signal propagation, Loran systems may suffer from large measurement biases, resulting in absolute accuracy on the order of hundreds of meters. However, Loran's repeatable accuracy is comparable to that of single-frequency (L1) GPS. In this paper, we explain how eLoran's absolute accuracy can be enhanced to the level of its repeatable accuracy, and we present a method for evaluation of eLoran's repeatable accuracy.

FACTORS AFFECTING ACCURACY

So what are the major factors that determine the accuracy of eLoran? eLoran is a ranging system, which means that the accuracy of our position fix is determined by the following three factors:

1. Accuracy of signal Time-of-Arrival (ToA) measurements.
2. Accuracy of the ToA to range conversion.
3. Geometry of the transmitter stations in view.

Transmitter geometry is a crucial factor in obtaining a good position fix; however, the impact of geometry on the accuracy performance of a ranging system is well understood [3] and will not be discussed in this paper.

Accuracy of the ToA to Range Conversion

One of the most important sources of error in Loran systems is due to spatial and temporal variations in the signal propagation velocity. The propagation velocity of Loran ground wave signals is a function of the Earth's surface conductivity and it also depends on the parameters of the atmosphere (temperature, pressure, humidity). Terrain elevation can also affect the signal propagation time, as eLoran ground waves obediently follow the Earth's surface and therefore travel a longer path than the theoretical point-to-point distance over an assumed smooth Earth. All of the factors mentioned above limit our ability to accurately convert the signal ToA measurements into distances, and thus contribute to the overall positioning error. In eLoran we account for these factors by means of so-called *Primary* (PF), *Secondary* (SF) and *Additional*

Secondary Factors (ASF). PF and SF allow us to model the signal propagation in the Earth's atmosphere over an all-sea water path. Any additional delay due to propagation over land is then taken into account using ASFs. In order to achieve the best possible positioning accuracy, ASFs in the area of interest need to be measured and stored in the receiver. Fluctuations in the ASF values should also be monitored and broadcast to the user in the form of differential corrections, e.g. using the eLoran data channel. Not taking ASFs into account can lead to ranging errors of up to 2 km [17]. Applying them correctly, on the other hand, gives the full eLoran accuracy, which approaches the repeatable accuracy of the system.

eLoran signal propagation may also be adversely affected by the presence of nearby conducting structures whose dimensions are an appreciable fraction of the signal carrier wavelength (e.g. bridges). Such structures can "absorb" some of the eLoran energy and re-radiate it [14]. The effects of re-radiation need further investigation and will not be discussed here.

Accuracy of the ToA Measurement

The third (and most varied) group of factors determining the positioning accuracy are those that affect our ability to accurately measure the actual ToAs of the eLoran signals. The ToA measurements are made in two stages. First, coarse measurements are made based on the shape of the leading edge of the eLoran pulse. When the approximate ToAs are known, the carrier phase of individual eLoran ground wave signals is measured to obtain more accurate ToA estimates. It is therefore the carrier phase distortion, which will be of interest in the following.

The ToA measurement errors are predominantly determined by the Signal-to--Noise Ratio (SNR) of the received signals. In the Loran frequency band, the dominant sources of noise are *atmospheric noise*, which is caused by lightning discharges, and *man-made noise* from, for example, switch-mode power supplies. Other sources of noise may include transmitter pulse timing jitter or receiver related noise. The latter is believed to be a minor component with modern eLoran receivers though [5].

Uncorrelated ToA measurement errors (e.g. due to atmospheric noise) can be suppressed by integrating (averaging) a certain number of received pulses before taking the measurement. This effectively increases the SNR of the received signals, but at the same time it places limitations on the allowable dynamics of the user platform.

Besides noise, another important source of ToA measurement error is interference caused by other radio signals. We can distinguish two types of interference to eLoran — *Carrier Wave Interference* (CWI) and *Cross-Rate Interference* (CRI). CWI originates from radio services operated near the eLoran frequency band and

was considered a major threat for Loran-C. With today's receivers though, most of the out-band CWI can effectively be suppressed, therefore CWI is no longer expected to be an issue. CRI emanates from eLoran itself and is currently the major source of interference to eLoran. What exactly is the cause of CRI then?

eLoran transmitters are organised in groups of usually 3 to 5 stations called 'chains'. The stations periodically broadcast groups of 8 or 9 specially shaped low--frequency, high-power, pulses. The interval between successive repetitions of the groups of pulses is unique to each chain and known as the *Group Repetition Interval* (GRI). Careful selection of GRIs and transmission times ensures that stations operating in a chain do not interfere with each other. However, the nature of the system is such that the signals from different chains overlap from time to time and may introduce errors into our ToA measurements – this is referred to as CRI.

Another effect of CRI is *transmitter dual-rate blanking*. Some Loran transmitters are dual-rated, i.e. they broadcast signals on two GRIs, and such transmitters are periodically faced with the impossible requirement of radiating overlapping pulse groups simultaneously. During the time of overlap, those pulses of one group that overlap any part of the other group's blanking interval are suppressed. The *blanking interval* extends from 900 μsec before the first pulse to 1600 μsec after the last.

Maritime eLoran

Accuracy is the major factor affecting the suitability of eLoran for maritime navigation. IMO standards for the region of Port Approach specify a stringent accuracy requirement of 10 meters (95 percent of the time). A number of studies in the past have shown that accuracies better than 10 m are achievable [1, 9]. Table 1 summarises measures that need to be taken in order to meet the 10 m accuracy requirement in the maritime environment.

Table 1. Meeting the maritime accuracy requirement

Accuracy Limiting Factor	Mitigation
Poor geometry	Installation of additional eLoran transmitters, perhaps using low power mini-eLoran stations as coverage gap fillers
ASF spatial variation	Detailed ASF maps stored in receivers
ASF temporal variation	Differential reference stations
Uncorrelated noise	Integration time ~ 5 sec is acceptable
Man-made noise	Careful receiver antenna installation

From what has been said so far, it follows that the major error sources in maritime eLoran are the residues of atmospheric noise, transmitter related noise, and CRI. These factors are also at the heart of the GLAs' coverage and performance model and will be investigated in greater detail in the following section.

THE GLA COVERAGE AND PERFORMANCE MODEL

The GLAs' coverage and performance model is implemented in the MATLAB™ environment. In the accuracy module of the coverage software, we first decide which eLoran stations to include in the analysis and we set up a region over which coverage is required. The coverage region is divided into grids consisting of rectangular elements of equal sizes, typically 0.1° in latitude by 0.1° in longitude. At each point in the grid the individual coverage limiting factors are modelled and the resulting data arrays are stored. When required, for coverage computation, these are then loaded into memory.

The level of repeatable accuracy is highly dependent on the variance of the measured ToA values. The higher the variance of the ToA, then the poorer is the positioning accuracy. The main driver of ToA variance is the signal-to-noise ratio (SNR) of the received signal. The lower the SNR, the higher the ToA variance and therefore the poorer the positioning accuracy. The calculation of SNR requires knowledge of the signal strength (or field strength) of the Loran signal, and the level of noise at the same location.

In the current implementation of the GLAs' coverage prediction software, ground wave field strength arrays are calculated using Millington's method. This employs a set of the 100 kHz propagation curves for different ground conductivities. Ground conductivity data is provided by a digital ground conductivity database developed at the University of Wales, Bangor, based on the World Atlas of Ground Conductivities [8].

As mentioned above, the dominant noise source in the Loran band is atmospheric noise. Atmospheric noise is computed at different percentiles and generated based on the model presented in ITU Recommendation P372-9 [7].

Most recently noise due to CRI has also been taken into account, as will be described below.

In addition to ground wave, the effect of sky wave propagation also needs to be taken into account, since there are likely to be geographical locations where the *wanted* ground wave is interfered with by its *unwanted* copy arriving via reflection

from the ionosphere. Sky wave field strength and sky wave delay arrays are computed. These are based on ITU recommendation 1147-2 [6].

Models implemented at Stanford University in their Loran Coverage Availability Simulation Tool [10] were also studied and we are in the process of incorporating these into our software.

When all the data arrays are available, algorithms within the software then test each grid point to see whether the eLoran signals meet certain acceptance criteria. For example, a signal of a particular station is used in the accuracy analysis only if its SNR is higher than –10 dB and the sky wave field strength to ground wave field strength ratio and sky wave delay are within the limits prescribed by the receiver Minimum Performance Standard [11]. With the (possibly) reduced set of signals at each grid point, repeatable accuracy is calculated and accuracy plots are generated. Selected parts of the model will now be presented in greater detail.

Modelling Errors Due to Atmospheric Noise

As explained earlier, atmospheric noise is one of the major sources of measurement error in eLoran. Our software allows us to evaluate the signal-to-atmospheric noise ratio for each station used in any point of the coverage area. Further, in [10] Lo *et al.* presented the following equation for the conversion of SNR to pseudorange measurement variance:

$$\sigma_s^2 = c_1 + \frac{337.5^2}{N \cdot SNR}, \tag{1}$$

where:
c_1 [m^2] accounts for transmitter related noise, which is assumed to be 6 m, one sigma ($c_1 = 36$ m^2) [10], N is the number of pulses used in signal integration, and SNR is the SNR of a single pulse, expressed as a linear ratio.

No explanation is given in that paper as to how this equation had been obtained. However, we have verified the equation ourselves both analytically and by numeric simulations; and we can confirm that the second term on the right hand side of Equation 1 gives an accurate estimate of pseudorange measurement variance under the assumption of white noise, at least in the range of SNR from –10 dB to +40 dB. This part of the equation is therefore being used in our coverage prediction software to model the measurement errors introduced by atmospheric noise. The usage of the c_1 constant is discussed further in this paper.

Modelling Errors Due to CRI

In order to meet the stringent eLoran standards, the impact of CRI within the system must be greatly reduced. This can, for example, be achieved through *CRI blanking* at the receiver end. With this technique, the eLoran receiver detects the pulses likely corrupted by CRI and discards them. The more pulses that are blanked, however, the higher is the influence of atmospheric noise and other disturbances on the ToA measurements, as the signal power available for tracking decreases significantly. We have designed methods of evaluating this blanking loss [16] and recently extended these to include the impact of sky wave borne CRI [15] (the presence of sky waves increases the probability of collision between the interfering pulse trains, depending on the sky wave delay). An example plot showing the blanking loss for one of the European stations is included in the case study below (figure 1).

Accounting for Other Sources of Error

Earlier in this paper we presented Lo *et al's* formula for the estimation of pseudorange variance due to atmospheric noise and *transmitter timing jitter* (Equation 1). In this formula the impact of the transmitter noise was modelled by an additive constant, equal to the equivalent in range of the assumed variance of the pulse timing jitter. We argue that this approach is too pessimistic, and we suggest a slightly modified version of this equation as explained in [15]:

$$\sigma_s^2 = \frac{337.5^2}{N \cdot SNR} + \frac{c_1}{N} + c_2 , \tag{2}$$

where:
N, SNR, and c_1 are as described in Equation 1 and c_2 [m^2] accounts for *other sources of variation* in the pseudorange measurements.

These may include: background CRI-induced noise caused by signals from distant interfering stations that cannot be processed out, residual CWI, receiver related noise, etc. The value of the c_2 constant has to be found experimentally. We have found that $c_2 = 12$ m^2 gives a good agreement with measurements from the GLAs' differential eLoran reference station in Harwich.

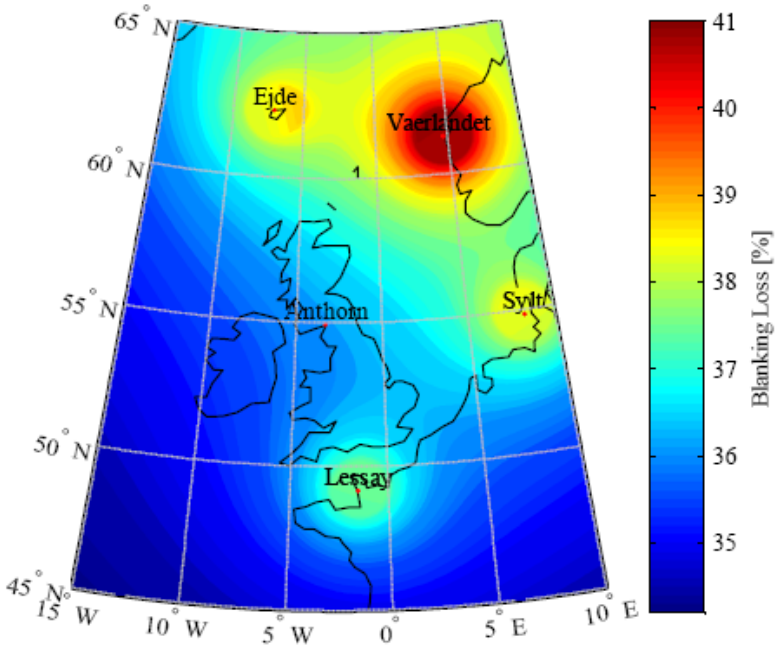

Fig. 1. Percentage of pulses blanked for the Anthorn station; height of the ionosphere: 91 km

Estimating Positioning Accuracy

In [16] we explained how the errors in pseudoranges translate into the position domain, assuming that the receiver utilises the Weighted Least Squares (WLS) position determination algorithm. We showed that the repeatable 2DRMS (Twice the Distance Root-Mean-Square) position accuracy can be estimated as:

$$\delta_{2DRMS} = 2\sqrt{\mathbf{C}_{1,1} + \mathbf{C}_{2,2}}, \tag{3}$$

where:

$\mathbf{C} = \left(\mathbf{A}^{\mathrm{T}}\mathbf{R}^{-1}\mathbf{A}\right)^{-1}$, $\mathbf{A}$ is the direction cosine matrix, which describes the geometry of eLoran stations relative to the user's position, and $\mathbf{R}$ is the pseudorange measurement covariance matrix.

This matrix is composed of the variances on each measurement obtained as described earlier.

Based on the value of δ_{2DRMS}, our software also estimates the R95 (95 percent radius) error. This estimation however is only valid under the assumption of Gaussian--distributed measurement errors.

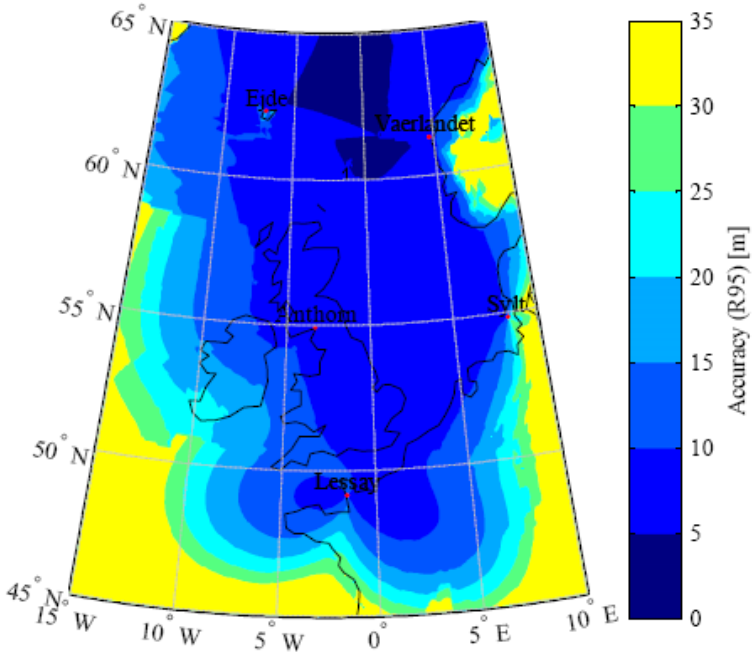

Fig. 2. Contours of repeatable eLoran accuracy (95%)

CASE STUDY

We will now demonstrate the use of the tools presented in this paper through a case study investigating the achievable repeatable accuracy of eLoran over the British Isles. Our transmission network will be formed by the 14 transmissions from the 9 European transmitters currently in operation, configured according to Appendix A. We assume that CRI within the network is mitigated through blanking. CRI originating from other Loran transmitters than those in Appendix A will not be considered in this study. The signal integration time is assumed to be 5 seconds.

The assessment of repeatable accuracy over the specified region followed the steps described in the previous section. First, the ground wave field strength arrays were calculated. We assumed that signal phase measurements are made 4 dB below the peak of the pulse, which corresponds to the location of the standard zero crossing on an undistorted eLoran pulse. Using the ITU noise model and the ground wave field strength arrays, SNR for all stations assumed in our analysis were estimated. In accordance with common practice [10], we used annual atmospheric noise not exceeded 95% of the time.

For each station, range limits were calculated based on the sky wave propagation parameters. Sky wave field strength values at 99 percentile for the winter night time period were used, providing a conservative estimate of own sky wave interference. The height of the ionosphere was assumed to be 91 km. The effects of sky wave propagation were also taken into account when evaluating the blanking loss for each station incurred as a result of mitigating CRI. Figure 1 shows the predicted blanking loss values for one of the transmitter stations used in our analysis.

Finally, pseudorange measurement variances were estimated using Equation 10 and the 2DRMS positioning accuracy was calculated using Equation 11. Figure 2 then shows the predicted R95 accuracy plot.

CONCLUSIONS AND FUTURE WORK

In this paper we have presented a set of tools for the assessment of eLoran accuracy performance, developed by a joint effort of the General Lighthouse Authorities of the United Kingdom and Ireland, the Czech Technical University in Prague, and the University of Bath. We have generated repeatable accuracy plots for the GLAs' service area using the current configuration of the European Loran transmitters. In doing so, we assumed that perfect ASFs were provided to the user, so that any biases in the measurements were eliminated. The resulting plots suggest that sub-10 m repeatable positioning accuracy should be achievable over most of Britain's coastal waters. Areas of insufficient coverage can be found on the west coast of Britain and over Ireland.

In the future we intend to include differential eLoran in the model. This requires a study of spatial decorrelation of the differential corrections as the user receiver moves away from the reference station. Also the accuracy of ASF maps used in user receivers needs to be assessed and included into the overall error budget. We also want to concentrate on collecting data to help model the effects of CRI. This should include modelling of advanced CRI mitigation methods, such as CRI cancelling, and background CRI noise from distant stations that cannot be processed out. Work is also underway on the availability and continuity components of the coverage prediction software. These will be described in follow-up papers.

ACKNOWLEDGEMENTS

The authors would like to thank Dr. Nick Ward of the General Lighthouse Authorities of the United Kingdom and Ireland (GLAs), and Prof. František Vejražka of the Czech Technical University in Prague for their support and assistance during the performance of this work.

Resilient PNT in e-Navigation

Paul Williams[1], Chris Hargreaves[1], Jan Šafář[2], Caspar K. Lebekwe[3], George Shaw[1], Nick Ward[1]

(1. The General Lighthouse Authorities of the United Kingdom and Ireland)
(2. The Czech Technical University)
(3. The University of Bath)

Dr. Paul Williams is a Principal Development Engineer with the Research and Radionavigation Directorate of The General Lighthouse Authorities of the UK and Ireland, based at Trinity House in Harwich, England. He is currently the technical lead of the GLAs' eLoran Work Programme. The work involves planning the GLAs' maritime eLoran trials and work on a wide range of eLoran related projects. He holds BSc and PhD degrees in Electronic Engineering from the University of Wales, is a Chartered Engineer, a Fellow of the Royal Institute of Navigation, a board member of the International Loran Association and is chairman of the Radio Technical Commission for Maritime Services Special Committee 127 on Standards for Enhanced Loran (eLoran) Systems.

Mr. Chris Hargreaves is a Trainee Development Engineer with the Research and Radionavigation Directorate of The General Lighthouse Authorities of the UK and Ireland. His duties involve the performance of project development work on many areas of radionavigation. His main area of interest is the GLAs' eLoran Work Programme, wherein he takes part in trials, develops software and data analysis techniques. He holds an MSci degree in Mathematics and Physics from the University of Durham, and is studying for an MSc in Navigation Technology at the University of Nottingham.

Mr. Jan Šafář was awarded the degree of Ing. (MEng) by the Czech Technical University in Prague, Czech Republic in 2007. Currently, he is a PhD candidate in the Department of Radio Engineering at the same university. He became involved in eLoran during a three month study period undertaken at the General Lighthouse Authorities of the United Kingdom and Ireland. His PhD project is focused on Group Repetition Interval Selection and Core eLoran Service Capacity.

Mr. Caspar K. Lebekwe was awarded the degree of MEng in Electronics and Communications Engineering at the University of Bath in 2008. He is currently a PhD candidate in the Department of Electrical and Electronics Engineering, sponsored by the General Lighthouse Authorities. His PhD project is focused on eLoran Service Volume Coverage Prediction.

Mr. George Shaw is a Principal Development Engineer working for the Research and Radionavigation directorate of the General Lighthouse Authorities of the UK and Ireland. He is responsible for strategy and systems studies that inform the future direction of maritime aids-to-navigation. His specialisation is in systems engineering and analysis of robust GNSS-based solutions for positioning and navigation across air, land and sea domains. He holds a MA in mathematics from the University of Cambridge, is a Chartered Engineer and a member of the Royal Aeronautical Society.

Dr. Nick Ward is Research Director of the General Lighthouse Authorities of the UK and Ireland, with responsibility for strategy & planning of research & development. His area of

specialisation is in radio-navigation and communications, including Automatic Identification Systems (AIS). He is currently vice chairman of the International Association of Marine Aids to Navigation and Lighthouse Authorities (IALA) e-Navigation committee. He is a Chartered Engineer, a Fellow of the Royal Institute of Navigation and a Member of ION.

Abstract
Resilient Positioning, Navigation and Timing (PNT) is an essential requirement for the successful implementation of the e-Navigation concept.

e-Navigation is defined by the International Maritime Organisation (IMO) and International Association of Marine Aids to Navigation and Lighthouse Authorities (IALA) as “the harmonized collection, integration, exchange, presentation and analysis of maritime information onboard and ashore by electronic means to enhance berth to berth navigation and related services, for safety and security at sea and protection of the marine environment”.

It comprises a number of structural components:

- electronic navigation charts;
- electronic positioning signals, supplemented by appropriate back-up systems;
- information on the vessel route, bearing, manoeuvring parameters and other status items in electronic format;
- transmission of positional and navigational information from ship to shore, shore to ship and ship to ship;
- clear, integrated display of the above information both on the shore and on the ship;

GNSS (in particular GPS) has become the primary means of navigation in many maritime applications. However, the vulnerability of GNSS to accidental or deliberate interference is well known and the need for more than one position input to e-Navigation is recognised. The requirement is for resilient PNT: it needs to be inherently reliable, secured against obvious external threats and capable of withstanding some degree of damage. A single, cross-sector solution that augments GNSS with an independent, dissimilar and complementary system is best for users. They will benefit from economies of scale to keep equipment costs low and existing networks - user, technology, business and regulatory - can be exploited. This will all lead to lower long-term average costs than other approaches.

eLoran is the only such complementary system that can be deployed in a timely fashion. This paper considers the vulnerability of GNSS, presents an overview of eLoran, discusses the drivers and requirements, briefly describes eLoran technology and projects being performed by the GLAs and reports on recent trials that demonstrate its performance.

1. INTRODUCTION. The Maritime Safety Committee of the International Maritime Organisation (IMO) has stated [1]:

'*e-Navigation systems should be resilient and take into account issues of data validity, plausibility and integrity for the systems to be robust, reliable and dependable. Requirements for redundancy, particularly in relation to position fixing systems should be considered.*'

Satellite navigation is now essential to the efficiency and safety of shipping. GPS drives ships' electronic charts, stabilises radar displays, and indicates vessels' positions both to other ships and to the Vessel Traffic Management Services and Search and Rescue authorities ashore. GNSS are now regarded as a utility to be taken for granted and have become the major electronic aid to navigation used by all mariners; as such their use is advocated by the General Lighthouse Authorities (GLAs).

Yet GPS is lost from time to time due to a range of vulnerabilities that affect all satellite navigation systems: solar disturbances, satellite failures and, increasingly, unintentional radio interference or deliberate jamming. Thus GPS, even when supported by Galileo and other satellite navigation systems, simply cannot meet the IMO requirement for a *resilient system* to support e-Navigation [2].

However, various solutions could be postulated to address the requirements implied by the IMO statement above. These might range from enhanced provision of physical and radar Aids-to-Navigation (AtoN), through "hardening" of GNSS, to a complementary electronic navigation system, such as eLoran, presently being trialled in the UK.

2. DRIVERS, REQUIREMENTS AND ELORAN

2.1. The Vulnerability of GNSS. There is now broad agreement that GNSS (GPS, Galileo, GLONASS and Compass) are all vulnerable to unintentional and intentional interference. This includes natural phenomena, such as ionospheric effects. The use of GPS jammers, long foreseen in navigation circles [3], has become a reality as criminals employ them to overcome tracking systems and steal vehicles. Low-powered jammers are readily available over the Internet for as little as $150 and can block GPS reception in a vehicle's vicinity. They can also block all mobile phone bands used in the area.

Today's jammers are already configured to jam GPS, Galileo and GLONASS civil and military signals simultaneously on both the L1 and L2 frequencies. It would be trivial to add L5. Some of these jammers are powerful, radiating 2W on each frequency.

The GLAs held GPS jamming trials in 2008 [4] and 2009 [5] to understand the impact of a loss of GPS on the safety of navigation. The results are presented in another GLA paper at this conference, and will not be elaborated upon further here.

2.2. Extending GNSS Performance. Extending GNSS performance is a driver for some eLoran developments. Specifically, ST Microelectronics [6] is exploring integrated eLoran and GPS at the chip scale to give consumer GNSS receivers the extreme sensitivity needed to start up deep inside buildings, including concrete underground carparks.

2.3. Resilient PNT *Resilient PNT* (positioning, navigation and timing) is today's requirement not just for the maritime sector but for critical infrastructure (e.g. transport, telecommunications, power distribution, finance, emergency services etc.) in general [7].

The UK Centre for the Protection of National Infrastructure uses the following definition for resilience: the equipment and architecture used are inherently reliable, secured against obvious external threats and capable of withstanding some degree of damage.

O'Rourke [8] states that resilient physical and social systems must be 'robust, redundant, resourceful and capable of rapid response', where:

Robustness: The inherent strength or resistance in a system to withstand external functionality

Redundancy: System properties that allow for alternate options, choices, and substitutions under stress

Resourcefulness: The capacity to mobilize needed resources and services in emergencies

Rapidity: The speed with which disruption can be overcome and safety, services, and financial stability restored

2.4. The Requirement – GNSS Interference Detection and Mitigation There is also a need for GNSS interference detection and mitigation that is being explored in the US [9] and UK [10]. In our safety-critical environment this needs to be available on board the ship. There are different ways of detecting interference, however, interference *mitigation* needs to ensure that a user's operation is not disrupted.

The requirement should be to maintain the user's concept of operations with a seamless transition from GNSS to a backup. This is what is really needed for e-Navigation. An inferior approach would provide a backup that does not maintain the user's concept of operations and requires manual intervention.

2.5. A Systemic Backup Users not only need resilient PNT, they also need it to be cost-effective and a systemic backup is the best solution. In this case, *systemic* means that the backup can be used within many user sectors – air, maritime, land, telecommunications, critical infrastructure etc.

Key benefits of a systemic backup include:

- short-term economies of scale – broad, cross-sector demand will ensure that cost of the systemic backup is very low. In practice, this means that chip-level integration with GNSS can be achieved swiftly and the cost to the user is small.

- linking into existing GNSS networks – these include technology research, product development and manufacturing, sales and marketing, user networks for retrofitting and regulation.

- lower long-term average costs – the cost of a systemic backup should always be lower than sector-specific backups and should decrease over time. On this basis, systemic backups should decrease the long-term average costs for many stakeholders.

2.6. The Solution – eLoran. At the highest level, the requirement is for resilient PNT (Section 2.4). GNSS will undoubtedly be one of the sources of PNT. The requirements for a GNSS complement are to:

- enable resilient PNT for use by critical infrastructure applications including maritime transport.
- be readily integrated with GNSS at chip-level.
- support interference detection and mitigation.
- maintain the user's concept of operations with a seamless transition to a complement when GNSS is lost.
- have the potential to be deployed world-wide.
- support maritime general navigation applications.
- be independent of GNSS.
- be dissimilar in terms of failure modes.
- provide similar levels of performance as GNSS

eLoran is the only system that can meet all these requirements in a timely fashion and support the development and implementation of e-Navigation. The GLAs firmly believe this and that is why the GLAs continue to encourage eLoran development, both cross-sector and cross-government within the UK and transnationally.

3. GLA ELORAN TECHNICAL PROJECTS

As a complementary, dissimilar and independent back-up for GNSS, eLoran *can* provide the resilient PNT information required by the future e-Navigation concept. The GLAs and others have shown this during various trials.

The GLAs are engaged in a number of technical projects aimed at developing the knowledge and processes required to establish eLoran services in their service areas. These will be presented briefly next. First of all, however, it is necessary to understand what defines maritime eLoran.

3.1 Defining Maritime eLoran. eLoran receivers are manufactured to assume that the ground-wave signals they receive have propagated over sea-water only. However, the propagation time of ground-wave signals varies with the type of surface over which the signal travels; fastest over sea-water, and more slowly over land. To account for any land along the propagation path, the receiver has built into it tables of propagation corrections called Additional Secondary Factors (ASFs). These tables are arranged in grid format and there would typically be a grid for each transmitter that the receiver is likely to use in a position solution in any particular geographical area – for example a harbour approach. ASFs are required for eLoran in the same way that tropospheric and ionospheric corrections are required in the GNSS receiver for GNSS signal propagation delays.

ASFs have a spatial component, which varies with geographical location (hence a grid of ASFs is published), and a time varying component, due to short-term weather variations and longer-term seasonal effects affecting ground conductivity. The time varying component affects the *repeatable* accuracy performance. Once the ASF grids have been published, and fixed in the mariner's receiver, the time varying component will need to be mitigated through the provision of differential-Loran (dLoran) broadcasts, in the same way that differential-GPS is used to mitigate the time varying effects of the earth's atmosphere on GPS; see Figure 1.

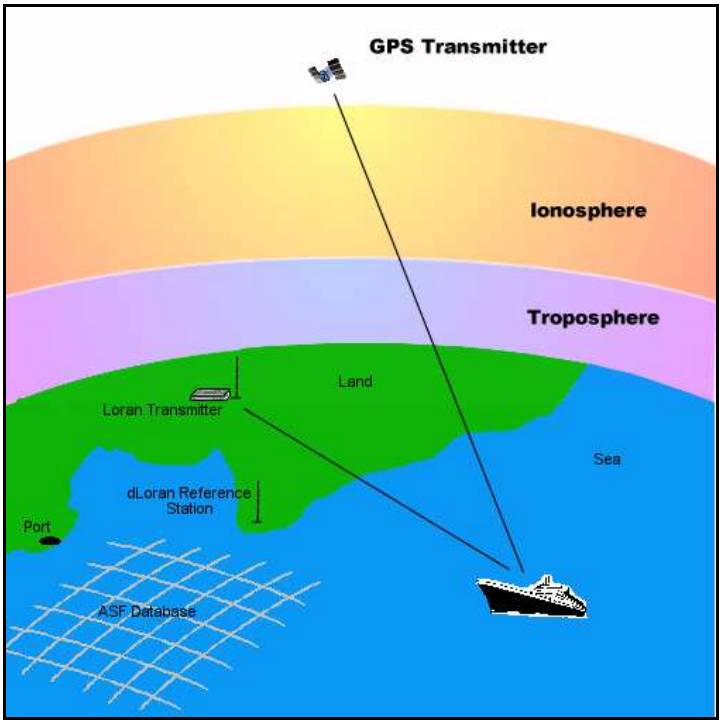

Figure 1 – ASFs and differential-Loran.

The eLoran temporal corrections may be transmitted to the user of the differential service using a data channel built into the Loran signal itself - the Loran Data Channel (LDC). In Europe this is likely to be Eurofix [11] – a data communications system based on the pulse positioning modulation of the last 6 pulses of the 8 pulse group transmitted from the station [11] - but the channel could equally be the US Ninth Pulse system [17].

e-Navigation's data communication system is also a possible future mechanism for the dissemination of pseudorange corrections for both differential-Loran and DGNSS.

In summary then, maritime eLoran requires the following:

- All in view eLoran receivers, which can form a least-squares position solution from Time of Arrival (TOA), or pseudorange, measurements made from individual eLoran transmitters, rather than hyperbolic Time Difference measurements

- Databases of ASF grid data stored within the receivers

- Differential-Loran corrections to account for changes in ASF values, transmitter timing and atmospheric effects over time – broadcast over LDC or the communications segment of e-Navigation

The GLAs' technical eLoran projects are aimed at understanding these components and more, with the aim of rolling out initial eLoran application services by mid- 2013. We will now briefly outline some of the major GLA eLoran projects.

3.2 ASF Measurement and Processing Best Practice

It is possible that the GLAs will become responsible for measuring and publishing ASFs for their service areas. In order to gain experience in ASF measurement, and develop the technical expertise required, the GLAs have procured three ASF measurement systems. Each unit contains an eLoran receiver, a GPS receiver, a precise clock, a PC, glue logic and processing hardware to make the precise measurements required to compute ASFs.

The project is investigating best practice in performing ASF measurement and post-processing, so that we can ensure the integrity and quality of the ASF data produced. Once the raw ASF data has been measured, it will need to be processed to minimise measurement noise. Processing may be divided into the spatial and temporal domains.

- **Temporal Domain** – There will be apparent variations of the ASFs over time during the performance of the spatial ASF surveying. These variations are due to transmitter timing variations, passing weather fronts, and changes in ground-wave propagation conditions. These temporal variations will need to be processed out of the raw spatial ASF data before grid processing can be performed. Temporal processing can be performed in post-processing or in real-time during ASF surveys using data from a differential-Loran Reference Station established near to the survey location.
- **Spatial Domain** – Spatial processing performed on the geographically distributed ASF data, measured during a mobile survey. The goal of spatial domain processing is to produce an ASF grid for eventual publication within a mariner's receiver. The spatial ASF measurements are made once-and-for-all at a particular date and time. In addition, the form that the ASF grid takes will affect the accuracy performance of the ASF data.

The GLAs are investigating the use of 2D surface interpolation of the ASF data. This allows the smooth transition from one grid point to the next as a vessel travels through the area.

It is not sufficient to simply publish ASF data, we also need to understand to what accuracy the ASFs are produced so that we can ensure integrity. It is therefore necessary to understand the contribution to the overall *ASF error budget* of each of the processes and techniques that we use. This will result in the generation of one or more error bounds on the ASF grid, which may be fed into a receiver's integrity monitoring algorithm. Figure 2 shows an interpolated ASF grid produced from raw ASF data collected during our Orkney Island trial (briefly discussed later). Figure 3 shows a plot of the standard error of the data of Figure 2. Figure 4 shows a screenshot of the ASF survey and validation software developed by the GLAs.

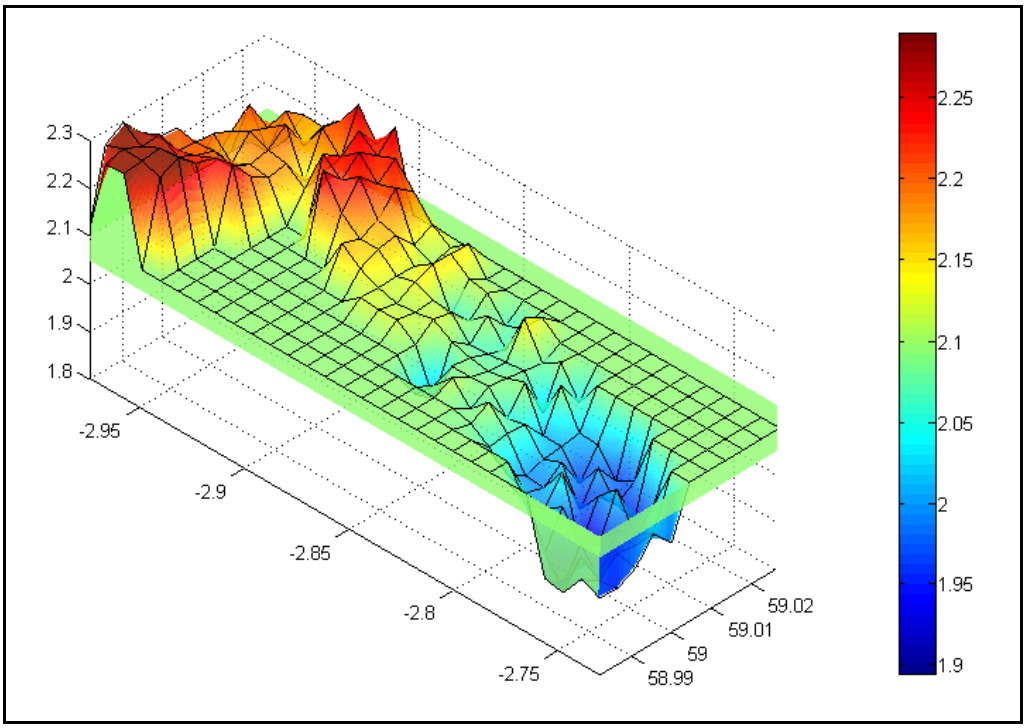

Figure 2 - Interpolated grid of Anthorn ASFs (vertical scale in microseconds) measured in a part of the Orkney Islands.

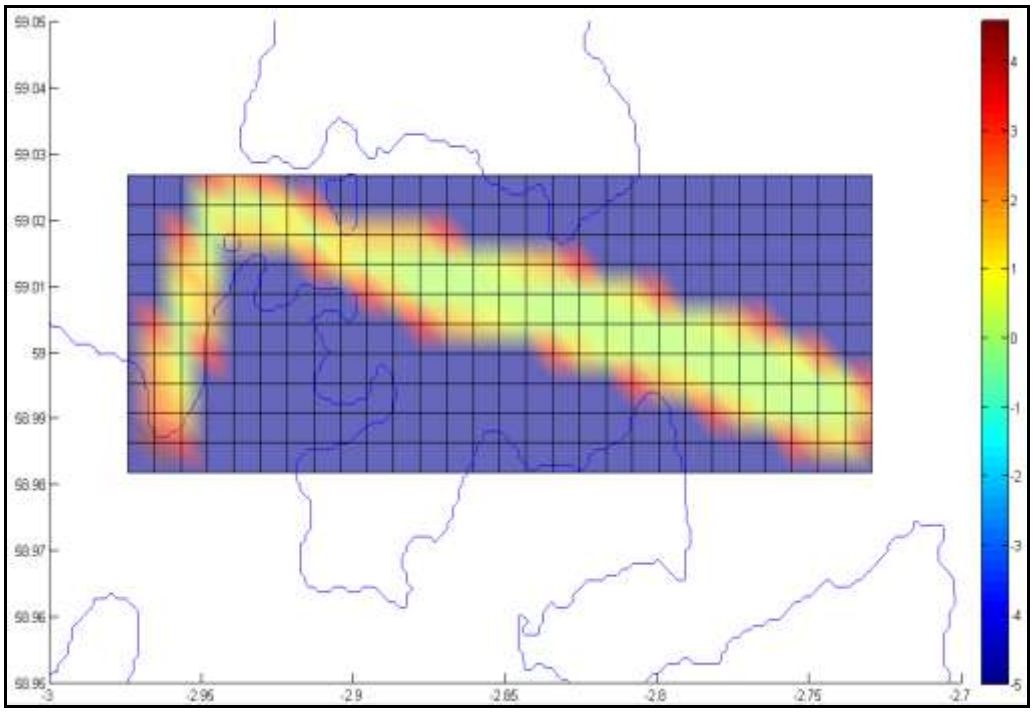

Figure 3 - Plot of the interpolated standard error of the ASF grid.

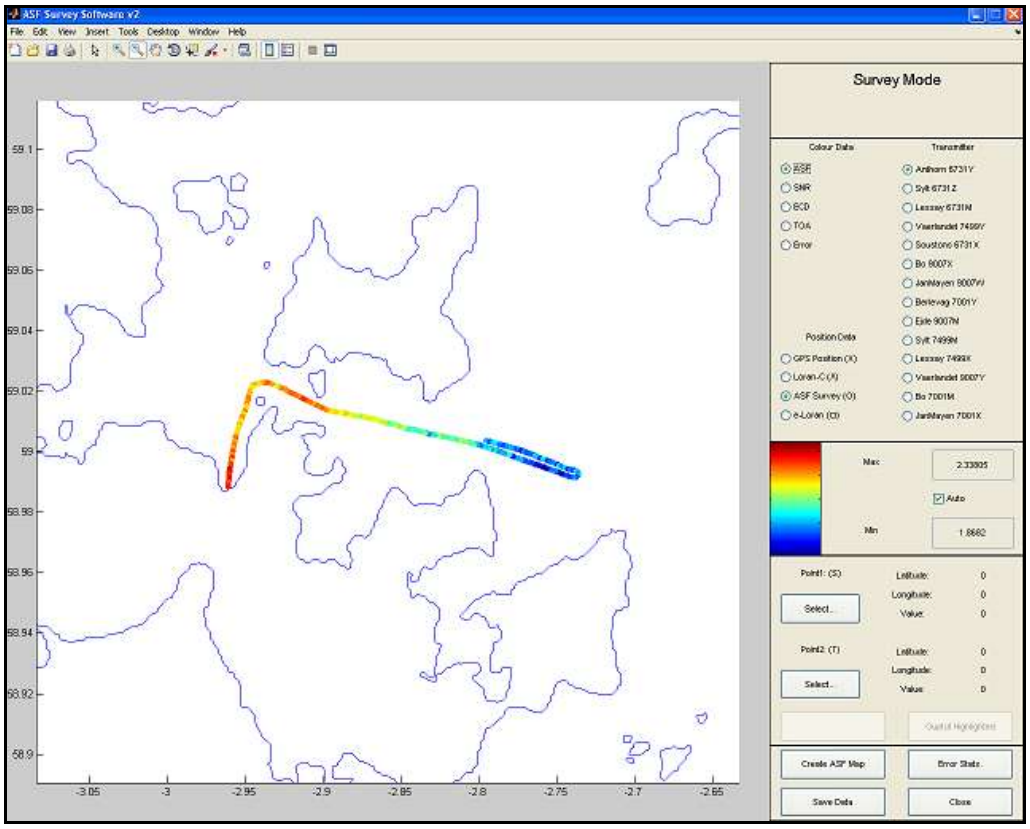

Figure 4 - Screen shot of the GLAs' ASF surveying software.

3.3 Real Time dLoran Service. The GLAs plan to produce a fully operational differential-Loran service (outlined in Section 3.1). Our main aim in this project is to understand how many Reference Stations are required to cover the GLAs' service areas. The answer to this question needs an analysis of such things as:

- The optimum update interval of the differential corrections to be broadcast. This depends on the radio frequency noise seen at the Reference Station site and the frequency of the variations typically seen in propagation measurements. It is very important to locate the receiving antenna of the differential Reference Station in an area of good Signal to Noise Ratio (SNR) and optimise the filtering of the differential measurements before they are broadcast.

- The degree of spatial decorrelation of the corrections from a Reference Station. The description of differential-Loran presented in Section 3.1 is an idealised situation. In reality there will be a degree of *spatial decorrelation* between the pseudorange variations seen at the reference station location and the variations seen by the mariner. This is because the signals received at the Reference Station travel over different land paths compared to the signals received at a user's vessel. Spatial decorrelation creates a geographical range limitation on the validity of the pseudorange corrections generated by the Reference Station. The error residual due to these spatial decorrelation effects will also need to be accounted for and a bound for them may need to be built into the overall ASF error budget.

Figure 5 illustrates a plot of a set of ASFs measured at the Harwich dLoran reference station and a set measured a few hundred metres away. It is possible to measure the decorrelation between the two sets and compute the dilution of precision due to the

phenomenon. The effect is very much dependent on the configuration of land and sea paths from the transmitters to the reference station, and no two reference station installations will present the same level of spatial decorrelation.

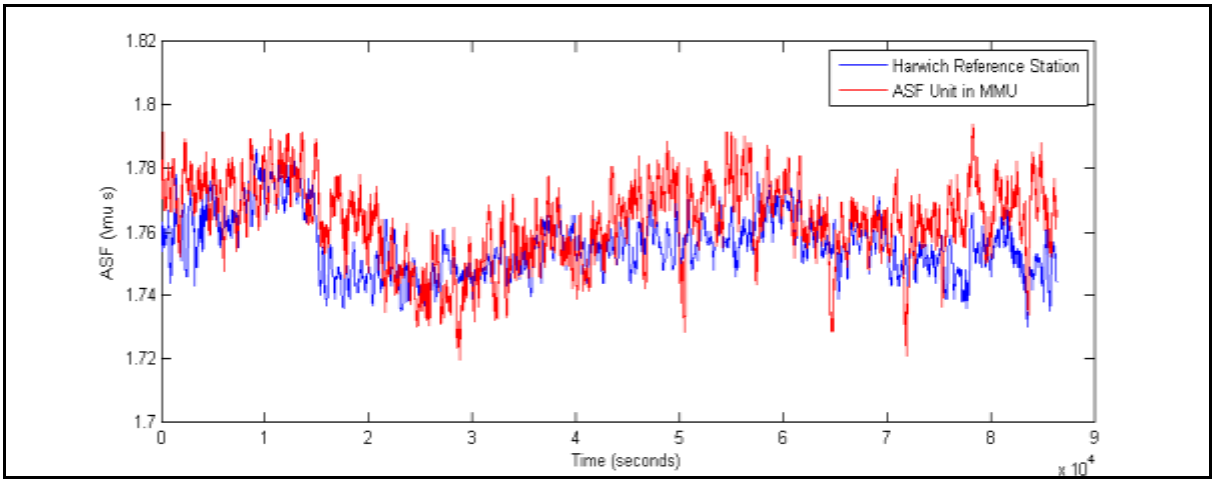

Figure 5 - Correlation of ASF measurements between two separate but close locations.

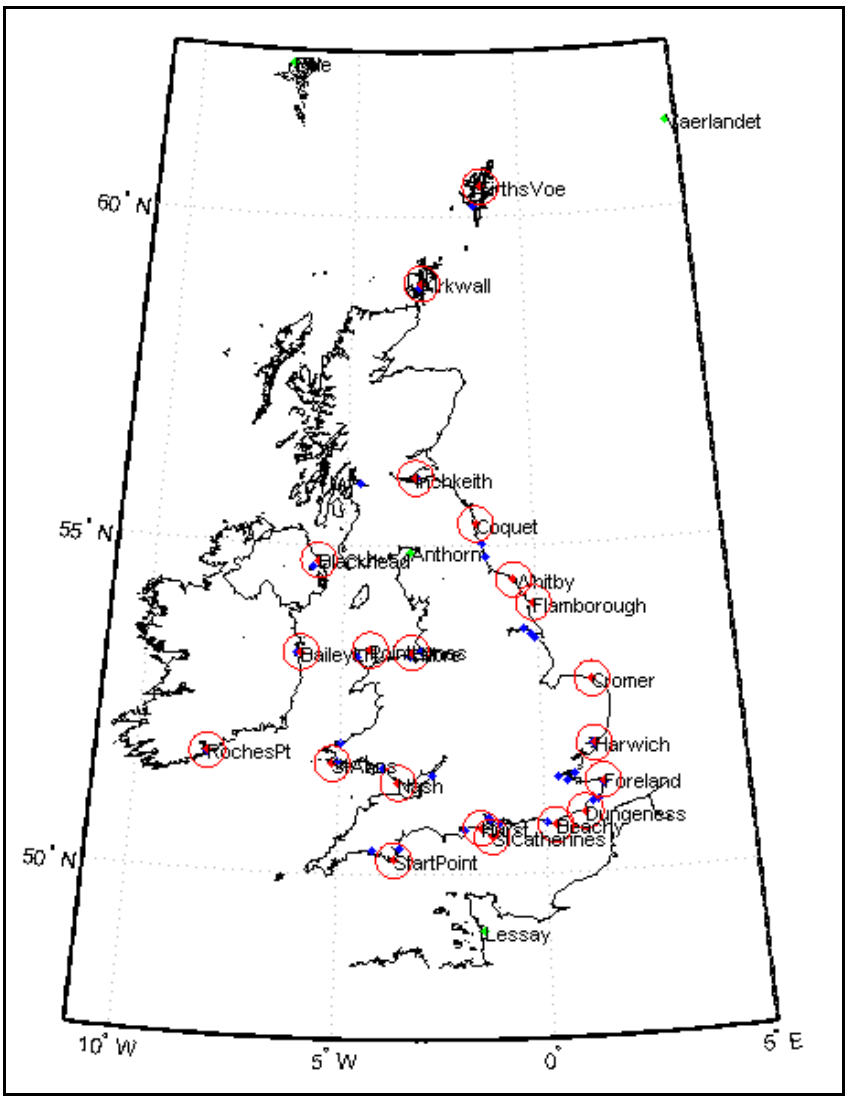

Figure 6- Possible locations of GLA dLoran reference stations at GLA AtoN.

The GLAs plan to undertake extensive measurement campaigns with monitors placed at a number of locations across the UK. This will enable us to gather evidence of long term seasonal variations and the degree of correlation at each end of the baselines defined by the locations of the monitor sites in a similar manner to that performed in the US [12].

The aim is to model the effect and build it into a coverage prediction model. Our eLoran coverage prediction capability (presented next) is being developed to include the effects of choosing the locations of differential-Loran reference stations. Figure 6 illustrates a possible future configuration of GLA differential-Loran reference stations. In this diagram, the red points represent differential-Loran reference stations located for convenience at GLA AtoNs – lighthouses and DGPS radio beacon sites. The red circles show an assumed 30km range of a reference station [12]. The blue diamonds represent an initial estimate of the ports and harbours able to support SOLAS class vessels and which will be required to be covered by differential-Loran. The diagram shows us constraining the reference station locations to GLA infrastructure. It can be seen, however, that in some circumstances this constraint may prohibit the coverage of some ports and either alternative locations would have to be sort or we would have to investigate whether a particular reference station's corrections can be safely used beyond the initial 30km range limitation. Should either of these two solutions prove difficult the GLAs have plans to investigate networked differential-Loran solutions – interpolating differential corrections between reference stations to form virtual differential stations.

3.3 Service Volume Coverage Prediction

The bulk of the technical work on our Service Volume Coverage Prediction project is being performed by a PhD student sponsored by the GLAs. The purpose of the study is to develop a software tool for use by the GLAs to investigate the structure and performance of possible future European eLoran transmitter networks. The work would support optimising infrastructure placement, developing a new operational concept as well as testing and providing feedback on new eLoran standards for equipment and signals.

From a scientific perspective, eLoran service coverage will be assessed in terms of meeting user requirements (accuracy, integrity, continuity and availability) throughout a geographic area of interest.

A sensitivity analysis is being undertaken to determine the level to which different service parameters need to be modelled, including:

- network topology – transmitter locations, mast heights, amplifier power, differential Loran reference stations and integrity monitors;
- signal design – shape and stability, group repetition intervals and data channel performance (bandwidth and bit error rate) ;
- signal propagation – atmospheric (primary factor) and ground conductivity (secondary and additional secondary factors), atmospheric activity (troposphere and ionosphere); and
- user equipment – antenna performance as well as all-in-view data processing techniques including station selection strategies and digital filtering.

The work is beginning to produce some very useful results. The plots of Figure 7, Figure 8 and Figure 9 show accuracy, availability and continuity plots respectively for eLoran over the British Isles.

Figure 7 shows the repeatable accuracy available over the service area. This plot assumes that differential-Loran, and ASFs are available over the entire service area. In reality this will not be the case, and the final version of the software will include the effects of limiting differential-Loran to various locations for the harbour entrance and approach application, for example.

Figure 8 shows the *system availability* of the Loran over the British Isles as it exists today. The plot takes into account the signal availabilities from each Loran transmitter contributing to the fix at each coverage grid location. This data has been derived from two years' worth of transmitter availability statistics obtained from the Loran Control Centre Brest (CCB), the operational centre for northwest European Loran based in France. The signal availabilities are then combined into a system availability statistic. It is important to realise that the performance figures here are meant as an illustration of coverage modelling capability and are not meant to represent true ***eLoran*** capabilities. The signal availability figures used in computing the system availability plots were obtained from measured statistical data for today's *modernised Loran-C*, which is still currently run using the old NELS standard operating procedures. We still have a way to go before eLoran becomes fully implemented in Europe, at which point we expect availability performance to be much improved.

This is the first time that the ability to predict Loran system *availability* has been possible in the UK and Europe! This is also true of the continuity plot shown in Figure 9.

All three of these plots illustrate the poor coverage to the west of the British Isles and indicate a requirement for an additional transmitter somewhere in the west of Ireland.

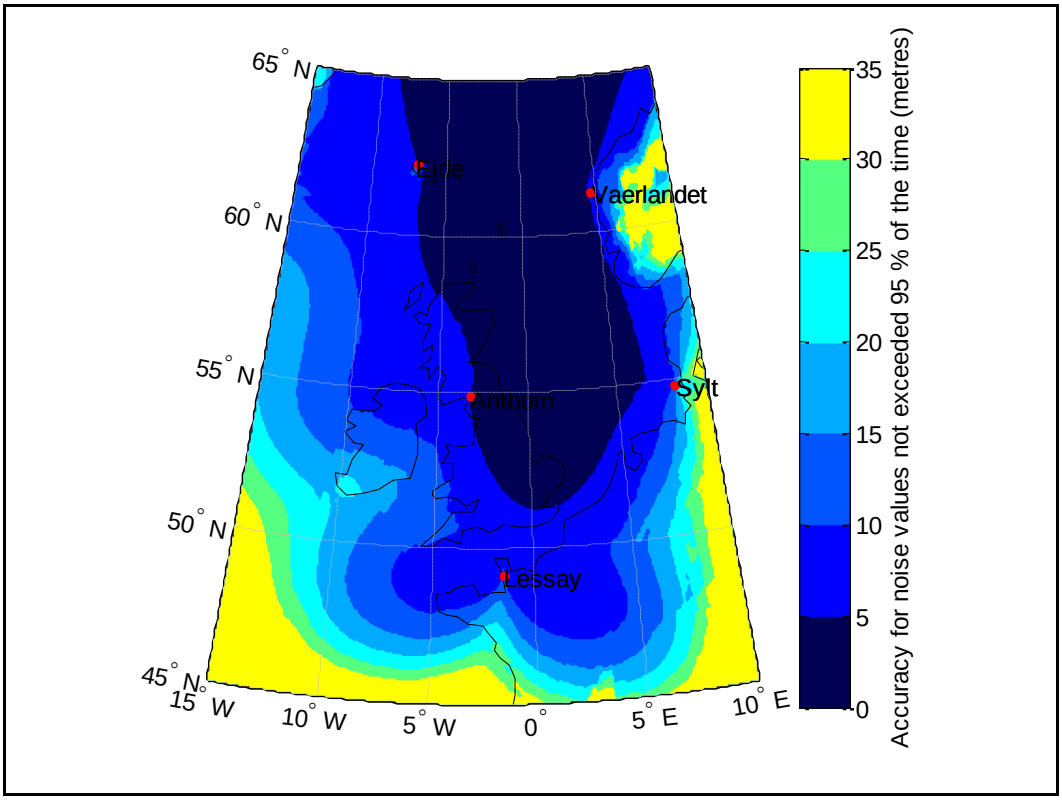

Figure 7 – Modelled accuracy contour plots.

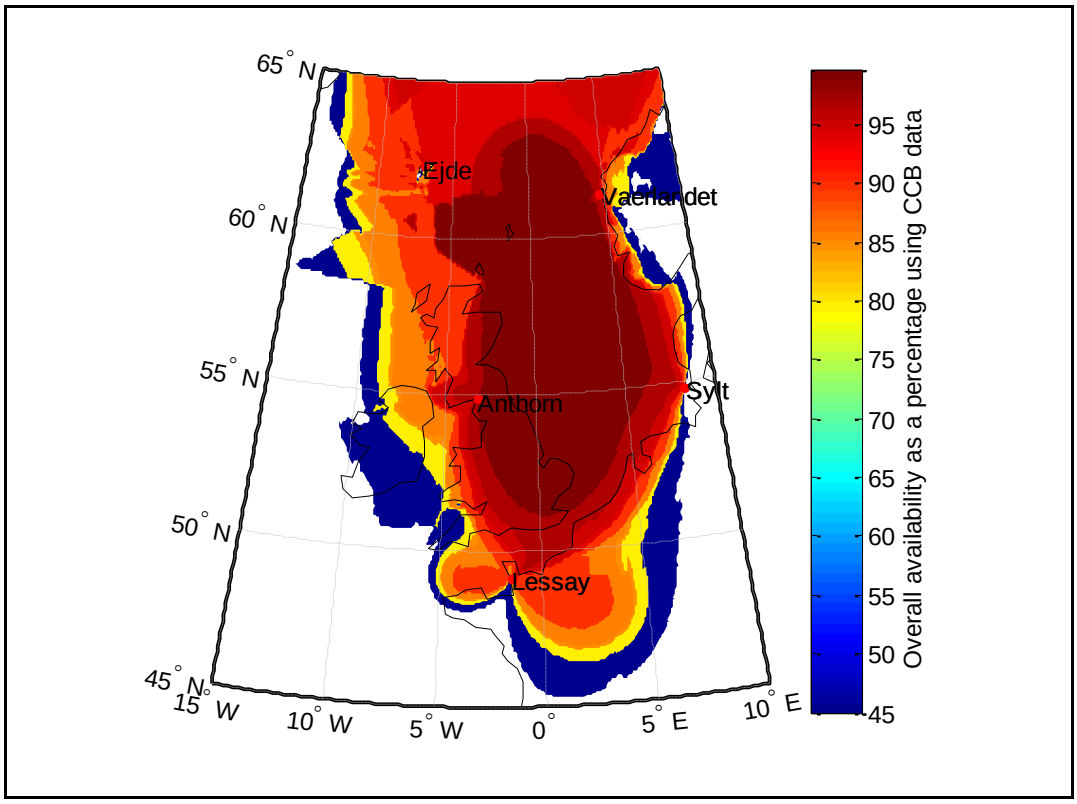

Figure 8 – System availability.

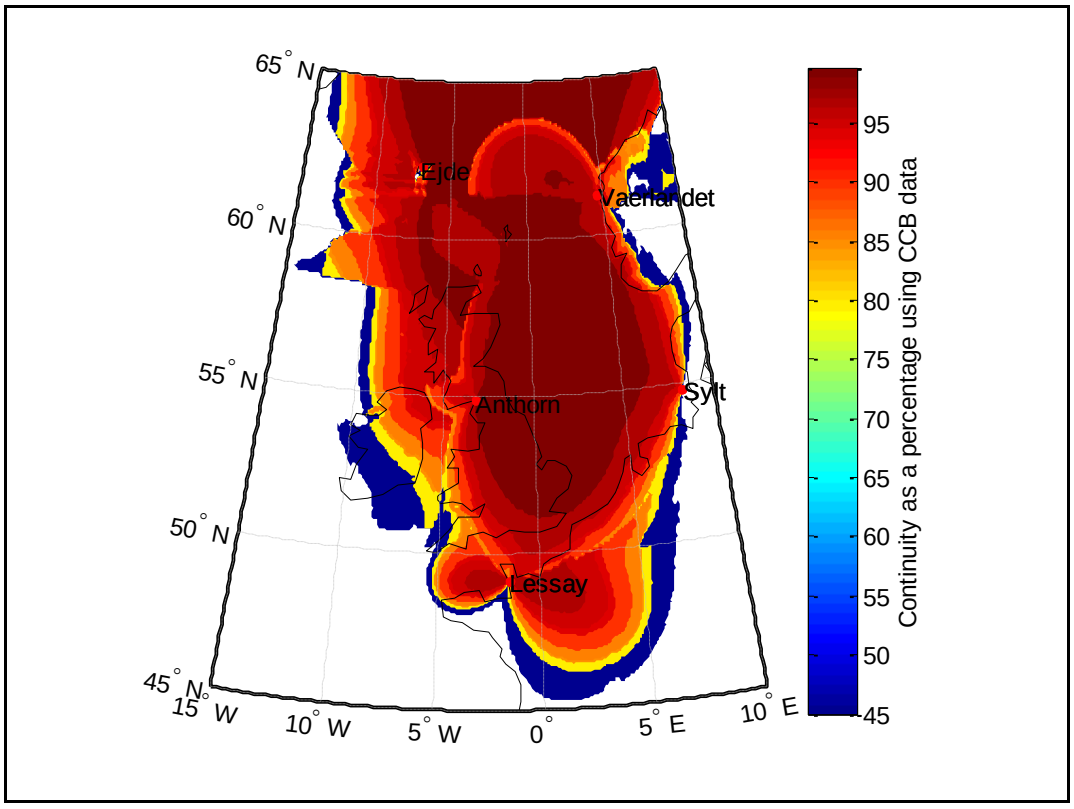

Figure 9 – Modelling of the continuity of the eLoran service.

3.4 GRI Selection and Crossrate analysis

The GLAs sponsor a second PhD student, *Jan Šafář* from the Czech technical University, who is focussing on some fundamental system design questions that arise when considering the introduction of new eLoran transmitter stations. The two main goals of the project are:

- to update existing Loran-C procedures for Group Repetition Interval (GRI) selection to reflect new eLoran standards

- to provide models of the effects of Cross-Rate Interference (CRI) between eLoran stations on the system's performance

Cross-Rate Interference is due to the 'collision' of pulses from different transmitters, on different Loran rates, arriving simultaneously at a receiver. This is the worst type of interference to Loran. However, it is a predictable characteristic and modern receivers can mitigate the effect to a greater or lesser extent. Figure 10 shows the loss of pulses of GRI 6731 using one type of receiver based mitigation called Cross-Rate blanking. In this form of mitigation, pulses from GRI 6731 that are interfered with by pulses from Loran signals from all other chains, including those via skywave, are removed – blanked by the receiver and therefore are not integrated and used in the position computation. The resulting loss of 'wanted' GRI 6731 pulses reduces the signal-to-noise ratio of the tracked signal. This has the potential to increase the variance of the Time Of Arrival (TOA) measurements made by the receiver, which in turn will result in poorer positioning accuracy. However, this loss of performance is small when compared to the consequences of not mitigating the effect.

Figure 11 and Figure 12 show that cross rate introduces a bias and a variance in pseudorange measurements. Figure 11 shows a plot illustrating the effect of each of the full possible range of GRIs (along the x-axis) cross rating with GRI 6731. The effect can be seen to produce a pseudorange (TOA) *bias* of between 3m and 6m as the cross rating GRI decreases in value from the right to the left. GRIs create interference to each other to a greater or lesser extent depending on their mathematical relationship to each other. For example some GRIs combine with 6731 quite catastrophically, while others that are quite numerically close are fine. This is reflected in the 'comb' structure of plot. Figure 12 shows the effect on the *variance* of the pseudorange measurements. In both of these pictures the red circles represent simulation results produced by Šafář using signals generated using a numerical Loran simulator written in Matlab™ with the resulting digital 'signals' fed into a software receiver, also written by Šafář. In a separate study Šafář also investigated a theoretical, frequency domain, analytical approach to solving the same problem so that the effects could be built into our coverage software. The results of this are shown as the blue dots in the figures. The results of the two separate approaches are astonishingly close! The techniques can also include the effects of cross rate mitigation methods.

The analysis techniques developed during this work will be built into the coverage modelling software described in Section 3.3 and will be required if and when it becomes necessary to install additional eLoran transmitters, and optimise the selection of their GRIs; either full power transmitters to extend coverage, or lower power mini or micro Loran stations as coverage gap fillers.

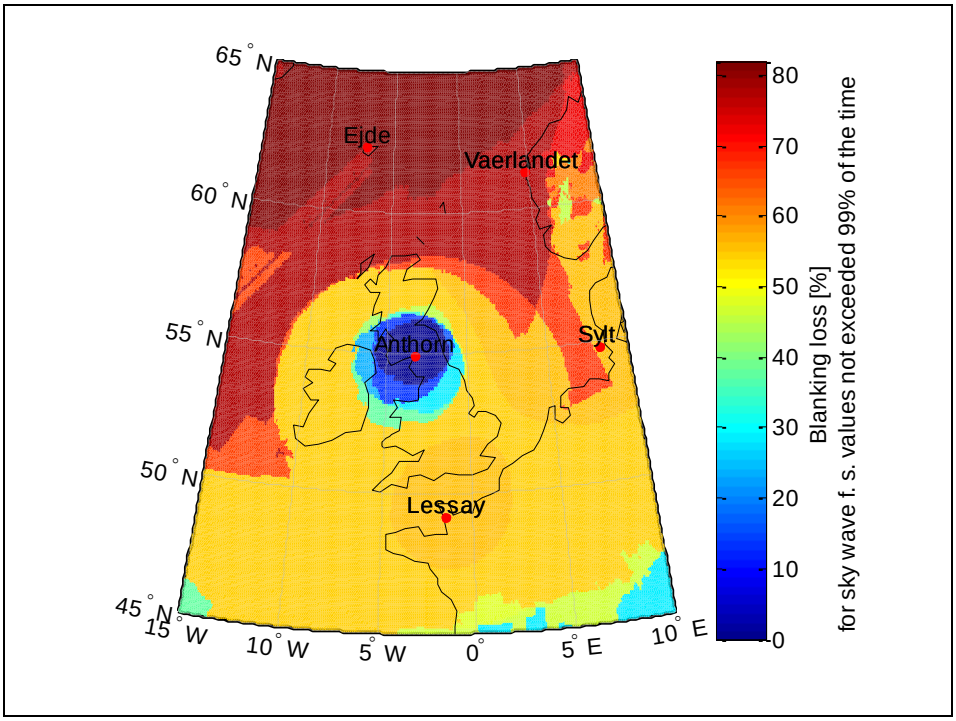

Figure 10 – Blanking loss due to eLoran cross rate interference for the signal of the 6731Y Anthorn station.

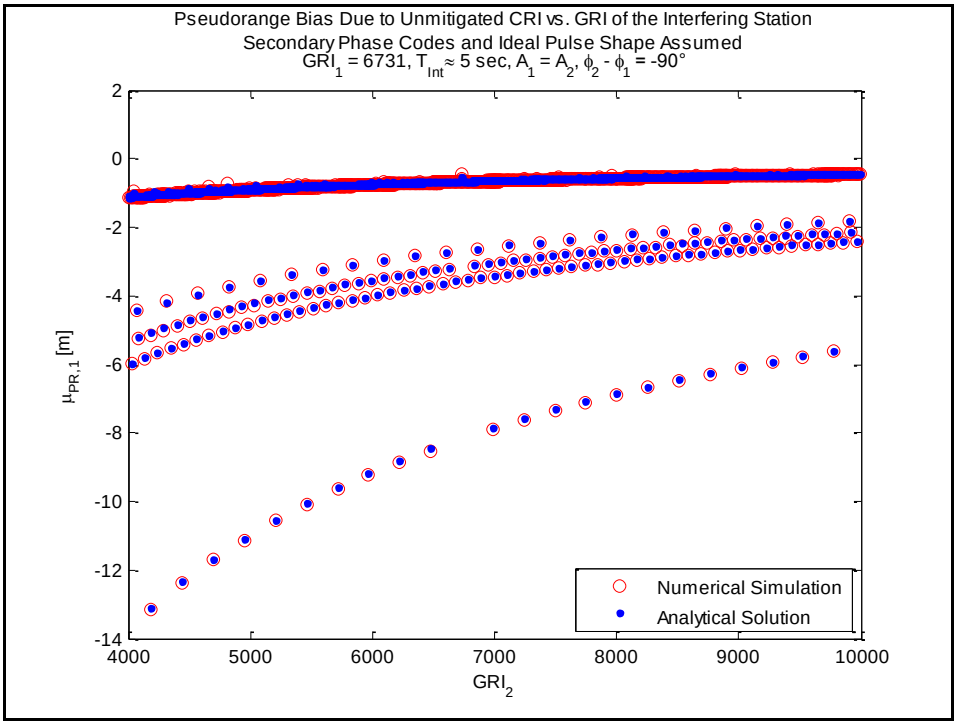

Figure 11 – Modelling the effect on pseudorange bias of a cross rating Loran signal.

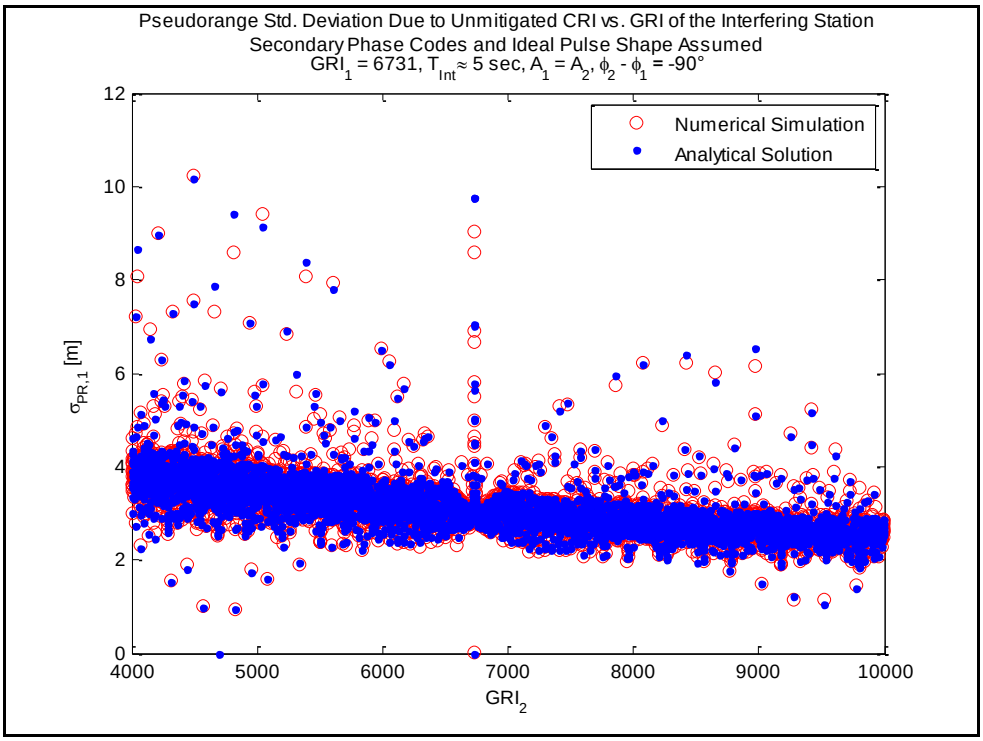

Figure 12 – Modelling the effect on pseudorange standard deviation of a cross rating Loran signal.

3.5 GAARDIAN and SENTINEL

Once we have rolled out our Core and Application Services, we would need to be able to monitor their availability and integrity, collecting long term performance data and generating integrity alerts as required. Hence we are interested in developing and monitoring the type of technology that would allow us to do this.

GAARDIAN is to be a network of data gathering and monitoring probes, to be located at the point of service for GNSS and eLoran timing, frequency and navigation users. It is the aim that the probes will provide detailed information on the availability and integrity of GNSS and eLoran signals to service providers through a web-enabled server interface. Users can access past and current data, and can be provided with alerts in real-time if and when service disruption occurs. In addition, the probes will be able to gather long-term data, which can be made available through the server for particular users.

The GAARDIAN project began as an initiative by the Technology Strategy Board (TSB), part of what is now called the Department for Business, Innovation and Skills (BIS) (previously DIUS). The Technology Strategy Board provides research funding to encourage the development of technology in areas that are considered vital to the future of the UK economy. The GLAs, as part of a consortium of seven organisations, led by Chronos Technologies Limited (CTL) submitted GAARDIAN as a proposal to the Technology Strategy Board to address the technology area ‘Data Gathering in Complex Environments’. The Technology Strategy Board awarded £2.2M funding to the project, and the project is almost complete, with the development of 15 prototype probes.

Under the work of the project the GLAs have been developing algorithms to detect potentially hazardous eLoran conditions and generate alarms as and when they occur, and collect summary performance data from these probes. We see the technology as a

potential prototype platform from which to develop a fully fledged integrity monitoring network.

SENTINEL is a proposed follow-on project to GAARDIAN that will research and develop a service to establish the extent to which Global Navigation Satellite Systems (GPS, GALILEO etc.) and eLoran Positioning, Navigation and Timing (PNT) signals can be trusted by users on a 24×7 basis. The SENTINEL service will be used to detect, quantify and locate accidental and deliberate GNSS interference (e.g. criminal jammers), natural PNT interference phenomena (e.g. weather, solar flares), at point of use, to enable decisions to be made on the degree to which a PNT service for safety/mission critical services with security or revenue generating impact can be trusted. This will provide alerts and be able to quantify and assess deliberate jamming to enable detection or mitigation by the appropriate agencies.

SENTINEL will build on the basic research being undertaken in the TSB funded GAARDIAN project and will be administratively lead by Chronos. The project will seek to deploy clusters of modified “GAARDIAN” probes up to a total of approximately 50 units deployed according to a strategy lead by ACPO ITS (Association of Chief Police Officers - Intelligent Transport Systems working group). The probes will be based on those being developed for the GAARDIAN project with an additional feature of RF signal detection. The team also includes members of the communications systems industry and academia. ACPO will bring interests from the wider governmental community to the project. The GLAs will further their eLoran algorithm development within the project and provide support for maritime trials of the system.

3.6 Standardisation

eLoran standardisation efforts began with a definition agreed by the International Loran Association [13] and in October 2007 the Radio Technical Commission for Maritime Services Special Committee-127 (RTCM-SC127) on eLoran systems was established. This Committee was set up to consider the need for the development of standards for eLoran position, navigation and timing (PNT) system components, including, but not limited to maritime eLoran receivers, and/or combined GNSS/eLoran receivers. Appropriate RTCM standards or reports are to be developed, addressing performance requirements, technical requirements, and/or test procedures, with a view to their use for the production of eLoran systems, and as the basis for eventual IMO, ITU and/or IEC recommendations or standards, as appropriate. The GLAs have recently taken over the chairmanship of the committee and are keen to encourage and progress standards development. The release of a draft RTCM eLoran Receiver Minimum Performance Standard (MPS) is imminent (November 2010).

3.7 eLoran Shipborne Monitoring

The aim of this project was to install automatic eLoran Monitoring Systems (LMS) aboard all six of the GLAs’ vessels; THV Patricia, THV Galatea, NLV Pole Star, NLV Pharos, THV Alert and ILV Granuaille.

Figure 13 – Reelektronika's Loran Monitoring System, front and rear panels.

Figure 13 shows the front and rear panels of the Loran Monitor System (LMS), six of which were procured from the Dutch Loran receiver manufacturer Reelektronika. The unit is a 3U 19 inch rack mountable unit containing a Reelektronika LORADD eLoran receiver, a u-Blox™ GPS receiver and a PC motherboard. Logging software running on the PC platform allows the automatic collection of data such as signal-to-noise ratio, pseudorange variations and positioning data, including standalone Loran, GPS-calibrated Loran, ASF corrected Loran with differential-Loran corrections, and GPS data.

The units are currently in operation aboard GLA vessels, working continuously to gather data automatically as the vessels perform their normal day-to-day business. In a future project R&RNAV engineers will gather the collected data, analyse it and write software to present the results in a convenient graphical form.

Figure 14 shows an example position plot of Anthorn signal-to-noise (SNR) data collected aboard THV Patricia during the month of September 2010. The data requires further post-processing in order to separate out day and night effects. In general an eLoran receiver should be capable of locking onto and tracking an eLoran signal down to an SNR of -10dB. The plot shows that this should be achievable from Anthorn off the east and southeast coast of the UK.

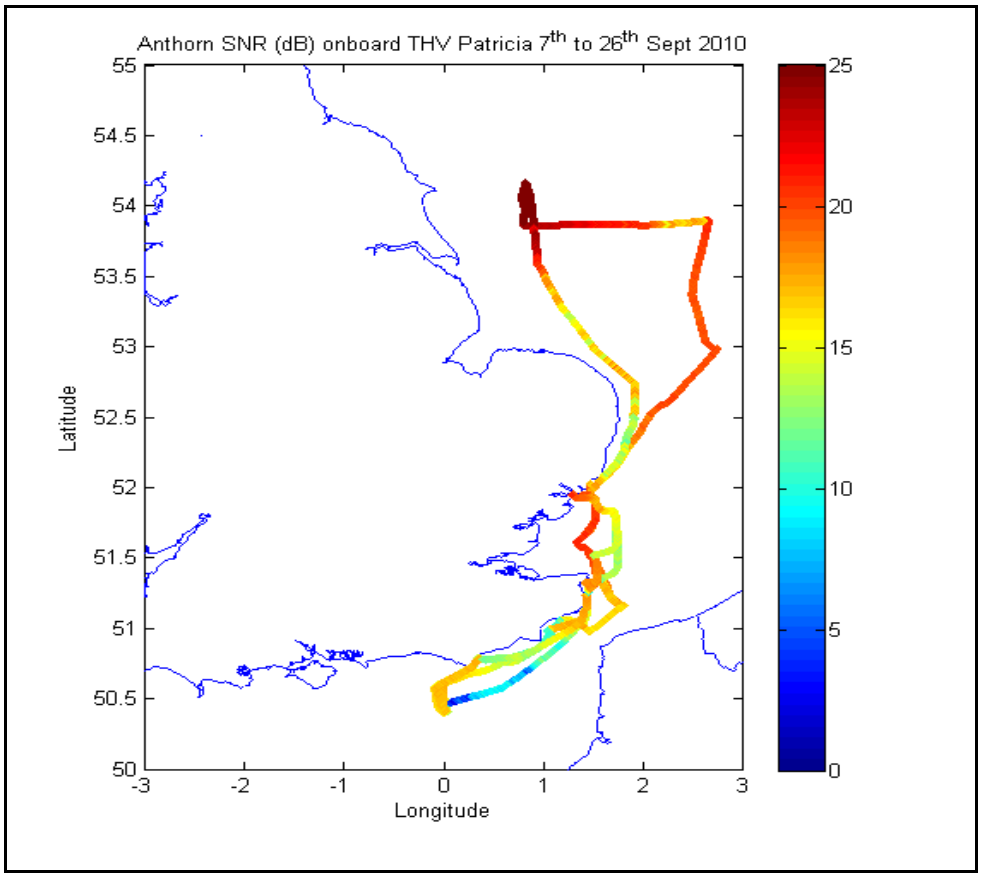

Figure 14 – Example eLoran signal-to-noise ratio data for Anthorn collected by THV Patricia during the month of September 2010.

4. SOME TRIAL RESULTS

4.1 Anthorn

Since 2007 the GLAs have run a Loran transmitter at Anthorn, in Cumbria. The station's day-to-day operation and maintenance is contracted out to Babcock. The transmitter is containerised and is run unmanned but monitored by staff at the Anthorn site, which is shared by other Babcock radio services. The station radiates 220kW and broadcasts as the 'Y' secondary of the 6731 chain (Figure 15).

Table 1 shows the monthly availability figures for Anthorn for the year up to September. These figures are the availability of the Loran signal from the transmitter and do not include authorised maintenance periods as agreed in the operating procedures of the Northwest European Loran System (NELS), the original organisation setup to run Loran-C in northwest Europen in the mid-1990s and which ran until the end of 2005. The outage of 1200 seconds in February was a single block of time and was traced to a problem with the X.25 data communications system in France. The figures correspond to an availability of 99.99% over the nine month period to September.

Figure 15 – European Loran transmitters. 'NELS' stations and Anthorn in green, Russian Chayka stations in red.

Month (2010)	Total Seconds	Monthly Outage (Seconds)	Seconds in month	Monthly Availability (%)
January	2678400	0	2678400	100
February	2419200	1200	2418000	99.95
March	2678400	0	2678400	100
April	2592000	0	2592000	100
May	2678400	0	2678400	100
June	2592000	0	2592000	100
July	2678400	0	2678400	100
August	2678400	0	2678400	100
September	2592000	0	2592000	100

Table 1 – Anthorn availability figures for the first 9 months of 2010.

4.2 Differential-Loran Reference Station

In addition to Core Service provision through the provision of an eLoran transmitter, the GLAs also plan to develop a differential-Loran Application Service, as outlined in Section 3.3. A prototype differential-Loran reference station has been running in Harwich since 2007, and we have been using the system to inform our various development projects. The Harwich dLoran reference station sends Loran pseudorange corrections up to Anthorn via a Virtual Private Network (VPN) over the Internet. The data is subsequently broadcast over the Eurofix Loran Data Channel (LDC).

In computing the value of the eLoran pseudorange correction to broadcast, the reference station integrates, or averages, a number of corrections over a particular time period. The operator of the reference station can choose the length of this integration period. The reference station generates corrections, broadcasts them and then receives them back over the LDC so that post-broadcast integrity checking can be performed. In this way, the resulting positioning accuracy of differential-Loran can then be measured at the reference station.

Figure 16 shows the results of some of the analysis work that we have performed on archived data collected by the Harwich dLoran reference station. The figure shows the variation of the 95%'ile differential-Loran positioning accuracy, with differential-correction averaging (integration) interval and correction update transmit interval. This was produced from corrections determined at the Harwich reference station, collected from January 2009 to the middle of October this year.

The plot of Figure 16 shows that in general as the integration interval increases, for a fixed update interval, the static positioning accuracy at the Harwich reference station improves. For a fixed integration interval, as the update interval increases, so the positioning accuracy worsens. Our aim is to achieve an optimally performing service based on investigating the effects of varying the integration interval. We need to do further work on this because the picture seems to imply that if you keep integrating corrections that you get better and better performance for a given update interval, but this is not necessarily true because of the effects of lag between the timeliness of the corrections and the time constant of propagation phenomena that cause the static pseudorange measurements to vary. The effect of employing a fixed integration interval is shown in Figure 17, which show approximately a year's worth of daily average positioning accuracy data collected at the Harwich reference station. With a fixed integration interval there appears to be an increase in positioning error in the winter because with this integration interval the broadcast pseudorange corrections are lagging the TOA variations due to the rapid propagation variations which are causing them. In the summer months the propagation variations are lower and the fixed interval results in lower lag. In order to obtain consistent corrections, and therefore a flat red line in Figure 17, the best approach may be to investigate the possibility of using a dynamic integration interval based on the variations of the pseudorange corrections measured over a particular period.

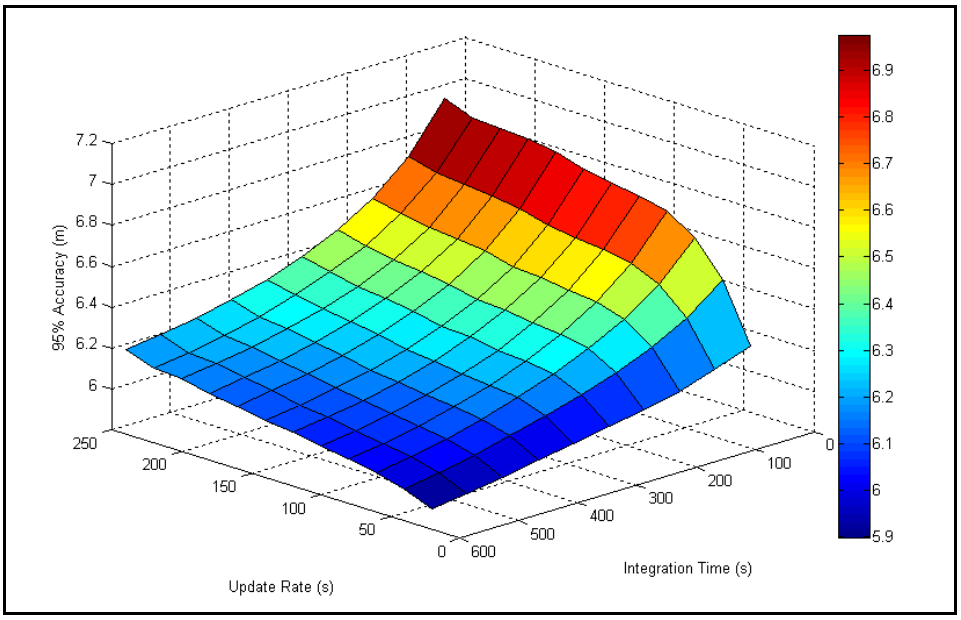

Figure 16 – Change in 95%'ile positioning error measured at Harwich reference station with time due to changing differential correction integration time and correction update rate.

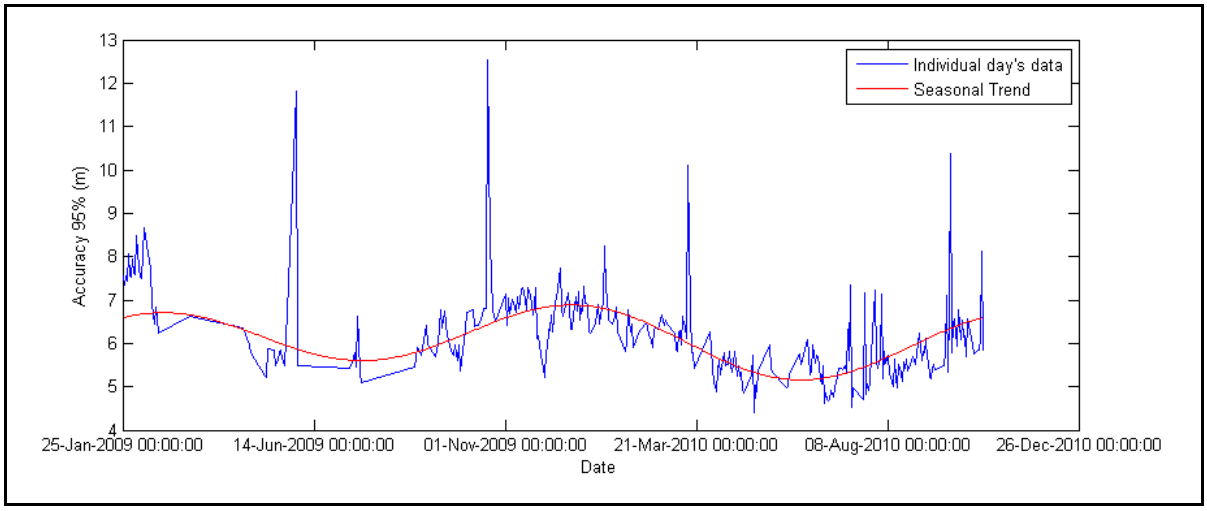

Figure 17 – Approximately 1 year's worth of daily averaged positioning accuracy data at the Harwich reference station. A fixed integration interval may not be appropriate for the entire year.

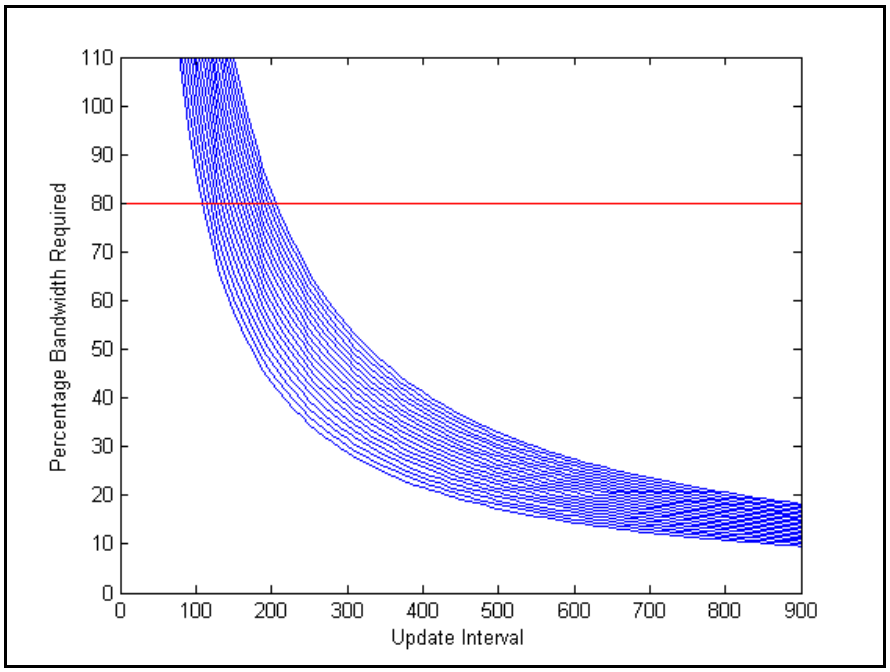

Figure 18 - Percentage bandwidth usage for a single transmitter (Anthorn on 6731) versus dLoran correction broadcast update interval (seconds). Number of Reference Stations: 21 to 40; number of eLoran transmitter pseudorange corrections per reference station: 4. Differential-Loran messages only.

Figure 19 – The GLAs' Mobile Measurement Unit (MMU).

In addition we will need to further investigate the broadcast update interval and its compatibility with the integration interval and other filtering methods used to generate the correction data. The required update intervals from our reference stations will also have a bearing on the amount of data bandwidth available from the LDC, as shown in Figure 18.

The ASF units we described in Section 3.2 can also be run as differential-Loran reference stations, thus providing portable units for our trials. Figure 19 shows our Mobile Monitoring Unit (MMU) fitted out with a portable reference station and a satellite broadband unit for sending corrections up to Anthorn for broadcast. This unit has been used very effectively during our recent GPS jamming trials and during some eLoran performance trials we performed in the Orkney Islands, which are discussed next.

4.3 Orkney Island Trials

Researchers worldwide have already shown that eLoran can meet the accuracy, availability, integrity, and continuity performance requirements for aviation non-precision instrument approaches and maritime harbour entrance and approach [15].

The GLAs have been developing initial proof-of-concept systems, and testing them in challenging environments. To demonstrate performance in an archipelago, the GLAs performed eLoran trials in the Orkney Islands, off the northern coast of Scotland [16]. This is an area of excellent eLoran geometry and signal strength from the transmitters at Ejde, Vaerlandet and Anthorn. Three routes were followed on three separate days. The total distance travelled was some 230 nautical miles with a total steaming time of about 23 hours at 10kts, the biggest trial performed to date.

Figure 20 - Pre-operational eLoran system tested in the challenging environment of Orkney, an archipelago off the northern coast of Scotland.

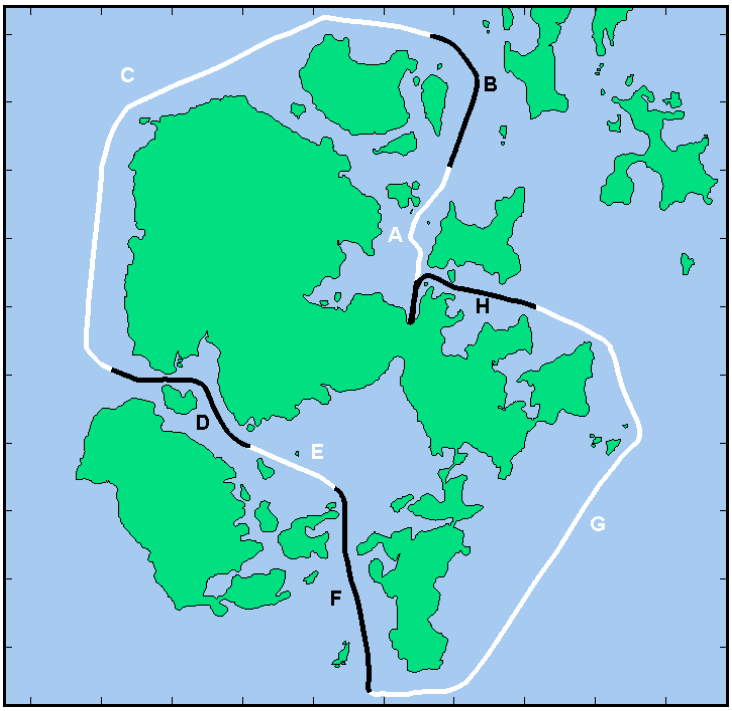

Figure 21 - Hoy Sound – segment D; a channel with complex land-sea signal paths. Accuracies of 11m (95%) achieved using eLoran.

To establish an eLoran system in the area for the duration of the trials, two things were required: a differential-Loran reference station and a map of ASFs stored within the receiver. A temporary differential-Loran Reference Station was installed at Kirkwall – the capital city of the Orkney Islands (Figure 20). ASFs were measured from the data collected during the performance of the routes. The most technically difficult part of the voyage occurred in the Hoy Sound (Segment D in Figure 21); a channel with complex land-sea signal paths. However, accuracies of 11m (95%) were achieved using eLoran. These accuracy levels are typical of those realised in widespread trials over the past four years.

The conclusion so far is that where there is good eLoran transmitter geometry and signal strength, and a maritime eLoran service has been established, complete with propagation correction maps (ASFs) and differential-Loran, there is no reason why eLoran should not provide close to (if not better than) 10m (95%) positioning accuracy. Other challenging areas include mountainous terrain and fjords, and these will need to be investigated in the near future. The GLAs have developed the capability to establish a temporary eLoran installation quickly and accurately for trial purposes, and to measure and analyse the system's performance.

5. OTHER OPTIONS TO PROVIDE RESILIENT PNT

The GLAs have analysed other technologies and their potential to provide resilient PNT. These include the use of physical and radar aids to navigation and hardening existing GNSS technology.

5.1 Physical & Radar Aton

Recognising current trends in maritime user radar equipage, it might be possible to expand or enhance the physical AtoN infrastructure to support a fall-back mode of radar positioning. This would assume a continuation of existing approaches and technologies to mark hazards, channels and traffic separation schemes, enhanced by the increased use of synchronised and sequenced lights and a major expansion of radar aids to navigation (radar reflectors, enhancers and radar beacons) to provide complete coastal coverage.

This could be used in conjunction with New Technology radars to provide absolute positioning, sufficient to allow continuation of navigation in the event of loss of GNSS. This possibility is explored in more detail in [14], but it must be stated that considerable R&D would be necessary to establish the feasibility and cost of such a solution, as well as international coordination and cooperative action by ship-owners and radar manufacturers, all of which would take many years to bring about.

5.2 HARDENING OF GNSS

This approach is a development of interference detection and mitigation outlined in Section 2.4. It further assumes that all SOLAS vessels would be equipped with multi-constellation GNSS receivers, initially provided when their existing equipment needs replacing, but fully equipped by no later than 2020. It would also be assumed that over time the users' GNSS receivers would incorporate more robust testing for the effects of interference and would alarm in an appropriate fashion if interference were detected.

Recognising the dependence of users upon GNSS based navigation, maritime authorities would need to undertake an infrastructure upgrade programme to enhance the capabilities of the IALA DGPS beacon infrastructure such that it supports multiple GNSS systems and various frequencies. Alternatively, or in addition, there would need to be a move towards international recognition of an integrated Satellite Based Augmentation System (SBAS) incorporating, for example WAAS, EGNOS, MSAS and GAGAN. There would also need to be increased R&D activities to support the standardisation of more robust user GNSS receiver equipment and to ensure its safe integration into future bridge systems.

This solution obviously requires concerted action from a wide range of stakeholders, coordinated through a number of international organisations, and would be a lengthy and perhaps costly process. National telecommunications regulators and their regional and international counterparts would need to ensure the adequate provision of means to deter, detect and respond to GNSS interference events. Finally, there would be a need for maritime authorities, including VTS operators and shipping organisations, acting through IMO, to develop reversionary procedures to which mariners can turn in the event of potentially hazardous GNSS interference.

6. CONCLUSIONS

The successful implementation of e-Navigation is dependent on resilient PNT. GNSS will undoubtedly be the primary source of that PNT, but to satisfy the requirement for resilience it will need complementary support. A GNSS complement must: enable resilient PNT for use by critical infrastructure applications including maritime transport; be readily integrated with GNSS at chip-level; support interference detection and mitigation; maintain the user's concept of operations with a seamless transition to a complement when GNSS is lost; have the potential to be deployed world-wide; be independent of GNSS and dissimilar in terms of failure modes, but provide similar levels of performance.

In the opinion of the GLAs, eLoran is the only system that can meet all these requirements in the timescale required to support the development and implementation of e-Navigation. For this reason the GLAs continue to encourage the development of eLoran within their organisation and within the wider national and international community.

7. REFERENCES

[1] IMO Maritime Safety Committee, MSC 85/26, 2009.

[2] IALA 2010 Conference, Cape Town, South Africa, Basker, Williams. Navigating eLoran, 2010.

[3] Last D. *GPS Forensics, Crime & Jamming*. 2nd GNSS Vulnerabilities and Solutions Conference, 2-5 September 2009, Baška, Krk Island, Croatia.

[4] Williams, P., Grant, A., Ward, N. and Basker, S., Reliable GPS: Interference, Jamming and the Case for eLoran, Proceedings of the Royal Institute of Navigation (RIN) NAV08 International Loran Association 37th Annual Meeting, London, 2008.

[5] Last D., Grant A., Ward N. *Demonstrating the Effects of GPS Jamming on Marine Navigation*. 3rd GNSS Vulnerabilities and Solutions Conference, 5-8 September 2010, Baška, Krk Island, Croatia.

[6] Mattos, P.G., *GNSS and eLoran Tightly Coupled*, Proceedings of the 22nd International Technical Meeting of the Satellite Division of the Institute of Navigation (ION GNSS 2009), Savannah, GA, September 2009, pp. 873-880.

[7] Basker S. *GPS Vulnerability*. Pres. IALA ad hoc meeting on eLoran, Haugesund, Norway, September 2007.

[8] O'Rourke, T.D. *Critical Infrastructure, Interdependencies, and Resilience*. The Bridge. Vol. 37, No.1. National Academy of Engineering, 2007.

[9] Merrill, J. *Update on US Interference Detection and Mitigation Plan (IDM)*. Proc CGSIC 49, Savannah, Sept 2009

[10] Curry C. *GAARDIAN - A UK Government Funded R&D Project Using eLoran to Investigate GPS Interference*. Proceedings of the 38th Convention of the International Loran Association, Portland, Maine, October 2009

[11] ITU Recommendation 589-3, '*International Telecommunications Union, Technical Characteristics Of Methods Of Data Transmission And Interference Protection For Radionavigation Services In The Frequency Bands Between 70 And 130 kHz.*'

[12] Swaszek, P., Johnson, G., Hartnett, R and Lo, S., 'An Investigation into the Temporal Correlation at the ASF Monitor Sites', *Proceedings of the 36th Annual Convention and Technical Symposium of the International Loran Association,* Orlando, Florida, 2007.

[13] 'Enhanced Loran (eLoran) Definition Document', Version 1.0, *International Loran Association*, October 2007

[14] ENC GNSS 2010, Ward, Bransby. Radar Aids to Navigation in the Age of GNSS.

[15] 'Loran's Capability to Mitigate the Impact of a GPS Outage on GPS Position, Navigation, and Time Applications', Narins, M. (Programme Manager), Prepared for the Federal Aviation Administration Vice President for Technical Operations Navigation Services Directorate, FAA, March 2004.

[16] Williams, P. and Hargreaves, C., 'eLoran Performance in the Orkney Archipelago', *Proceedings of the 38th Convention of the International Loran Association, Portland, Maine,* October 2009.

[17] B. B. Peterson, A. Hawes, and K. Shmihluk, 'Loran Data Channel Communications using 9th Pulse Modulation (ver 1.0)', Loran Support Unit, 2 Jan 2006.

BIBLIOGRAPHY

[1] Editorial, Loran-C in Europe-not the end, but a new beginning. Technical report, 1999. (Cited on page 32.)

[2] Private conversation with Dr. Fullekrug, 2009. (Cited on pages xiii, 19, and 35.)

[3] International Loran Association and other. Enhanced loran (eloran). definition document (for consultation-comments to ila by 1 april). *Report Version: 0.1. Report Version Date*, 12, 2007. (Cited on pages xiii, xvii, 5, 8, 9, and 11.)

[4] J. Darrah A. Donahue L. Hirsch D. Jewell D. W. Klepczynski J. Levine K. Lewis E. Stear P. Ward B. Parkinson, J. Doherty and P. Rambow. Independent Assessment Team (IAT) Summary of Initial Findings on eLoran. Technical report, Institute for Defense Analyses, 2009. (Cited on page 5.)

[5] Ernest G Baxa Jr. Continued investigation of potential application of omega navigation to civil aviation. 1978. (Cited on page 123.)

[6] M. Beckmann. *Carrier Wave Signals Interfering with Loran-C*. PhD thesis, Technical University of Delft, 1992. (Cited on pages 13, 34, 35, and 47.)

[7] M. Beckmann. Interference detection and suppression methods for loran- c receivers, proc. 19th annual technical symposium, wild goose association. Oct. 1990. (Cited on page 47.)

[8] C. O. Lee Boyce, Sherman Lo, J.D. Powell, and Per Enge. *Atmospheric Noise: Data Collection and Analysis, Proceedings of the International Loran Association 34th Annual Meeting, Santa Barbara, CA,*. October 2005. (Cited on pages 38, 54, and 55.)

[9] C. O. Lee Boyce, Sherman Lo, J.D. Powell, and Per Enge. *Analysis of Noise and Cycle Selection in a Loran Receiver, Proceedings of the International Loran Association 35th Annual Meeting, Groton, CT,*. October 2006. (Cited on pages 38 and 55.)

[10] Lee Boyce, Sherman Lo, Powell, J.D. Powell, and Per Enge. *Mitigating Atmospheric Noise for Loran, Proceedings of the Institute of Navigation GNSS Conference, Fort Worth, TX,*. September 2006. (Cited on pages 38 and 54.)

[11] Lee Boyce, Sherman Lo, J.D. Powell, and Per Enge. *Noise Assessment and Mitigation for Loran for Aviation, Proceedings of the Institute of Navigation Annual Meeting, Cambridge, MA,*. June 2005. (Cited on page 29.)

[12] C.O. Lee Boyce Jr. *Atmospheric Noise Mitigation for Loran*. PhD thesis, Stanford University, Stanford, CA, 2007. (Cited on pages 38, 40, 54, 55, and 56.)

[13] Brest. *European Loran-C System Control Centre of Brest Report version 1 2008-2009*. CCB. (Cited on page 147.)

[14] P. Brunavs. Phase lags of the 100 khz radio-frequency ground wave and. approximate formulas for computation,. *Canadian Hydrographic Service*, 1977. (Cited on pages 99, 111, 112, and 131.)

[15] Hargreaves C, Williams P, and Bransby M. ASF quality assurance for eLoran. In *Proceedings of the 2012 IEEE/ION Position, Location and Navigation Symposium*. IEEE, apr 2012. (Cited on pages 99 and 115.)

[16] John A. Volpe National Transportation System Center. Vulnerability assessment of the transportation infrastructure relying on the global positioning system. Technical report, August 20, 2001. (Cited on page 5.)

[17] British Atmospheric Data Centre. *www.badc.nerc.ac.uk/data/dataset*. (Cited on page 80.)

[18] CCIR (International Radio Consultative Committee). *Characteristics and Applications of Atmospheric Noise Data, Report 322-3, ITU, Geneva.* 1988. (Cited on pages 29 and 55.)

[19] Nick Ward David Last, Paul Williams. eloran and amateur radio-a study in coexistence. 2008. (Cited on page 35.)

[20] Richard George Farnsworth. *Loran- C Coverage Prediction in Western Europe*. PhD thesis, University of Wales, Bangor,, 1990. (Cited on page 18.)

[21] Richard George Farnsworth. *Loran- C Coverage Prediction in Western Europe*. PhD thesis, University of Wales, Bangor,, 1990. (Cited on pages 27, 28, 29, 30, 31, 33, 34, 36, 44, 48, 51, 56, 99, and 162.)

[22] Kenneth A Fisher. The navigation potential of signals of opportunity-based time difference of arrival measurements. Technical report, AIR FORCE INST OF TECH WRIGHT-PATTERSON AFB OH SCHOOL OF ENGINEERING AND MANAGEMENT, 2005. (Cited on page 97.)

[23] Radio Technical Commission for Maritime Services. *"Recommended Standards for Maritime Users"*. (Cited on page 52.)

[24] B. Forsell. *Radio Navigation System*. Prentice Hall, 1991. (Cited on page 44.)

[25] Hua Fu and Pooi Yuen Kam. MAP/ML estimation of the frequency and phase of a single sinusoid in noise. *IEEE Transactions on Signal Processing*, 55(3):834–845, mar 2007. (Cited on page 71.)

[26] Martin Fullekrug. University of bath, private communications. (Cited on page 56.)

[27] R. Hartnett G. Johnson, P. Swaszek. *4 down, 50 to go, an Update on Harbor Surveys in the US,Proc. 36th Annual Technical Symposium, International Loran Association, Orlando, FL.* 16-17 October 2007. (Cited on page 131.)

[28] Grace Xingxin Gao, Matteo Sgammini, Mingquan Lu, and Nobuaki Kubo. Protecting gnss receivers from jamming and interference. *Proceedings of the IEEE*, 104(6):1327–1338, 2016. (Cited on page 6.)

[29] A.J Grant. *Availability, Continuity, and Selection of Maritime DGNSS Radio beacons*. PhD thesis, University of Wales, Bangor, 2003. (Cited on pages 33, 54, 148, 149, 156, and 159.)

[30] Alan Grant, Paul Williams, Nick Ward, and Sally Basker. Gps jamming and the impact on maritime navigation. *The Journal of Navigation*, 62(2):173–187, 2009. (Cited on page 6.)

[31] Markus Günter Graulich. Weather influence on loran-c. 1987. (Cited on page 80.)

[32] U.S. Coast Guard. *Specification of the Transmitted Loran-C Signal MI6562.4. Washington, DC: U.S. Department of Transportation.* 1981. (Cited on pages 10, 51, and 131.)

[33] Hui Hua, Gong Wang, and Jianmin Shi. The availability assessment for reactor trip system based on markov model. In *2014 10th International Conference on Reliability, Maintainability and Safety (ICRMS)*. IEEE, aug 2014. (Cited on page 146.)

[34] Ling-Ling Huang, Yang Fu, Yang Mi, Jia-Lin Cao, and Peng Wang. A markov-chain-based availability model of offshore wind turbine considering accessibility problems. *IEEE Transactions on Sustainable Energy*, 8(4):1592–1600, oct 2017. (Cited on page 146.)

[35] S-W Hwang, Y. S. Choi, S. J. Lee, and S. H. Yang. An analysis on ASF variations and temperature. In *2014 IEEE/ION Position, Location and Navigation Symposium - PLANS 2014*. IEEE, may 2014. (Cited on page 99.)

[36] Shin M. Y. Lee S. J. Yang S. H. Lee C. B. Hwang, S. W. Asf correction technique using multiple eloran monitor sites in korea. *The Institute of Navigation*, 26:597–603, February 2009. (Cited on pages xv, 99, 118, 119, and 122.)

[37] J. Johler. Propagation of the low-frequency radio signal. *Proceedings of the IRE*, 50(4):404–427, apr 1962. (Cited on pages 99, 100, and 101.)

[38] J. Johler and R.H Doherty. *"Analysis of Groundwave Temporal variations in the Loran-C Radionavigation System"*. 76-222-1,USCG, June 1976. (Cited on page 99.)

[39] J Ralph Johler, WJ Kellar, and Lillie C Walters. *Phase of the low radiofrequency ground wave*, volume 573. US Department of Commerce, National Bureau of Standards, 1956. (Cited on pages xvii, 99, 100, and 102.)

[40] GW Johnson, PF Swaszek, Jan-Hendrik Oltmann, and Michael Hoppe. Feasibility study of r-mode using mf dgps transmissions. *German Federal Waterways and Shipping Administration, Milestone*, 2. (Cited on pages 73 and 96.)

[41] Rohan Kapoor, Subramanian Ramasamy, Alessandro Gardi, and Roberto Sabatini. Uav navigation using signals of opportunity in urban environments: A review. *Energy Procedia*, 110:377–383, 2017. (Cited on page 96.)

[42] Joseph F Kasper. Evaluation of omega configurations for airways system operations. In *Proc. ION Nat'l. Air Meeting*, 1971. (Cited on page 123.)

[43] D. Last and Y. Bian. *Carrier-wave interference to Loran-C: a statistical evaluation, vol. 29, pp. 1260-1274*. Oct. 1993. (Cited on page 33.)

[44] J.D Last, M.D Searle, and R.G Farnsworth. *"The Northwest European Loran-C Systems: Coverage and Performance Predictions",*. Navigation, Journal of The Institute of Navigation, Vol. 40, No. 3, pp.209-226., 1993. (Cited on pages 46, 48, and 99.)

[45] Williams P. Last, D. and K. Dykstra. *Propagation of Loran-C Signals in Irregular Terrain, Modelling and Measurements: Part 1: Modelling,Proceedings of the 29thAnnual Meeting of the International Loran Association, Washington, DC,*. November 2000. (Cited on page 35.)

[46] Caspar. K Lebekwe. *Private Conversation with Dr Paul Williams at the GLAs*. (Cited on pages 32, 33, 46, 146, 154, and 179.)

[47] Morris P. Lo, S. and P. Enge. *Early Skywave Detection Network: Preliminary Design and Analysis, Proceedings of the 34th Technical Symposium of the International Loran Association, Santa Barbara, CA,*. October 2005. (Cited on page 39.)

[48] Morris P. Lo, S. and P Enge. *Early Skywave Detection Network: Preliminary Design and Analysis, Proceedings of the International Loran Association 34th Annual Meeting, Santa Barbara, CA*. October 2005. (Cited on page 48.)

[49] Sherman Lo. *Loran Integrity Analysis for Required Navigation Performance 0.3, Proceedings of the 5th International Symposium on Integration of LORAN-C/Eurofix and EGNOS/Galileo, Munich, Germany,*. June 2004. (Cited on pages 8, 35, 37, 48, 74, and 137.)

[50] Sherman Lo. *Loran Integrity Analysis for Required Navigation Performance 0.3, Proceedings of the 5th International Symposium on Integration of LORAN-C/Eurofix and EGNOS/Galileo, Munich, Germany,*. June 2004. (Cited on page 137.)

[51] Sherman. Lo. *"Loran Availability and Continuity Analysis for Required Navigation Performance 0.3", Proceedings of GNSS 2004 The European Navigation Conference, Rotterdam, The Netherlands,*. May 2004. (Cited on pages 8, 37, 48, 58, 137, 151, 159, 162, and 166.)

[52] Sherman Lo. *The Loran Integrity Performance Panel (LORIPP), Proceedings of the ION-GPS Meeting, Portland, Oregon*. September 24-27, 2002. (Cited on pages 8, 35, 37, and 55.)

[53] Sherman Lo, Peter Morris, and Per Enge. *Early Skywave Detection Network: Preliminary Design and Analysis, Proceedings of the International Loran Association 34th Annual Meeting, Santa Barbara, CA*. October 2005. (Cited on page 137.)

[54] Sherman Lo, Peterson, Benjamin, and Per Enge. *Proving the Integrity of the Weighted Sum Squared Error (WSSE) Loran Cycle Confidence Algorithm, Navigation: The Journal of the Institute of Navigation, Vol. 54 No.4,*. 2007. (Cited on page 39.)

[55] Sherman Lo, B. Peterson, L. Boyce, and P. Enge. *The Loran Coverage Availability Simulation Tool, Proceedings of the Royal Institute of Navigation NAV08/International Loran Association 37th Annual Meeting, London, UK,*. October 2008. (Cited on pages 13, 18, 37, 40, 48, 73, 152, and 159.)

[56] Sherman C Lo, Benjamin B Peterson, Tim Hardy, and Per K Enge. Improving loran coverage with low power transmitters. *Journal of navigation*, 63(01):23–38, 2010. (Cited on page 10.)

[57] Wenzel Lo, S., Morris R., P., and P. Enge. *Modeling and Validating Bounds Loran Temporal ASF Bounds for Aviation, Navigation: The Journal of the Institute of Navigation,*. January 2008. (Cited on page 137.)

[58] G. Millington. *"GroundWave Propagation over an inhomogeneous Smooth Earth"Proceedings of the Institute of the Electrical Engineers, Vol. 96 Part III, pp. 44-53*. 1949. (Cited on pages 28 and 46.)

[59] Andre Nieuwland. An improved cycle identification algorithm, proc. 21st annual technical symposium, wild goose association. Aug. 1992. (Cited on page 47.)

[60] NOAA. *www.noaa.gov*. (Cited on page 76.)

[61] US Department of Defense and Department of Transportation. "Federal Radionavigation Plan 2001 FRP 2001, ". Technical report, 2001. (Cited on pages 7 and 151.)

[62] General Lighthouse Authorities of the United Kingdom, Ireland Research, and Radionavigation. *The Case for eLoran, Version 1.0,*. May 2006. (Cited on pages 5, 6, 7, 37, 99, and 145.)

[63] Kyung Ryoon Oh, Jong Chul Kim, and Gi Wook Nam. Development of navigation algorithm to improve position accuracy by using multi-dgps reference stations' prc information. *Positioning*, 1(09):0, 2005. (Cited on pages xv, 119, and 120.)

[64] International Maritime Organization. *"World-Wide Radionavigation System ", Resolution A.815 (19)*. 1995. (Cited on page 18.)

[65] W. Pelgrum. *Noise - From a Receiver Perspective,in Proceedings of the 34th Annual Convention and Technical Symposium of the International Loran Association*. 2005. (Cited on pages 39, 54, 55, and 56.)

[66] Wouter J. Pelgrum. *New Potential of Low Frequency Radionavigation in the 21st century Ph.D. Thesis,*. ISBN 978-811198-1-8., University of Delft,. (Cited on pages 12, 18, 36, 38, 46, 54, 56, 61, and 99.)

[67] Wouter J. Pelgrum. *New Potential of Low Frequency Radionavigation in the 21st century Ph.D. Thesis,*. ISBN 978-811198-1-8., University of Delft,. (Cited on page 174.)

[68] B. B. Peterson. *Feasibility of Increasing Loran Data Capacity using a Modulated Tenth Pulse, Proceedings of the International Loran Association 36th Annual Meeting, Orlando, FL*. October 2007. (Cited on page 62.)

[69] D.C Poppe. *Coverage and Performance Prediction of DGPS Systems Employing Radio Beacon Transmissions*. University of Bangor, 1995. (Cited on pages 18, 44, 46, 48, 50, 52, 63, 123, 150, 151, and 159.)

[70] U.S. Department of Homeland Security Press Office. *Statement from DHS Press Secretary Laura Keehner on the Adoption of National Backup System to GPS,*. February 7, 2008. (Cited on page 5.)

[71] K. Bridges R. Hartnett and G. Johnson. *A Methodology to Map Airport ASF's for Enhanced Loran, Proc. Institute of Navigation Annual Meeting, Cambridge, MA,*. 27-29 June 2005. (Cited on pages 39 and 99.)

[72] Theodore S Rappaport et al. *Wireless Communications: Principles and Practice*, volume 2. prentice hall PTR New Jersey, 1996. (Cited on page 46.)

[73] John F Raquet, Mikel M Miller, and Thao Q Nguyen. Issues and approaches for navigation using signals of opportunity. In *Proc. of ION NTM*, pages 1073–1080, 2007. (Cited on page 96.)

[74] FAA (AND-700) report to DOT. *An Analysis of Loran-C Performance, its Suitability for Aviation Use, and Potential System Enhancements,*. July 2002. (Cited on pages xvi, xvii, 5, 6, 7, 8, 142, 145, and 151.)

[75] REUTERS. Europe gives up on eloran, 2016. (Cited on page 6.)

[76] P. Williams S. G. Gug, T. Ikeda and T.G.Jeong. *Far East Radionavigation Service (FERNS) Update,In Proceedings of NAV08/ILA37,*. 2008. (Cited on page 27.)

[77] Jan Šafář. *Analysis, Modelling and Mitigation of Cross-Rate Interference in Enhanced Loran*. PhD thesis, Radioelectronics, University of Prague, 2014. (Cited on pages 5, 6, 7, 13, 16, 21, 36, 40, 46, 48, 53, 54, 57, 58, 62, 73, 77, 80, 123, 137, 151, 169, 170, 172, 173, 174, and 179.)

[78] Jan Šafář, Caspar. K Lebekwe, and Paul Williams. Accuracy performance of eloran for maritime applications. *Annual of Navigation*, pages 109–121, 2010. (Cited on pages 24, 46, 57, and 59.)

[79] Charles A Schue III. The next generation lf transmitter and its impact on loran, eloran, and tactical (e) loran systems. In *Proc. RIN NAV08 and 37th ILA Technical Symposium*, 2008. (Cited on page 10.)

[80] A.D. Spaulding and F.G. Stewart. *An Updated Noise Model for Use in IONCAP, Report 87-212, National Telecommunications and Information Administration, US Department of Commerce*. January 1987. (Cited on pages 29 and 54.)

[81] K. Spies and J. Wait. On the calculation of the ground wave attenuation factor at low frequencies. *IEEE Transactions on Antennas and Propagation*, 14(4):515–517, jul 1966. (Cited on page 101.)

[82] M. A. Uman. *The Lightning Discharge, Dover Publications, Inc., Mineola, NY*. 2001. (Cited on page 54.)

[83] International Telecommunication Union. *"Ground-wave Propagation Curves for frequencies between 10 kHz and 30 MHz, Recommendation 368-7"*. 1992. (Cited on page 46.)

[84] International Telecommunication Union. *Prediction of Sky-Wave Field strength at Frequencies between about 150 and 1700kHz Recommendation ITU-R P.1147-1*. 1999. (Cited on pages 33, 48, and 51.)

[85] International Telecommunication Union. International telecommunication union, itu-r p.372-9, radio noise. 2001. (Cited on pages 29, 34, 38, 55, and 152.)

[86] International Telecommunications Union. *"World Atlas of Ground Conductivities ", Recommendation ITU-R P.832-2,*. 1999. (Cited on pages 44 and 46.)

[87] International Telecommunications Union. *"Radio Noise, Recommendation ITU-R P.372-9"*. 2001. (Cited on page 29.)

[88] RF Van Essen, GWA Offermans, AWS Helwig, and D Van Willigen. Regional area augmentation concept for eurofix, reducing spatial decorrelation effects through multi-station dgnss. In *26th Annual Technical Symposium of the International Loran Association, Ottawa, Canada*, pages 6–9, 1997. (Cited on pages 119 and 120.)

[89] D. Van Willigen, G.W.A. Offermans, A.W.S. Helwig, and E.J. Breeuwer. *New Views on the System Aspects of Eurofix, Proceedings of the 25th Annual Technical Symposium of the International Loran Association, San Diego, CA*. November 3-7, 1996. (Cited on page 123.)

[90] Durk Van Willigen, René Kellenbach, Cees Dekker, and W. van Buuren. edloran-next generation of differential loran. (Cited on pages xv, 115, 116, and 117.)

[91] J.R. Wait. The ancient and modern history of EM ground-wave propagation. *IEEE Antennas and Propagation Magazine*, 40(5):7–24, 1998. (Cited on page 101.)

[92] Robert Wenzel and Kirk Montgomery. *Early Skywave Examples from U.S. Coast Guard Primary Control Monitor Set Data, Proceedings of the 32nd Technical Symposium of the International Loran Association, Boulder, Colorado*. 3-7 November 2003. (Cited on page 77.)

[93] Robert Wenzel, Peter Morris, and Kirk Montgomery. *An Examination of Loran Signal Propagation Temporal Variation Modeling, Proceedings of the International Loran Association 35th Annual Meeting, Groton, CT, October*. 2006. (Cited on page 80.)

[94] Alwyin Williams. *Prediction of Coverage and Performance of Datatrak Low-Frequency Tracking SystemPrediction of Coverage and Performance of Datatrak Low-Frequency Tracking System*. PhD thesis, University of Wales, Bangor, 2004. (Cited on pages 6, 28, 30, 33, 34, and 62.)

[95] P. Williams, C. Hargreaves, J. Safar, C. K. Lebekwe, G. Shaw, and N. Ward. *Resilient PNT in e-Navigation, in Proceedings of the Royal Institute of Navigation NAV10 Conference and Exhibition, 2010*. 2010. (Cited on pages 24, 27, 46, 141, and 147.)

[96] Z. Wu, T. S. M. Maclean, D. J. Bagwell, and M. J. Mehler. Propagation over an inhomogenous irregular surface. *Radio Science*, 23(1):33–40, jan 1988. (Cited on pages 104 and 109.)